Diss. ETH No. 19801

Parallelization of Design and Simulation: Virtual Machine Tools in Real Product Development

A dissertation submitted to the
ETH ZURICH

for the degree of
Dr. sc. ETH Zürich

presented by
PASCAL MAGLIE
M. Sc. Mechanical Engineering, EPFL
born August 28th 1980
citizen of Italy

accepted on the recommendation of
Prof. Dr. K. Wegener, examiner
Dr. P. Pahud, co-examiner
Dr. G. Kress, co-examiner

2012

Acknowledgements

Contents

VI

Symbols and abbreviations

Symbols

α	mass proportional Rayleigh damping factor
β	stiffness proportional Rayleigh damping factor
β_c	variable stiffness multiplier
β_j	material dependent constant stiffness multiplier
γ	phase of eigenvector components
γ_{ref}	reference phase of eigenvector
δ	decay constant
ϕ	eigenvector matrix
ϕ_{rn}	component n of eigenvector r
$\phi_{rn,s}$	component n of scaled eigenvector r
ϕ_{mk}	measured eigenvector k
ϕ_{sl}	simulated eigenvector l
η	loss factor
Λ	logarithmic decrement
ω	angular frequency
ω_0	resonance angular frequency
ω_r	angular frequency for mode r
Ω	eigenvalue matrix
ρ	density
υ	kinematic viscosity
ζ	constant damping ratio
ζ_{mr}	modal damping ratio
a	acceleration
A	state matrix
$A, A1, A2 \dots$	notation for A rotary axes of a machine tool
A_{tot}	assembled state matrix
A_i	state matrix of volume i

A_r	reduced finite element state matrix
B, B^T	input matrix
$B, B1, B2 \dots$	notation for B rotary axes of a machine tool
B_{tot}	assembled input matrix
B_i	input matrix of volume i
B_r	reduced finite element input matrix
C, C^T	output matrix
$C, C1, C2 \dots$	notation for C rotary axes of a machine tool
C_i	output matrix of volume i
C_r	reduced finite element output matrix
C_{tot}	assembled output matrix
d	damping of a single mass-spring-damper system
d	bearing inner diameter
d_c	critical damping coefficient
d_{cpl}	linear guideway physical damping coefficient
d_m	average bearing diameter
D	bearing outer diameter
D	feedthrough matrix
$D, [D]$	damping matrix
$\tilde{D}$	damping matrix expressed in modal coordinate system
D_ζ	frequency dependent damping matrix
D_i	damping matrix of volume i
D_k	element damping matrix
D_r	reduced finite element damping matrix
D_{tot}	assembled feedthrough matrix
E	Young's modulus
EX_Y	cross-talk deviation in direction X caused by an acceleration of axis Y
EX_Z	cross-talk deviation in direction X caused by an acceleration of axis Z
EY_X	cross-talk deviation in direction Y caused by an acceleration of axis X
EY_Z	cross-talk deviation in direction Y caused by an acceleration of axis Z
EZ_X	cross-talk deviation in direction Z caused by an acceleration of axis X
EZ_Y	cross-talk deviation in direction Z caused by an acceleration of axis Y
f_0, f_1	lubrication and type dependent coefficient for bearing friction
$F, F(t)$	force
$\tilde{F}$	generalized force expressed in modal coordinate system
F_{drive}	drive force
F_{TCP}	force acting at the TCP

$G(s)$	original transfer function
$G_r(s)$	reduced transfer function
i	complex number $(i^2 = -1)$
i	volume index
I	identity matrix
I_{xx}	component $(1,1)$ of the 3x3 symmetrical moment of inertia tensor
I_{yy}	component $(2,2)$ of the 3x3 symmetrical moment of inertia tensor
I_{zz}	component $(3,3)$ of the 3x3 symmetrical moment of inertia tensor
I_{xy}	component $(1,2)$ of the 3x3 symmetrical moment of inertia tensor
I_{xz}	component $(1,3)$ of the 3x3 symmetrical moment of inertia tensor
I_{yz}	component $(2,3)$ of the 3x3 symmetrical moment of inertia tensor
j	coupling index
j	jerk
k	stiffness of a single mass-spring-damper system
$K, [K]$	stiffness value, stiffness matrix
$\tilde{K}$	stiffness matrix expressed in modal coordinate system
KM	drive local stiffness coefficient
KN	linear guideway local normal stiffness coefficient
KQ	linear guideway local transversal stiffness coefficient
K_r	reduced finite element stiffness matrix
$K_r^L\{A^T, C\}$	r-th left Krylov subspace
$K_r^R\{A, B\}$	r-th right Krylov subspace
K_A, KA	coupling rotation stiffness coefficient about local direction X
K_B, KB	coupling rotation stiffness coefficient about local direction Y
K_C, KC	coupling rotation stiffness coefficient about local direction Z
K_X, KX	coupling linear stiffness coefficient in local direction X
K_Y, KY	coupling linear stiffness coefficient in local direction Y
K_Z, KZ	coupling linear stiffness coefficient in local direction Z
$KTCP\_X$	TCP stiffness value in direction X
$KTCP\_Y$	TCP stiffness value in direction Y
$KTCP\_Z$	TCP stiffness value in direction Z
K_{ax}	bearing local axial stiffness
K_{basis}	partial stiffness of a machine tool kinematic chain
K_{c1}, k_1	partial stiffness of a machine tool kinematic chain
K_{c2}, k_2	partial stiffness of a machine tool kinematic chain
K_i	stiffness matrix of volume i
K_{rad}	bearing local radial stiffness

K_{tot}, k_{tot}	total stiffness of a machine tool kinematic chain
m	mass of a single mass-spring-damper system
m_i	moment i of a transfer function
$M, [M]$	mass, mass matrix
$\tilde{M}$	mass matrix expressed in modal coordinate system
M_i	mass matrix of volume i
Mr	friction torque
M_r	reduced finite element mass matrix
n	rotation speed
O	null matrix
$PosX$	local X position of geometric center of the couplings of an axis
$PosY$	local Y position of geometric center of the couplings of an axis
$PosYM$	local Y position of the driving point of a linear axis
$PosZ$	local Z position of geometric center of the couplings of an axis
$PosZM$	local Z position of the driving point of a linear axis
P_1	equivalent bearing load
q	generalized FE variable expressed in modal coordinate system
$\dot{q}$	first derivative of q
$\ddot{q}$	second derivative of q
Q	heat
$ROTX$	rotation degree of freedom A
$ROTY$	rotation degree of freedom B
$ROTZ$	rotation degree of freedom C
R_ϵ	Strain Energy Ratio
R_a	first orientation of coupling local coordinate system
R_b	second orientation of coupling local coordinate system
R_c	third orientation of coupling local coordinate system
R_s	stiffness scaling factor
R_x	orientation of a linear axis guideway system
s	path
s	Laplace variable
s_0	expansion point for Taylor Series Expansion
t	time
T	generalized finite element nodal temperature
u	generalized finite element nodal displacement
UX	translation degree of freedom X
UY	translation degree of freedom Y

UZ	translation degree of freedom Z
U_x	nodal displacement X
U_y	nodal displacement Y
U_z	nodal displacement Z
v	speed
$Volume\_i$	defined notation for ANSYS volume components
v_i	basis vector i of the Krylov subspace
V_r	basis matrix r of the Krylov subspace
w_i	basis vector i of the Krylov subspace
W_r	basis matrix r of the Krylov subspace
$U(s)$	generalized finite element input in the Laplace space
x	generalized finite element variable, state vector
$\dot{x}$	first derivative of x
$\ddot{x}$	second derivative of x
x_{drive}	displacement at the axis reader head
x_{TCP}	TCP displacement
$X, X1, X2 \ldots$	notation for X linear axes of a machine tool
$X(s)$	generalized finite element variable in the Laplace space
$Y, Y1, Y2 \ldots$	notation for Y linear axes of a machine tool
z	reduced state vector
$\dot{z}$	first derivative of z
$\ddot{z}$	second derivative of z
$Z, Z1, Z2 \ldots$	notation for Z linear axes of a machine tool

Abbreviations

ACK	Axis Construction Kit
ANS	SGI export option for direct solving in ANSYS
APDL	Ansys Parametric Design Language
BTA	Balanced Truncation Approximation
CAD	Computer Aided Design
CAE	Computer Aided Engineering
CAM	Computer Aided Manufacturing
CMS	Component Mode Synthesis
CRS	SGI export option for coupled reduced analysis
DBS	Digital Block Simulation
DOF	Degree Of Freedom
EMA	Experimental Modal Analysis
ETH	Eidgenössische Technische Hochschule
FE/FEM	Finite Element / Finite Element Method
FFT	Fast Fourier Transform
FRF	Frequency Response Function
GC	Gravity Center
GUI	Graphical User Interface
HNA	Hankel Norm Approximation
IGES	Initial Graphics Exchange Specification
IWF	Institut für Werkzeugmaschinen und Fertigung
LTI	Linear Time Invariant
MAC	Modal Assurance Criterion
MOR	Model Order Reduction
ODE	Ordinary Differential Equation
RAM	Rapid Access Memory
RBS/*RBS*	Rigid Body Simulation / SGI export option for rigid body analysis
SGI	Structure Gateway Interface
SME	Small and Medium-sized Enterprise
SPA	Singular Perturbation Approximation
STEP	STandard for the Exchange of Product model data
STL	Standard Tessellation Language
SVD	Singular Value Decomposition
TCP	Tool Center Point
WPP	Workpiece Point
XML	Extensible Markup Language

Abstract

A machine tool is a mechatronic system, whose complexity and precision requirements, necessary to the current strategic and technologic differentiation in the global market, are becoming increasingly challenging. The design of machine tool structures is subject to the usual conflicts present in product development: high productivity and efficiency require shorter machining times, leading to the construction of lightweight axes, in order to achieve higher accelerations. On the other hand, the increasing requirements regarding surface quality and precision necessitate high static and dynamic stiffness, leading inevitably to larger masses.

The combination of a multitude of contradicting conditions requires detailed design criteria, whose reliability is adapted to the complexity of modern multi-axis machine tools, in order to reduce the number of real prototypes before the series production. The precept of the *right first time* has become indispensable in the reality of Swiss small and medium-sized enterprises, because production is often characterized by small series, in order to offer customized solutions to the client.

These aspects have led to the increasing interest of the machine tool industry for simulation. The systematic integration of detailed virtual studies of the structural dynamic behavior into the design process aims at simultaneously improving the product quality and shortening the time to market launch. To achieve this, there is a need for tools and guidelines embedded into the development concept, without impinging on existing procedures.

Hence, during the work on the present thesis, industrial applicability represents a constant priority. The focus is set on five main issues: the modeling of coupling elements, the automation of simulation models creation, the reduction of computation times, the flexibility of the analyses and the relevance of the obtained results.

A test-bed is developed for the targeted investigation of linear guiding systems properties in various configurations. This helps to establish how the specifications provided by the component manufactures are best integrated into a finite element model. Among different variants, the optimal modeling guidelines with regard to the elasticity module of the carriages and rails, as well as the boundary conditions at the coupling interfaces are determined. From a selection of frequency responses measured on the same test-bed, an efficient identification process for the guideway damping coefficients is illustrated with the help of a finite element model . The validation of the models is then performed on two multi-axis machines, a tool-grinding center and a machining center. Both structures are loaded statically and dynamically. The deformations, resp. the harmonic responses resulting from the measurements and from the simulations are compared and demonstrate an excellent concordance of results. The method is also applied to the bearings of spindles and rotary axes and to the ballscrews.

The computation time of finite element models is too high for them to be realistically integrated into the design process, which usually requires many simulations in order to improve various aspects of the structure. To support the use of simulation tools at the different design stages, two methods aiming to reduce the model size are discussed: the first is of physical nature and reproduces the structural behavior by means of a rigid body model. The second is based on a mathematical order reduction of the matrices generated by the finite element model.

A stand-alone program is developed and serves as an efficient environment for rigid body simulations. By means of static, modal and harmonic analyses focusing on the relative deviations between the tool tip (TCP: Tool Center Point) and the workpiece center (WPP: Workpiece Point), it is possible to explore the influence of selected parameters on the dynamic behavior of the structure. A sensitivity and a parametric analysis enable the determination of the optimal kinematic configuration by acting on the fundamental characteristics of the machine. With help of the *Strain Energy Ratio*, defining the ratio between the energy stored in the coupling elements and the deformation energy of the structure, a scaling factor for the coupling stiffness coefficients is derived. Its role is to compensate for the compliance loss at the interfaces between the rigid bodies of the model. The objective is to establish rules which are valid for any machine tool and for all loading conditions, in order to improve the reliability of rigid body analyses.

In the next phase, a higher complexity level is necessary so as to generate advanced models including the axis controls. A toolbox, composed of a series of grouped Matlab macros, is developed to perform mechatronic analyses of the entire machine structure. A dimensional reduction by means of the program *MOR for ANSYS* is applied to the finite element mat-

rices of the different volumes and the resulting systems are subsequently automatically assembled, connected by the coupling elements and completed by the control algorithms. The validity of the method is first verified by comparing the results of the original finite element simulation and the corresponding reduced order simulation. The cross-talk deviations on a real two-axis machine are investigated by means of measurements. The experimental conditions are then reproduced in the compact model and the obtained results are confronted with the measurements. The observed concordance is very promising for further applications of reduced coupled simulations of machine tools in the time-domain.

The concept of *Structure Gateway Interface* (SGI) is introduced so as to centralize the creation of the various simulation models, including the implementation of the coupling parameters. This central platform based on ANSYS Workbench relies on a discretized geometry of a structure with an arbitrary number of linear and rotary axes and spindles. A series of macros uses the predefined components of the volumes and interfaces in order to automatically build the complete machine tool model. After these pre-processing operations, three options are available: simulate the unaltered model in ANSYS (option *ANS*), export the mechanical and geometrical data required for simulation in the rigid body stand-alone program (option *RBS*) or export the matrices which, after order reduction, are used to perform the mechatronic simulation in Matlab with the dedicated toolbox (option *CRS*).

Kurzfassung

Eine Werkzeugmaschine ist ein mechatronisches System, dessen Anforderungen an Komplexität und Genauigkeit, bedingt durch die aktuell notwendige strategische und technologische Differenzierung im globalen Markt, immer anspruchsvoller werden. Die Auslegung von Werkzeugmaschinen-Strukturen kommt nicht um die Konflikte herum, die in der üblichen Produktentwicklung vorkommen: Hohe Produktivität und Effizienz verlangen kürzere Werkstückbearbeitungszeiten, was die Konstruktion von leichten Achsen erfordert, um hohe Beschleunigungen erreichen zu können. Andererseits benötigen die wachsenden Anforderungen an Oberflächenqualität und Genauigkeit hohe statische und dynamische Steifigkeit, was unvermeidbar zu grösseren Massen führt.

Die Kombination einer Vielzahl von widersprechenden Bedingungen erfordert detaillierte Design-Kriterien, deren Zuverlässigkeit für die Komplexität moderner mehrachsiger Werkzeugmaschinen geeignet ist, um die Anzahl realer Prototypen vor der Serienfertigung zu minimieren. Das Motto des *right first time* ist in den Realitäten der Schweizerischen kleinen und mittleren Unternehmen unumgänglich geworden, weil die Produktion sich oft durch kleine Serien auszeichnet, um den Kunden massgeschneiderte Lösungen anzubieten.

Diese Aspekte begründen das zunehmende Interesse der Werkzeugmaschinenindustrie für die Simulation. Die systematische Integration von umfassenden virtuellen Analysen des dynamischen Verhaltens im Designprozess zielt darauf ab, sowohl die Produktqualität zu verbessern, als auch die Markteinführungszeit zu verkürzen. Um dies zu erreichen müssen allerdings Werkzeuge und Richtlinien vorhanden sein, die vollkommen im Entwicklungskontext eingebunden sind, ohne die schon existierenden Abläufe durcheinanderzubringen.

Somit stellt während den Entwicklungsarbeiten in der vorliegenden Doktorarbeit die industrielle Anwendbarkeit stets eine Priorität dar. Der Fokus liegt auf fünf Hauptpunkten: Die Modellierung von Kopplungselementen, die Automatisierung der Erstellung der Simulationsmodelle, die Reduktion der Rechenzeiten, die Flexibilität der Analysen und die Relevanz der gewonnenen Resultate.

Ein Prüfstand wird für die gezielte Untersuchung der Eigenschaften von Wälzführungseinheiten in verschiedenen Anordnungen entwickelt. Es wird festgelegt, wie die Steifigkeitsangaben der Komponentenhersteller am besten in ein Finite-Elemente-Modell integriert werden. Unter verschiedenen Varianten werden die optimalen Modellierungsrichtlinien bezüglich der Elastizitätsmodule der Wagen und der Schienen und der Randbedingungen der Kopplungsschnittstellen bestimmt. Mittels einer Auswahl von gemessenen Frequenzantworten auf dem gleichen Prüfstand wird ein effizientes Verfahren zur Identifikation von Dämpfungskoeffizienten der Führungen mit Hilfe eines reduzierten Finite-Elemente-Modells erläutert. Die Validierung der Modelle erfolgt dann an zwei mehrachsigen Werkzeugmaschinenstrukturen, einer Werkzeugschleifmaschine und einem Fräsbearbeitungszentrum. Hierbei werden die Strukturen statisch und dynamisch belastet. Die Verformungen, bzw. die Frequenzgänge aus Messung und Simulation werden miteinander verglichen, woraus eine sehr gute Übereinstimmung resultiert. Die Validierungsmethode wird dabei auch auf Rotationslager von Spindeln und Rotationsachsen und auf Kugelgewindetriebe angewandt.

Die Rechenzeit von Finite-Elemente-Modellen ist zu hoch, um in den Entwicklungsprozess konkret integriert werden zu können, weil eine Vielzahl Simulationen üblich erforderlich ist, um diverse Aspekte der Struktur zu verbessern. Um die Anwendung von Simulationswerkzeugen während den verschiedenen Stadien der Entwicklung zu unterstützen, werden zwei Methoden zur Reduktion der Grösse des Modells diskutiert: die erste ist physikalisch motiviert und bildet das Strukturverhalten als Starrkörpermodell ab. Die zweite besteht darin, eine mathematische Ordnungsreduktion der Systemmatrizen durchzuführen, die aus dem Finite-Elemente-Modell generiert werden.

Ein Stand-alone Programm wird entwickelt und dient als Umgebung für Starrkörpersimulationen. Anhand von statischen, modalen und harmonischen Analysen, die auf die relativen Verlagerungen zwischen Werkzeugspitze (TCP: Tool Center Point) und Werkstück Mittelpunkt (WPP: Workpiece Point) fokussieren, wird das dynamische Strukturverhalten untersucht. Eine Sensitivitätsstudie und eine parametrische Studie erlauben darauf, die optimale kinematische Konfiguration bezüglich den wesentlichen Parametern der Maschine zu bestimmen. Die Kennzahl *Strain Energy Ratio* definiert das Verhältnis zwischen der in den Kopplungselementen eingelagerten potentiellen Energie und der in der Struktur gespeicherten Deformationsenergie. Daraus wird insbesondere ein Anpassungsfaktor bestimmt, um die Steifigkeitswerte der Verbindungsstellen für Starrkörpermodelle zu skalieren. Er zielt darauf ab, den Nachgiebigkeitsverlust an den Schnittstellen zwischen den starren Körpern des Modells auszugleichen. Das Ziel ist somit, Regeln zu ermitteln, um die Zuverlässigkeit von Starrkörperanalysen für beliebige Werkzeugmaschinen und bei beliebigen Lastfällen zu erhöhen.

In der darauffolgenden Phase ist ein höherer Komplexitätsgrad erforderlich, um fortgeschrittene Modelle inklusive Achsenregelung zu generieren. Eine Toolbox, bestehend aus einer Reihe von Matlab Makros, wird entwickelt, um mechatronische Simulationen von gesamten Maschinenstrukturen durchzuführen. Eine dimensionale Reduktion wird mit Hilfe des Programms *MOR for ANSYS* auf die Finite-Elemente Matrizen der einzelnen Volumen angewandt und die resultierenden Systeme werden dann auf automatisierter Weise zusammengesetzt, durch die Kopplungselemente verbunden und um die Regelungsalgorithmen ergänzt. Die Gültigkeit der Methode wird zuerst geprüft, indem die Resultate von originalen Finite-Elemente Simulationen und von entsprechend ordnungsreduzierten Simulationen verglichen werden. Anhand von Messungen, werden Cross-Talk Abweichungen auf einer realen zweiachsigen Maschine untersucht. Die experimentellen Bedingungen werden im kompakten Modell abgebildet und die gewonnenen Simulationsergebnisse mit den Resultaten der Messungen gegenübergestellt. Die gute festgestellte Übereinstimmung ist für weitere Anwendungen von reduzierten gekoppelten Simulationen von Werkzeugmaschinen im Zeitbereich sehr erfolgversprechend.

Das Konzept von *Structure Gateway Interface* (SGI) wird zur Vereinheitlichung der Erstellung der verschiedenen Modelle und zur Implementierung der Kopplungsparameter entwickelt. Diese ANSYS Workbench -basierte zentrale Plattform beruht auf einer diskretisierten Geometrie einer Struktur mit beliebig vielen Linear- und Rotationssachsen und Spindeln. Eine Reihe von Makros verwenden vordefinierte Komponenten der Volumen und Schnittstellen, um das gesamte Modell der Werkzeugmaschine automatisch zu erstellen. Nach diesen Pre-processing Operationen stehen drei Optionen zur Verfügung: Das Modell in ANSYS unverändert simulieren (Option *ANS*), die mechanischen und geometrischen Eigenschaften exportieren, die für die Simulation im Stand-alone Starrkörperprogramm erforderlich sind (Option *RBS*) oder die Matrizen exportieren, die nach Ordnungsreduktion, für die mechatronische Simulation in Matlab, mit der dafür vorgesehenen Toolbox, verwendet werden (Option *CRS*).

Résumé

Une machine-outil est un système mécatronique dont la complexité et la précision suivent des tendances toujours plus exigeantes, nécessaires à une différentiation stratégique et technologique dans le marché global actuel. La conception des structures de machines-outils n'échappe pas aux conflits présents habituellement dans le développement de produits: haute productivité et efficacité exigent des temps de passage de la pièce à usiner aussi courts que possible, ce qui se traduit par la nécessité de concevoir des axes légers, pouvant être soumis à d'importantes accélérations. D'un autre côté, les exigences sur la qualité de surface et la précision revues indéfiniment à la hausse requièrent haute rigidité statique et dynamique, ce qui entraîne inévitablement des masses plus élevées.

La combinaison d'une multitude de contraintes souvent contradictoires fait appel à des critères de design, dont la fiabilité doit être à la hauteur de la complexité des machines-outils multi-axes modernes, afin de minimiser le nombre de prototypes réels avant la mise en série. La devise du *right first time* est devenue incontournable dans les réalités des petites et moyennes entreprises suisses, vu que la production est souvent caractérisée par des séries limitées, pour offrir aux clients des solutions sur mesure.

Ces aspects justifient l'intérêt croissant que porte l'industrie des machines aux outils de simulation. L'intégration systématique de l'étude virtuelle détaillée du comportement structurel dans le processus de conception a pour but d'en améliorer la qualité, tout en abrégeant le temps nécessaire à la mise sur le marché. Pour atteindre cela, il est nécessaire d'avoir à disposition des outils et des directives qui s'insèrent dans le contexte de développement, sans en bouleverser les procédures déjà en vigueur.

C'est ainsi que tout au long des développements dans la présente thèse, l'applicabilité au niveau industriel constitue constamment une priorité. L'accent est mis sur cinq points principaux: la modélisation des éléments de couplage, l'automatisation de l'élaboration des modèles de simulation, la réduction des temps de calcul, la flexibilité des analyses et la pertinence des résultats obtenus.

Un banc d'essai est développé pour l'étude ciblée des propriétés des guidages linéaires à corps roulants. Il est établi comment intégrer les valeurs des rigidités fournies par les fabricants des composants dans un modèle éléments finis. Parmi différentes variantes, les règles de modélisation optimales concernant le module d'élasticité des chariots et des rails, ainsi que les caractéristiques des contraintes aux interfaces sont déterminées. A partir d'une sélection de réponses en fréquence mesurées sur le même banc d'essai, un procédé efficace d'identification des coefficients d'amortissement dans les guidages à l'aide d'un modèle éléments finis est illustré. La validation des modèles est ensuite effectuée sur deux machines multi-axes, dont un centre de meulage d'outils et un centre d'usinage. Les deux structures sont soumises à des charges statiques et dynamiques. Les déformations, respectivement les réponses harmoniques découlant des mesures et des simulations sont comparées, démontrant une très bonne concordance des résultats. Par le biais de ces analyses, la méthode de validation est en outre appliquée aux paliers rotatifs des broches et des axes de rotations et aux vis à billes.

Le temps de calcul des modèles éléments finis est trop élevé pour pouvoir être concrètement intégré dans le processus de conception, qui requiert en général une multitude de simulations servant à améliorer divers aspects de la structure. Pour favoriser l'emploi d'outils de simulation pendant les différents stades de la conception, deux méthodes de réduction de la taille des modèles sont discutées: la première est de nature physique et reproduit le comportement de la structure à l'aide d'un modèle corps-rigide. La deuxième se base sur une méthode mathématique de réduction dimensionnelle des matrices générées par le modèle éléments finis.

Un programme stand-alone est développé et sert d'environnement pour simulations corps-rigide. A l'aide d'analyses statiques, modales et harmoniques focalisant sur les déviations relatives entre la pointe de l'outil (TCP: Tool Center Point) et le centre de la pièce (WPP: Workpiece Point), il est possible d'explorer l'impact de paramètres sélectionnés sur le comportement dynamique de la structure. Une étude de sensitivité et une étude paramétrique permettent d'établir la configuration cinématique optimale en agissant sur les caractéristiques essentielles de la machine. A l'aide du *Strain Energy Ratio*, définissant le rapport entre l'énergie potentielle emmagasinée dans les éléments de couplage et l'énergie de déformation dans la structure, un facteur d'ajustement des coefficients de rigidité dans les joints pour les modèles corps-rigide est déterminé. Son rôle est de compenser la perte d'élasticité aux interfaces entre les corps rigides du modèle. L'objectif est ainsi d'émettre une règle valable pour toute machine-outil et dans tous les cas de charge envisageables pour conférer une meilleure fiabilité aux analyses corps-rigide.

Dans la phase suivante, un degré de complexité plus élevé est nécessaire pour générer des modèles plus avancés incluant la commande des axes. Une toolbox, composée d'une série de macros Matlab, est développée pour effectuer des simulations mécatroniques de l'entière structure des machines. Les matrices éléments finis des différents volumes sont soumises à une réduction dimensionnelle à travers le programme *MOR for ANSYS* et les systèmes résultants sont assemblés, interconnectés par les éléments de couplage et complétés par les algorithmes de commande, le tout de manière hautement automatisée. La validité de la méthode est tout d'abord vérifiée en comparant les résultats des simulations éléments finis originales et des simulations réduites correspondantes. En se basant ensuite sur des essais, les déviations dues au cross-talk sur une machine réelle deux-axes sont étudiées. Les conditions expérimentales sont reproduites dans le modèle compact et les résultats obtenus sont confrontés avec les mesures. La bonne correspondance constatée est très prometteuse dans l'optique d'ultérieures applications de simulations couplées réduites de machines-outils.

Le concept de *Structure Gateway Interface* (SGI) est introduit pour centraliser l'élaboration des différents modèles, y compris l'implémentation des paramètres de couplage. Cette plateforme centrale basée sur *ANSYS Workbench* s'appuie sur une géométrie discrétisée d'une structure avec un nombre quelconque d'axes linéaires et rotatifs et de broches. Une série de macros utilise des composants prédéfinis des volumes et interfaces pour construire automatiquement le modèle complet de la machine-outil. Au terme de ces opérations de pre-processing, trois options sont à disposition: simuler le modèle tel quel dans ANSYS (option *ANS*), exporter les données mécaniques et géométriques requises pour la simulation dans le programme stand-alone corps-rigide (option *RBS*) ou exporter les matrices, qui après réduction, sont utilisées pour effectuer la simulation mécatronique dans Matlab à l'aide de la toolbox prévue à cet effet (option *CRS*).

Chapter 1

Introduction

The needs and demands of the industry have considerably developed over the last decades. This new context, affected by the global opening and by the effects of an ever-growing competitiveness, decreasing prices and a prevalent demand for qualitative high-class products, has brought new facets to the product development of machine tools. In order to accommodate to the new market requirements regarding multi-function capabilities, customizability, energy efficiency, etc., actions have to be taken which enable a reduction of development times and of prototyping costs and a higher reactivity to changing customer needs. New design concepts having to satisfy major productivity standards lead to increasingly complex systems with better dynamic properties and as a consequence higher precision. However, the integration of the improved and more elaborated characteristics of the different components of a machine-tool has the opposite effect of extending the development phase. A realistic simulation requires therefore the use of sophisticated tools to integrate the elaborate characteristics of all components. It becomes indeed inevitable to consider all the interactions between the several subsystems of multi-axis assemblies, as the one in figure 1.1, in order to correctly predict the deformations caused by the generated axis motions and the process loads.

The fast emergence of rotary axes has been driven by the increasing requirements for flexibility of the production process and notably enables the fabrication of workpieces with complex geometries in less take-ups than a traditional three-axis machine. But this gain of productivity and adaptability comes with the drawbacks associated with more elaborate systems. Higher investment costs and more critical technical challenges increase the risks related to design errors. A five-axis machine is indeed characterized by a complex dynamical behavior resulting from the interaction between the different sub-systems which compose it. The use of rotary axes generates frequent and fast orientation changes of the tool and/or workpiece, which lead to significant dynamic loads due to the necessary
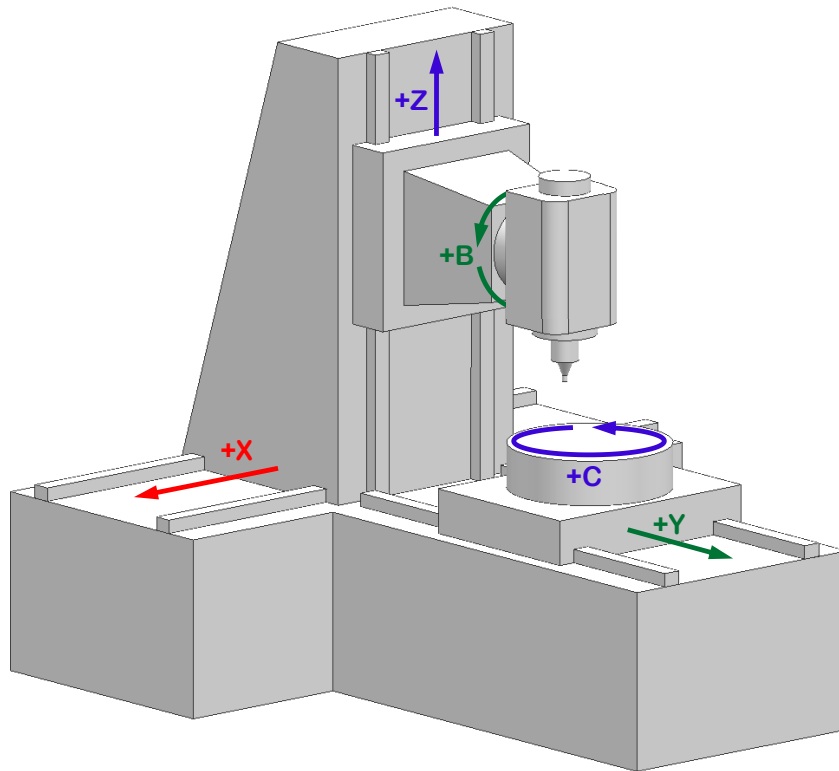
Figure 1.1: Standard axis arrangement of a five-axis machine tool.

accelerations of the linear axes. The accelerations of the rotary axes act also dynamically on the subordinate linear axes, creating complex inertial interactions. These inertial aspects add to the ever growing process loads as a consequence of the arising of hard-to-machine materials and of the prevalence of high feed rates and respective accelerations.

The process model connects the cutting force with the feed velocity of the tool, its rotational speed, the cutting depth, the tool geometry and the properties of the materials in contact. It closes the dynamical loop of the machine tool structure, thus enabling the determination of optimal cutting parameters and the prediction of chatter phenomena due to regenerative effects. Hence the understanding of the full vibrational behavior of a machine tool presupposes simultaneously a correct cutting model and a reliable model of the entire mechanical chain through the complete axis arrangement, starting from the tool tip and ending at the workpiece.

A further complexity level originates in the coupling effects generated by the feed drives, whose layout cannot be separated from the structural analysis of machine tools. Gain factors, velocity profiles, acceleration and jerk settings, bandwidth, etc. all directly or indirectly influence the deviations of the tool from its nominal path, resulting from the

interplay between the dynamical behavior of the drive trains and the mechanical structures of the mobile components.

The interaction between all these perturbation sources creates permanently changing structural configurations leading to unwanted vibration phenomena, which during roughing as well as during finishing phases, become always more difficult to model with a simplified analytical approach. Modern simulation methods for multi-axis machine tools can roughly be classified into two categories: the Finite Element Method (FEM) and the Rigid Body Simulation (RBS):

- Rigid body simulation is fast and efficient, but doesn't take into account all the deformation and vibrational characteristics of the structural parts of complex machines. In conventional machine tools, the structural parts are much stiffer than the couplings, justifying the assumption of the compliances concentrated in the joints. In modern machine tools, the assumption is not appropriate, due to the lightweight characteristics of the structural parts resulting from higher dynamics requirements. The corresponding RBS simplification level is adapted to preliminary qualitative evaluations, but due to the evident precision and reliability limits, caution has to be taken in function of the machine configurations and the loading conditions.

- FEM simulation is certainly more appropriate for the analysis of complex compliant systems, providing a model with an arbitrarily high level of detail. However, the extensively large number of degrees of freedom which have to be handled renders this method inapplicable for the tasks of most researchers and engineers, which dispose of limited time and computational resources. Besides, the complex nature of FE models, originated from CAD geometries, renders the translation, pre-processing and every subsequent change of the model highly problematic and time expensive.

There is therefore an increasing demand for new simulation concepts being able to handle the high complexity level of modern five-axis machine tools, and being simple enough to be efficiently operated on standard computers available to most developers and which can easily be integrated into the design process. These are the two absolute prerequisites to the ultimate objective of designers, which is the optimization of the product performance. Instead of that, the trend in the machine tool industry in terms of simulative effort is rather to run FE models at various phases of the design process in order to verify the static and modal behavior of selected configurations of the structure and, if needed, perform manual changes based on the colorful pictures provided by the simulation, without a systematic way of evaluating the effective quality of the machine and methods to derive the necessary directions of enhancement.

In order to efficiently incorporate modern simulation and optimization methods into the
industrial context, the focus is set here on the development of an integrated environment
and methodology for the evaluation of machine tools, based on the rigid body approach and
on the order reduction technique. The idea is to achieve the parallelization of design and
simulation. A central platform can be accessed at various development stages to improve
targeted properties of the complete mechatronic machine tool structure (figure 1.2), with
a growing complexity and sophistication level of the virtual models adapted to the various
detailing phases of the product development.
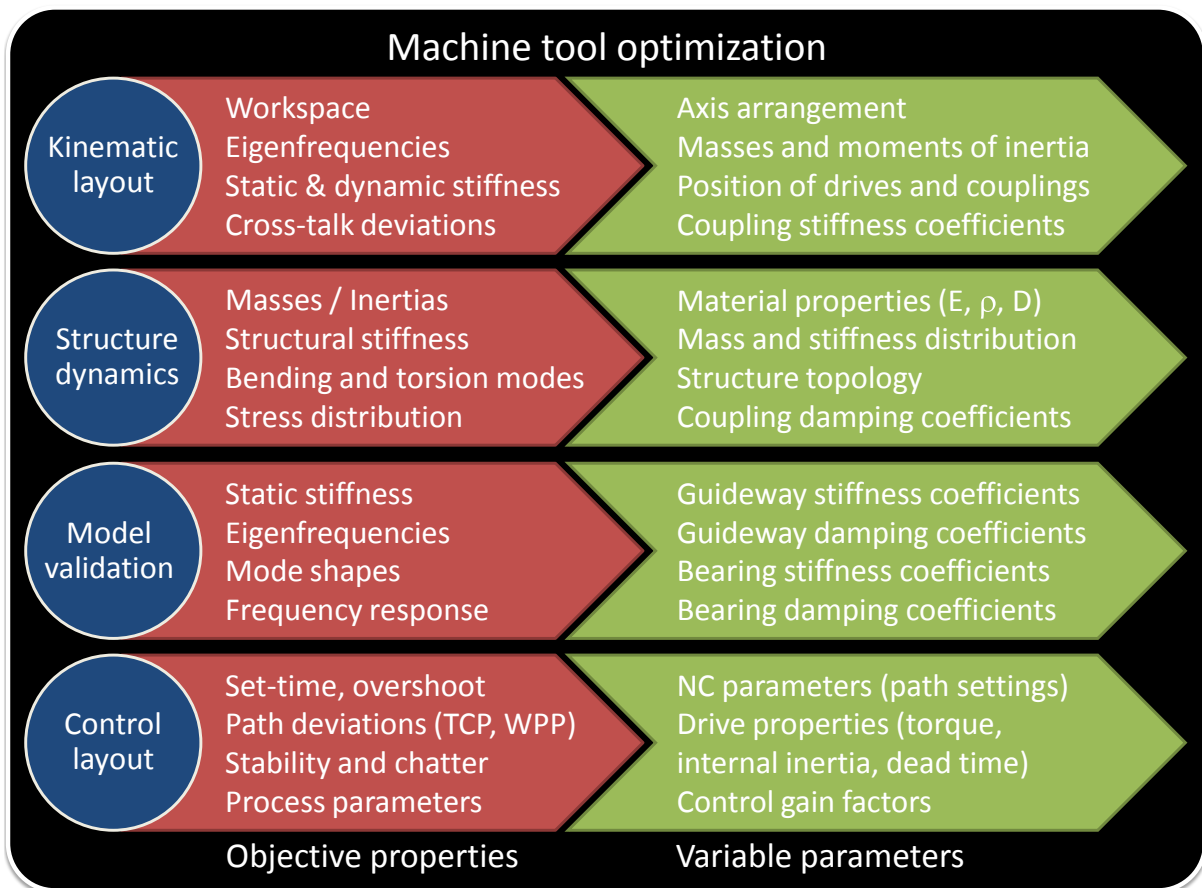
Figure 1.2: Range of optimization options of the mechatronic system *machine tool*.

During the layout phase, the simplified characteristics of a rigid body model are perfectly
adapted to the selection of an appropriate kinematic configuration of the axes. Thanks
to the extremely low computational effort, numerous iterations can be performed in order
to establish the fundamental structure parameters, e.g. masses, centers of mass, drive
positions, rail and carriage distances, stiffness and damping coefficients of the couplings,
etc. The different static and dynamic analyses inherent to this study rest systematically

on the relative deviations between the tool and the workpiece, for all the possible loadcases and in all conceivable workspace positions. In the subsequent concept phase, the model is completed with the flexibility of the structural components, derived from the order reduction of the system matrices of the original ANSYS model. It is thereupon possible to carry out quantitative analyses taking into account the compliances in the couplings as well as in the axis bodies, without excessively increasing the computation times. Detailed and accurate simulations, containing in particular the axis control algorithms, complement the design phase, preceding the construction of the first, and ideally last prototype.

The thesis starts with a review of the prevailing methods used to evaluate the behavior of machine tools in chapter 2. An extensive survey of modern simulation approaches is presented (section 2.1), ranging from commercial rigid body analysis tools (section 2.1.1) to the multitude of capabilities offered by models originating from finite element packages (section 2.1.2), including the associated order reduction methods (section 2.1.3). In section 2.1.4, the advantages and disadvantages of the described simulation methods are listed and the possibility of combining them into different environments are summarized. The following section 2.1.5 is dedicated to the important properties of the various coupling elements present in machine tools. Convictions and uncertainties regarding the corresponding stiffness and damping coefficients are addressed. The chapter ends with the research gap (section 2.2) motivating the research conducted in the field of simulation of machine tools and summarizing the achievements of this thesis.

In chapter 3, the fundamental concept of the *Structure Gateway Interface* (SGI) is introduced to emphasize how the process translating a CAD geometry into a simplified mathematical representation is handled, using the capabilities of the FE-software package ANSYS. First the role of this central design platform is highlighted in section 3.1, describing the different steps and interfaces leading to the obtention of a ready-to-solve model. Subsequently, the pre-processing phase in ANSYS Workbench is examined in detail, including the preparation of the model (section 3.2) and the macros which have been developed taking into account the specific features of machine tools (section 3.3). Three options are available after the complete building of the model: the *ANS* option executes the normal simulation in ANSYS (chapter 5), the *RBS* option exports a data set needed for Rigid Body Simulations (chapter 6) and the *CRS* option exports a data set used to perform Coupled Reduced Simulations (chapter 7).

Chapter 4 focuses on the determination of modeling guidelines concerning finite element models of machine tools. After a section concentrating on experience-based meshing aspects (section 4.1), modeling issues of the coupling elements are addressed (section 4.2). On the basis of static and modal experiments, conducted on a test-bed explicitly de-

signed to investigate the properties of linear guideways in different configurations, general modeling rules are formulated to specify how the manufacturers' catalogue values are best integrated into a FE model (section 4.2.1). The same test-bed is also used to illustrate how damping coefficients of coupling elements can be identified, based on frequency response functions using simple experiments (section 4.2.2).

In chapter 5, the acquired modeling guidelines are applied on two different machine tools, which are used to experimentally validate the finite element models. In section 5.1, static experiments are carried out by measuring the force at the TCP resulting from predefined displacements of the feed axes and comparing the results with the equivalent finite element analyses. In section 5.2, resonance modes and frequencies are identified on the basis of experimental modal analyses (EMA) and matched with the corresponding results of the finite element modal analyses. A section introducing the *Strain Energy Ratio* R_ϵ completes the chapter (section 5.3). Resting on the output of different models, various studies outline the energy distribution between coupling elements and structural components for several loadcases and in several axis configurations. The interpretation of the potential impact of R_ϵ on the design process of machine tools is sketched.

In chapter 6, the files obtained with the export option *RBS* are imported into a stand-alone GUI (Graphical User Interface) developed for the specific purposes of investigating the behavior of machine tools based on a rigid body approach. Section 6.1 refers to the details of the export option *RBS* of the *Structure Gateway Interface*. After highlighting the export data process (section 6.1.1), the single output files generated with help of the developed ANSYS scripts are described in detail (section 6.1.2). Section 6.1.3 features additional modeling guidelines for the integration of coupling stiffness and damping coefficients in rigid body models of machine tools. Based on the *Strain Energy Ratio*, scaling factors for the stiffness values of coupling elements, essential for reliable rigid body analyses, are derived. The different modules of the stand-alone program are recapitulated in section 6.2 and next the various analysis capabilities are reviewed in section 6.3. Using the existing finite element models of the two machine tools introduced in chapter 5, the strengths and limits of the corresponding rigid body models are discussed by comparing results of static and modal analyses (section 6.4).

In chapter 7, on the basis of the output issued with the export option *CRS*, the implemented process necessary to perform advanced mechatronic analyses of the complete machine tool system in Matlab is described. Section 7.1 focuses on the details of the export option *CRS* of the *Structure Gateway Interface*. Similarly to section 6.1, the export data process is first summarized (section 7.1.1) and then the detailed content of the files generated with help of the developed ANSYS scripts is presented (section 7.1.2).

In section 7.2, the operating mode of the stand-alone reduction algorithm *MOR for ANSYS* is illustrated, leading to the construction of reduced state-space representations of the single bodies. The assembly principle of the different subsystems is briefly described in section 7.3 and the following section 7.4 addresses the way the coupling properties are integrated, connecting the various inputs and outputs of the bodies by means of a specifically designed *coupling matrix*. The benefits of the presented modular reduction process are demonstrated in the subsequent section 7.5. The chapter ends with the incorporation of the control systems to the machine tool structural model (section 7.6). The whole method is validated by means of experiments investigating cross-talk deviations at the TCP as function of axis acceleration and by matching the results with the outcome of the corresponding simulations of the reduced mechatronic model.

At last, in chapter 8, the results and benefits of the present thesis are summarized. The vision for future research work in the field of simulation and its integration in the design process of machine tools is finally proposed.

Chapter 2

State of the art

The present chapter, covering the current trends in machine tool dynamic analyses, provides the foundation motivating the research on innovative methods for dynamic evaluations of structures, seen as mechatronic entities. Over the last two decades, many advanced experimental and simulative tools, mostly originated from the aeronautical and automotive industry, have penetrated the machine tool sector and have proved their efficiency in accelerating the development phase of new machining concepts. As a result, the analytical dimensioning process based on the engineers' experience is now supported by powerful computational methods able to simulate a broad variety of models, ranging from simple mass-spring-damper systems to complex non-linear finite element models. These modern modeling and simulation methods used to evaluate the dynamic properties of machine tools are presented in the following sections. A broad overview of advanced methods based on virtual models of machine tools is given in [1] and [2]. Current and future promising techniques to master the workspace characteristics of complex parallel kinematic concepts, to obtain improved prototypes by applying advanced optimization methods, to integrate motion control algorithms in order to account for their reciprocal effects with the structure, to extend flexibility and reconfigurability of modern machine tools in innovative manufacturing concepts or to implement cutting models and consider stability issues resulting from the interaction between the machining process and the vibrational traits of the machine are reviewed.

The measurable machine behavior is a combination of the geometric [3, 4], the thermal [5, 6], the static and the dynamic behavior. The dynamic behavior directly influences the quality of the workpiece and is observable through several effects like following error, overshoot, regenerative chatter, cross-talk deviations, etc. In general, there are a few weak spots (bottlenecks) which govern dynamic errors in machine tools and their identification is an essential condition for a targeted improvement.

A comprehensive study of the dynamic behavior is supported by various methods:

- Determination of selected frequency responses (resp. eigenmodes) of the machine tool structure, determined by the mass distribution, the stiffness and damping properties in the guideways and bearings and by the structural compliances (for higher frequency ranges)

    - Experimental modal analysis, relating a set of strategic force to acceleration signals distributed over the whole structure
    - Simulation models based on rigid body and finite element models

- Test of the structure including the control loop (control gain, acceleration and jerk settings), feed-forward, filters, dead-time, measuring system, etc.

    - Simulation of drives including machine structural components
    - Experiments: evaluation of internal signals, cross-talk measurements, subsequent FFT (Fast Fourier Transform) and cross-talk interpretation

- Stability measurements (process parameters)

    - Online measurements on operating machine
    - Integration of process model into a virtual structure

2.1   Simulation and modeling of machine tools

The modeling and simulation tools applied during product development in most engineering fields are divided into two distinct approaches: The *Rigid Body Simulation* (RBS) originates in the simulation of non-mechanical models, in particular in applications of electrical and control engineering. The *Finite Element Method* (FEM) was developed for the investigation of mechanical systems and generated a multitude of applications in the field of structure analysis. Modern applications of both RBS and FEM methods to the simulation of complex mechatronic systems like machine tools are reviewed in the following sections. Advanced techniques consisting in reducing the dimension of finite element models and combining them with rigid body models are then discussed. Machine tool components assure the coupling function between ground, bed and axes of the machine. Their characteristics are of great importance for the static and dynamic behavior of machine structures. The way the stiffness and damping properties of such components are derived and integrated in machine tool models are finally examined.

2.1.1 Rigid Body Simulation (RBS)

As summarized by Zirn [7], the most basic models of machine tools consist of servo axes as main structural subsystems (figure 2.1). The elaborate electro-mechanical system of the drive mechanism is coupled to the flexible transmission devices, which through the position measurement systems are part of the semi-closed or closed position feedback control loop. The flexible structural parts between servo axes and both tool and workpiece are on the other hand outside the control loop, because the positions of the tool and workpiece are normally not measured. Vesely [8], Zaeh [9] and Oertli [10] also focused on specific model approaches for ballscrew drives in prevision of a more realistic integration into machine tool models. Due to the increasing lightweight characteristics of machine tool parts and the resulting high accelerations, designers are forced to consider their interplay with the compliances of the feed drives.
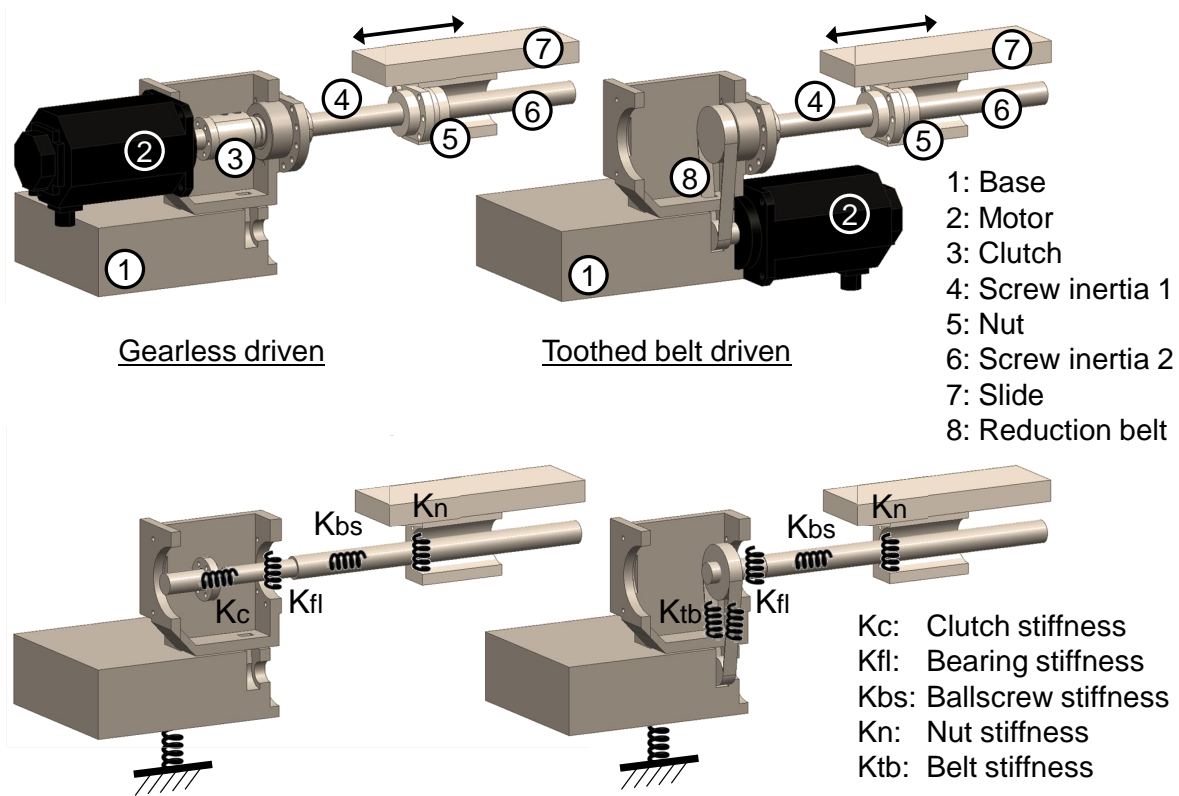

Figure 2.1: *Gearless driven* and *toothed belt driven* feed drive units as main subsystems of a machine tool model.

The *Siemens Mechatronic* software package [11] offers such simulation capabilities in terms of integration of control systems and structures (figure 2.2). The axis arrangement of a machine tool, consisting of connected rigid masses, is enhanced by the respective one-

dimensional drive trains. These are composed of serially connected springs and dampers corresponding to the couplings within the motion system, from the motor to the ballscrew nut. The model is extended by the sensor systems, allowing to incorporate and test various feedback control algorithms.
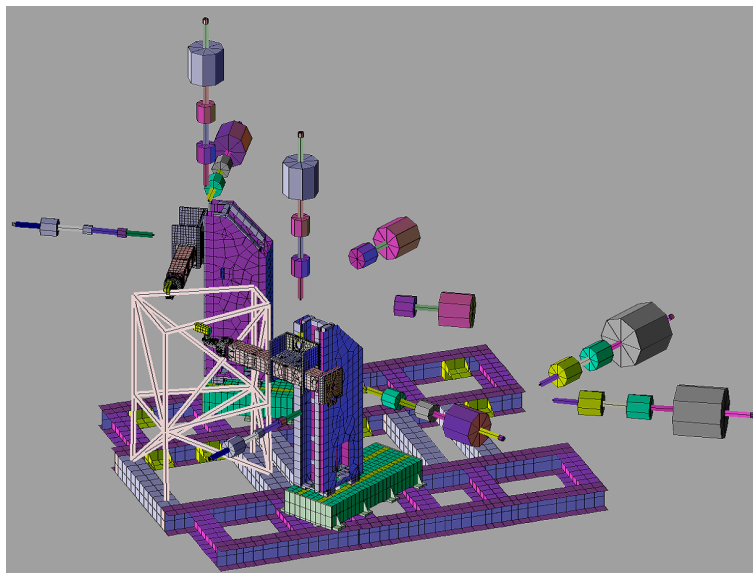

Figure 2.2: Mechatronic model of a Schuler machine with the SIEMENS software package.

Especially in complex five-axis machine tools, the cross-coupling between the different axes is relevant for the overall behavior of the structure and cannot be neglected. To overcome this disadvantage present in the modeling types described above, a higher complexity level is required. Often the axes of a machine tool featuring one (linear or rotational) relative degree of freedom are modeled as rigid bodies, described by their mass and inertia properties. These rigid bodies are connected by punctual elastic elements (figure 2.3), which stand for simplified representations of connecting or guiding components (linear guideways, rotational bearings, ballscrew systems, machine bed mounting elements, etc.) [12]. The study of such a model, where all the compliances are concentrated at the connecting points, is referred to as Rigid Body Simulation (RBS).

MSC Adams (figure 2.4) is probably the most widely used program based on the rigid body approach. The user can either build a mechanism using pre-defined standard components (cuboids, cylinders, etc.) or directly import a geometry from a universal transfer format file (Parasolid, STEP, IGES) previously exported from a CAD (Computer Aided Design) model. The bodies of the mechanism are then connected by various coupling elements to choose among a multitude of standard connections (standard joints, spring-damper elements, etc.).
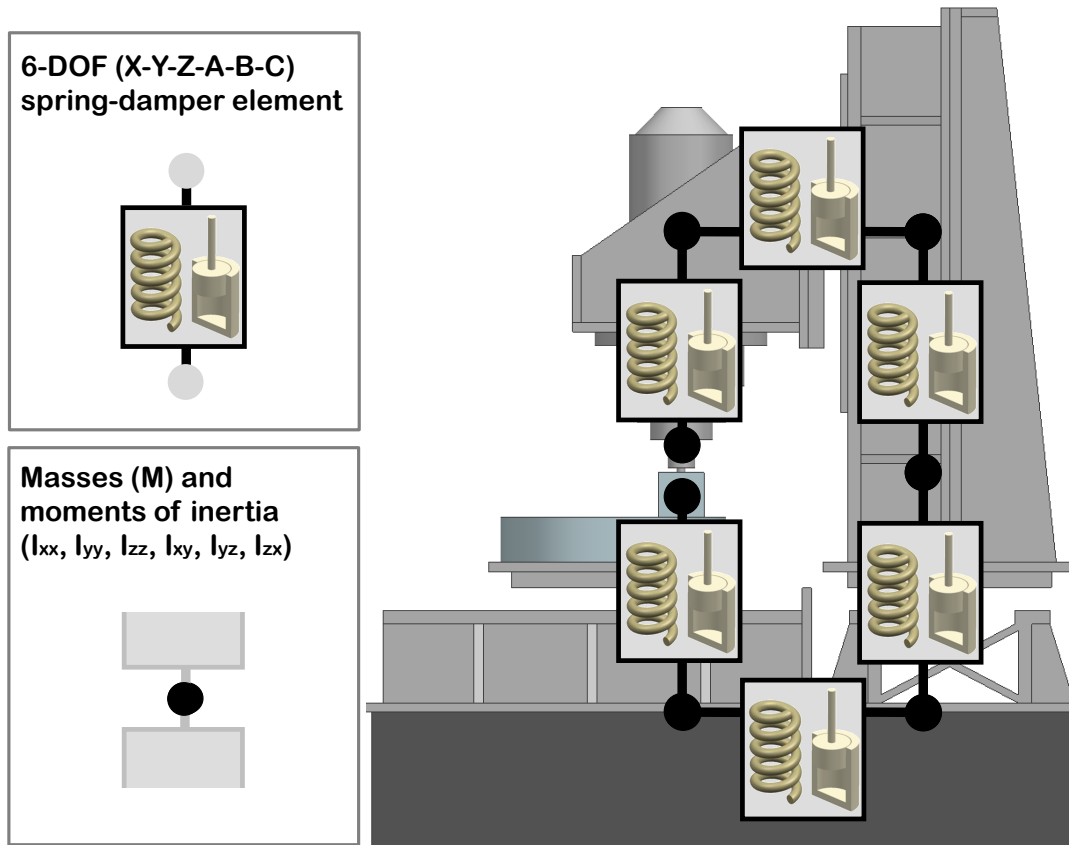
Figure 2.3: Schematic *Rigid Body Model* of a machine tool.

The efficacy of rigid body simulations in terms of computing time has brought many other software providers to integrate a rigid body module into their standard package. A comparison of different packages for rigid body calculations has been presented in [13]: *MSC.Adams*, *Recurdyn*, *LMS Virtual.Lab*, *SIMPACK* and *ITI SimulationX* are the most popular among them. *Matlab/Simulink* is an environment for multidomain simulation and model-based design for dynamic and embedded systems. Also classified as *Digital Block Simulation* (DBS) tool, it provides an interactive graphical environment and a customizable set of block libraries to design, simulate, implement and test a variety of time-varying systems, including controls. These features made the software very popular within machine tool designers for the tuning of axis control systems [14, 15]. The *SimMechanics* toolbox uses a block-diagram schematic approach for modeling control systems around mechanical devices. The block library has been extended with mechanical elements allowing to easily incorporate rigid bodies and joints into a Simulink model [16]. In figure 2.5, a machine tool model composed of four bodies is shown on the lefthand side (body numbers also referenced in figure 2.6). The box on the righthand side illustrates the replacement of constraints by joints, necessary for dynamical investigations.

1. Revolute joint
2. Hook joint
3. Fixed joint
4. Translational joint
5. Constant velocity
6. Point-curve constraint
7. Cylindrical joint
8. Coupler joint
9. Curve-curve constraint
10. Spherical joint
11. Screw joint
12. General constraint
13. Planar joint
14. Gear

15. Translation spring-damper
16. Force
17. Contact
18. Torsion spring-damper
19. Torque
20. Tire
21. Bushing
22. Force vector
23. Modal force
24. Field
25. Torque vector
26. Gravity
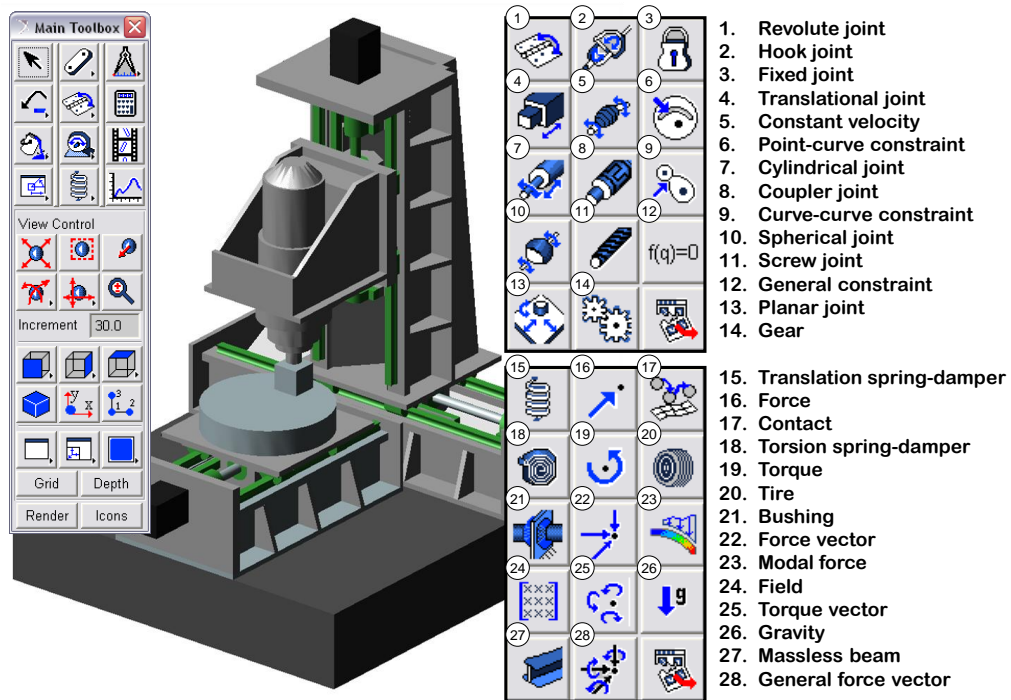27. Massless beam
28. General force vector

Figure 2.4: Machine tool modeled in MSC Adams and selection of joint elements and boundary conditions.
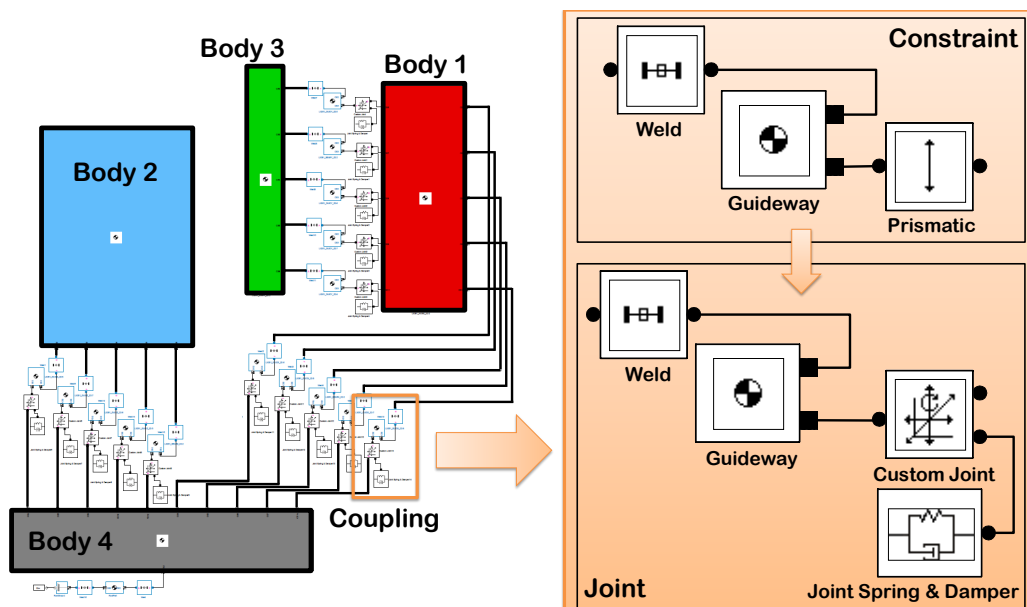

Figure 2.5: Model of a machine tool in SimMechanics with customized joints.

The *SimMechanics Link* utility bridges the gap between geometric modeling and block diagram modeling and simulation, by combining the SimMechanics software with CAD programs. The different bodies of a CAD assembly are translated into STL (Standard Tessellation Language) files describing the geometrical properties. The kinematic characteristics are stored into a physical modeling file XML (Extensible Markup Language) containing all the necessary information on mass and inertia of the single parts and their mutual constraints. This set of files can then automatically be imported and visualized into SimMechanics (figure 2.6). The *parts* of a CAD model become *bodies* and the *constraints* of a CAD model become *joints*.
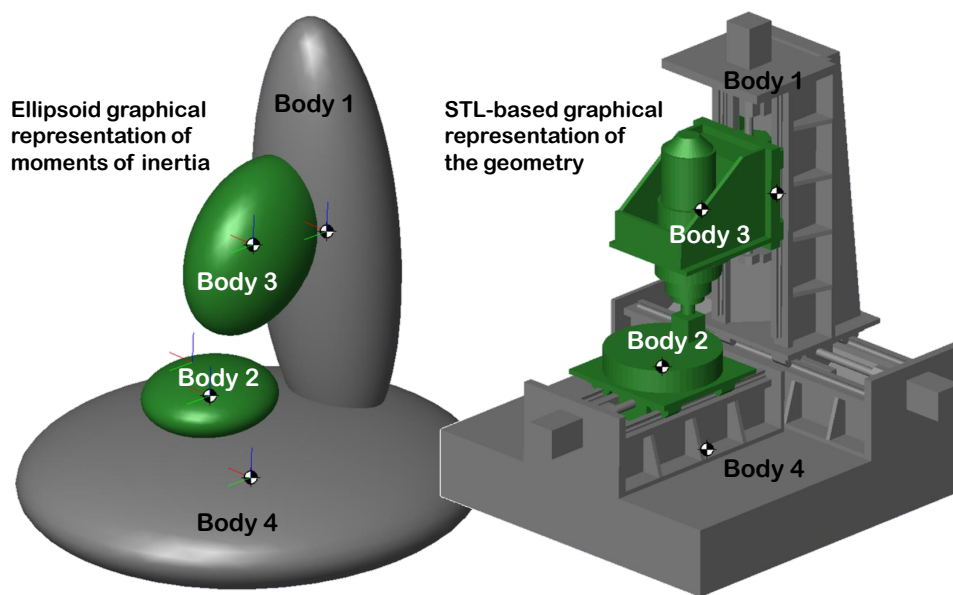
Figure 2.6: View of a machine tool model in SimMechanics
left: inertial-based ellipsoids - right: STL-imported geometry.

FE software providers also developed rigid body based toolboxes. *ANSYS Rigid Dynamics* is e.g. an add-on allowing to analyse a fully rigid system whose components are interconnected through customizable joints (figure 2.7).

The majority of these tools, thanks to their high customizability, are applicable to any type of structures, from airplane fuselages to micro-electronics devices, giving the user nearly unlimited freedom. However, a machine tool manufacturer needs to model machine tools and machine tools only. In contrast to other engineering fields, whose custom-made simulation solutions are driven by more substantial budgets, no specialized software packages for the specific needs of machine tool designers are commercially available and benefit from a widespread diffusion and acceptance.

Figure 2.7: ANSYS joint capabilities with the Rigid Dynamics Module.

Axis Construction Kit (ACK) is a tool programmed in Matlab which has been developed at the Institute of Machine Tools and Manufacturing (IWF) of the ETH Zurich [17] (figure 2.8). With the help of a Graphi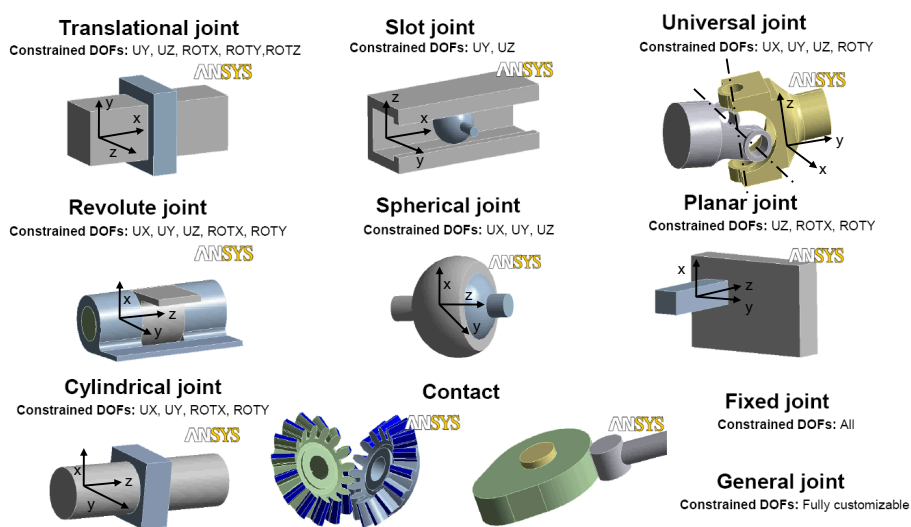cal User Interface (GUI) [18], it is possible to define a machine tool structure starting from basic body shapes. Defined by their masses and inertias, the rigid bodies are interconnected by spring-damper elements. This rigid body simulation environment is especially useful for early conception phases, while the detailed kinematic configuration is still open. The characteristics of the resulting model don't differ from models created with *MSC Adams* or *SimMechanics*. The differentiation of ACK comes rather from two main concerns which prevailed during the past and ongoing research activities at IWF: first the ability to quickly set up and modify a machine tool model in order to investigate as many axis arrangements and positions as possible, and secondly the straightforward evaluation strategy, in order to get clear information on machine tool specific qualities (static and dynamic stiffness, cross-talk deviations, natural frequencies, etc.) without laborious manual post-processing work.

The disadvantages of such programs originated in research projects is the lack of applicability and accessibility on the industrial level, due to software integration and user-friendliness issues. On the technical level, the limits of the method lie in the validity of the rigid body assumption, which cannot be systematically applied to modern lightweight structures.
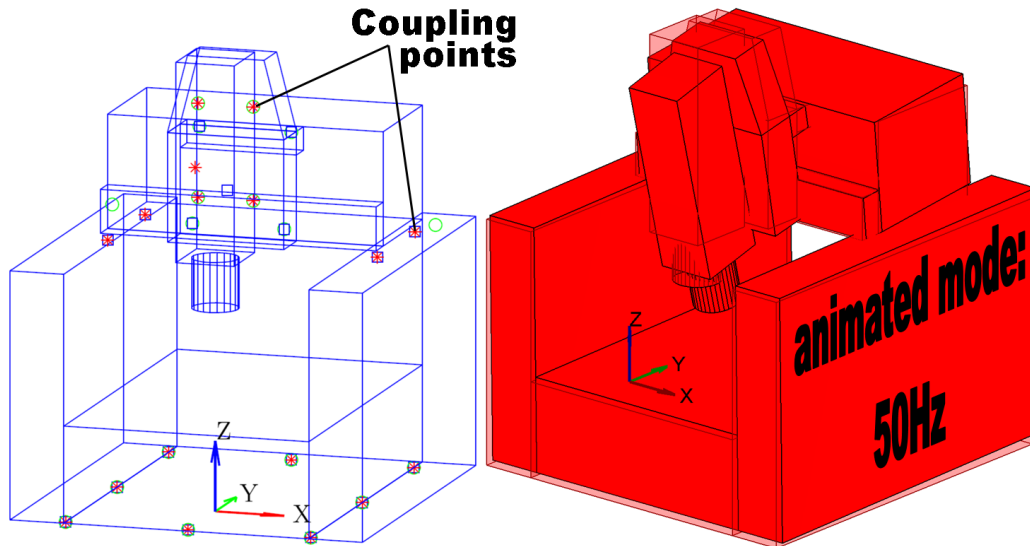
Figure 2.8: Example of a machine tool modeled with ACK [17].

2.1.2   Finite Element Method (FEM)

The importance of the *Finite Element Method* (FEM) for virtual analyses of machine tools has constantly increased over the last two decades and, having taken advantage of the sudden advances in the interfacing capabilities with most CAD packages, is today the most common simulation approach among machine tool manufactures and research institutes. It started with deformation and stress calculations in single machine components subject to static or cyclic loading and has evolved to an indispensable tool for the evaluation of dynamic properties of complete machine tools. Assuming the use of correct elements and a mesh which is fine enough, a FE model provides complete and accurate results for a broad range of analyses (figure 2.9): static (linear and non-linear), dynamic (modal, harmonic and transient), thermal (steady-state and transient). All key issues on the behavior of a machine tool a designer has to deal with are standard modules in most commercial FEM software. *ANSYS*, *MSC.Nastran*, *ABAQUS* and *COMSOL* are among the most diffused commercial packages.

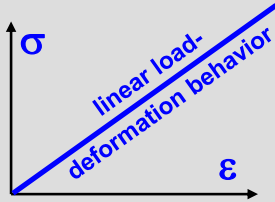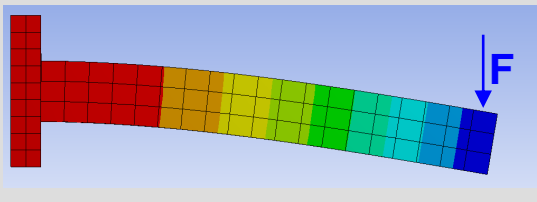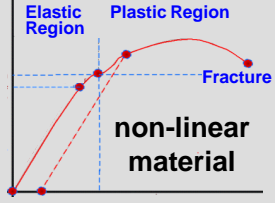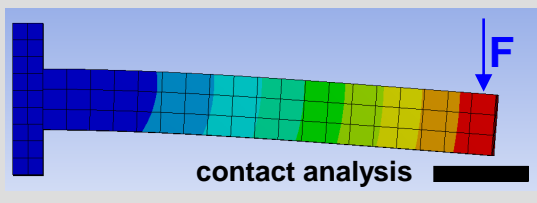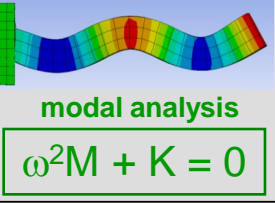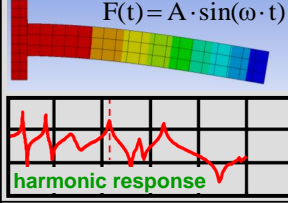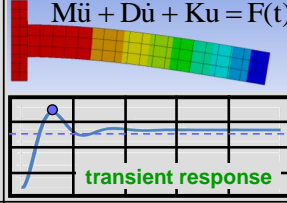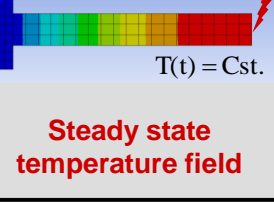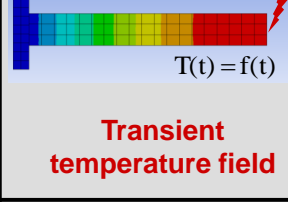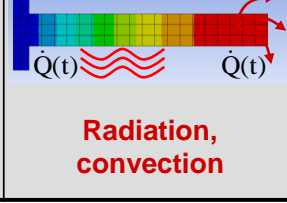| F :	force	A :	constant	M :	mass matrix	u :	displacements
F(t) :	force	Cst :	constant	D :	damping matrix	T :	temperature
t :	time	ω :	angular frequency	K :	stiffness matrix	Q :	heat

Linear static analysis	σ — linear load-deformation behavior — ε		**F**
Non-linear static analysis	**Elastic Region** **Plastic Region** **Fracture** **non-linear material**		**F** contact analysis
Dynamic analysis	**modal analysis** $\omega^2 M + K = 0$	$F(t) = A \cdot \sin(\omega \cdot t)$ **harmonic response**	$M\ddot{u} + D\dot{u} + Ku = F(t)$ **transient response**
Thermal analysis	$T(t) = Cst.$ **Steady state temperature field**	$T(t) = f(t)$ **Transient temperature field**	$\dot{Q}(t) \qquad \dot{Q}(t)$ **Radiation, convection**

Figure 2.9: Analysis capabilities of a commercial FE software package

A finite element analysis involves the following steps:

- Meshing: the spatial domain is discretized into a collection of simple elements, which can be one-, two- or three-dimensional, depending on the formulation of the problem. Based on their coordinates, the elements and their corresponding nodes are then numbered.

- Element equations: the element equations are derived for every single element using the physics of the problem and typically using the Galerkin's method or the variational principle [19].

- Assembly: in the next step, the element equations for the whole mesh are assembled into a set of global equations that model the properties of the entire system.

- Boundary conditions: degrees of freedom whose values are known a priori are constrained using boundary conditions, which modify the global equations.

- Solving: the primary unknowns of the equation system are solved at every node. For structural problems, the primary unknowns are node displacements U_x, U_y and U_z.

- Post-processing: derived variables (e.g. stresses) are calculated using the nodal values of the primary variables and the results are represented in tabular or graphical form.

For a linear structural problem [20], the assembly of the element equations results in an second order *Ordinary Differential Equation* (ODE) of the form:

$$M \cdot \ddot{x}(t) + D \cdot \dot{x}(t) + K \cdot x(t) = F(t) \tag{2.1}$$

where M is the mass matrix, D is the damping matrix, K is the stiffness matrix, F is the external load vector and x is the vector of unknowns, which in structural analyses are the nodal displacements.

The general solution of the inhomogeneous equation (2.1) is a superposition of the solution of the homogeneous equation and of an excitation-specific particular solution. Due to the damping effect, which is always present in reality, the long-term behavior of the oscillating system is significantly determined by the particular solution and is often of great interest for the study of the dynamic behavior of structures. In practice, the particular solution is found after decoupling the equations system by transformation into the modal space. The resulting system has the form of equation (2.2):

$$\tilde{M} \cdot \ddot{q}(t) + \tilde{D} \cdot \dot{q}(t) + \tilde{K} \cdot q(t) = \tilde{F}(t) \tag{2.2}$$

where $\tilde{M} = \Phi^T M \Phi = I$, $\tilde{D} = \Phi^T D \Phi$, $\tilde{K} = \Phi^T K \Phi = \Omega$, $\tilde{F} = \Phi^T F$, Φ is the eigenvectors matrix and $\Omega = diag[\omega_i^2]$ is a diagonal matrix containing the eigenvalues of the undamped system. In case of proportional damping, the resulting system is exclusively composed of diagonal matrices and its solving becomes straightforward.

In structural problems, the transfer behavior between the inputs (forces) and outputs (displacements) of a *Linear Time Invariant* (LTI) system in the frequency domain is of great interest, because many important characteristics of the dynamics can be determined from the transfer function (2.5), which is the ratio of the output Laplace Transform to the input Laplace Transform, assuming zero initial conditions.

Taking the Laplace Transform of the governing equation (2.1) results in (2.3):

$$M \cdot s^2 X(s) + D \cdot sX(s) + K \cdot X(s) = F(s) = U(s) \qquad (2.3)$$

Collecting all the terms involving $X(s)$ and factoring leads to (2.4):

$$[M \cdot s^2 + D \cdot s + K] \cdot X(s) = F(s) = U(s) \qquad (2.4)$$

Integrating the output equation $Y(s) = C \cdot X(s)$, the transfer function of the second order system is (2.5):

$$G(s) = \frac{Y(s)}{U(s)} = \frac{C}{M \cdot s^2 + D \cdot s + K} \qquad (2.5)$$

Even though the development of machine tools and structures in general has greatly benefitted from the expansion of the FE method, a drawback remains: while the computation of static loadcases on single parts takes ordinarily a few minutes, the solving of a modal analysis of an entire machine tool can take up to several hours. As for more complex and time-consuming dynamical analyses in the frequency and time domains, where numerous subsequent simulation steps are required, a systematic use of FE models during the conception phase becomes impracticable.

2.1.3   Model Order Reduction (MOR)

Conventionally, in one sequence of a structural analysis of a machine tool, the nodal displacements are computed for a mesh which, due to increasingly complex systems, easily exceeds 100.000 degrees of freedom (DOF). Furthermore this computation step is part of a design process which should take into account several machine configurations, the integration of the control algorithm and possibly a few optimization procedures at different levels. Although modern computers are able to handle engineering problems of this size, designers in an industrial context have to cope daily with limited hardware and time resources. Hence the consideration of full mechatronic models of this size becomes prohibitive, making of order reduction a decisive milestone for future efficient machine tool modeling and simulation.

Model Order Reduction (MOR) consists in reducing the size of a structure model by selecting the relevant degrees of freedom (figures 2.10 and 2.11). It is actually no new research field and various techniques have been developed through the last decades, which can be divided into various classes: as related in [21] there are three categories depending
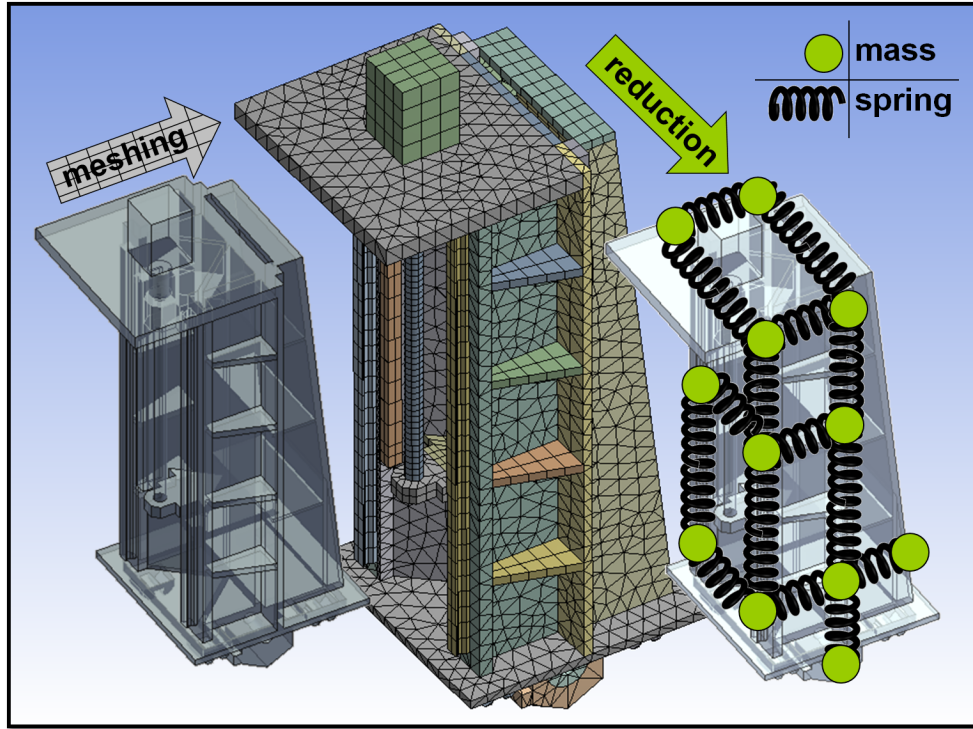
Figure 2.10: Schematic model order reduction of a machine tool part.

$$\boxed{M\ddot{x}(t)+D\dot{x}(t)+Kx(t)=Bu(t)} \boxed{y(t)=C^{T}x(t)}$$

$$\boxed{M_{r}\ddot{z}(t)+D_{r}\dot{z}(t)+K_{r}z(t)=B_{r}u(t)} \boxed{y(t)=C_{r}^{T}z(t)}$$

$$M \quad + \quad D \quad + \quad K \quad = \quad B$$

$$= \quad C^{T}$$

$$M_{r} \quad + \quad D_{r} \quad + \quad K_{r} \quad = \quad B_{r}$$

$$= \quad C_{r}^{T}$$

$x(t) \in \Re^{n}$	$M,D,K \in \Re^{n \times n}$
$u(t) \in \Re^{m}$	$B \in \Re^{n \times m}$
$y(t) \in \Re^{p}$	$C \in \Re^{n \times p}$

$M_{r} = V^{T}MV \in \Re^{k \times k}$	$B_{r} = V^{T}B$	$\in \Re^{k \times m}$
$D_{r} = V^{T}DV \in \Re^{k \times k}$	$C_{r} = V^{T}C$	$\in \Re^{k \times p}$
$K_{r} = V^{T}KV \in \Re^{k \times k}$		
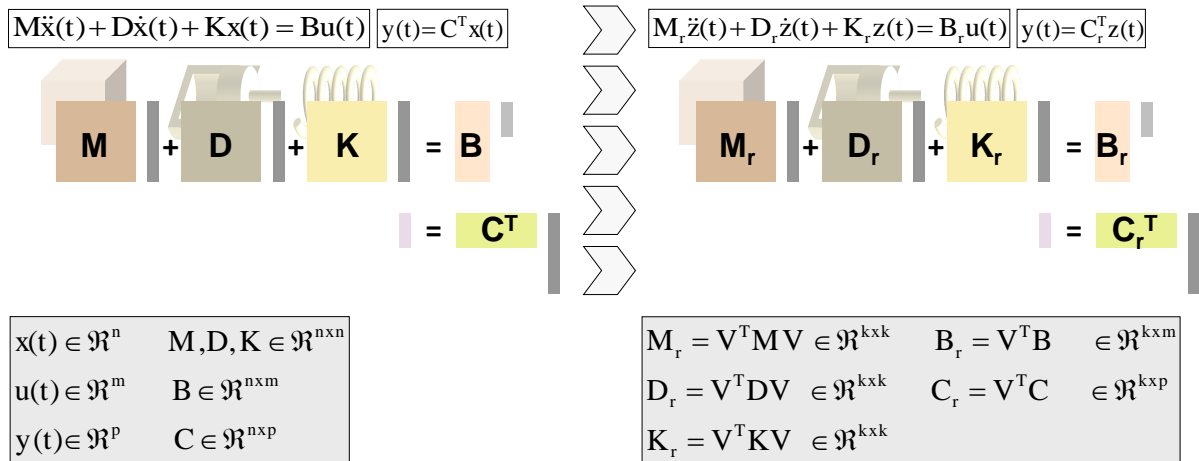
Figure 2.11: Principle of matrix transformation in model reduction.

on the fundamental nature of the method. Benner [22] and Bonin [23] distinguish between *modal truncation*, *modern balancing* and *moment-matching* methods. Bechtold [24] and Antoulas [25] group the reduction methods into *Guyan-based*, *control theory* (SVD) and *Padé approximants* (Krylov). Over the past years many of these techniques have been used in practical applications: in the late 60's already, Craig and Bampton [26] introduced the

concept of substructuring to reduce the simulation time of large airplane structures. Based on eigenvalue computations or modal truncation, their method constitutes the fundament of what is today known as *Component Mode Synthesis* (CMS) and has been implemented in most CAE (Computed Aided Engineering) tools like ANSYS (figure 2.12) [27, 28, 29, 30, 31, 32]. Hatch [33] gave many examples on how to reduce simple structures in Matlab using static and dynamic condensation. Berkemer [34] and Fleischer [35] make use of modal reduction techniques (see equation (2.2)) to incorporate reduced finite element bodies into their machine tool models. After transformation of the system into the modal coordinate system, the matrices are projected onto the resulting space and the states associated with the higher frequency modes are eliminated or truncated.
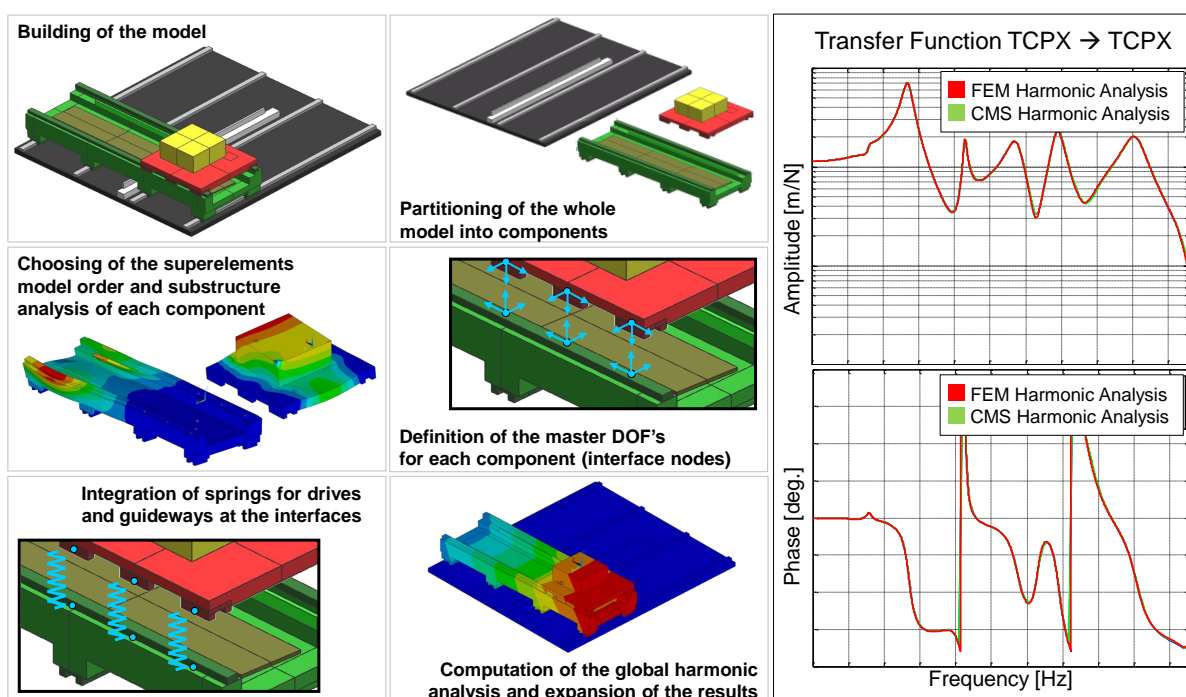
Figure 2.12: Application example of the CMS method in ANSYS [36].

Applications of modern balanced truncation techniques for the analysis of different structures, from gyroscopes to machine tools, are found in [37] and [38]. The principle is similar to the modal truncation, except that the projection, based on the calculation of the singular values, is energetically optimal. Through solving of the *Lyapunov equations*, only the least controllable and observable states, whose contribution to the energy transfer is minimal, are truncated. These characteristics earned these techniques, which comprise the *Balanced Truncation Approximation* (BTA), the *Singular Perturbation Approximation* (SPA) and the *Hankel Norm Approximation* (HNA), the classification as control theory methods [24].

Interpolatory model reduction also belongs to the modern reduction techniques, which have an inherent mathematical approach compared to the traditional methods from the engineering world. They allow structural features in the original model to persist in the reduced model and, insofar as it is possible, leave the overall input/output response characteristics unchanged [39]. The desired result is a compact model that can reliably and inexpensively replace the original exact model. They include rational *Krylov-based* interpolation methods as a special case. Instead of using modal or control-based subspaces [40], the matrices are projected onto the so-called Krylov subspace, which is computed using the *Lanczos* or *Arnoldi* algorithms, or some modified versions of these. The broader framework allows retention of special structure in the reduced models, such as symmetry, second- and higher order structure, state constraints, internal delays and infinite dimensional subsystems [41, 42, 43]. Fassbender [44] recently tested different Krylov subspace methods for first and second order systems and compared their relative performance on the example of a simple machine tool structure.

Benner [22] outlined that modern reduction methods, based either on balanced realization or moment-matching, are largely preferred over classical methods, based on eigenvalues computation: their advantages in terms of computational cost and automation level are decisive criteria in current applications. Bechtold [24], in her survey of existing reduction techniques, evidenced why, due to their computational efficiency, the Krylov methods (based on moment-matching, as in equation (2.9)) are even more adapted to large scale systems than control theory methods (based on realization techniques). Current research in this field also led to the development of error indicators [45, 46], giving an a priori estimation of the deviation between the reduced and the original models. A further extension of the method consists in implementing parameter preserving order reduction [47], allowing to modify the system behavior by varying key parameters directly in the reduced model.

In table 2.1, the different categories of methods discussed above are recapitulated: classical methods include Guyan-based and modal truncation methods, whereas under modern reduction methods are comprised modern balancing and interpolatory methods.

MOR for ANSYS (figure 2.13) is the result of years of research effort at IMTEK [48, 49, 50, 51, 52] and is today a commercially available stand-alone program for order reduction of ANSYS models. The algorithm behind the software belongs to the Krylov subspace (or moment-matching) methods, whose fundamental idea is to find a low-order subspace to project the system matrices onto. The building of the Krylov subspace is carried out using the Arnoldi process, which leads to a reduced system whose transfer function $G_r(s)$ has the same moments as the original transfer function $G(s)$ up to a chosen degree.

Table 2.1: Table recapitulating the existing model order reduction methods.

| Guyan-based and modal truncation methods	Modern balancing (realization) methods	Padé approximant (interpolatory) methods
• Static condensation • Dynamic condensation • Modal superposition • Component Mode Synthesis (CMS)	• Balanced Truncation Approximation (BTA) • Singular Perturbation Approximation (SPA) • Hankel Norm Approximation (HNA)	• Krylov Subspace methods (moment-matching)

Increasing computational efficiency
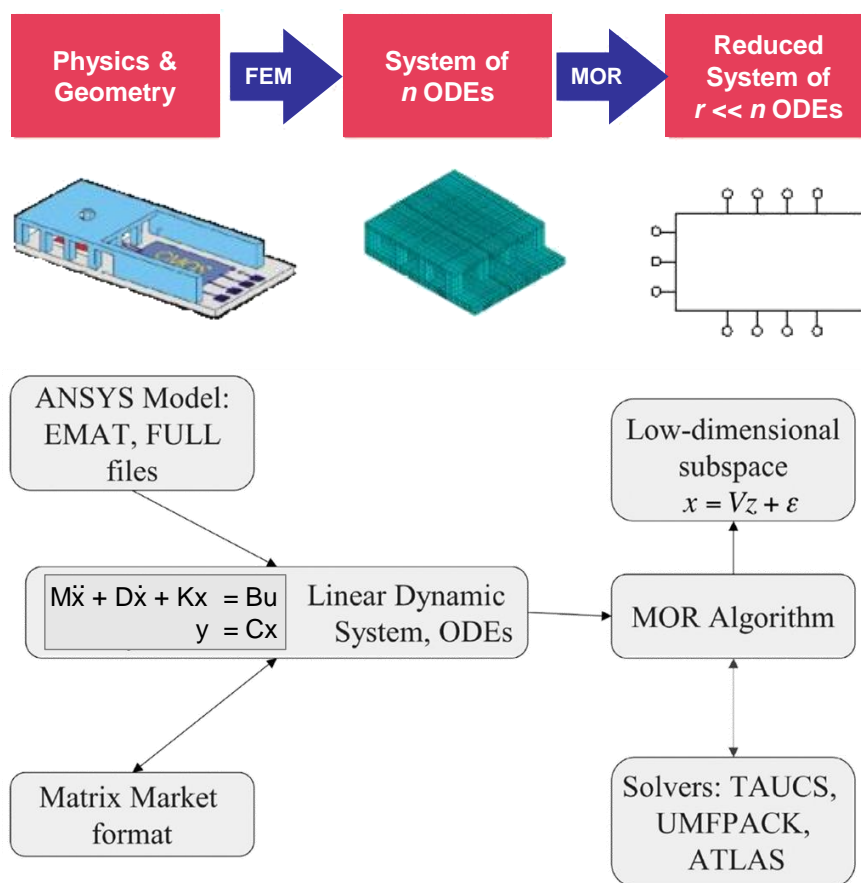
Figure 2.13: MOR for ANSYS algorithm [49].

In the first order state-space system in the form of (2.6), $x(t)$ is the state vector, $u(t)$ the input vector, $y(t)$ the output vector, A the state matrix, B the input matrix and C the output matrix.

$$
\begin{aligned}
A\dot{x}(t) &= x(t) + Bu(t) \\
y(t) &= C^T x(t)
\end{aligned}
\tag{2.6}
$$

Through the *Laplace Transform* it is translated into the frequency domain (2.7):

$$
\begin{aligned}
sAX(s) &= X(s) + BU(s) \\
Y(s) &= C^T X(s)
\end{aligned}
\tag{2.7}
$$

The resulting transfer function is formulated as follows (2.8):

$$
G(s) = \frac{Y(s)}{U(s)} = -C^T(I - sA)^{-1}B
\tag{2.8}
$$

The *Taylor Series Expansion* of $G(s)$ about $s_0 = 0$ is given in (2.9):

$$
G(s) = -C^T(I + sA + s^2A^2 + \dots)B = \sum_{i=0}^{\infty} m_i s^i
\tag{2.9}
$$

where $m_i = -C^T A^i B$ are called the moments about s_0.

The Krylov-based methods consist in finding a function (2.10):

$$
G_r(s) = \frac{P_{r-1}(s)}{Q_r(s)} = \frac{a_{r-1}s^{r-1} + \dots + a_1 s + a_0}{b_r s^r + b_{r-1}s^{r-1} + \dots + b_1 s + 1}
\tag{2.10}
$$

as a Padé approximant of $G(s)$ and whose Series Expansion about s_0 matches the first $2r$ moments of the Series Expansion of $G(s)$, as expressed in (2.11):

$$
\begin{aligned}
G(s) &= G_r(s) + O(s^{2r}) \\
\lim_{s \to s_0} O(s^{2r}) &= 0
\end{aligned}
\tag{2.11}
$$

A numerically stable way of computing the moments requires the determination of the Krylov subspaces, whose vectors v_i and w_i in (2.12) represent the corresponding stable basis vectors:

$$
\begin{aligned}
r - th \text{ right Krylov subspace: } K_r^R\{A, B\} &= span(v_1, v_2, \dots, v_r) \\
r - th \text{ left Krylov subspace: } K_r^L\{A^T, C\} &= span(w_1, w_2, \dots, w_r)
\end{aligned}
\tag{2.12}
$$

There exists two main approaches to create the basis matrices V_r and W_r for the Krylov subspaces: the Lanczos algorithm and the Arnoldi process. The Lanzos algorithm delivers a more accurate approximation, is numerically more efficient and guarantees preservation of the system invariance. The Arnoldi process is yet preferred in most cases, because it guarantees numerical stability, the stability and passivity properties of the original system are preserved and it enables a complete output approximation (figure 2.14).
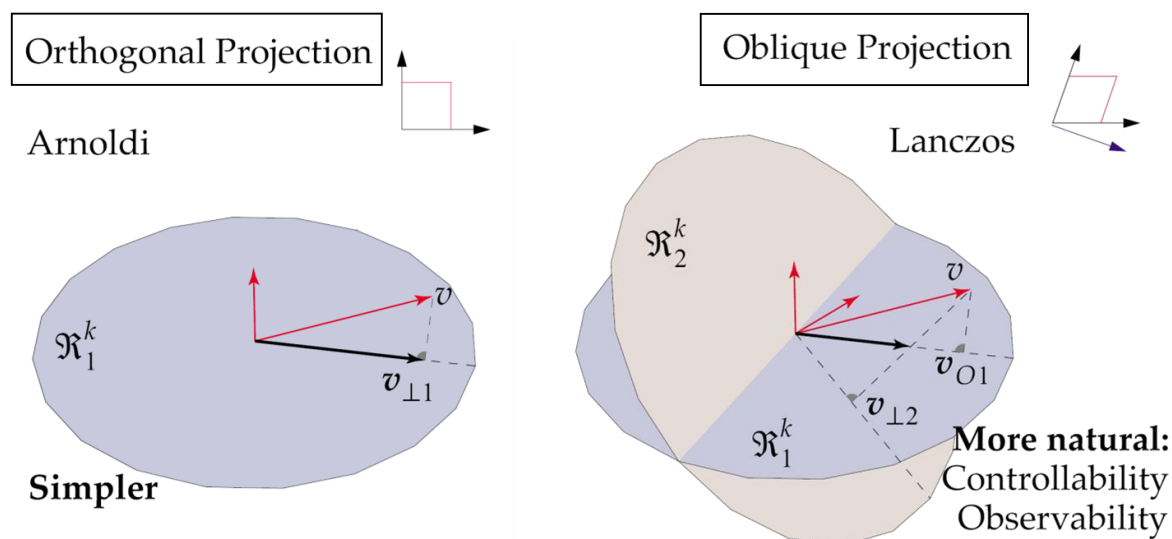
Figure 2.14: MOR for ANSYS algorithm [49].

The mentioned advantages in terms of computational efficiency, the commercial availability, the stand-alone nature, the wide applicability of the method and the fact that the algorithm is based on the system matrices of a commercial software like ANSYS led to many applications of MOR for ANSYS, particularly in the field of MEMS (Micro-Electro-Mechanical Systems). However, due to the specific features of machine tools, the handling of the model size, the structure complexity and particularly the numerous degrees of freedom at the axis interfaces (couplings) have so far prevented the diffusion of MOR for ANSYS (like any other reduction method to that matter) as a systematic design tool.

2.1.4   Combination of RBS and FEM

RBS and FEM are the two absolute leading approaches when it comes to the study of the static and dynamic behavior of machine tools. Their advantages and disadvantages are summarized in table 2.2.

Table 2.2: Rigid Body Simulation vs. Finite Element Method analyses.

Rigid Body Simulation	Finite Element Method
+ good interfacing capabilities	+ good interfacing capabilities
+ simple model building	− not automated and complex pre-processing and meshing
+ small models / fast calculations	− large models / long computation times
− approximated body properties	+ exact body properties
− less accurate results (quantitative considerations possibly hazardous, e.g. by structural deformations)	+ more accurate results (quantitative considerations mostly reliable, even by structural deformations)
+ large axis motions possible	− implementations of axis motions only through self-programmed algorithms
+ efficient integration of control	− control integration makes computation times even longer
− not straightforward and unadapted post-processing	+ graphical and user-friendly post-processing
− **not adapted to the specific needs of machine tools**	− **not adapted to the specific needs of machine tools**

Modern machine tool designs are characterized by transmission components getting always stiffer and by structures getting always more lightweight [32]. The complete distributed compliance of the structure needs to be considered while evaluating the combined performance of structure and control system. To predict the machining results exactly, large motions of flexible axes have to be calculated, initiating the challenge of integrating large machine movements under consideration of small deformations in the structural components, the ratio of these two orders of magnitude being very high in machine tool dynamics.

In the last years, many efforts have been made to bring together the benefits of both rigid body and finite element simulations by combining heterogeneous models into one

mixed model. Hence Siedl and Zaeh recently showed how dynamic positioning motions of machine axes could be achieved by differentiating the components of the structure into rigid, modal and nodal bodies. The relative nodal method has been used, which is able to handle flexible bodies with all degrees of freedom [13, 53]. Weule [54] and Kipfmueller [55] presented how such a mixed description can be exploited to simulate and optimize the structure of a hybrid kinematic machine tool. Zirn [56] and Montavon [57] introduced the notion of *coupling matrix* to link the inputs and outputs of rigid, respectively of flexible bodies, belonging to a same machine tool model.

These contributions may vary in their approach, in the applied software tools, in the implementation technique, but all have one common denominator: the objective to obtain a model simple enough to have reduced computation times but complex enough to include all the needed dynamic properties of the structure. In the last five years, this vision led the way to the novel modeling techniques known as coupled simulation. In the field of machine tools, coupled simulation stands for all the methods consisting in combining structure and control into one realistic mechatronic model able to reliably capture the global dynamic behavior of a machine tool and serving as solid basis during the development of a new virtual design. This is possible either by integrating the feed drive control into the structural model (integrated simulation) or by implementing an interface between two different models, one containing the structure and one the control algorithm (co-simulation) [58].

Table 2.3 proposes a classification of the existing ways of combining different simulation environments, taking as examples one *RBS* tool (MSC Adams), one *FEM* tool (ANSYS Workbench) and one *DBS* tool (Matlab/Simulink), and a non exhaustive list of references to application examples is given in table 2.4.

2.1.5   Modeling of components

The importance of modeling the properties of the connections between the moving axes of a machine tool has been pointed out as simulation techniques for entire structures spread out. As the part of the displacement occurring in the joints can vary from 30 to 90% of the overall displacement [74] depending on the application, wrong modeling assumptions can lead to substantial errors. In standard machine tools, connections can be classified into four groups: linear guiding systems for the motion of linear axes, rotation bearings for the motion of rotary axes and spindles, ballscrew systems for the transmission of the drive force, and mounting elements for the connections of the machine bed to the ground foundation. Due to their wide application, the modeling efforts in this work focus principally on linear guideways and rotation bearings with rolling elements, on standard

Table 2.3: Different combinations for mechatronic analyses of machine tools.

Platform / Model	RBS	FEM	DBS
RBS		ANSYS + rigid-body module	MATLAB + Simulink & SimMechanics
FEM	ADAMS + flexible-body module		MATLAB + model order reduction
DBS	ADAMS + coupled control	ANSYS + coupled control	

RBS: Rigid Body Simulation	FEM: Finite Element Method	DBS: Digital Block Simulation
	mixed structural model: FEM & RBS	
	mechatronic model (structure & integrated control)	
	mechatronic model (control & equivalent structure)	

Table 2.4: Reference list associated to table 2.3

Platform	Model		References
FEM	RBS	:	[59, 60, 61]
DBS	RBS	:	[62, 63, 16, 64]
RBS	FEM	:	[65, 66, 54, 67]
DBS	FEM	:	[31, 38, 56, 8]
RBS	DBS	:	[68, 69, 70, 71]
FEM	DBS	:	[58, 72, 73]

ballscrew drive systems and on standard frame mounting devices (figure 2.15). For details about alternative systems, an overall review on joints and drives technologies is proposed in [2]. Two key factors need to be considered in this regard: the stiffness and the damping coefficients.
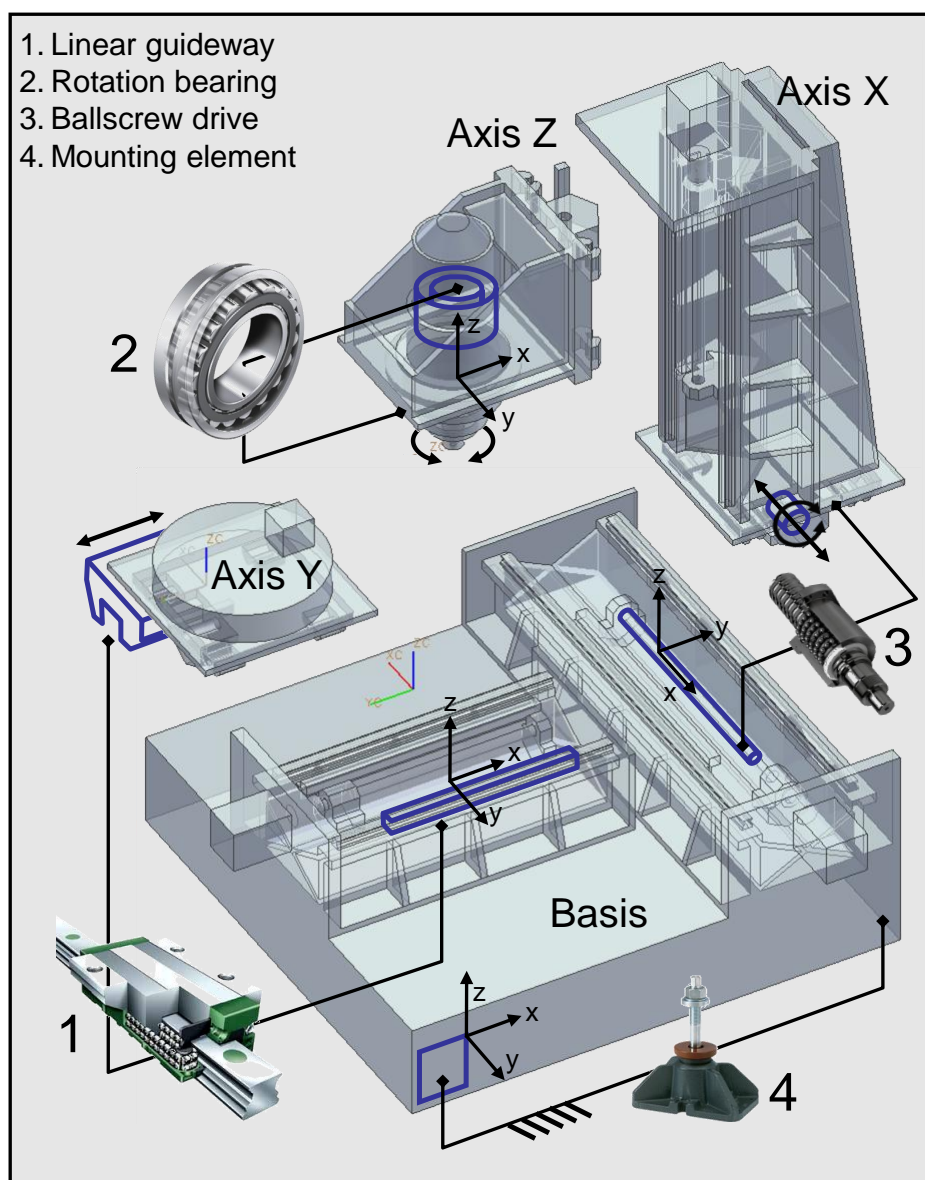
Figure 2.15: Standard machine tool components with corresponding local coordinate systems.

Modeling of stiffness

The global stiffness of a machine tool is a result of the arrangement of successive structural parts (bodies) and couplings (joints) in the mechanical chain leading from the TCP (Tool Center Point) to the WPP (Workpiece Point).

The linear and isotropic modeling of structural stiffness of machine bodies by means of material specific Young's moduli has proven to be perfectly adapted for the investigation of machine tool dynamics.

Table 2.5: Stiffness coefficients in local coordinate systems of machine tool components (figure 2.15).

Type	coefficient K_x	coefficient K_y	coefficient K_z	coefficient K_a	coefficient K_b	coefficient K_c
Linear guideway	0	lateral stiffness	normal stiffness	roll stiffness	pitch stiffness	yaw stiffness
Rotation bearing	radial stiffness	radial stiffness	axial stiffness	tilt stiffness	tilt stiffness	0
Ballscrew drive	drive stiffness	radial stiffness	radial stiffness	torsional stiffness	tilt stiffness	tilt stiffness
Mounting element for machine bed	lateral stiffness	lateral stiffness	vertical stiffness	tilt stiffness	tilt stiffness	tilt stiffness

Concerning the joint stiffness, the modeling is characterized by two distinct layers: the component modeling and the stiffness coefficients. For the first layer, one modeling technique has become increasingly predominant and consists in defining a generalized 6-DOF spring-damper element at each coupling location, whose required coefficients vary depending on the connection type (table 2.5).

In FE environments like in ANSYS, it is possible to implement punctual elements to which the six single stiffness values can be assigned. The element type *COMBIN14* is widely used for this purpose and greatly simplifies the definition of local springs, even though it requires some effort in order to properly select the concerned nodes and properly orient the local coordinate system, which for large structures can involve arduous manual work. But assuming this step is accomplished, the next issue concerning the second layer is to actually decide what coefficients should be chosen for the single couplings, according to table 2.5.

The whole set of stiffness coefficients of rotation bearings (in single or multiple assembly configurations) for rotary axes and spindles is normally accessible on the corresponding catalogue specifications. Special attention has to be brought to the influence of the preload level in the bearing stiffness as well as to the velocity-dependent stiffness variation in high speed spindles [75].

Table 2.6: Damping coefficients in local coordinate systems of machine tool components (figure 2.15).

Type	coefficient D_x	coefficient D_y	coefficient D_z	coefficient D_a	coefficient D_b	coefficient D_c
Linear guideway	friction coefficient	lateral damping	normal damping	roll damping	pitch damping	yaw damping
Rotation bearing	radial damping	radial damping	axial damping	tilt damping	tilt damping	friction coefficient
Ballscrew drive	drive damping	radial damping	radial damping	torsional friction	tilt damping	tilt damping
Mounting element for machine bed	vertical damping	lateral damping & friction	lateral damping & friction	tilt damping	tilt damping	tilt damping & friction

For the modeling of feed drive systems, the integration of available data on the stiffness coefficients of the various chain components (fixed bearing + ballscrew spindle + nut) have been extensively studied in the past years to obtain very detailed models, see [76, 8, 62, 9, 7]. In the work of Oertli [10], the modeling of electromechanical drives for machine tools by means of elaborate stiffness matrices requiring a larger number of coefficients than in table 2.5 are of great interest for the detailed simulation of the drive chains.

The lateral K_y and normal K_z stiffness coefficients of linear guideways are commonly derived from catalogue specifications. Rotational stiffness coefficients are not systematically at hand but are provided by the manufacturers if explicitly asked. One important knowledge remains however unknown: the boundary conditions characterizing the method leading to the catalogue values. Some manufacturers use an experimental setup to identify the stiffness values of their linear guideway components. Some manufacturers focus on virtual models to calculate the stiffness coefficients.

Another way of obtaining reliable data about the stiffness of rolling linear guideways or bearings is to carry out an experimental identification using the real machine and an adequately parameterized RBS or FEM model, like it is commonly done for numerous structural applications in the field of machine tools, e.g. in [77, 78, 79, 80, 81, 82, 83, 84, 85].

But the trend being to reduce the experimental effort in favor of a fully virtual analysis, in the future a comprehensive experimental verification should only be carried out on one final consolidated prototype.

When a machine tool is solidly mounted on a concrete foundation or floor, the resultant structural natural frequencies are very likely to be in close proximities to some of the disturbance frequencies caused by the rotational elements contained in the machine, typically the spindle. Deliberate use of flexible mounting mechanisms shifts the whole set of the rigid motion frequencies far lower than the disturbing frequencies [86]. For this reason, flexible mounting devices have become standard for the fixation of machine tool beds. However, even if the reciprocal effect between machine bed rigid modes and process excitation is greatly reduced, the effects are not negligible. The stiffness values taken from catalogue specifications do not guarantee reliable values for the specific applications. Targeted experimental modal analysis and subsequent parameter updating by identifying dominantly low-frequency rigid eigenmodes is a rapid and efficient way of obtaining accurate values for a specific application [16].

When implementing joints into a machine tool model, the resulting effective stiffness is naturally given by the coefficients of the spring elements, but is also greatly influenced by the surrounding structure components. Hence the questions which arise are: how should the spring element be connected to the fixed part respectively to the moving part? Should the carriage, the rail, the bearing rings, etc. be explicitly represented in the model? If yes, should they have their default Young's modulus or should they be modeled as rigid parts? How valid are these values when transferred to a rigid body model? These questions don't have trivial answers if the exact manufacturers' experimental or virtual setups are not considered.

Modeling of damping

As decisive factor in the amplitude level of the relative dynamic displacements at the natural frequencies between TCP (Tool Center Point) and WPP (Workpiece Point), realistic models of damping phenomena are absolute prerequisites for quantitative statements on mechatronic properties of entire machine tools.

The prediction of the damping characteristics of machine tools is extremely difficult due to their dependency on many different influences. Measurements of the dynamic behavior of similar machine tools or components and the validation of existing simulation models is the best way to find adequate initial values for future simulations.

As in the case of stiffness, damping effects in machine tools have different sources. They can be classified into three distinct categories:

1. Structural damping originates inside the material, due to internal frictional effects, causing the dissipation of energy as the structural parts deform during oscillations. The damping characteristics of a machine tool structure can vary notably depending on the used material. A classic choice consists in building the machine on a steel or cast iron basis. Welded structures are preferred when lightweight and dynamics is a prerogative, but can evidence lower damping capacity. Alternative materials like polymer concrete are often considered for massive stationary machine frames [87, 88, 89, 90]. Composite structures filled with metallic foam [91] or with concrete [92] offer a good compromise between weight, stiffness and damping coefficient.

   In FE-analyses, material damping is frequently described by proportional viscous damping, known as Rayleigh damping [93, 94] and formulated as in equation (2.13):

$$[D] = \alpha \cdot [M] + \beta \cdot [K] \tag{2.13}$$

$$
\begin{aligned}
D \quad &: \quad \text{damping matrix} \\
M \quad &: \quad \text{mass matrix} \\
K \quad &: \quad \text{stiffness matrix} \\
\alpha, \beta \quad &: \quad \text{constant factors}
\end{aligned}
$$

Modal damping is another possibility to implement structural damping. Given the second-order equation of a single spring-mass system (2.14):

$$m\ddot{x} + d\dot{x} + kx = 0 \tag{2.14}$$

and assuming a solution of the form $x = e^{st}$, the characteristic equation of the system is formulated as (2.15):

$$ms^2 + ds + k = 0 \tag{2.15}$$

The solution of equation (2.15) is:

$$x = e^{\left(\frac{-dt}{2m}\right)} \left[Ae^{t\left[\left(\frac{d}{2m}\right)^2 - \frac{k}{m}\right]^{1/2}} + Be^{-t\left[\left(\frac{d}{2m}\right)^2 - \frac{k}{m}\right]^{1/2}} \right] \tag{2.16}$$

where A and B are arbitrary constant factors depending on initial conditions.

It is observed that the behavior of the damped system depends on the numerical value of the radical in the exponential of equation (2.16). In this context, the critical damping coefficient d_c, reducing the radical to zero, is defined as (2.17):

$$d_c = 2\sqrt{mk} = 2m\omega_0 \tag{2.17}$$

where ω_0 is the natural frequency of the system. The damping ratio ζ gives the relation of the actual damping to the critical damping (2.18):

$$\zeta = \frac{d}{d_c} = \frac{d}{2\sqrt{mk}} = \frac{\Lambda}{2\pi} = \frac{\delta}{\omega} = \frac{\eta}{2} \tag{2.18}$$

$$
\begin{aligned}
d &: \quad \text{damping coefficient} \\
m &: \quad \text{mass} \\
k &: \quad \text{stiffness} \\
\Lambda &: \quad \text{logarithmic decrement} \\
\delta &: \quad \text{decay constant} \\
\omega &: \quad \text{angular frequency} \\
\eta &: \quad \text{loss factor}
\end{aligned}
$$

In ANSYS [95] the damping matrix $[D]$ is required for harmonic, damped modal and transient analyses. In its most general form it is defined as follows (2.19):

$$[D] = \alpha \cdot [M] + \beta \cdot [K] + \sum_{j=1}^{N_{mat}} \beta_j \cdot [K_j] + \beta_c \cdot [K] + [D_\zeta] + \sum_{k=1}^{N_{ele}} [D_k] \tag{2.19}$$

α : constant mass matrix multiplier (input on ALPHAD command)

β : constant stiffness matrix multiplier (input on BETAD command)

β_j : material dependent constant stiffness matrix multiplier

(input on MP,DAMP command)

ζ : constant damping ratio (input on DMPRAT command)

β_c : variable stiffness multiplier

(constant damping ratio, regardless of frequency) $\beta_c = 2\zeta/\omega$

D_ζ : frequency dependent damping matrix

(calculated from the specified damping ratio for mode r: $\zeta_r = \zeta + \zeta_{mr}$,

where ζ_{mr} is the modal damping ratio for mode r

(input on MDAMP command)

D_k : element damping matrix

Since the values of α and β are generally not known directly, they can be derived from the modal damping ratio ζ_{mr}, which is the ratio of actual damping to critical damping for a particular mode of vibration r. Exploiting the proportional Rayleigh representation and after transformation into modal coordinates, ζ_{mr} is expressed as in (2.20):

$$\zeta_{mr} = \frac{\alpha}{2\omega_r} + \frac{\beta\omega_r}{2} \qquad (2.20)$$

In many practical structural problems, as it is the case for machine tool components, the mass proportional damping factor α may be ignored, as it is mostly relevant in applications evidencing low frequencies and high amplitudes. For applications with higher frequencies and low amplitudes, as in machine tools, only the stiffness proportional damping factor β is considered. It is important to note that only one value of β can be input at each load step, so from equation (2.20), the calculation of β should be based on the dominant natural frequency for the load step in question.

In table 2.7, damping ratio values relevant for machine tool structures are summarized [96].

Table 2.7: Typical damping ratios for machine structures.

Material	Damping ratio
Steel	0.001–0.002
Cast iron GG-25	0.002–0.004
Polymer concrete	0.02–0.03
Welded structure	0.004–0.08
Machine bed	0.04–0.08

2. The above considerations lose their validity when several mixed damping sources are found on a single system. It is therefore necessary to integrate other forms of damping using specific element types. Joints damping is a form of energy dissipation taking place in machine elements connecting the moving components, like linear guiding systems, bearings and ballscrew drives, whose functioning technological principle commonly consists of rolling bodies (balls or cylinders).

As it is the case for stiffness, the modeling of joint damping is divided into the component modeling layer and the damping coefficients layer. The same 6-DOF *COMBIN14* elements, defined locally between the axes, are considered for the first layer. The second layer consists then in assigning the required viscous linear damping and friction coefficients of table 2.6. The correct implementation of this form of damping is all the more crucial as it represents the largest damping contribution of the overall machine tool [97, 98, 99]. Many efforts have been made for the identification of universally applicable damping parameters of rolling elements. Popov [100], De Vicente [101], Al-Bender [102] examined the in-depth behavior occurring at the interface of a rolling contact. Dietl [103, 104] and Shamine [84] focused on the dynamic characteristics of rolling bearings and on methods to experimentally identify their dynamic properties. Albert [105], Brecher [106], Neugebauer [107], Rossteuscher [108], Wu [109], Groche [110] conducted comprehensive analyses on different test-beds in order to investigate the damping mechanisms in linear rolling guiding elements for different operating conditions.

In [111], an overview of damping parameters for different mechanical components related to machine tools is given. Indicative values regarding rolling bearings, used in rotary axes and spindles, are summarized in table 2.8. The experimental set-up in [110] also evidenced the relevant variance in the results when identifying damping parameters of linear guideways (table 2.9).

The sensitivity to operating parameters leads to uncertainties greatly affecting the dynamical modeling of machines based on mechanical rolling elements:

Table 2.8: Typical damping values for rolling bearings [111].

Component	Damping value
Rolling bearing (inner diameter $55mm$)	$2000 - 9000Ns/m$
Rolling bearing (inner diameter $90mm$)	$5500 - 12000Ns/m$
Rolling bearing (inner diameter $120mm$)	$50000 - 550000Ns/m$
Rolling bearing (inner diameter $160mm$)	$200000 - 1000000Ns/m$

Table 2.9: Typical physical damping values for linear guideways [110].

Component	Damping value
Ball linear guideway (carriage size $35mm$)	$4000 - 10000Ns/m$
Roller linear guideway (carriage size $35mm$)	$3500 - 14500Ns/m$
Ball linear guideway (carriage size $45mm$)	$4000 - 14000Ns/m$
Roller linear guideway (carriage size $45mm$)	$6500 - 10500Ns/m$

The friction torque in a rolling bearing has two distinct contributions: a first one involving the viscosity of the lubrication and the rotation speed of the bearings, and a second one including the effects of the bearing load. It is expressed as in equation (2.22) (see table 2.10).

$$Mr = 10^{-7}f_0(v \cdot n)^{2/3}d_m^3 + f_1 P_1 d_m \qquad (2.21)$$

$$\text{for } v \cdot n \geq 2000$$

Mr :   friction torque $[Nmm]$

v :   kinematic viscosity at operating temperature $[mm^2/s]$

n :   rotation speed $[min^{-1}]$

P_1 :   equivalent bearing load $[N]$

d_m : $(d + D)/2$:average diameter $[mm]$

with inner and outer diameters d and D

f_0, f_1 :   lubrication and type dependent coefficients $[-]$

(f_{0r} and f_{1r} in reference [DIN ISO 15312] conditions)

Table 2.10: Typical friction coefficients for rolling bearings [112].

Component	f_{0r}	f_{1r}
Deep groove ball bearing	$1.7 - 2.3$	$0.00010 - 0.00020$
Self-aligning ball bearing	$2.4 - 4$	0.00008
Angular contact ball bearing	$2 - 7$	$0.00025 - 0.00035$
Four point bearing	$2 - 3$	0.00037
Cylindrical roller bearing with cage	$2 - 4$	$0.00020 - 0.00040$
Cylindrical roller bearings full complement	$5 - 12$	0.00055
Needle-roller bearing	$5 - 10$	0.00050
Self-aligning roller bearing	$4.5 - 6.5$	$0.00017 - 0.00036$
Tapered roller bearing	$3 - 4.5$	0.00040
Axial cylinder roller bearing	$3 - 4$	0.00150
Axial self-aligning roller bearing	$2.5 - 3.3$	$0.00023 - 0.00033$

Despite the non-linearity in the first part of equation (2.22), using the correct empirical coefficients f_{0r} and f_{1r}, the friction torques in spindle bearings are possibly realistic, since the operating conditions are generally well known. This assumption is unacceptable when it comes to bearings used in rotary axes, since the rotation speed is constantly varying, frequently changing direction and regularly passing through zero values. This adds to the non-linearities due to the stick-slip and hysteresis effects occurring at very low speeds. In controlled units like rotary axes and ballscrew drives, the friction effects of the whole drive train as well as damping resulting from the control itself ought to be considered. This makes the modeling of friction for actuating mechanisms in machine tools all the more complex.

The same considerations apply to linear rolling guideway systems. In the linear axes of machine tools there is no stationary operating mode characterized by constant speed. All the non-linear phenomena like stick-slip and hysteresis affect the dynamical behavior of the linear drives in direction of motion. This adds to the already mentioned damping effects in the drive train and in the feed control. It appears therefore unrealistic to count on quantitative friction parameters valid for all operating conditions. The complexity is taken a step further if the varying loads on the single carriages are considered. The constantly changing mass distribution caused by axis displacements, the inertial loads resulting from axis accelerations and the additional loads as a consequence of the machining process forces make the instantaneous load-dependent friction unpredictable. Brecher [106] investigated the influence of the different factors on the friction force for a selection of linear guideways. It confirmed that, even though the speed dependent behavior is relatively linear between 5000 and $40000 mm/min$ (table 2.11), the low-speed region remains a complex issue.

A recurrent conclusion to these exhaustive studies is that, regarding viscous damping effects in direction of motion (friction effects) as well as the viscous damping effects square to the direction of motion, the damping coefficients are affected by significant uncertainties. Many factors have a fundamental influence which makes the determination of robustly realistic parameters for use on concrete applications extremely difficult: speed, lubrication, temperature, loading conditions, preload, gaskets, type of rolling element, manufacturing tolerances, assembly conditions, fastening torque, manufacturer, time of service, previous load cycles, etc. [1, 99, 106]

3. The third damping source is less known but probably as important as the other ones. In machine tool assemblies, there are countless spots responsible for energy dissipation, but due to their unrevealed nature they are often included into the general proportional material damping or even ignored. Many of these contributions, which are not within the force flow between the tool and the workpiece, don't need to be considered, as their effect on the machining process is irrelevant. At most some measures are taken to damp disturbing vibrations if they generate excessive noise. On the other side, damping effects in welded structures [113], protective covers [114], bolted parts [115, 116, 117], gaskets, cables, etc. actively participate to the compliance behavior between tool and workpiece. Petuelli [118] conducted a series of experiments on a lathe, analysed the damping behavior of the structure at different assembly stages and evidenced that material damping accounts for only 10% of the overall machine damping.

Table 2.11: Typical friction coefficients for linear guideways [106].

Component	Friction force			
Load on carriage (additional to preload)	$0kN$	$10kN$	$20kN$	$30kN$
$v = 5000mm/min$				
Ball linear guideway (carriage size $35mm$)	$15 - 20N$	$30 - 35N$	$50 - 55N$	$95 - 100N$
Roller linear guideway (carriage size $35mm$)	$30 - 35N$	$40 - 45N$	$45 - 50N$	$55 - 60N$
Ball linear guideway (carriage size $45mm$)	$25 - 30N$	$40 - 45N$	$65 - 70N$	$100 - 105N$
Roller linear guideway (carriage size $45mm$)	$65 - 70N$	$65 - 70N$	$75 - 80N$	$85 - 90N$
$v = 40000mm/min$				
Ball linear guideway (carriage size $35mm$)	$30 - 45N$	$40 - 55N$	$60 - 75N$	$100 - 115N$
Roller linear guideway (carriage size $35mm$)	$55 - 70N$	$55 - 70N$	$65 - 80N$	$70 - 85N$
Ball linear guideway (carriage size $45mm$)	$45 - 60N$	$55 - 70N$	$70 - 85N$	$105 - 120N$
Roller linear guideway (carriage size $45mm$)	$125 - 140N$	$125 - 140N$	$130 - 145N$	$135 - 150N$
Guideway wipers	$10 - 40N$			

Due to the uncertainties associated with damping and friction properties in the connections between structural parts, the study of the dynamic behavior of a machine tool, as opposed to the study of the static behavior, still needs some further assessment in order to gain enough reliability.

By experimentally investigating the Frequency Response Function (FRF) of the TCP compliance and the corresponding mode shapes, it can help the design engineer to validate the simulation models in order to find realistic values for the stiffness and damping behavior of the machine components. The calibration of the parameters of spring-damper elements is extremely time-consuming, because of the large amount of unknown coefficients which need to be identified (guiding systems, rotation bearings and the various mechanical com-

ponents of the ballscrew drives). A solution is to split the problem: first the stiffness parameters are identified using the undamped model. Then the complexity and uncertainty levels are increased and the damping parameters are identified using the damped model. But even in this case, the simultaneous manual calibration of all stiffness and damping coefficients of a complex five-axis machine tool is prohibitive.

2.2   Research gap

Constraints, needs and acceptance of CAE methods on the industry level do not match those of a research-oriented institution. Not until the end of the nineties, machine manufacturers began to systematically integrate CAD-CAE-based methods into their design process. The reason for this time delay compared to other engineering fields is the small-scale nature of the machine tool industry, which does not dispose of financial means important enough to justify such a radical changeover in the product development philosophy. Hardware costs have been constantly decreasing over the last decade, so that it is no obstacle to the use of computers in the design process anymore. The cost of an annual license for a CAE program is namely high, but ideally, if one could choose between a FE license and an additional machine prototype, a quick cost estimation would solve the dilemma. What prevents from investing into the simulation department must then lie in the costs associated with the exploitation of CAE tools, or better said with the ratio between costs and benefits, as the conviction that the effort put into advanced simulation methods will pay off in the long term is not commonly assumed in the machine tool field yet.

Rigid body simulation has been established as a very useful and efficient tool for the investigation and optimization of mechanical systems. In the field of machine tools, research efforts have led to the development of programs enabling the implementation of typical machine tool components and joints.

The most widespread simulation technique among machine tool designers is the finite element method. Combined with the experience of engineers with analytical computations, it has become reliable enough to be incorporated into the design process, particularly for the study of single machine structure components by means of static analyses.

Modern techniques for reduction of the size of FE models have evidenced, in many engineering applications, how the computation times can be reduced without compromising the accuracy of the simulations. Extensive research work has been carried out during the last years to find ways to combine reduced finite element models with rigid body models, opening a multitude of possibilities for the integration of drives and controls into the simulation models.

The weakness of the rigid body approach lies in the actual creation of the model to simulate, since no commercial tools are available, which are adapted to the specific modeling features of machine tools, in particular of the joints. Non-commercial tools like ACK are supposed to solve this problem, but the lack of functional integrated environments allowing a systematic and automatic variation and evaluation of the model prevents their industrial acceptance. The increasing dynamics of machine tools accentuates the effects of inertial loads. This means that both the stiffness and the mass of the moving parts have to be taken into consideration as design criteria. This results in more compliant structures and represents a limiting issue to the use of rigid body models.

Finite element models benefit of a broad acceptance among machine tool designers. But since complex structural parts, joints and drives systems have made their way into models of entire machine tools, the engineer experience becomes less helpful, the preparation and implementation efforts become higher, many uncertain key parameters have to be dealt with and the computation times become prohibitive. Besides, changes in the kinematic arrangement and axis positions, due to the nodal-based nature of joints implementation, are associated with large additional effort.

The combination of RBS and reduced FEM models is supposed to take advantage of the strengths of both methods. The deficiencies lie in the integration of the different involved software packages, in order to achieve a functional and efficient synergy. Derivation of rigid body model characteristics, pre-processing and meshing of FE models, reduction of FE system matrices and implementation of mixed coupling properties invoke many interfacing and transfer processes between numerous heterogeneous programs. The lack of a common basis for the development of functional models is a severe restriction to the industrial application of modern simulation tools.

The above considerations represent an important obstacle to the possibility for designers and CAD/CAE engineers in small and medium-sized enterprises (SME) to make of advanced simulation tools an inherent part of product development. Figure 2.16 illustrates how this affects the conventional use of simulation during the various design phases. Instead of that, already in the layout phase, simulation should provide flexible and efficient tools to easily vary and evaluate the model configuration without having to rebuild it. Successively in the concept phase, compliant bodies should also be taken into account with the help of modern model order reduction techniques.

An adequate simulation model is hence supposed to have its complexity, accuracy and reliability levels grow synchronously with the maturation stage of the machine development. If at every design phase the simulation model is exactly as detailed as needed to make the corresponding constructive decisions, then the use of simulation is considered to be
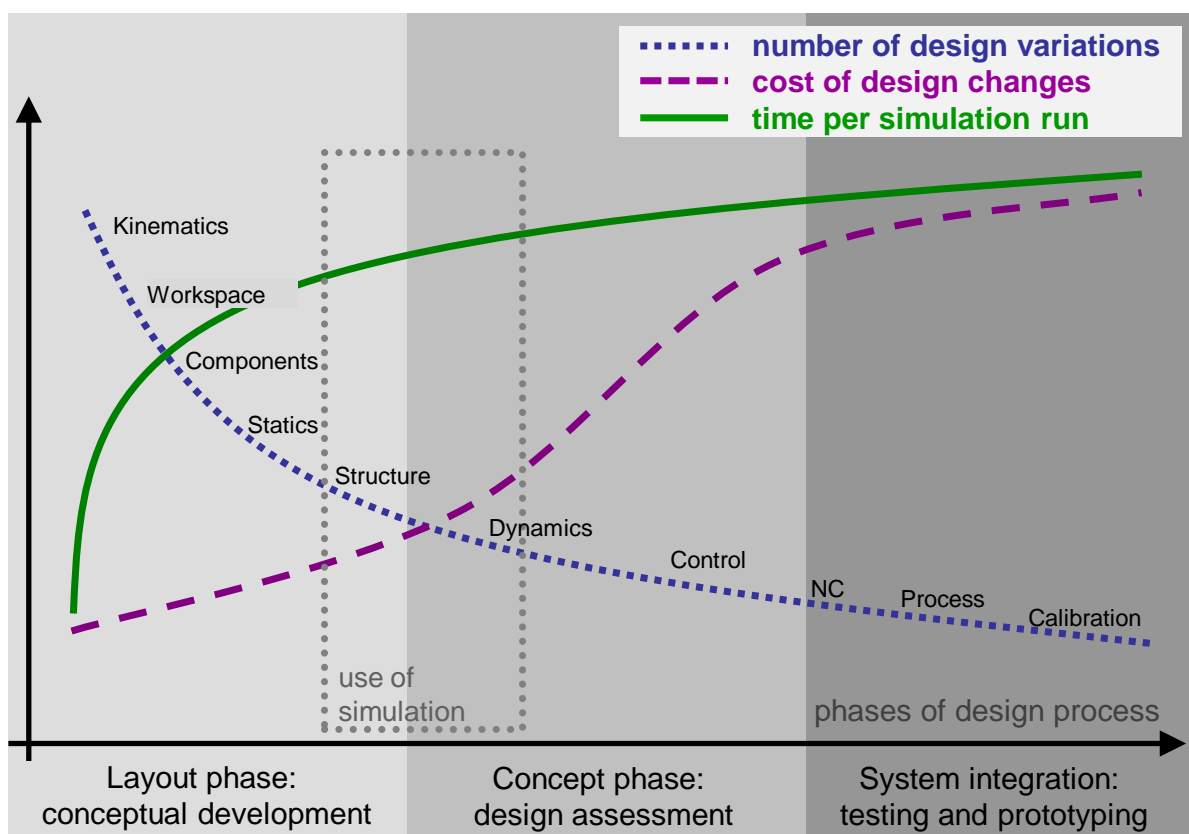
Figure 2.16: Simulation effort with conventional use of simulation methods.

optimal. The best design alternatives are promoted to the detailing phase, where full FE simulations are conducted on the limited remaining set of models in order to verify the behavior of the model resulting from the simplified analyses. If this succeeds, a prototype is built and all experimental verifications are carried out during the testing phase. The overall ambition is that the virtual model is so reliable that the prototype is reduced to a pure formality not before the end of the development phase, preceding the series production. The research work carried out in this thesis in the field of machine tools and their dynamic properties is composed of two major issues:

- The determination of guidelines for machine tool models, in particular for the properties of couplings interconnecting the moving axes. These aspects are critical for two reasons: first because it is a well established truth that compliances in joints contribute to a great extent to the resonant peaks in the low frequency range. On the second hand, the optimal implementation method of such mechanical components within finite element and rigid body models remains vague, data specifications from manufacturers giving minimal information in form of either direction-dependent sin-

gle values or in form of force-displacement diagrams. Matching of results of static and modal analyses with the corresponding FE simulations are used to formulate a series of significant and robust rules to corroborate the use of idealized spring models for the virtual development of complete machine tools. The certified implementation of the stiffness values has also the advantage of strengthening the model accuracy for the identification of other parameters. In particular damping coefficients could not be identified using a model whose joint boundary conditions are approximative or whose stiffness coefficients erroneous.

- The second issue in this thesis is the development of an integrated platform to improve the efficiency of the modeling, solving and post-processing phases during the design of machine structures. The result is a *Structure Gateway Interface* (SGI) involving the automated creation of a machine tool FE model with its joints elements, the automated export and the completion and evaluation of efficient reduced analyses. From the common environment, the designer can choose what analyses are needed at a certain development stage and automatically generates the corresponding model files. The priority of the *Structure Gateway Interface* and of the simulation tools is to meet the demanding industrial requirements:

  - Widespread software packages (commercial CAD and FEM programs) as basis for the creation (pre-processing) of the models
  - Automated assistance for the creation of FE-models specific to the needs of machine tools, regarding in particular the kinematics and the axis couplings
  - Fully automated export of complete models for reduced-size computations
  - Different degrees of complexity to be deployed during different design phases
  - Automated assistance for the execution and evaluation of analyses targeted for the needs of machine tools, considering in particular the TCP-WPP relative deviations and the investigation of the entire workspace

An application-oriented stand-alone software, specifically developed for machine tool rigid body analyses, supports the designer in the first drafts of structure design. Through an efficient and functional graphical interface and the benefits of pre-formatted post-processing tools, the study of many machine variants in a very short time is made accessible to the demanding industrial reality.

A stand-alone reduction algorithm, combined with automated routines developed in Matlab, is used for coupled reduced analyses, including the control systems. It enables more accurate evaluation of the quality criteria in the full working range and the tuning of the feed control parameters.

Through the integration of innovative and efficient simulation methods to bypass the increase of computational times associated with a higher model complexity, without compromising the accuracy and reliability of the analyses, the potential of the parallelization of design and simulation becomes accessible to SME, as outlined in figure 2.17. It leads to the *democratization of simulation-driven product development.*
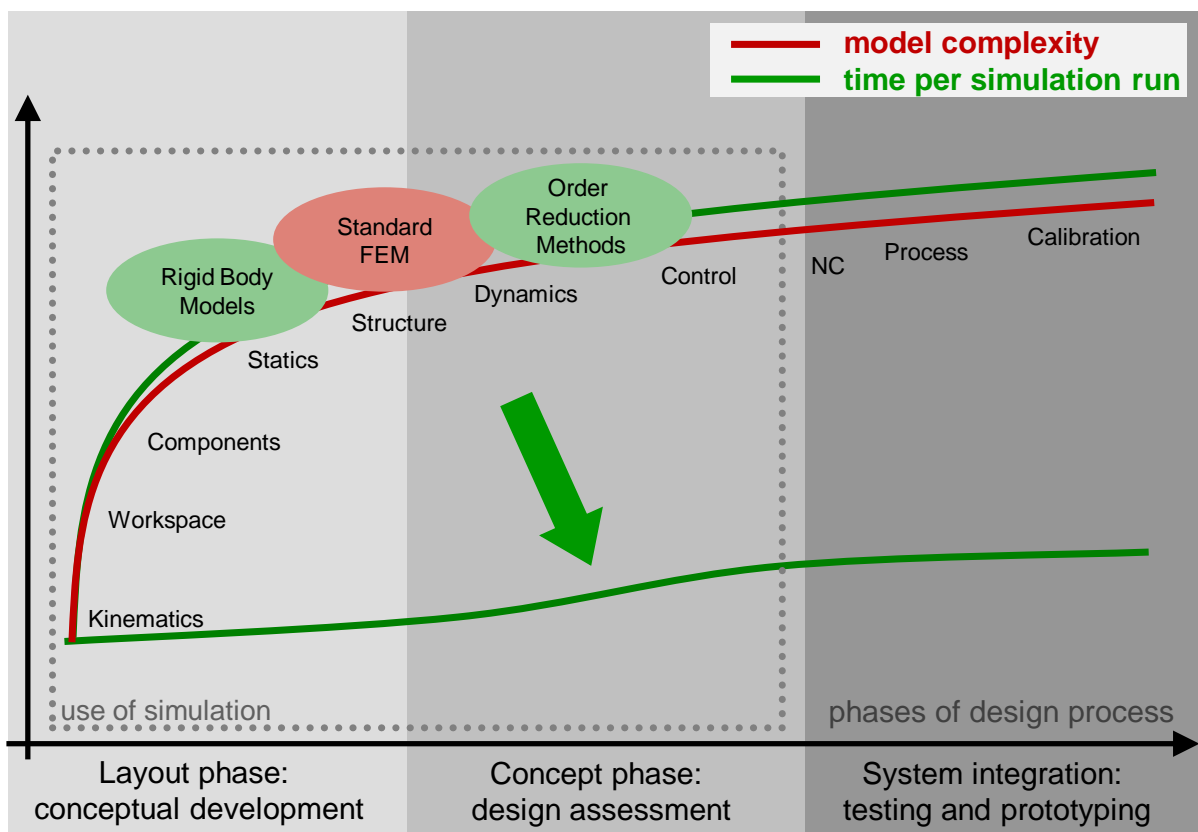

Figure 2.17: Benefits of modern simulation methods in terms of simulation effort.

Chapter 3

Automated creation of a machine tool model

The two major steps involved in the investigation of static and dynamic properties of machine tools are the creation and the evaluation of the model. When considering the structure of a whole machine tool, the time leading to the complete setup of the system to be actually solved is commonly larger than the time for the solving of the problem itself. This has mainly two reasons:

- first the reduction of a complete machine tool model (consisting of numerous parts) to the required complexity level is extremely delicate and every single modeling assumption needs to be implemented very meticulously.

- secondly the pre-processing steps and the obtention of a ready-to-solve model implies extensive manual work representing a bottleneck process, whereas the solving phase can often run as a hidden background process on a remote computer

That's why prior to the actual solving of a finite element problem, every designer is confronted to a pre-processing phase requiring considerable effort, depending on the complexity of the geometry to analyse. As mentioned, it is not only critical because it is associated with a large time, and thus cost investment, but also due to the importance of a thorough preparation, in order to avoid each single modeling error which could lead to some major inaccuracies of the final simulation result. Erroneous definition of material properties, wrong units of punctual stiffness parameters, contacts which should be defined and have been forgotten, contacts which should be deleted and have been overlooked, etc. are all single details which can have fatal consequences. As it has been pointed out in

chapter 2, no software specifically adapted to the development of machine tools is commercially available. Various packages, toolboxes, add-ons, etc. exist, but the integration of all the involved platforms is often intricate. The objective here is to identify one ideal platform, a *Structure Gateway Interface* (SGI), to base the whole modeling process on and which supports the designer from the initial CAD geometry to a fully functional and efficient simulation model.

3.1 Role of a Structure Gateway Interface (SGI)

The process leading from a CAD geometry of a machine tool to the solving of the corresponding system of mathematical equations is often laborious and consists of different steps taking place in heterogeneous programs. The focus consists in developing one common intermediate environment which fulfills the interfacing requirements. The finite element method is seen as a central simulation tool to unify the various steps identified above. The interfacing problem is then restricted to two phases:

- From CAD to FEM: Geometrical defeaturing
  operations for reduction of the complexity level

- From FEM to DBS: Translation of the geometrical data
  into a physical model describing the structural behavior

The benefits and challenges of the transfer between a CAD and a FEM model are described in section 3.1.1. It includes the defeaturing of the geometry and the creation of a physical model through the discretization phase. The developments in this work don't focus on this part, except for showing concrete machine tool applications of the existing methods (section 4.1.1). The research consists predominantly in the steps involved in the transfer from a FEM to a DBS model, starting from a meshed geometry, which are described in section 3.1.2 and detailed in chapters 6.1 and 7.1. Section 3.1.3 finally outlines the requirements of the whole transfer process and the significant role of a *Structure Gateway Interface* (SGI) in efficiently solving models of machine tools, as schematized in figure 3.1.

3.1.1 From CAD to FEM

In the development department of a SME, the new design of a machine tool is nowadays strongly CAD-based. Specialists with longtime experience are able to put together a new structure in a CAD environment much faster than any engineer can achieve it in
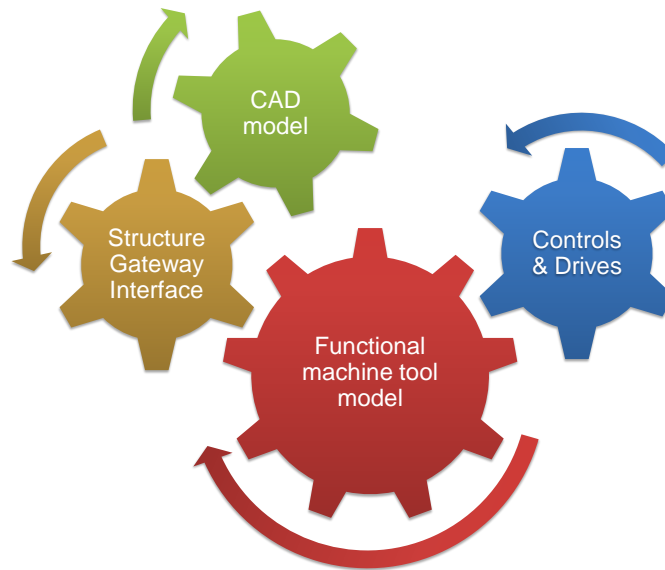
Figure 3.1: Structure Gateway Interface between a CAD model and a functional machine tool model.

a CAE environment. Modern CAD-packages have integrated the possibility to perform analyses of the structural properties of an assembly or sub-assembly using FE-simulations to predict the physical behavior and analyses of the manufacturing process using CAM-simulations (Computer Aided Manufacturing) to visualize the virtual resulting workpiece. This could promote some leading CAD-software package to the ideal candidate for the searched platform. But CAD packages are traditionally not oriented towards physical simulation, at least not yet, and this makes their use not adapted to the needs of complex machine tool analyses.

Advances in modern FE-packages in terms of user-friendliness, meshing efficiency, solver performance and post-processing graphics capabilities have turned them into an indispensable tool for engineering tasks. But in accordance with the arguments above about the CAD supremacy in development departments, what may have literally boosted the popularity of FE programs among the industry are the interfacing capabilities between CAD and CAE environments. Design changes and updates have been indeed extremely simplified since associative and bi-directional interfaces allow a very efficient and straightforward parameter-based communication between these heterogeneous environments. In addition to that, most FE packages now support a very robust and faultless import from standard transfer formats like STEP, IGES and Parasolid. In a nutshell, the advantage of this improved inter-compatibility can be formulated as follows: if a model geometry is available in a CAD program, obtaining the same geometry in a FE program is today considered as a standard, elementary and unproblematic task.

In evaluating the ideal platform for simulation-based product development, this gives commercial FE environments an unsurpassable asset. It takes advantage of the undeniable benefits of the FE-discretization technology, which is the most powerful way to translate complex geometric and physical data into a mathematical formulation, without giving up the fundamental skills of CAD experts.

It is then assumed that the resulting model in the FE environment is ideally configured to be automatically meshed. However it has to be noted that this assumption is often associated with underestimated effort. Although quite some progress has been achieved in the field of automatic defeaturing methods, in most cases there are three applicable ways of getting a FE-suitable machine tool model out of a CAD geometry: the first is creating a CAD-model following exigent and stringent rules in prospect of further simulations. The second is using available in-built CAD-based defeaturing algorithms, which nonetheless, due to the numerous problem typologies, often lack robustness and efficiency and end up in manual operations. The third consists in applying modern defeaturing functions directly in the FE program, just before the meshing, in order to make it ready for meshing. Boolean operations, parts moving or deleting, defeaturing algorithms (automatic or semi-automatic deleting of small holes and other details irrelevant for the structural properties) are some of the possibilities available (see section 4.1.1). New ways in direction of automated topological defeaturing of structures could be explored in order to reduce the effort in obtaining valid simulation models.

The transfer from an original CAD model to a meshed FEM model, whose size doesn't exceed the needs, constitutes the first part of the *Structure Gateway Interface* and is presented in figure 3.2.

3.1.2   From FEM to DBS

The second and main part is, starting from the meshed FEM model, to obtain efficient and valid models based on a DBS (Digital Block Simulation) environment like Matlab, for the specific requirements of machine tool dynamic analyses. This means the FE program has to:

- Set the global configuration parameters of a machine tool,

- Define the properties of the structural parts as well as of the coupling elements

- Convert the model into an external environment using a simplified representation
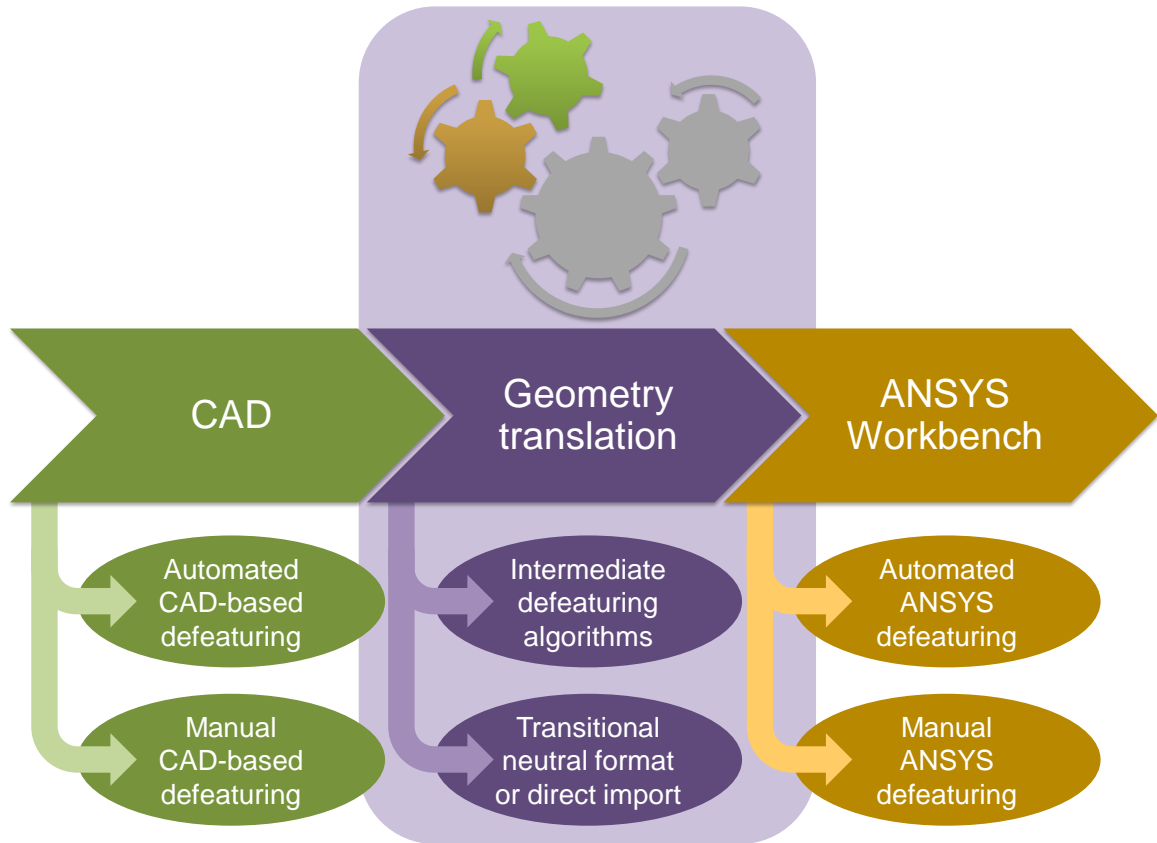
Figure 3.2: From a CAD model to ANSYS Workbench.

Modern FE packages offer the possibility to integrate scripting within a simulation in order to customize the analysis. The major contributions of the present work to the *Structure Gateway Interface* consists in developing macros to automate the three steps above for the specific characteristics of machine tools, as it is shown in figure 3.3.

3.1.3 Structure Gateway Interface

The role of a changeover between a native CAD structure and an elementary but accurate CAE structure is essential to understand the vision of the presented work. The gap between these two poles needs to be bridged. ANSYS Workbench fulfills these requirements, that is why it was chosen as basis for the *Structure Gateway Interface* between a CAD model and a functional machine tool model. As leading and most widespread software provider for structural FE-analyses, it best fulfilled the need of universality. Since the release of ANSYS Workbench, it is possible to ally the standard interfacing capabilities, the flexibility of classic script-based simulations, the powerful highly-automated meshing capabilities and the accessibility of innovative project and analysis management user interfaces.
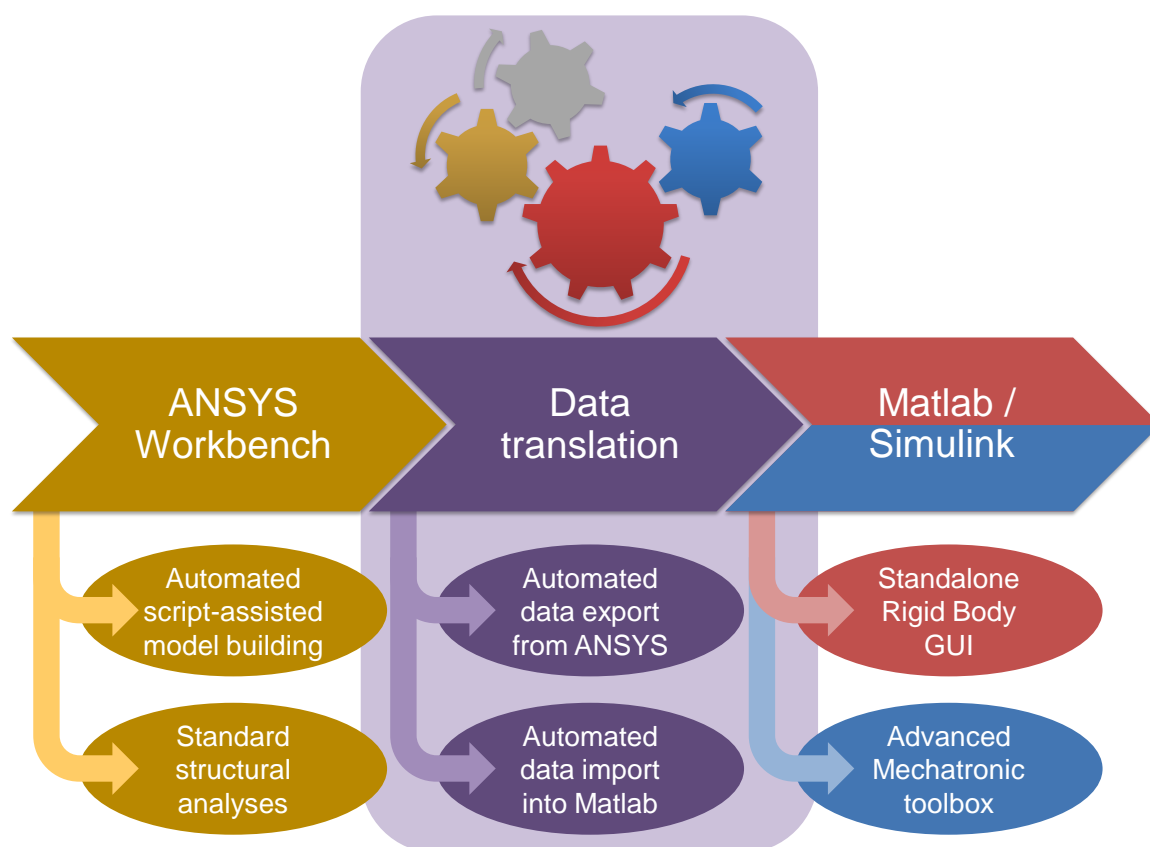
Figure 3.3: From ANSYS Workbench to a machine tool model.

The role of a *Structure Gateway Interface* consists hence in executing the following steps, also summarized in figure 3.3, for any machine tool model to be analysed:

1. Automated grouping of nodes and elements
2. Implementation of coupling properties
3. Simple derivation of mechanical properties
4. Exporting of global system matrices

As already mentioned, the transition from the starting CAD geometry to the final FE model is composed of two interfacing issues: the first one consists in importing the CAD model into ANSYS Workbench (figure 3.2), and the second one consists in exporting the required model information from ANSYS to Matlab (figure 3.3).

After a defeaturing phase, which clearly needs further developments to enable efficient automated functions to replace long and laborious manual operations, the CAD-interfacing and pre-processing capabilities of ANSYS Workbench are used in order to import the geometry of a machine tool structure and prepare it for simulation. A standard analysis with

ANSYS Workbench normally begins with the *DesignModeler* module, a CAD-like inter-
face which allows modifications of the geometry. The meshing of the model structure and
the grouping of nodes and elements into components constitutes the pivot point between
the two phases of the SGI and leads to the script-assisted building of the machine tool FE
model. In the ANSYS *Simulation* environment, the different axes of the structure, as well
as their coupling properties need to be defined. The complete configuration of the machine
tool FE model, the correct definition of all joint parameters and the actual writing of files
into the working directory are covered by the corresponding operations (steps 1 to 4), but
would be extremely time-demanding if they had to be done manually for every structure
variation. Instead of that, the interface comprises a series of *APDL* (Ansys Parametric
Design Language) scripts which execute the above functions in an automated way and,
depending on the type of desired output, automatically export the corresponding content.
The subsequent step is then the simulation and validation of the resulting reduced models
in a Matlab based environment, where the stored ANSYS data are imported and auto-
matically manipulated in order to create a new model suitable for the purposes of efficient
simulation driven design.

The *Structure Gateway Interface* involves a considerable effort in software development
taking into account the know-how concerning the specificities of machine tool systems.
Steps 1 and 2 are detailed in the next two sections 3.2 and 3.3, which lead to the complete
machine tool model depicted in figure 3.9. Step 3 is discussed in chapter 6.1. Step 4 is
discussed in chapter 7.1.

3.2   Preparation of a model in a FE environment

The structure of a machine tool is composed of several parts, which are either solidly
joined by standard fixings (welds, screws, bolts, etc.) in case they belong to a same body,
or joined by rotating bearings, resp. by linear guiding systems, when defining the interface
between two axes with a relative degree of freedom. In order to facilitate the handling
of the model in the subsequent steps, at this stage, in the *DesignModeler* environment
of ANSYS Workbench, all the linear and rotary axes are defined as single components.
The bodies belonging to a sub-assembly are not merged into one body, but share common
faces, edges and consequently the corresponding nodes. This has the advantages that no
contacts need to be defined at the connections between two adjacent parts and yet they
can be assigned different material properties.

The resulting model, adequately divided into axis sub-assemblies, is then transferred to the
Simulation environment of ANSYS Workbench. During this phase, ANSYS executes an

automatic contact search which identifies all contact pairs in the model. Since there are no
contacts within a sub-assembly, there are two types of remaining contacts: contacts within
a single sub-assembly which have been missed and all contacts between the different sub-
assemblies representing the couplings. The former must be eliminated by checking and
updating the model in *DesignModeler*, the latter have to be systematically deleted to
clear the concerned faces for the upcoming customized implementation of spring-damper
elements. At this point the meshes of all the axes of the structure are generated and
machine tool specific pre-processing script-based tasks are carried out.
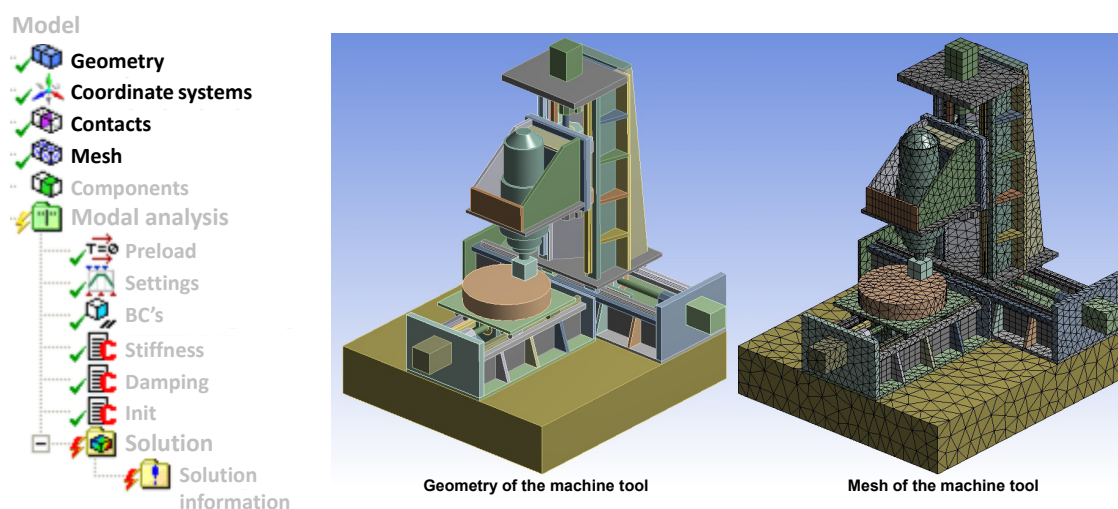
Figure 3.4: Geometry and mesh of a three-axis machine tool.

The elements of all bodies belonging to a same axis are grouped into a single volume
component, which greatly facilitates accessing the system matrices and the mechanical
properties in the subsequent steps. In the example covered here (figure 3.4) the structure
is divided into four sub-assemblies: a linear axis X (Volume_1), a linear axis Y (Volume_2),
a linear axis Z (Volume_3) and the machine bed (Volume_4). The bearings of the spindle
are not modeled and the corresponding parts belong to the axis Z. This kinematic structure
is therefore expressed as follows: $[Tool - Z - X - Bed - Y - Workpiece]$. In figure 3.5,
these model components are highlighted in red and the component names can be found in
the project tree on the left.

A joint location consists of two corresponding sets of faces defining the contact between
carriage and rail, between drive nut and ball screw, between the inner and outer rings
of a bearing or between the two adjacent connecting parts of a machine bed mounting
element (see figure 2.15). The nodes of all faces belonging to the two corresponding sets
are grouped into two different area components, as shown in the project tree on the left
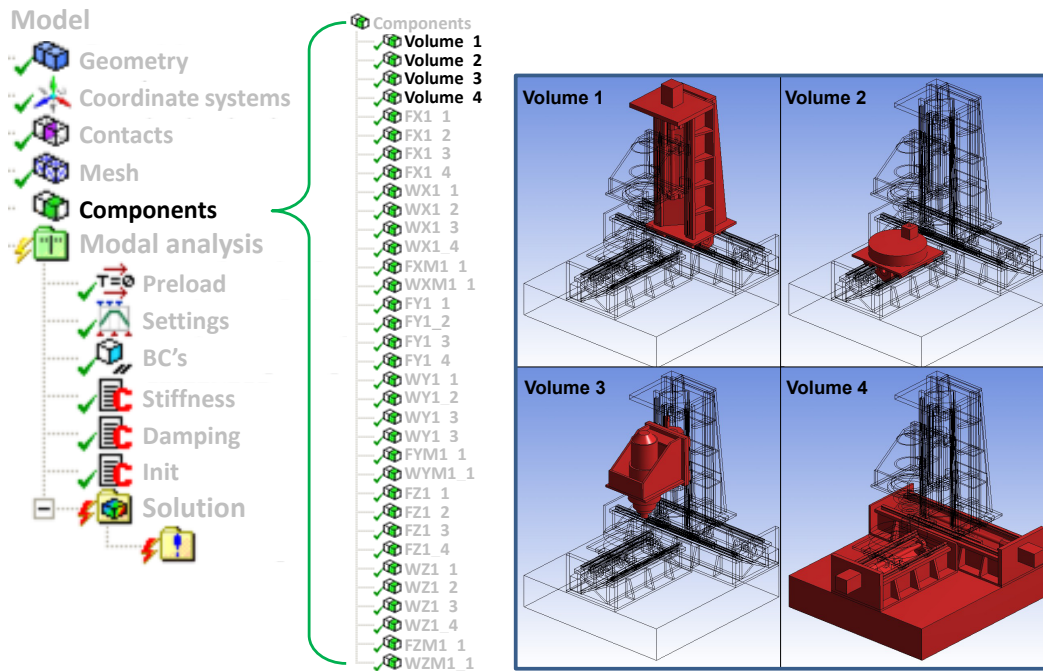of figure 3.6.

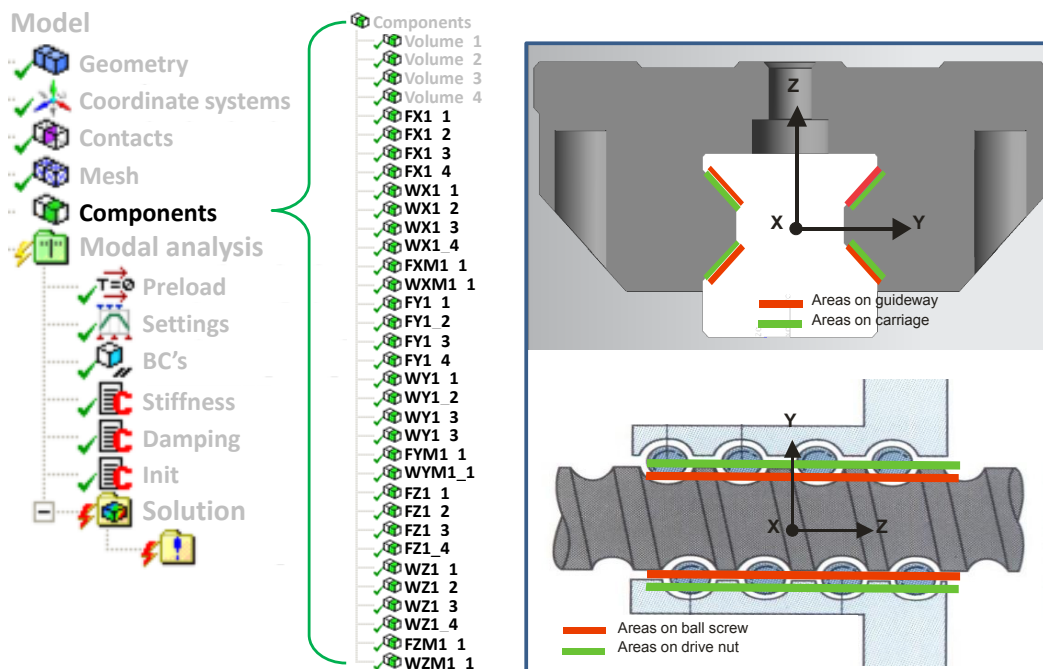Figure 3.5: Axis components (sub-assemblies) of a three-axis machine tool.

Figure 3.6: Coupling components (areas) of a three-axis machine tool.

Assuming the machine structure is in the form described throughout this chapter, with clearly delimited axes, clean connection locations and a suitable mesh, the definition of the volume and area components mentioned above is the sole manual operation required from the program user. Based on a predefined and intuitive naming convention, they constitute the initiation of the construction of the final FE model of the machine tool.

3.3 Pre-processing simulation scripts

The remaining inputs needed are entered in text form in the APDL scripts added to the project tree in the pre-processing analysis pipeline (figure 3.7) and have been developed and optimized for the specific modeling purposes of machine tool structures.
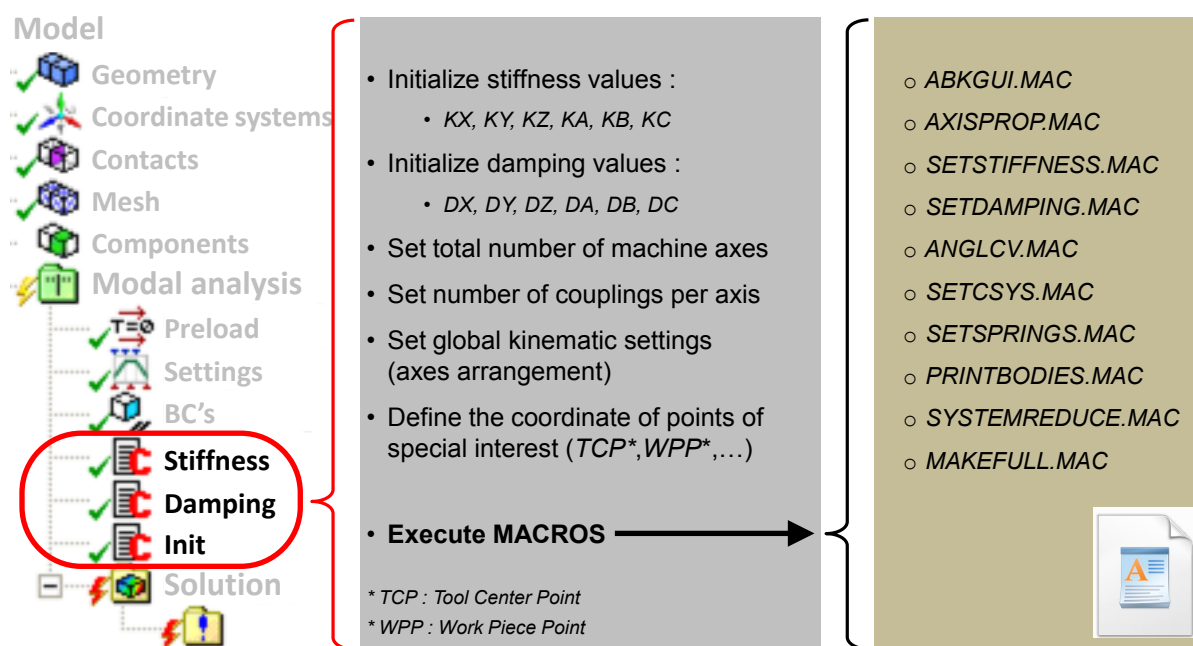
Figure 3.7: Process structure of APDL scripts and macros.

In the STIFFNESS and DAMPING scripts, all parameters of the spring-damper elements are entered, giving an extended overview of all manually defined coupling properties: for each interface, two six-dimensional vectors are needed, which contain the three translational and the three rotational stiffness (KX, KY, KZ, KA, KB, KC), resp. damping (DX, DY, DZ, DA, DB, DC) values between the two corresponding mass elements represented in figure 3.8. The values are entered in the following standardized form:

$$AXIS\_(name)\_(number)\_K(dir) = \dots [N/mm] \text{ or } [Nmm/rad]$$
$$AXIS\_(name)\_(number)\_D(dir) = \dots [Ns/mm] \text{ or } [Nmms/rad]$$

where $name$ is the axis denomination (X, Y, Z, A, B, C), $number$ indicates the axis number in case more than one axis has the same denomination and dir indicates one of the six possible stiffness or damping directions, relatively to the local coordinate system (see figure 3.8).
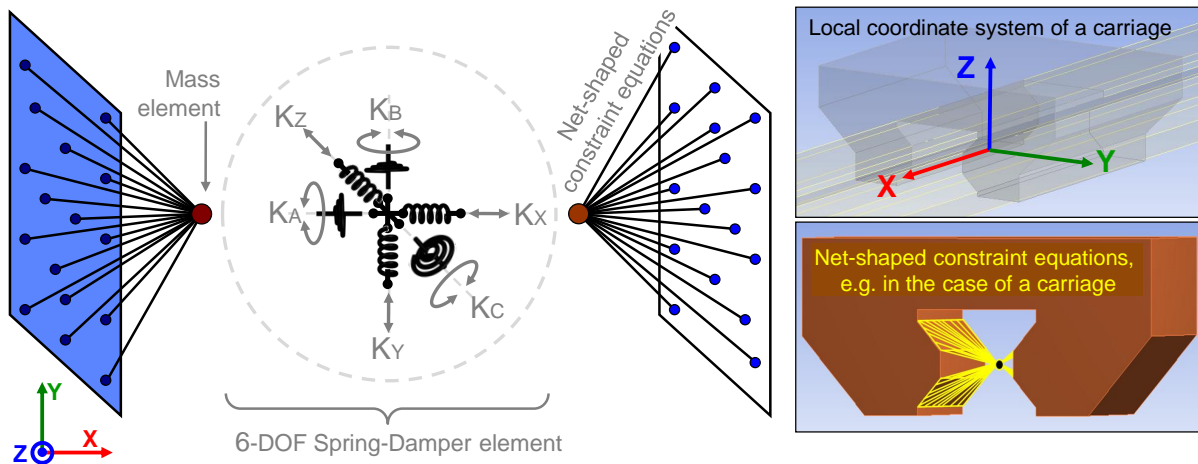

Figure 3.8: Standard implementation of couplings, with constraint equations and local coordinate system.

In the INIT script, the configuration parameters of the machine tool are set. The additional data to be entered concerns purely machine tool specific information, as outlined in figure 3.7. The process is completed by the execution of a first series of ANSYS APDL macros, which use the inputs from the named components (volumes and areas) created in the *Simulation* model and the parameter values defined in the STIFFNESS and DAMPING scripts to completely build the machine tool model. These macros are mainly responsible for taking axis after axis and identifying its position, its orientation, its mechanical properties, its adjacent axes, the joint locations with every adjacent axis and assigning the actual stiffness and damping values to all corresponding joints. At every coupling location, two identical mass elements are automatically created at the median position of the nodes composing the shorter joint component (typically the areas of the carriages, inner rings and nuts). Subsequently the respective net-shaped constraint equations connect one mass element to the moving part (carriage, drive nut, bearing inner ring) and one mass element to the fixed part (rail, ball screw, bearing outer ring). Between the mass elements, a 6-DOF spring-damper element is created applying the previously defined stiffness and damping values relative to the standard local coordinate systems defined at each coupling (figure 3.8).

At the end of the INIT script, the machine tool model is finalized and fully determined, as schematized in figure 3.9 for a two-axis machine tool with a basis, a horizontal axis with a direct measuring system and vertical axis containing the TCP. The standard ANSYS simulation run is stopped here before entering the solution phase. An option key then redirects the simulation into three possible choices (figure 3.10), which are associated with their corresponding set of further ANSYS macros:

- Executing of standard FEM simulation in ANSYS - Key *ANS*

- Export of data for Rigid Body Simulation - Key *RBS*

- Export of data for Coupled Reduced Simulation - Key *CRS*
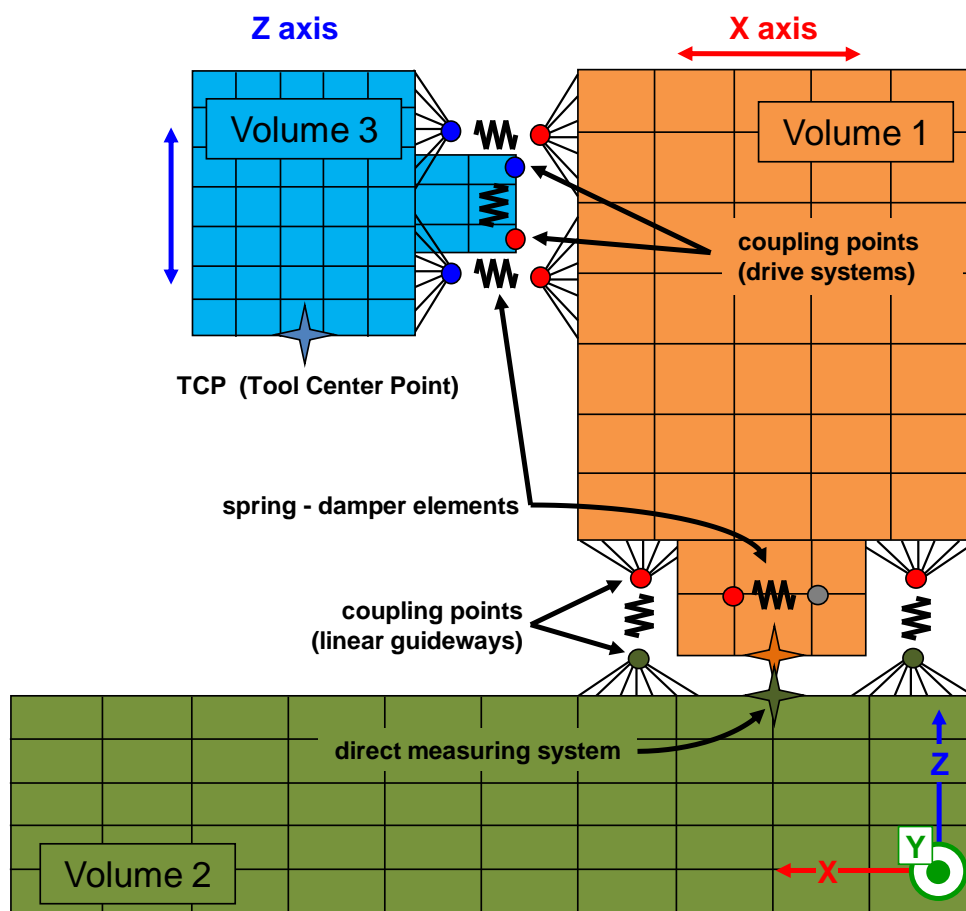
Figure 3.9: Finalized and fully determined machine tool model.
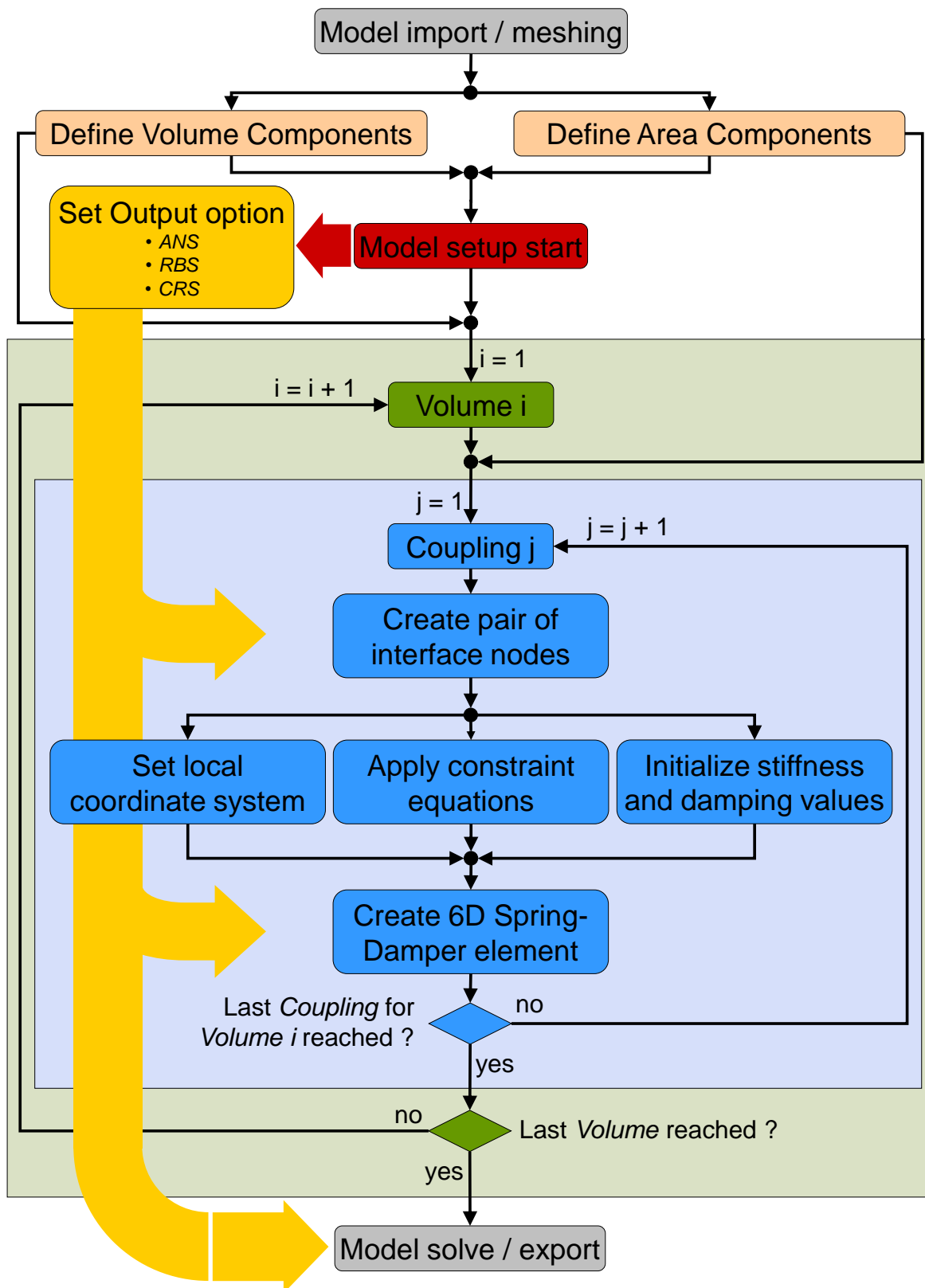
Figure 3.10: Process flow diagram of the simulation scripts in ANSYS
– with the three available option keys *(ANS - RBS - CRS)*.

Using the *ANS* option, the simulation run resumes where it stopped, and since at this stage the model is already complete and ready, the solving of the full finite element equations system starts. Depending on the user's choice, a static, modal, harmonic or transient analysis is performed, followed by the results evaluation during the post-processing phase: displacements, stresses, eigenfrequencies, eigenmodes and frequency responses can be graphically represented in the simulation environment.

With the *RBS* option, the mechanical data of the machine axes, including masses and moments of inertia, as well as the stiffness and damping values and positions of the couplings are exported and stored into one archive format file. This data set includes all the information for subsequent rigid body analyses performed in a Matlab-based stand-alone environment (chapter 6).

The *CRS* option is used for the export of the full system matrices in the standard ANSYS *.full* file format, containing the mass matrix M, the damping matrix D, the stiffness matrix K, the input matrix B and output matrix C. Additionally the parameters of the couplings, including the stiffness values, the damping values and the numbers of the connecting nodes are automatically stored. These files are required in the Matlab based mechatronic toolbox, allowing reduced coupled simulations of complete machine tools taking into account the flexibility of the structural parts (chapter 7).

Chapter 4

Rules for modeling machine tools

The present chapter is intended to give an overview of modeling techniques and rules concerning different critical aspects of machine tool models and to fulfil the needs of analyses focusing on the overall dynamical behavior. The discussion comprises two main issues:

- simplification and meshing methods for machine parts
  (intended as axis structural bodies)

- modeling guidelines for the crucial properties of the couplings/joints
  between the machine axes (connecting the axis structural bodies)

The objective is to give reliable and general guidelines providing a solid foundation for designers when investigating new machine concepts.

4.1   Meshing of a machine tool

The meshing of a complex machine tool structure is a crucial step in the process leading to an applicable simulation model. As mentioned in section 3.1, one of the main functions of a platform like ANSYS Workbench is to take advantage of its ever growing meshing power. In the logic of a transfer from a given CAD model to an efficient simulation model as automated and fast as possible, the meshing process is properly integrated if it's carried out in relatively short time and if the resulting FE model has just the sufficient size to meet the accuracy requirements, depending on the application case.

4.1.1   Meshing of structures

The direct use of a complex CAD model for machine tool FE analyses often leads to extremely large models having up to 10^6 DOFs. In this case, even a static analysis can become impracticable due to both arduous meshing effort and high computation times. It is therefore common practice to simplify a CAD model to obtain a smaller and more functional FE model.

In the *DesignModeler* environment of ANSYS Workbench, many functions have been integrated to modify the geometry in prevision of a facilitated meshing process. An assembly representing an X-Y table with a rotary axis B is used to illustrate the correlation between the effort of geometry manipulation and the resulting model size and computation time. In the most unfavorable (and unrealistic) case where a CAD geometry is directly exported without any geometry processing at all, the starting configuration in the finite element environment could look like in figure 4.1: 400 parts compose the assembly.
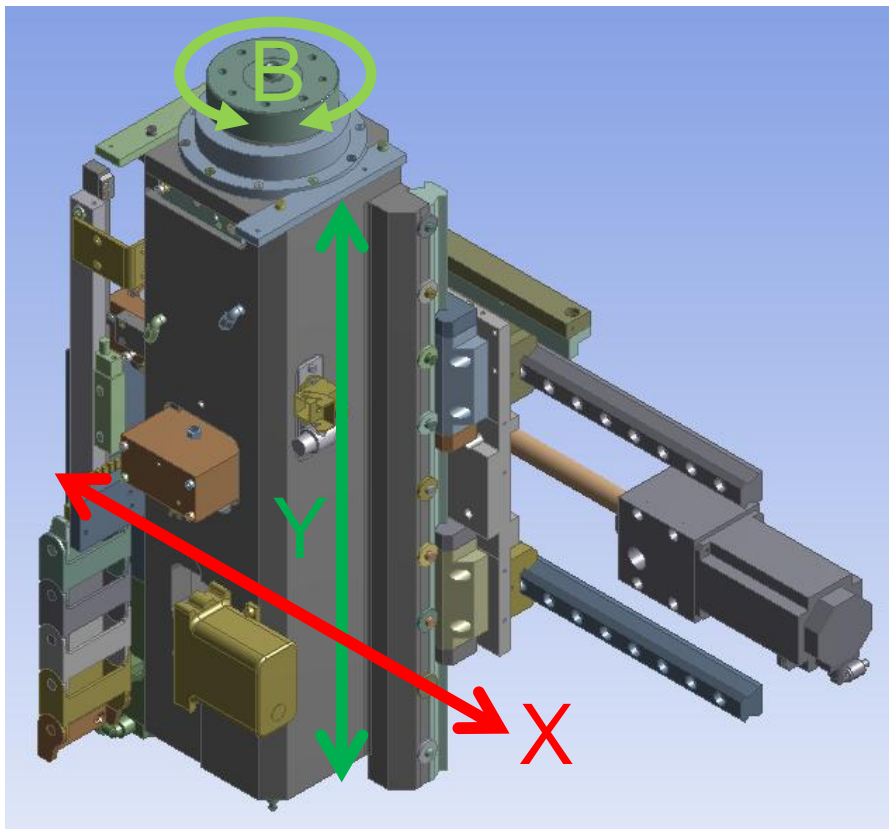
Figure 4.1: Typical geometry of a machine tool assembly without geometry processing.

The meshing progress is evaluated at five different stages, characterized by distinct successive simplification processes which are standard procedures in ANSYS *DesignModeler*:

– Unaltered model (figure 4.1) (not solved due to mesh size)
0. Elimination of small parts – set as Reference model (figure 4.2 left)
1. Automatic "Repair Hole" operations
2. Additional "Face Delete" operations
3. "Virtual Topology" and "Pinch" operations
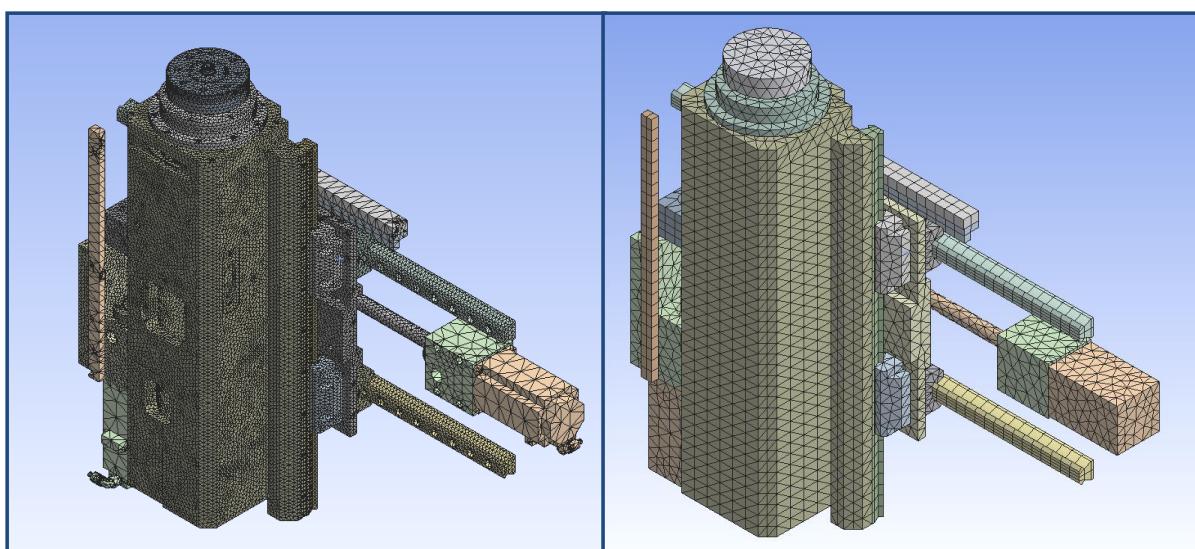4. Additional "Face Delete", "Slice" and "Boolean" operations (figure 4.2 right)

Figure 4.2: Meshed models at defeaturing steps 0 and 4 of geometry of figure 4.1.

The first step consists in eliminating all small parts, which have no structural relevance (screws, bolts, joints, plastic parts, hydraulic parts, etc.). Since the number of the parts to exclude is often higher than the number of parts to keep, the best strategy is to group the needed parts, and once all axes are defined, group the remaining parts into a separate set, which can be suppressed before proceeding to the simulation. In this example, the remaining parts after this first operation amount to 40, which corresponds to a reduction of 90% in parts number.

The second step takes advantage of modern defeaturing methods implemented in ANSYS *DesignModeler*. The "Repair Hole" algorithm allows selecting a minimal diameter, below which all holes are automatically deleted. This does not manage to act on every single hole (those with complex forms or those crossing each other are not recognized), but for a large variety of applications it is efficient enough to remove most of them.

The third and fourth steps apply the "Face delete", "Virtual Topology" and "Pinch" features to bypass the problems caused by construction constraints: small offsets between adjacent faces (needed for assembly), fillets, chamfers, complex cavities and pockets, etc.

The fifth and last step consists of additional manual operations to eliminate all unwanted features which managed to pass all previous defeaturing levels.

As discussed in section 3.2, the suggested method is based on the creation of components, making two adjacent volumes share their common faces and edges. The alternative is to consider the single parts isolated and to rest on the definition of contacts. There is no absolute solution which is best-suited in every case. It strongly depends on the type of structure considered. If a model is composed of a few parts, thus generating a limited and manageable number of contacts, it is advisable to use the contact capabilities, as merging topologies can lead to a more laborious mesh and a poorer elements quality. If a model is composed of many interconnected parts, it is difficult to keep an overview of all generated contacts, which, on the one hand is an important source of errors, and on the other hand leads to a larger equations system due the several extra constraint equations. In the case of a machine tool, the designer is frequently confronted to a structure with many parts, which is why, based on experience, the cases treated in this work are handled without contacts, at the expense of mesh quality and size, as depicted in figure 4.3.

With contacts enabled
(highlighted region)
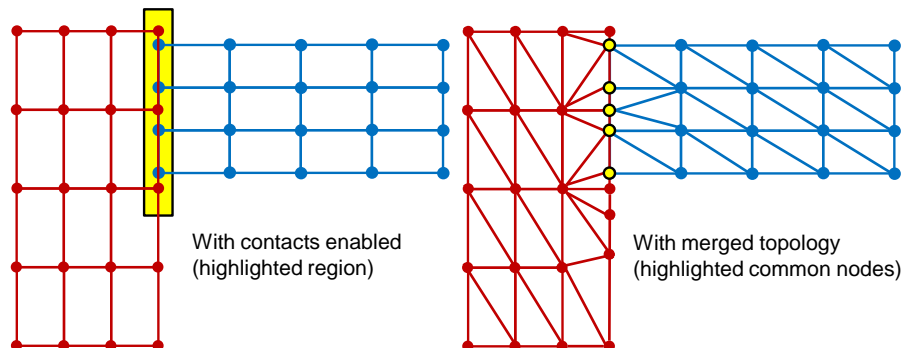
With merged topology
(highlighted common nodes)

Figure 4.3: Left: a regular plane mesh of two sweepable bodies connected through contacts. Right: a tetrahedron mesh connected by merging the adjacent edges and faces.

The comparative study to investigate the effects of subsequent simplification steps focuses on different criteria to evaluate the different models:

- Manual processing time
- Mesh size (number of nodes)
- Computational times (for static and modal analyses)
- Results (of static and modal analyses)

In figure 4.4, pre-processing related data are summarized. The interpretation of the different plots is intended to point out the correlation between the time needed to obtain a model and the gain in computation times:

Hence the first step leading to Model 1 seems ineluctable due to the huge size reduction. The benefits of the second simplification step leading to Model 2 are also relevant when looking at the further diminution of the number of nodes. For the remaining steps it then all depends on the number of iterations which are envisaged. There is no point investing one hour defeaturing a model to gain ten minutes of simulation time for a single analysis. But if several variations of the structure are foreseen, requiring possibly up to hundred iterations, then it could be worth going all the way to Model 4.
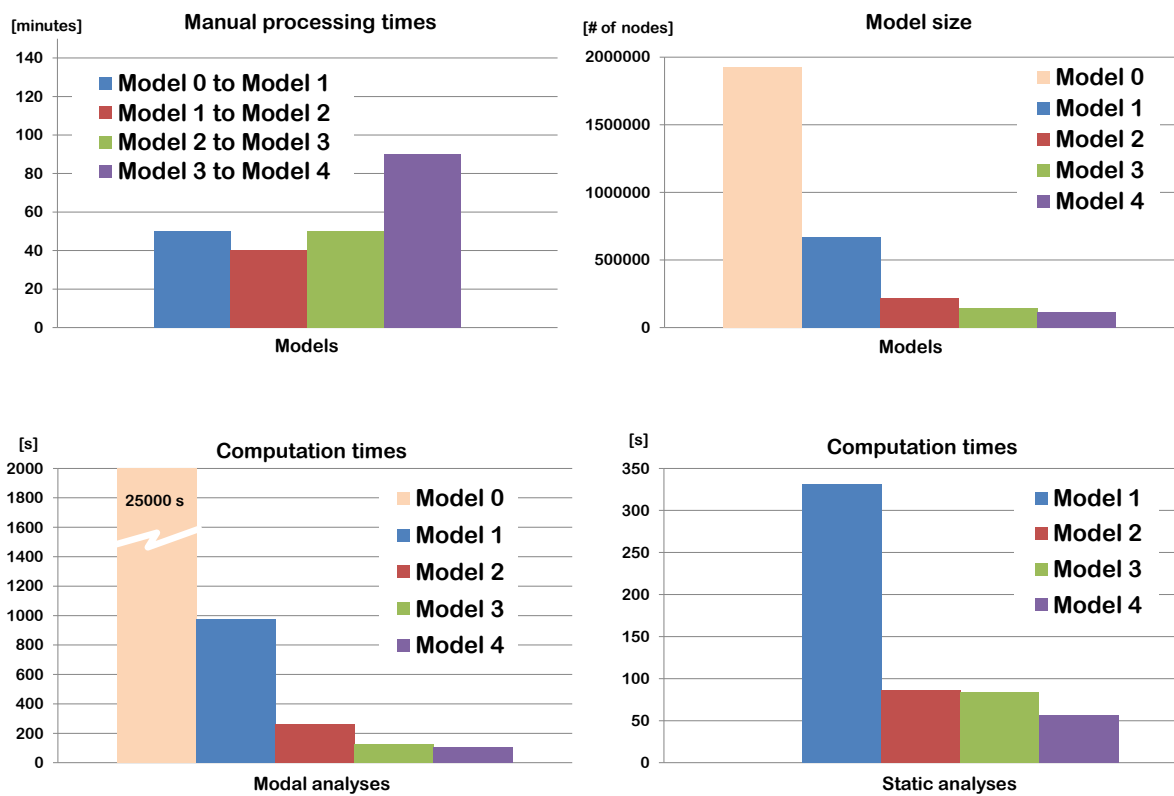
Figure 4.4: Comparison of manual processing times with analysis computation times.

As shown in figures 4.5 and 4.6, the decision of the model to use can exclusively be based on criteria concerning mesh size and computation times. The accuracy of the simulation is indeed not affected by this choice, as both the results of the static and modal analyses evidence differences under 5%.
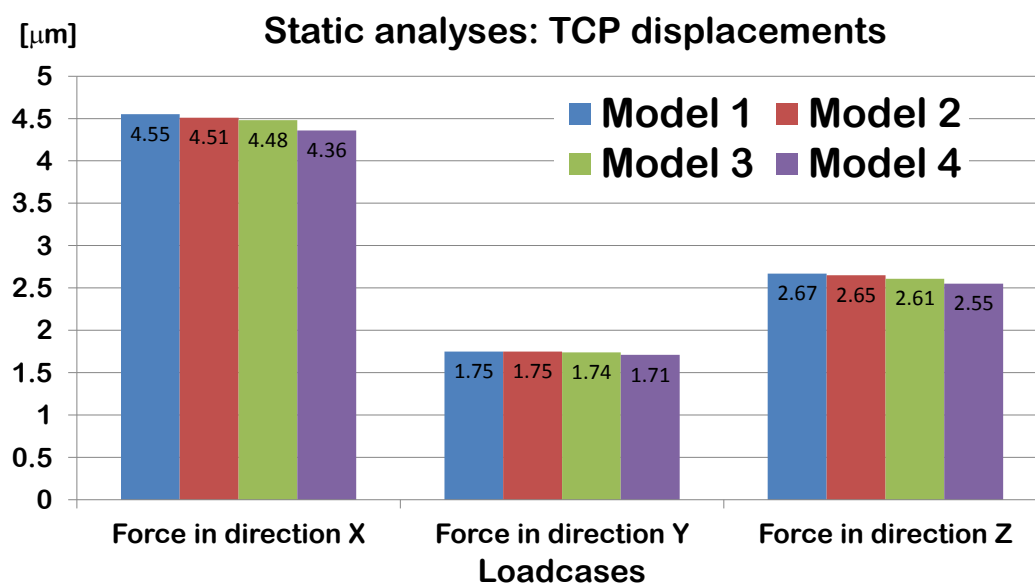
Figure 4.5: Comparison: results of static analyses for all models.
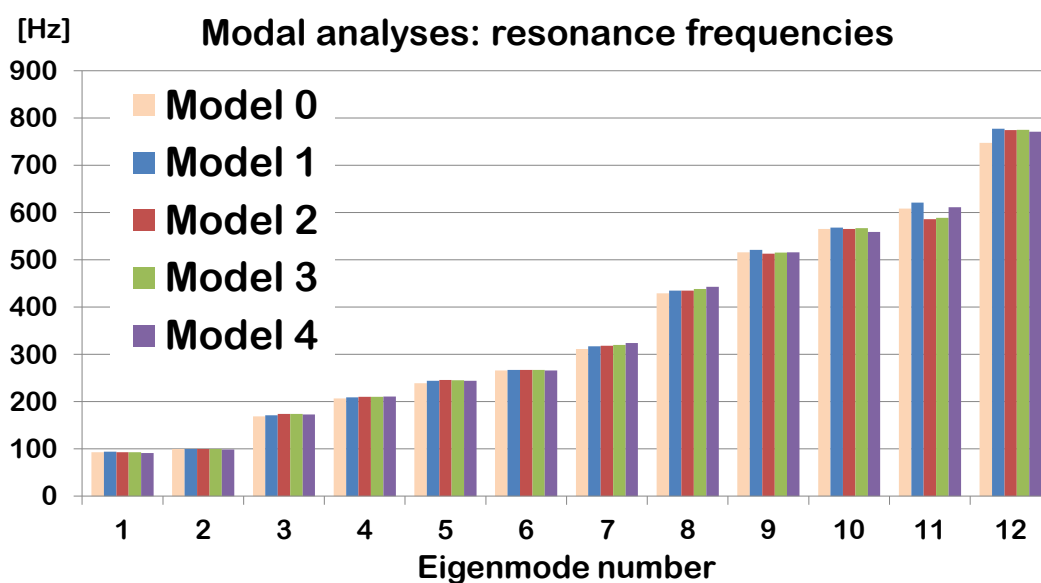

Figure 4.6: Comparison: results of modal analyses for all models.

Two other important aspects when processing a structure in a FE environment concern the element size and the element type: Choosing the mesh dimension for the discretization of a machine tool structure consists in identifying the minimal element size assuring a satisfactory result accuracy. Three different overall mesh sizes are tested on a basic two-axis machine tool structure composed of linear axes: a medium element size corresponding

approximately to the DEFAULT ANSYS settings, a COARSE element size 30% larger than the DEFAULT settings and a FINE element size 30% smaller than the DEFAULT settings. Of course there might be cases where specific parts of machine structures require special attention and an appropriate mesh, for example for thin geometries subject to high loads. The selection of the element types used to mesh a machine tool model is a compromise between mesh effort and resulting solving time. For structures typically imported from CAD models, three possibilities are available and are investigated here: a shell-based mesh, where entire "thin" plate-shaped 3D structural parts are transformed into 2D surfaces, a tetrahedron mesh consisting of 10-nodes volume elements and a hexahedron-dominant mesh where 20-nodes volume elements are created where applicable.

In figure 4.7, the outcome of the mesh survey is recapitulated, based on experiences in modeling machine tools. As expected, the shell model evidences the smallest mesh size and the shortest computation times. The hexahedron model, even though having a mesh size inferior to the tetrahedron model, requires higher solving times, because of the more time-consuming meshing process.

The results of static and modal analyses conducted on the models with different element sizes and types complete the analysis. For every one of the three quadratic mesh types, the results of the static analyses don't show any significant difference between the three corresponding element sizes. However, if the displacements obtained with the tetrahedron and the hexahedron meshes are quasi equivalent, the shell mesh reveals a more compliant behavior, which amounts to approximately 15% compared to the other two models. This is presumably due to the "thin plate" assumption adopted among the structure, whose criterion of a width-to-thickness ratio of at least 10 (ideally at least 20) is rarely fulfilled. The same erroneous effect is also outlined by the resonance frequencies found using the DEFAULT mesh size.

> *The bottom line is that a tetrahedron mesh with a reasonable element size is appropriate, allying a very low meshing effort and an accuracy equivalent to a hexahedron mesh. In contrast to structural analyses of single parts focusing on local strength aspects and the corresponding fatigue failures, the study of global static and dynamic behavior of entire machine tools allows a larger mesh size and a lower mesh quality.*

4.1.2 Meshing of components

The meshing of machine tool components, like carriages and rails of guiding systems, bearing elements and ball screw drives doesn't require special element types. Standard
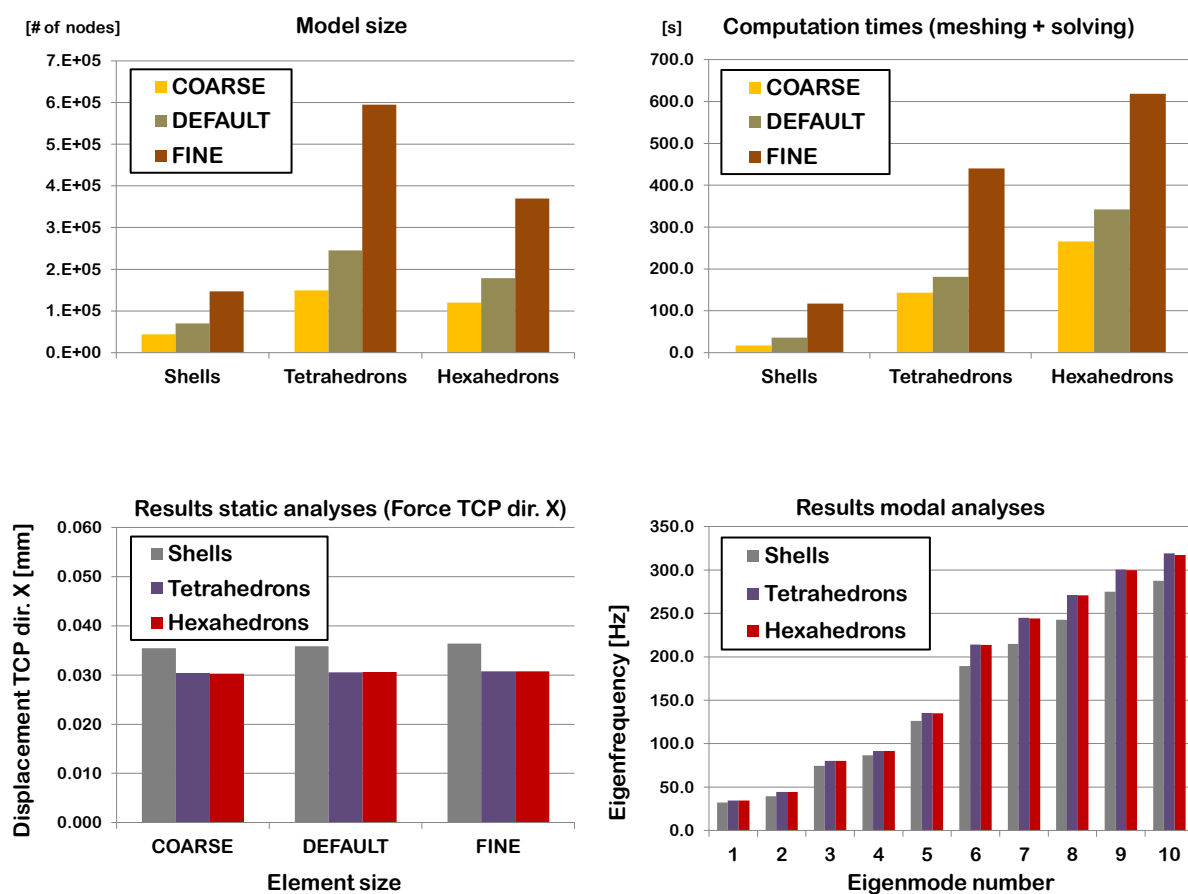
Figure 4.7: Comparison: mesh size and element type.

volume tetrahedron or hexahedron elements are mostly well suited, since in most cases, the components are modeled as volumes and due to the intention to consider the compliances of each component itself in the dynamic simulations. Some attention has to be put on the mesh size though. The couplings of the machine bodies, being defined by discrete spring-damper elements, involve two mass elements connected to the respective adjacent bodies by constraint equations, as described in section 3.3. In order to avoid local singular effects due to high load concentration, the components connected to the mass elements through the constraint equations need to have a mesh which is fine enough to assure a sufficient and uniform distribution of forces and moments on all the concerned nodes. For this reason, the mesh size of carriages, rails and bearings is chosen half the size of the global settings in the applications covered in the presented work.

4.2   Modeling of coupling elements

Components are defined as all the mechanical parts required for the internal motions bet-
ween machine axes and which are in most cases purchased from external suppliers (see
figure 2.15). Hence standard models obtained from the various providers are incorpo-
rated into the CAD geometry and their integration into the machine model needs to be
defined: linear guideways, ball screws, bearings and machine bed mounting elements are
characterized by the way they interact with the rest of the structure and by the inter-
nal stiffness and damping properties. For the former, it is favorable to apply the same
methodology as in section 4.1.1, that is using merged topology instead of contacts. For
the latter, standard contacts are replaced by alternative spring-damper elements. Their
implementation and their detailed characteristics are treated in a more comprehensive
manner in sections 4.2.1 and 4.2.2.

As mentioned in section 3.3, the area components at the interface locations are used to
create net-shaped constraint equations in order to distribute the joint loads over enough
nodes to avoid unrealistic local deformations. As shown in figure 4.8, the mechanical parts
(carriages, rails, bearing rings, ballscrews, nuts, etc.) are maintained in the model and
their geometry is used to define the connecting areas. For every set of areas, the associated
component is composed of all nodes belonging to those areas. At this stage the *APDL*
scripts, which are a result of the presented research work, execute the following sequence
of automated commands, subsequently for each interface, which will finalize the model of
the machine tool:

- Two additional nodes are created at the centroid location of the shorter part of the
  component (normally the carriage, bearing inner ring, nut, etc.).
- The additional nodes are meshed with a *MASS21* element (a small mass value is
  assigned to the elements).
- Through a set of constraint equations, one mass element (master node) is attached
  to the elements (slave nodes) of the moving part (carriage, bearing inner ring, nut,
  etc.) and the other mass element (master node) is attached to the elements (slave
  nodes) of the fixed part (rail, bearing outer ring, ballscrew, etc.).
- The script automatically retrieves the needed stiffness and damping coefficients from
  the *STIFFNESS* and *DAMPING* scripts (see figure 3.8) for the interface in question.
- The stiffness and damping values are used to initialize six *COMBIN14* elements
  between the two related master nodes at each joint location, which define all interface
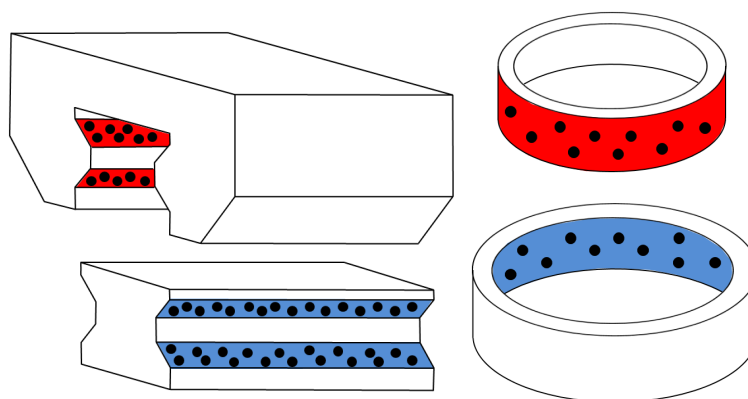 characteristics.

Figure 4.8: Component faces used to define the axis couplings, depicted with the belonging nodes.

4.2.1   Component stiffness parameters

The above section describes the "architecture" of the interfacing elements, but some crucial issues which greatly influence the final results need to be clarified in order to have joint models as accurate as possible. For this purpose, the following points concerning the modeling of linear guiding systems require further investigation:

- Given catalogue values, which Young's modulus is better suited for the modeling of carriages and rails? Shall the value of standard steel be used or shall the components be modeled as rigid?

- Given catalogue values, what is the optimal influence length of the net-shaped constraint equations for carriages and rails? (see figure 3.8)

- Given catalogue values, which type of constraint equations better corresponds to the real behavior of linear guidings, *CERIG*, which defines a fully rigid region between the master node and the slave nodes, or *RBE3*, which distributes the forces and moments of the master node to the slave nodes with customizable weighting rules?

The objective is to evaluate to what extent the boundary conditions inherent to the experimental setup or to the simulation model of the manufacturers (often consisting of one rigidifying half-space on the carriage side and one on the rail side) influence the way the coefficients have to be implemented in a machine tool FE model.

A comparative study between various simulation models and experimental data on a test-bed is intended to provide indications concerning the modeling method to reproduce the behavior of linear guiding systems. The tested components, called *A* and *B*, supplied by two different manufactures, have the following characteristics:

- Linear guideway manufacturer A: Size 35, roller elements, preload 8% of dynamic load rating, O-configuration.

- Linear guideway manufacturer B: Size 35, roller elements, preload 10% of dynamic load rating, X-configuration.

These two types are selected because they represent two of the most commonly used elements for standard middle-sized machine tools.

The test-bed consists of two plates of $700mm$ x $700mm$ connected by a variable number of carriages in different arrangements, as depicted in figure 4.9. Two options are investigated to test experimentally the characteristics of the rail-carriage interactions:

- applying vertical static loads at the coupling locations and measuring the relative vertical displacement between carriage and rail

- carrying out an experimental modal analysis and identifying the resonance modes of the upper plate in a frequency range of $0 - 1000Hz$
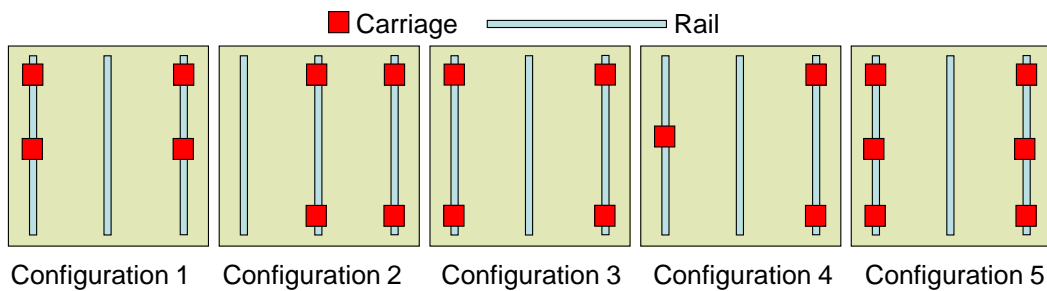
Figure 4.9: Five different carriage configurations are used in the experimental analyses on the test-bed.

For the component of supplier A in *configuration 3*, both options are evaluated to check the coherence between the two experimental methods. For the static case, a vertical force of $4kN$ is applied by means of a calibrated spring and a mechanical probe is used to capture the local elongation δ of the nominal distance h between the top side of the upper plate and the top side of the lower plate, as illustrated in figure 4.10. For the modal analyses, 3D acceleration sensors are used to retrieve the desired mode shapes resulting from a harmonic excitation generated by an impulse hammer. A grid of 36 points on the upper plate is selected, as shown in figure 4.11. Additionally, 8 points are selected on the lower plate, to ensure that the identified modes originate exclusively from the compliances in the connecting guideways.
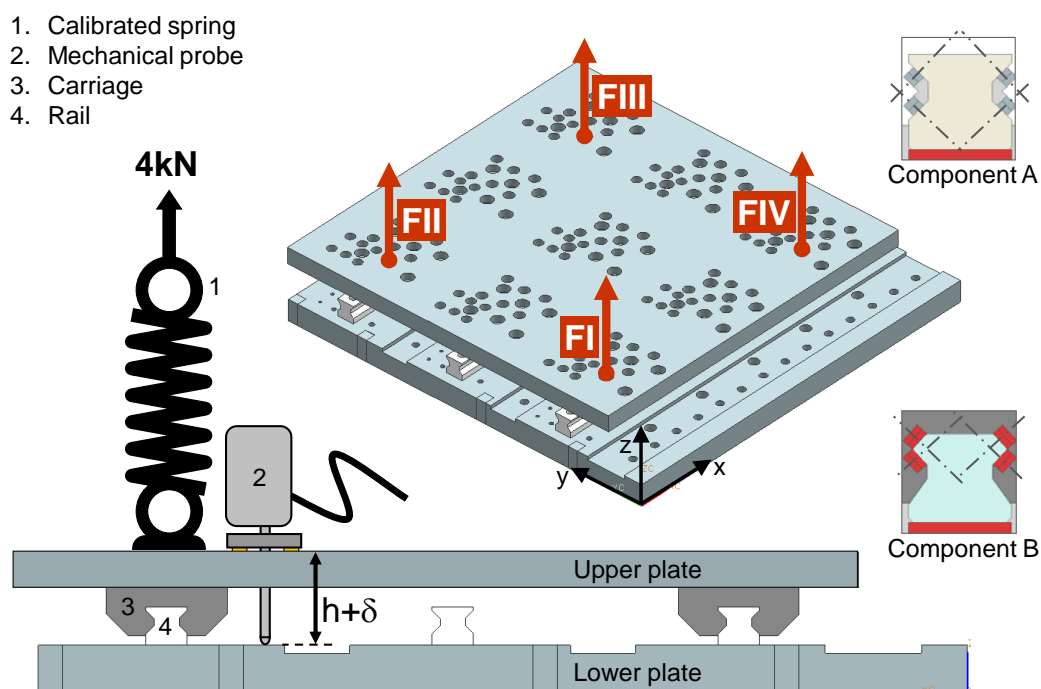
Figure 4.10: Experimental setup for static measurements on the test-bed.

In order to establish modeling guidelines for linear guiding systems, a detailed FE model of the test-bed allowing six distinct modeling variants of the rail-carriage couplings is generated (table 4.1):

Table 4.1: Description of the six modeling variants of the rail-carriage couplings.

	Young's modulus rails over carriage length	Young's modulus carriages over carriage length	Influence length of constraint equations (in % of carriage length)
ALL_STR	rigid *	rigid *	100 %
SEM_STR	rigid *	E = 210 GPa	100 %
SEM_FLX	E = 210 GPa	rigid *	100 %
ALL_FLX_2	E = 210 GPa	E = 210 GPa	100 %
ALL_FLX_1	E = 210 GPa	E = 210 GPa	50 %
ALL_FLX_0	E = 210 GPa	E = 210 GPa	25 %
			* rigid: E = 1000 • 210GPa
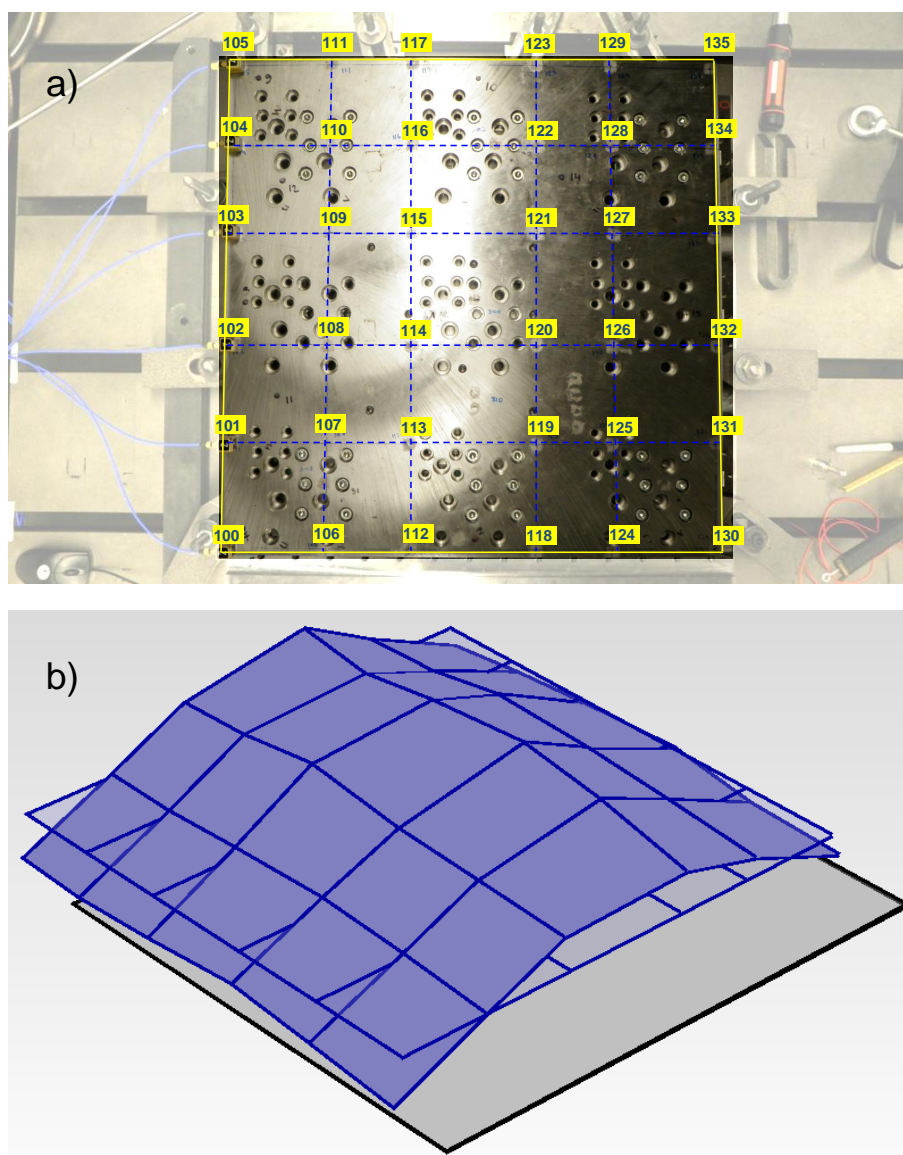
Figure 4.11: Experimental setup for modal measurements on the test-bed.
a) Grid of 36 $(100 - 135)$ measurement points on the upper plate
b) Illustrative identified mode shape after evaluation of the measurement data

Both the static and modal loadcases are reproduced using the FE model. The experimental results serve as reference to select the preferential modeling technique to be incorporated into the simulation model.

The comparison of the static analyses are based on the average deviation between measured and simulated data for the four successive forces shown in figure 4.10. The relative displacements between upper and lower plates for a force of $4kN$ are simulated (figure 4.12a), measured (figure 4.12b) and juxtaposed for a direct evaluation.

The best results are obtained using the modeling variants *ALL_FLX_2* and *SEM_STR*, which evidence an error of about 6%, as it can be deduced from figure 4.13.
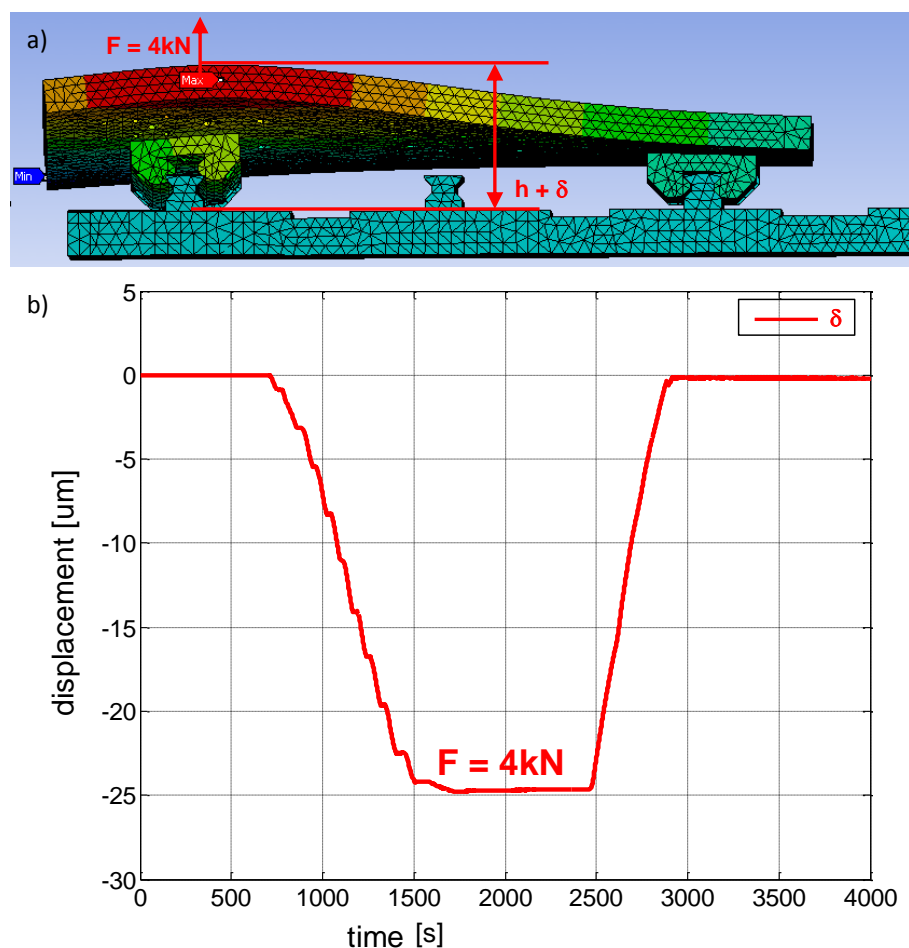

Figure 4.12: Simulated (a) and experimental (b) static compliances
of the test-bed with components A in carriage configuration 3.

Looking at the results of the modal analyses of the test-bed with components *A* and *B* in the five configurations described in figure 4.9, the best matches are obtained with the modeling techniques *ALL_FLX_1*, *ALL_FLX_2* and *SEM_STR_2*, as recognizable in tables 4.3 and 4.4. The summarized values represent the percentage errors of the nine first eigenfrequencies between the different FE models and the experimental results. The matching process takes into consideration both the form of the mode shapes and the corresponding eigenfrequencies, as illustrated in figure 4.15 for components *A* in configuration 3 and with the modeling variant ALL_FLX_2. In order to rigorously verify the correspondence of the eigenvectors, the analysis of figure 4.15 is completed by the computation of the MAC (Modal Assurance Criterion) matrix.
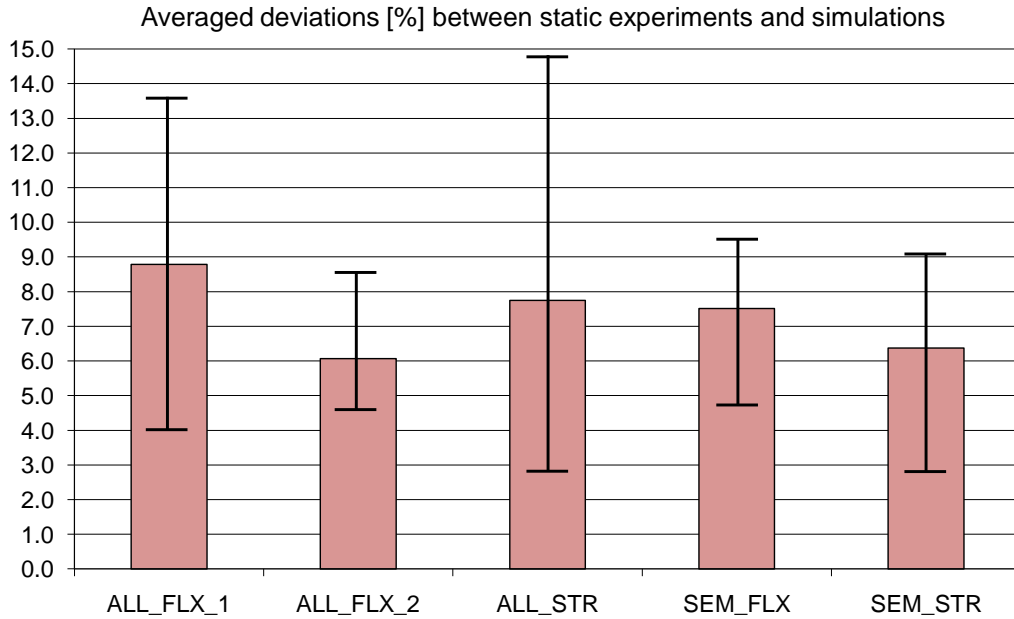
Figure 4.13: Matching of static compliances of the test-bed with components A in carriage configuration 3 (for the first five modeling variants (table 4.1)).

If the experimental modal analysis is carried out in optimal conditions, no phase shift occurs between the single measured points. For the measurements of simple structures, where proportional damping can be assumed, or in structures with relatively low damping, this is mostly the case. In complex structures, with local damping effects (as e.g. in linear guideways), other methods should be used, like e.g. the phase resonance method [119]. Another solution is to transform the measured eigenvectors to correct possible phase shifts. The measured complex eigenvectors must indeed be compared with the undamped eigenvectors resulting from the FE simulations. In order to eliminate the effect of damping on the phase, the measured eigenmodes are renormed. This transformation (figure 4.14) is carried out by means of a process which scales the eigenvector relatively to a reference point, according to the equations (4.1):

$$\begin{aligned} \text{original: } \phi_{rn} &= a + bi = Ae^{\gamma i} \\ \text{scaled: } \phi_{rn,s} &= A \cdot cos(\gamma - \gamma_{ref}) \end{aligned} \qquad (4.1)$$

The MAC matrix is then computed between the new scaled experimental eigenvectors and the corresponding simulated eigenvectors, according to equation (4.2). The MAC describes the angle between two vectors, thus verifying their orthogonality.
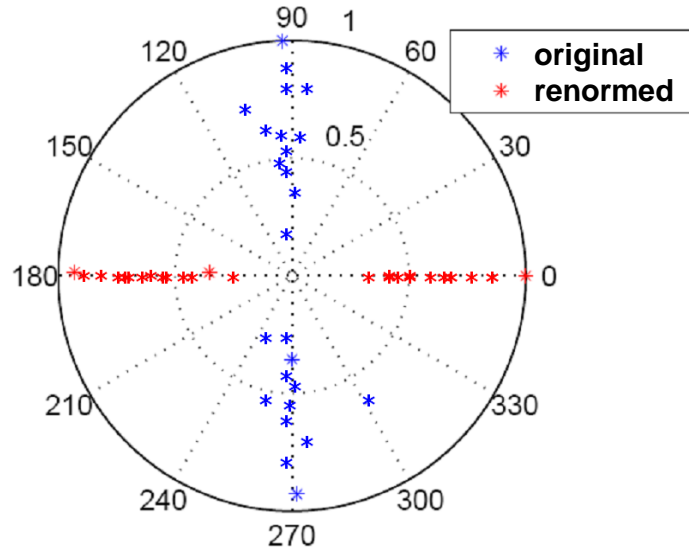
Figure 4.14: Illustration of the scaling process of the eigenvectors.

$$MAC(k,l) = \frac{(\phi_{mk}^T \phi_{sl})^2}{(\phi_{mk}^T \phi_{mk})(\phi_{sl}^T \phi_{sl})} \tag{4.2}$$

ϕ_{mk} :   measured eigenvector k

ϕ_{sl} :   simulated eigenvector l

ideal case: $MAC(k,l) = \begin{cases} 1 \text{ for } k = l \\ 0 \text{ otherwise} \end{cases}$

For the case considered here, the MAC matrix of the first nine eigenmodes takes the form depicted in table 4.2. The results outline a diagonal minimum value of 0.78, which indicates a good correlation between the eigenvectors. For the rest of the matching process, the comparison is limited to the visual inspection of the mode shapes and to the eigenfrequency deviations.

For the model ALL_FLX_2, which is the easiest to implement, an average error of ca. 2.5% for components A and of ca. 5.5% for components B is observed.

The results establish the following general modeling guidelines, which best fit the experimental data with respect to the stiffness parameters of linear guiding systems:

> *The carriage and the rail must be assigned the standard Young's modulus of steel, that is $2.1 \cdot 10^5 MPa$, and the influence domain size of the constraint equations of type* CERIG *must equal the length of the carriage.*
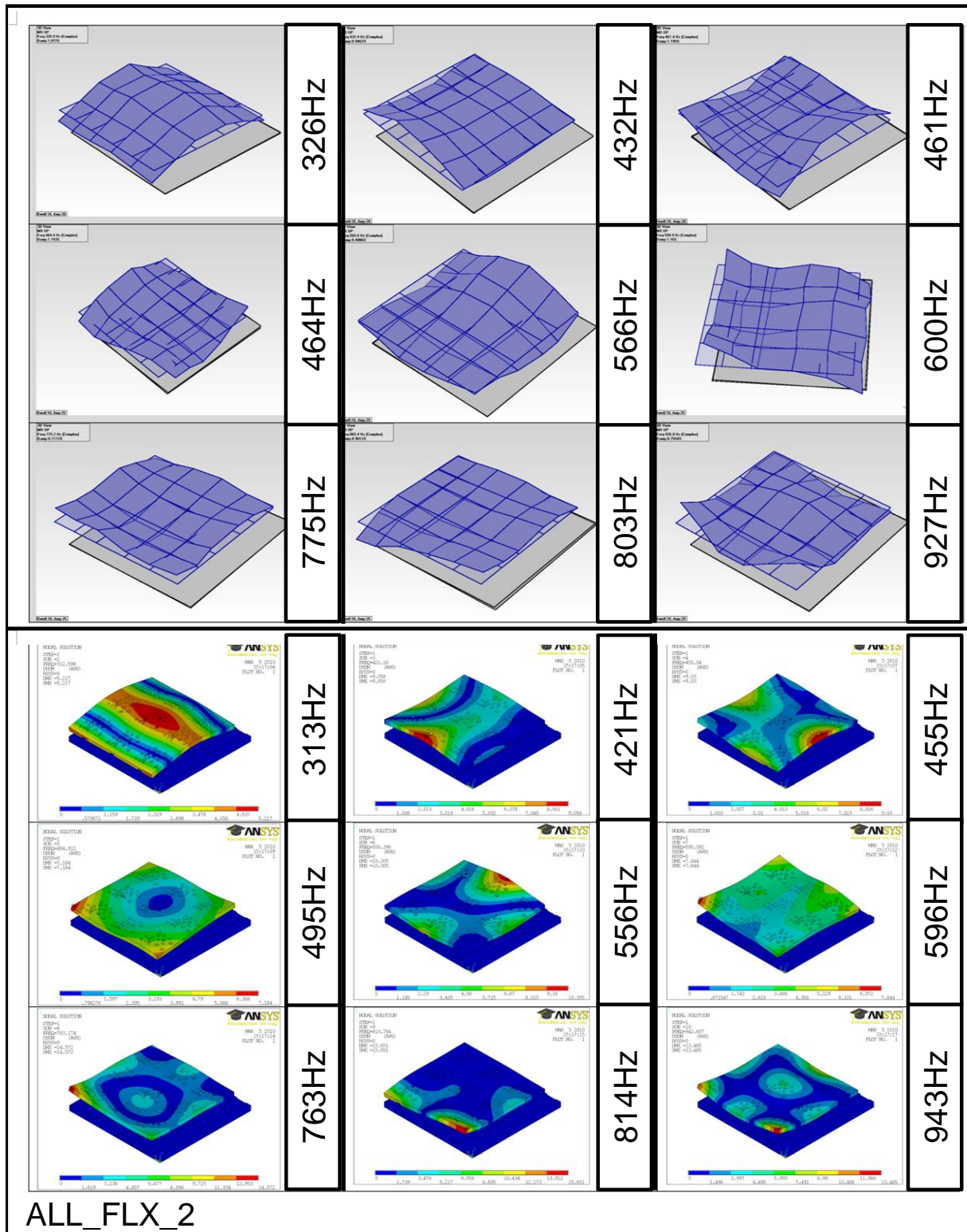
Figure 4.15: Simulated (modeling variant ALL_FLX_2) and experimental resonance modes of the test-bed with components A in configuration 3.

Table 4.2: MAC matrix of the first 9 eigenmodes of the test-bed with components A in configuration 3.

MAC	Mode 1	Mode 2	Mode 3	Mode 4	Mode 5	Mode 6	Mode 7	Mode 8	Mode 9
Mode 1	0.95	0.09	0.02	0.01	0.01	0.01	0.14	0.02	0.07
Mode 2	0.01	0.81	0.07	0.12	0.07	0.01	0.18	0.00	0.01
Mode 3	0.10	0.07	0.94	0.13	0.07	0.01	0.00	0.02	0.00
Mode 4	0.04	0.12	0.34	0.78	0.03	0.00	0.00	0.00	0.00
Mode 5	0.03	0.05	0.01	0.01	0.86	0.16	0.05	0.00	0.04
Mode 6	0.01	0.00	0.04	0.02	0.18	0.82	0.09	0.12	0.00
Mode 7	0.02	0.28	0.02	0.01	0.12	0.00	0.86	0.37	0.43
Mode 8	0.00	0.03	0.00	0.01	0.09	0.10	0.09	0.83	0.03
Mode 9	0.05	0.01	0.02	0.00	0.17	0.01	0.23	0.08	0.90

Table 4.3: Matching of resonance modes of the test-bed with components A
(Average deviations of eigenfrequencies of corresponding modes 1–9).

Component A		Modeling variants					
	Modes 1-9	ALL_FLX_0	ALL_FLX_1	ALL_FLX_2	ALL_STR	SEM_FLX	SEM_STR
CONFIGURATION 1	AVERAGE DEVIATION	2.8 %	2.0 %	1.9 %	3.9 %	2.8 %	2.1 %
CONFIGURATION 2	AVERAGE DEVIATION	3.4 %	2.3 %	2.3 %	6.5 %	5.9 %	3.1 %
CONFIGURATION 3	AVERAGE DEVIATION	4.1 %	2.9 %	2.4 %	5.1 %	3.0 %	2.6 %
CONFIGURATION 4	AVERAGE DEVIATION	3.1 %	2.6 %	2.7 %	5.5 %	4.1 %	3.2 %
CONFIGURATION 5	AVERAGE DEVIATION	4.2 %	3.4 %	3.0 %	6.4 %	4.7 %	3.6 %

These guidelines are tested and confirmed by the correlation between FE simulations and measurement data on real machines by comparing results of static and modal analyses (sections 5.1 and 5.2). The same static and modal analyses also serve as validation of the modeling methodology for rotary bearings. The recommendation is based on the same principle, i.e.:

Table 4.4: Matching of resonance modes of the test-bed with components B
(Average deviations of eigenfrequencies of corresponding modes 1–9).

Component B		Modeling variants					
	Modes 1-9	ALL_FLX_0	ALL_FLX_1	ALL_FLX_2	ALL_STR	SEM_FLX	SEM_STR
CONFIGURATION 1	AVERAGE DEVIATION	7.2 %	5.8 %	5.9 %	5.5 %	6.4 %	4.8 %
CONFIGURATION 2	AVERAGE DEVIATION	7.0 %	5.6 %	7.0 %	9.8 %	9.4 %	7.4 %
CONFIGURATION 3	AVERAGE DEVIATION	8.7 %	5.2 %	4.8 %	7.2 %	6.1 %	4.8 %
CONFIGURATION 4	AVERAGE DEVIATION	7.3 %	3.8 %	4.4 %	6.9 %	5.4 %	4.5 %
CONFIGURATION 5	AVERAGE DEVIATION	9.9 %	6.5 %	6.0 %	7.1 %	6.0 %	5.6 %

> *The influence domain size of the constraint equations must equal the width of the bearings, but with* RBE3 *constraint equations, instead of* CERIG*, which avoid an unnatural stiffening of the whole component.*

Concerning the coupling behavior occurring at the interfaces between the nut and the ballscrew of a drive system, the assumption is made that the only coefficient needed to be integrated into the models is the longitudinal stiffness (K_x). Complex stiffness matrices as the ones used in [10] are not considered. This represents a major simplification of the dynamic behavior of the drive system, but is legitimated by the fact that the analyses of complete machine tools carried out in this thesis mainly focus on the global structural behavior at the TCP and not on the detailed dynamic phenomena in the drive components.

The design of the test-bed also enables different configurations of the guiding system, which means that the distances between carriages, resp. between rails can be changed. The supposition is that, depending on the configuration, the lateral stiffness coefficients (K_y) to be implemented in the FE model need to be adjusted in order to correctly reproduce the experimental behavior. This is verified with help of the experimental modal analyses carried out with both components A and B in the five configurations shown in figure 4.9. The evaluation of the influence of the configuration focuses on the yaw mode, consisting of a rotation of the top plate about the vertical axis. The eigenfrequencies of these measured modes in all configurations are compared with the corresponding eigenfrequencies obtained with the simulation models. No significant correlation between the relative error and the configuration can be identified from the plot in figure 4.16. It can be nevertheless established, that the lateral stiffness coefficients provided by the manufacturers tend to be too high for component A and too low for component B.
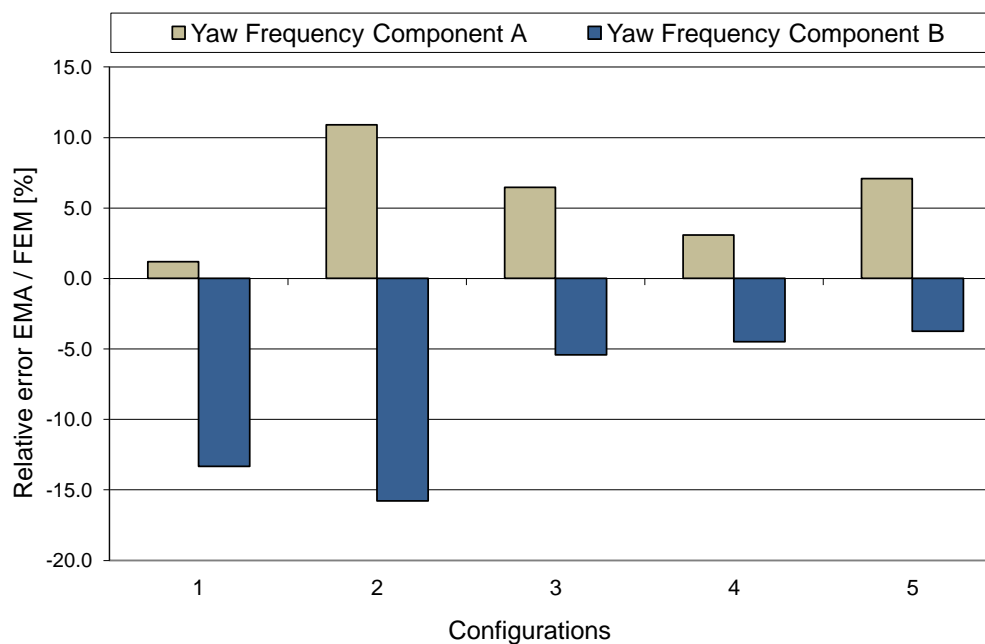
Figure 4.16: Matching of the measured and simulated yaw eigenfrequencies for components A and B.

4.2.2 Component damping parameters

The previous section focused on the stiffness parameters of machine tool couplings, in particular of linear guideways. Various identification methods are available to reliably estimate stiffness values and lead to acceptable model errors of static and modal analyses. When investigating a machine tool in the time or frequency domain, additional information concerning damping in coupling elements is required. As discussed in section 2.1.5, this is associated with a much larger parameter uncertainty, the effective damping depending on several factors. Given a structure whose static and modal behavior is well known, it is however possible to identify case specific damping values in a fast and straightforward manner. The test-bed introduced in section 4.2.1 serves as basis to illustrate the principle: using the components of type A in *configuration 4* (3 carriages), preselected experimental harmonic responses are reproduced using the simulation model and the default physical damping (the start value is set to $3.5 Ns/mm$) parameters are adjusted until a satisfactory match is obtained.

Two resonance modes, dominated respectively by a vertical and a horizontal relative displacement between the rails and the carriages, are targeted (figure 4.17). The corresponding measured resonance peaks are isolated and compared with the varying peaks

obtained via simulation. The final fit results in the two matching transfer functions displayed in figures 4.18 and 4.19. The two criteria used to identify an appropriate value of the physical damping coefficient in the carriages are the amplitude and the width of the peaks. It has to be noted that the physical stiffness coefficients are not adjusted, the values provided by the manufacturer are used in the finite element model.
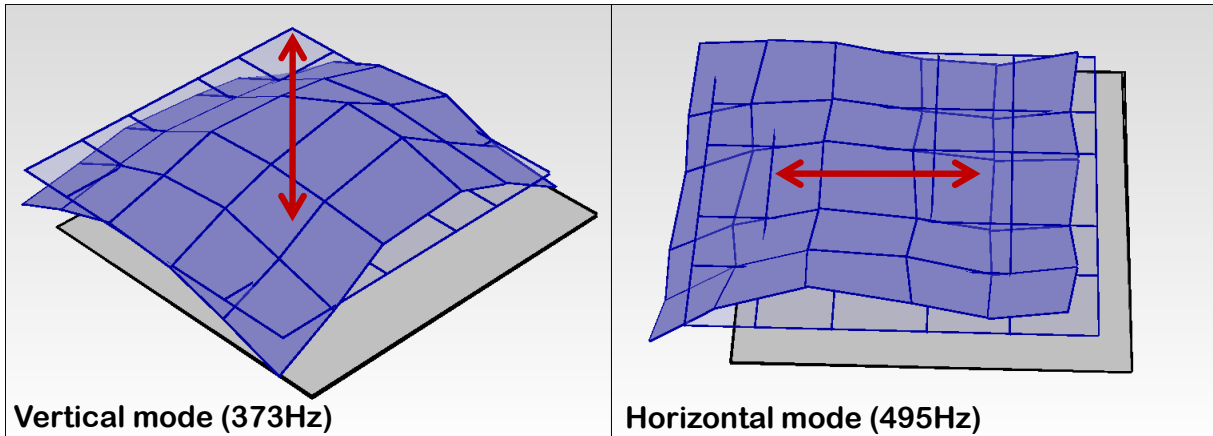

Figure 4.17: Resonance modes used as targets for damping parameters matching.

The fitting of the two resonance modes is achieved with vertical and horizontal damping parameters in all three carriages of ca. $12 Ns/mm$. These values are valid for this structure, in this configuration and in the given conditions. It is probable that a part of the structural damping comes from the plate fixings, where local friction effects are likely to occur. It is hence difficult to isolate the damping contribution coming purely from the interaction between the rollers and the carriages, respectively the rails and from the guideway wipers. Such detailed investigations would need a proper experimental setup whose concern is primarily damping identification. The point to evidence here is a methodology which, based on a few simple measurements, allows a fast identification of machine tool parameters. How the simulation model is derived will be presented more in detail in chapter 7. As illustration of the effectiveness of the simulation model, a damping sensitivity analysis confronting material damping to coupling damping is presented in figures 4.20 and 4.21. First the value of the structural β damping (nominal value: $\beta = 1e^{-6}s^{-1}$) is varied, and then the values of the physical damping d_{cpl} in the carriages (nominal value: $d_{cpl} = 12 Ns/mm$). Using a multiplication factor between 0.5 and 1.5, the observation that the damping sources in machine tools are essentially concentrated in the coupling joints finds further evidence, since the effect of varying the β coefficient is practically null.
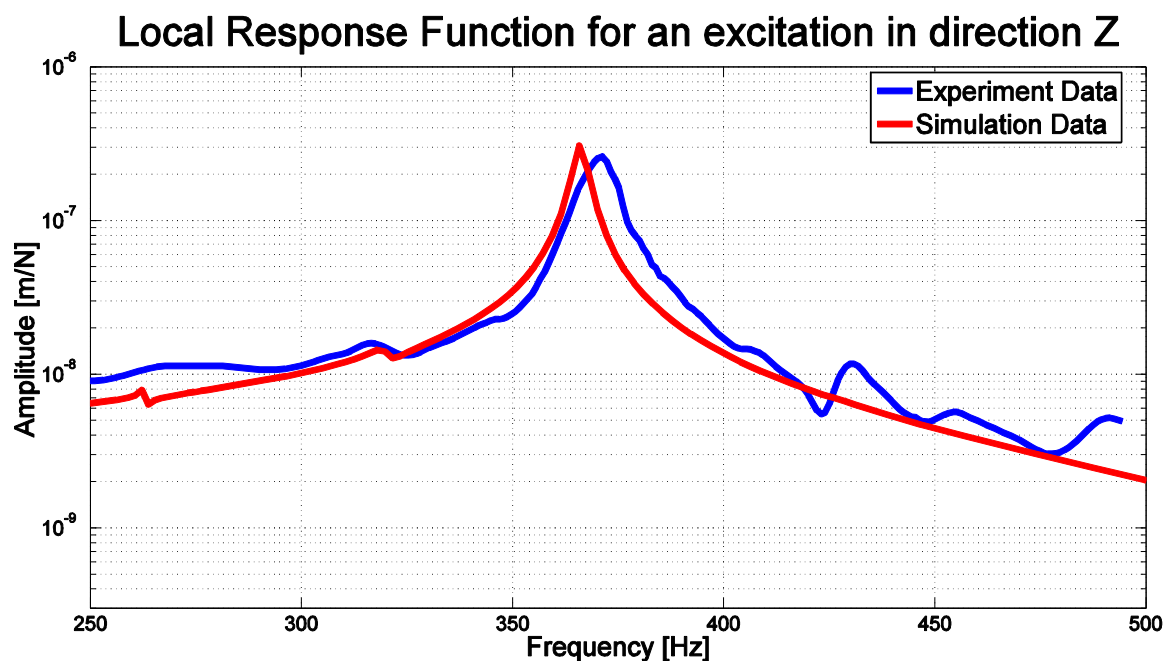
Figure 4.18: Superposed experimental and simulated harmonic responses
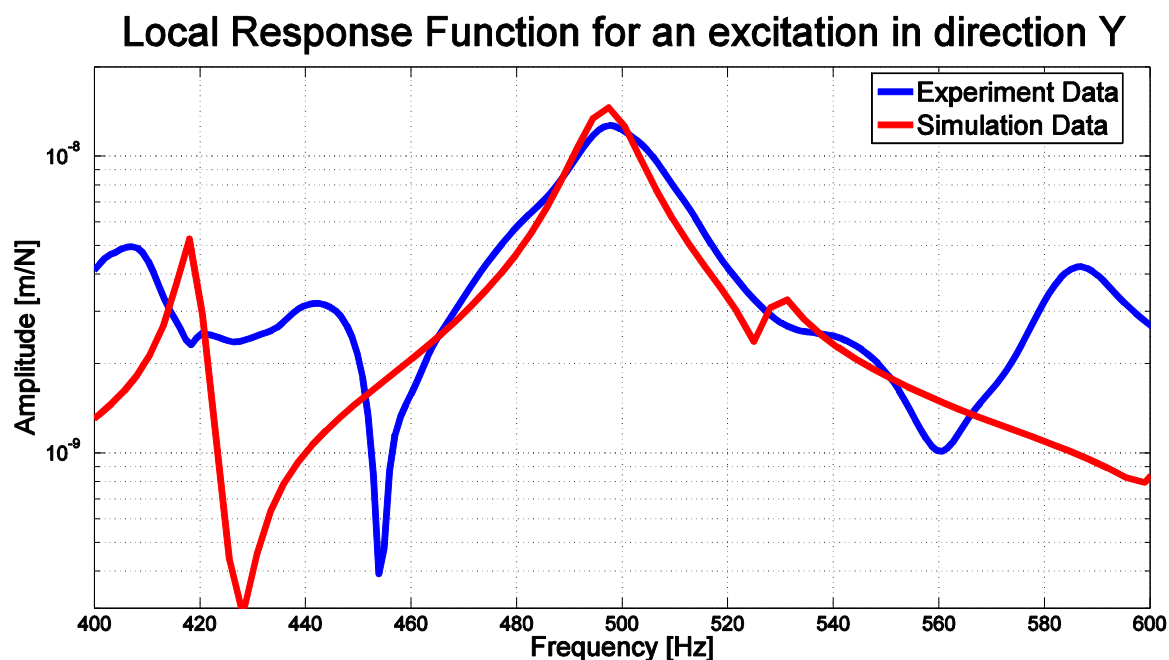of the vertical mode (373Hz) after adjusting of damping parameters.

Figure 4.19: Superposed experimental and simulated harmonic responses
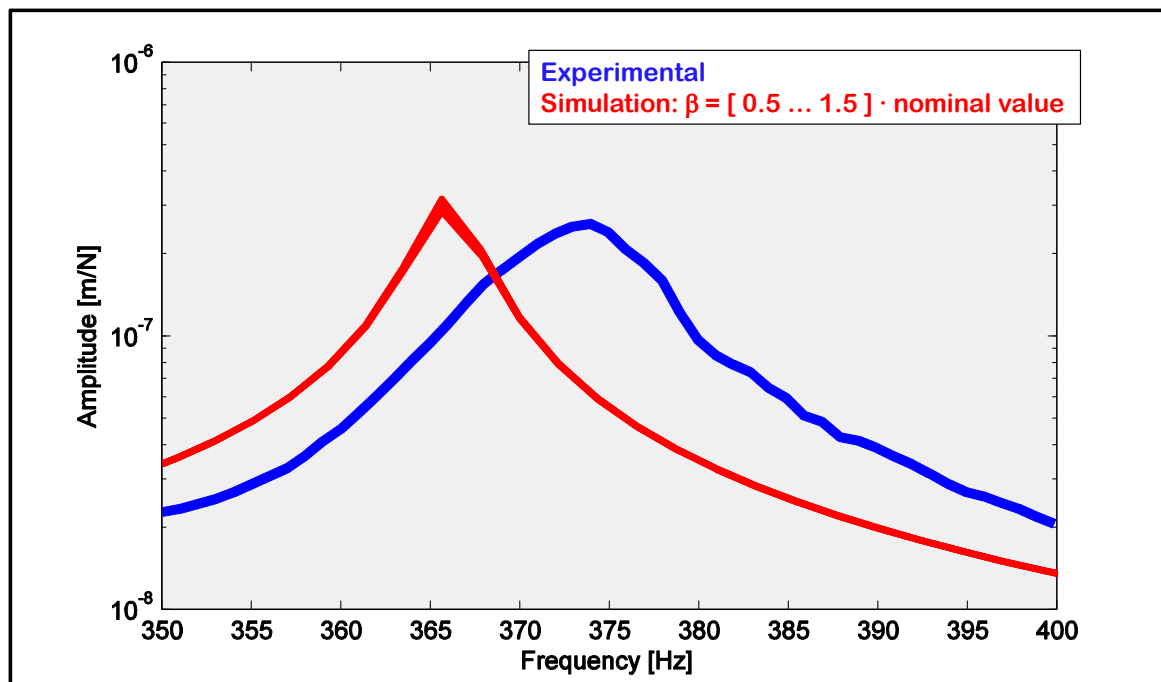of the horizontal mode (495Hz) after adjusting of damping parameters.

Figure 4.20: Effect of structural beta damping variation on simulated local harmonic response (Variation irrelevant → all red curves superposed).
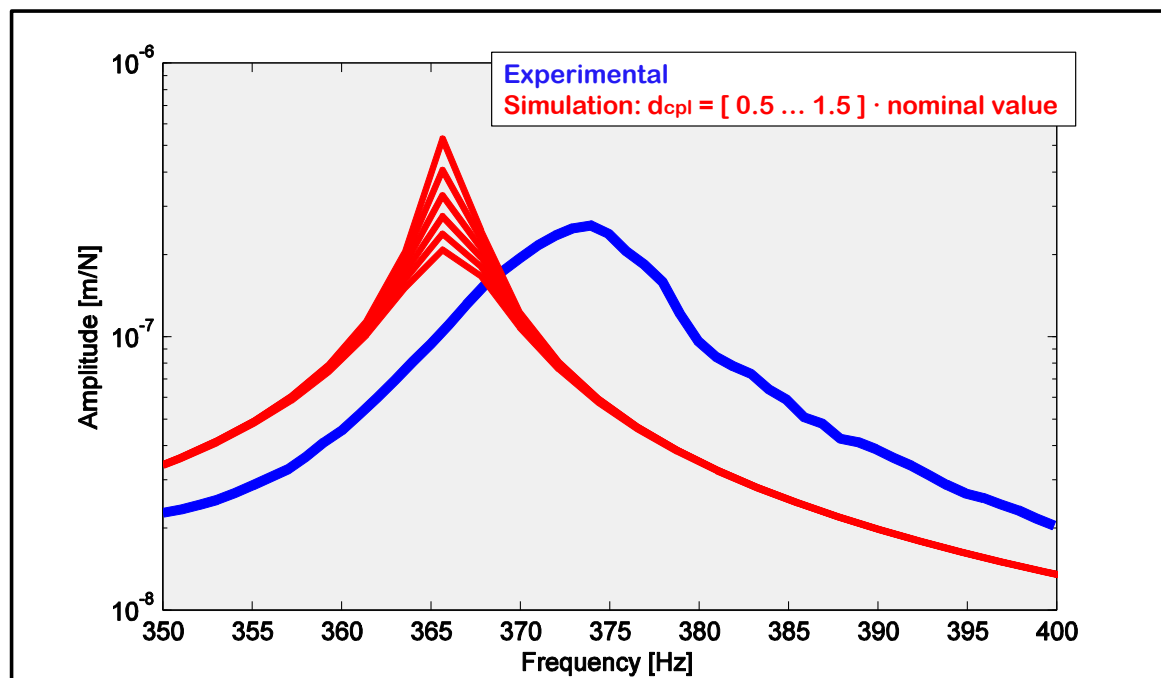

Figure 4.21: Effect of physical coupling damping variation on simulated local harmonic response.

Chapter 5

Analysis of machine tools

Roller linear guiding systems of size 35 are often used in machine tools. It was shown that, provided that the established modeling rules are observed, the catalogue stiffness values made available by guideway systems suppliers can be integrated in a FE simulation model. In order to verify the modeling guidelines derived in chapter 4, a series of experimental tests are carried out on two real machines called A and B and reproduced by means of detailed simulation models, as described in the following sections 5.1 and 5.2. The two structures investigated in the present chapter consist of a machine bed made of spheroidal steel and of linear guiding systems corresponding to the components of types A and B introduced in section 4.2.1.

5.1 Experimental static analysis of machine tools

The objective of the static analyses carried out on the machine tools is to evaluate the static stiffness of the entire structural loop at the TCP, i.e. the relative displacement between workpiece and tool resulting from a force acting on both sides in opposite directions.

5.1.1 Experimental setup for static measurements

For this purpose, a piezo force sensor is mounted at the workpiece location and is brought in contact with an area on the tool side in order to generate the desired mutual load. For every motion direction X, Y and Z of the machine axes, feed steps of $10\mu m$, measured at the axis linear scale, are executed through the axes numerical control. The resulting force variation is measured online and represented in graphical form, as exemplarily illustrated in figure 5.1.

Given the perfectly linear behavior in the considered force range, the experimental static stiffness is evaluated at the maximum measured force.
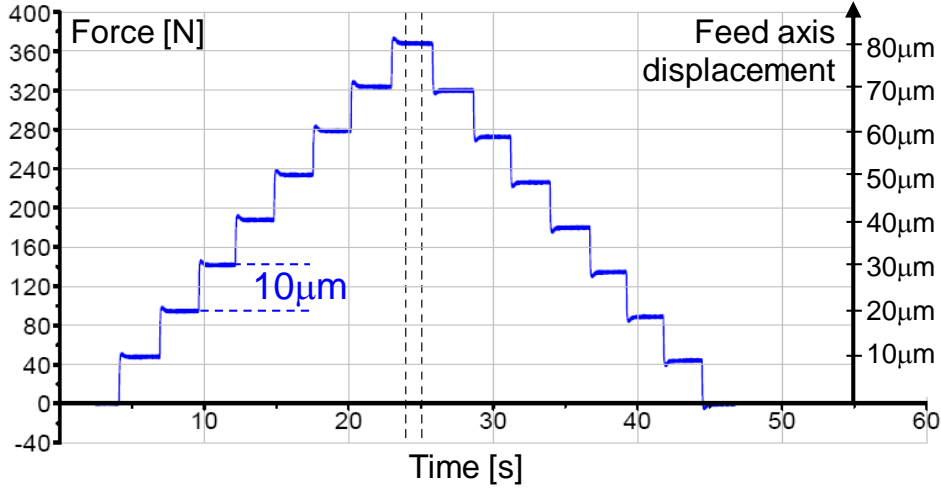

Figure 5.1: Typical force-displacement relation for a static measurement run.

5.1.2   Static comparison principle

In order to reproduce the measurements, a complete FE model is generated and configured in the same axis positions as the measured machine, including the piezo mounting parts. Two forces equal in amplitude but of opposed directions are applied at the contact location between the piezo extremity and an area on the housing of the tool side. The structural stiffness is then given by superposing the resulting displacements of the two nodes the forces are applied to. The approximated static equivalence of the model with the experimental conditions is achieved by setting an artificially high drive stiffness to avoid any relative displacement at the encoder. This principle is illustrated in figure 5.2.

$$\frac{1}{K_{tot}} = \frac{1}{K_{basis}} + \frac{1}{K_{c1}} + \frac{1}{K_{c2}} = \frac{x_{TCP}}{F_{TCP}}$$

5.1.3   Validation of machine FE models with static analyses

For a comprehensive validation of the static behavior, different loadcases are implemented on the machines of both manufacturers. For machine A, four different loading configurations are investigated, one in axis direction X, one in axis direction Y and two in axis direction Z. The respective positions of the piezo and the contact locations are shown in figures 5.3 and 5.4.
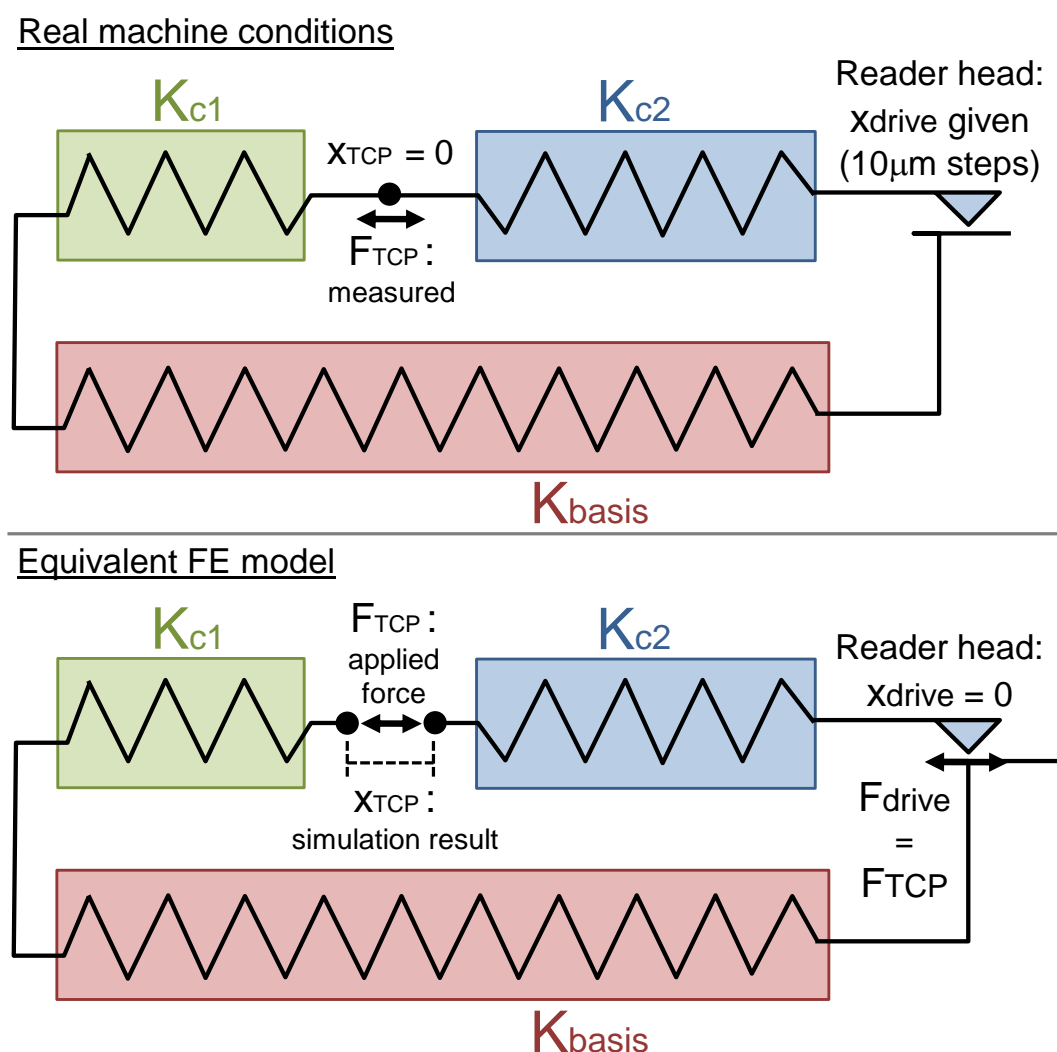
Figure 5.2: Equivalence principle between experimental conditions and
a schematized representation of the corresponding FE simulation model.

- FORCE_X: Piezo on workpiece spindle - Load applied on main spindle housing
- FORCE_Y: Piezo on axis B table - Load applied on main spindle housing
- FORCE_Za: Piezo on workpiece spindle - Load applied on main spindle flange
- FORCE_Zb: Piezo on axis B table - Load applied on main spindle flange

For machine B, three loading conditions are examined, one in each axis direction, as illustrated in figures 5.5 and 5.6.

- FORCE_X: Piezo on workpiece spindle - Load applied on main spindle
- FORCE_Y: Piezo on workpiece spindle - Load applied on main spindle
- FORCE_Z: Piezo on workpiece spindle - Load applied on main spindle
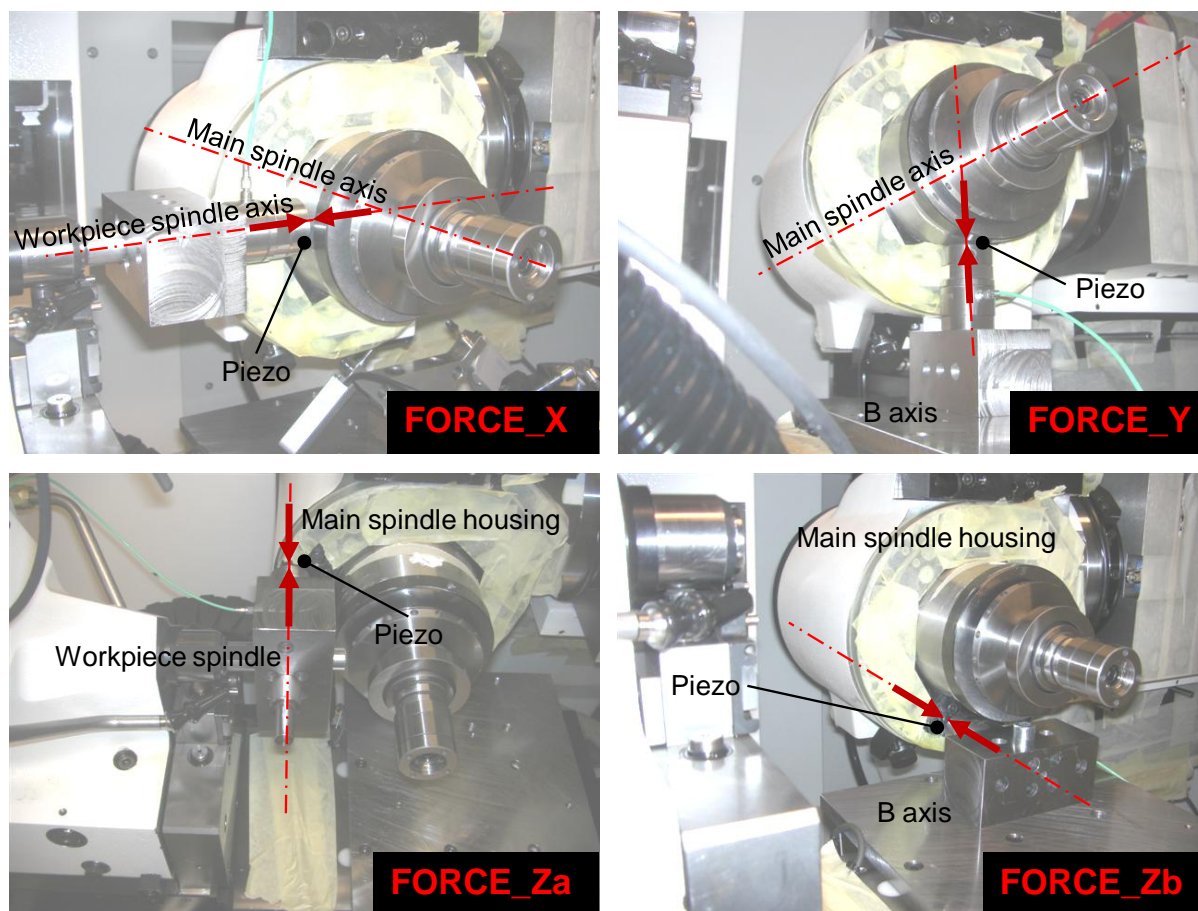
Figure 5.3: The four different measured static loadcases for machine A.
Kinematic description of machine structure A: [Tool-C1-A-Z-Bed-X1-Y-B-X2-C2-Workpiece]

The four static stiffness values obtained for machine A deduced from the measurements are compared with the outcome from the FE simulations. The results are summarized in figure 5.7, showing the relative error between the virtual and the real stiffness values. For both loadcases in direction Z, the deviations are under 7%. For the forces in directions X and Y, the results reveal deviations of 20%, respectively 30%.

To this matter, the source of error is presumably due to the boundary conditions of the rotary axes A and B. The positions of the encoders play indeed an important role: the axis displacements or rotations on the real machine are zero where the reader heads are located, whereas the active control of the axes in the FE models is represented by a high stiffness at the drive locations. The compliance between these two locations is thus neglected in the FE model, leading to the observed higher stiffness values compared to the experimental results.
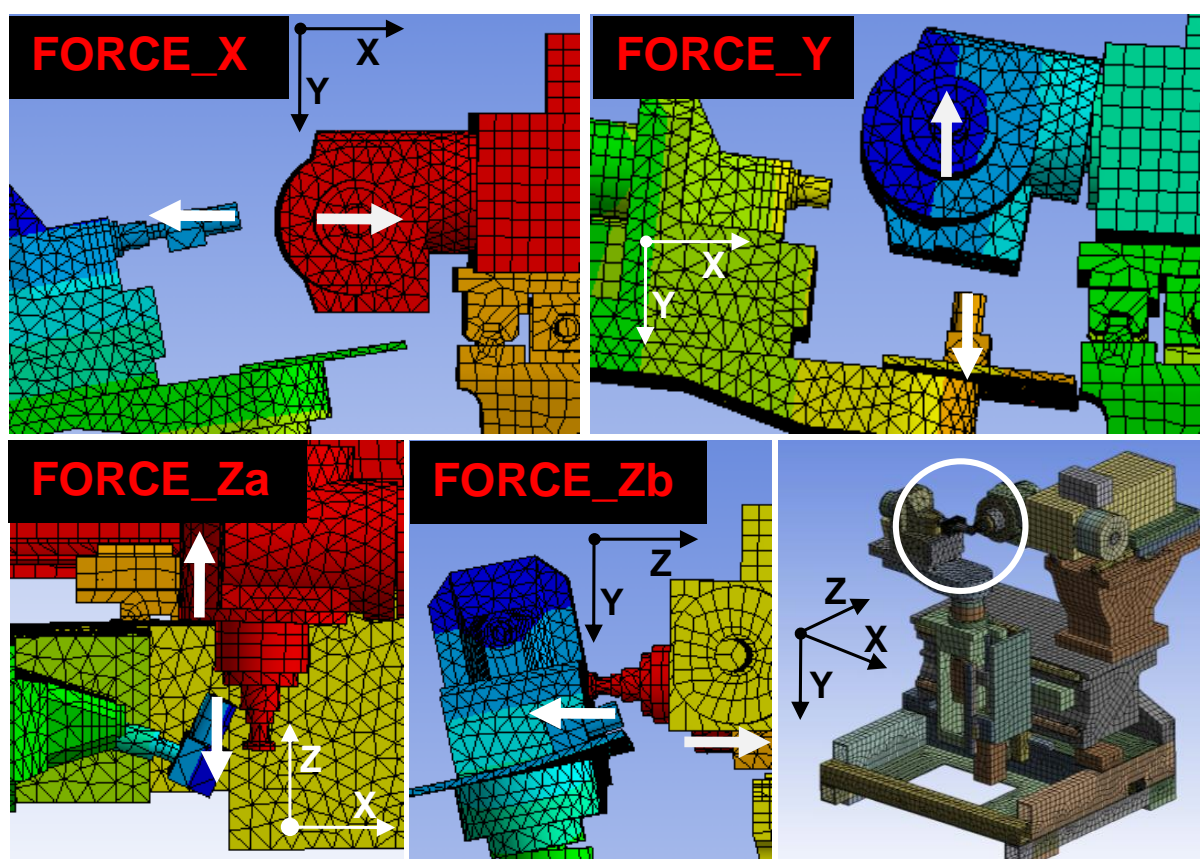
Figure 5.4: The four different simulated static loadcases for machine A.

The same matching procedure is repeated for machine B and the results are recapitulated in figure 5.8, displaying a relative error between the calculated and the real stiffness values under $+8\%$.

5.2   Experimental modal analysis of machine tools

The objective of the experimental modal analyses is to identify the most relevant eigenmodes, especially those occurring in the low frequency domain. These modes involve relative displacements between the machine bodies due to the joint compliances and are therefore adapted to the validation of the modeling guidelines of the couplings.

5.2.1   Experimental setup for dynamic measurements

Experimental Modal Analysis (EMA) [120, 121] is a way to describe a structure in terms of its natural characteristics which are the frequencies, the modal damping ratios and the
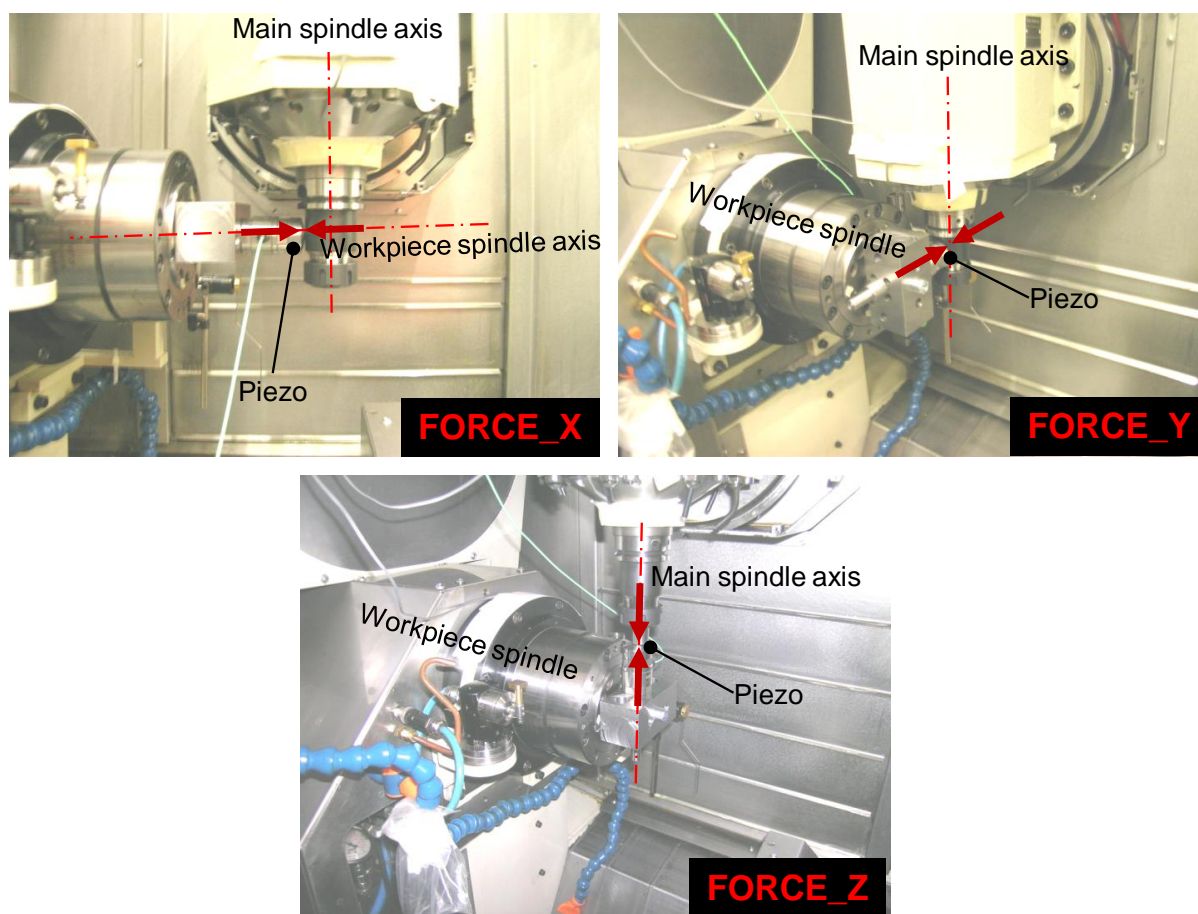
Figure 5.5: The three different measured static loadcases for machine B.
Kinematic description of machine structure B: [Tool-C-B-Z-Y-X-Bed-A-Workpiece]

corresponding mode shapes - in one word its dynamic properties. By means of an impulse hammer with integrated force measuring sensor, the machine structure is impacted at one or several locations in one or several directions. Accelerations are measured using three-dimensional accelerometers, placed at key positions on the structure, with special attention paid at the connections between the different moving parts (or machine axes). The relations between the quasi-Dirac excitation and the resulting acceleration signals, after going through a Fast Fourier Transform, describe the frequency response functions, which once synchronized, help identifying the global dominant resonance peaks. The following curve fitting process leads finally to the identification of the vibration modes of the structure, with the corresponding eigenfrequencies and modal damping ratios (figure 5.9). Experimental modal analysis is very well established for the evaluation of all kind of structures, and machine tools are no exception. Aside from allowing an efficient diagnosis of a machine by detecting possible structural weaknesses, it is also a powerful tool for validating a virtual model by updating parameters affected by uncertainties [122, 123, 124, 125, 126].
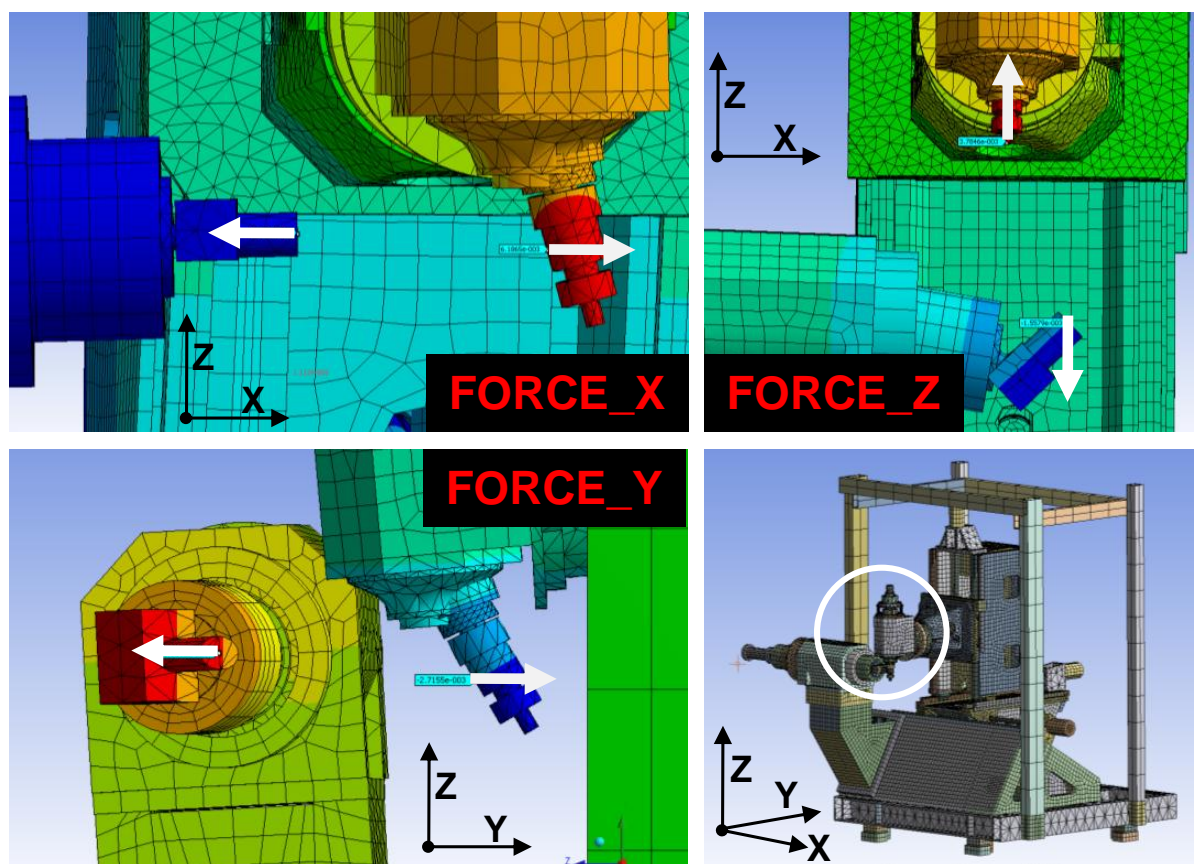
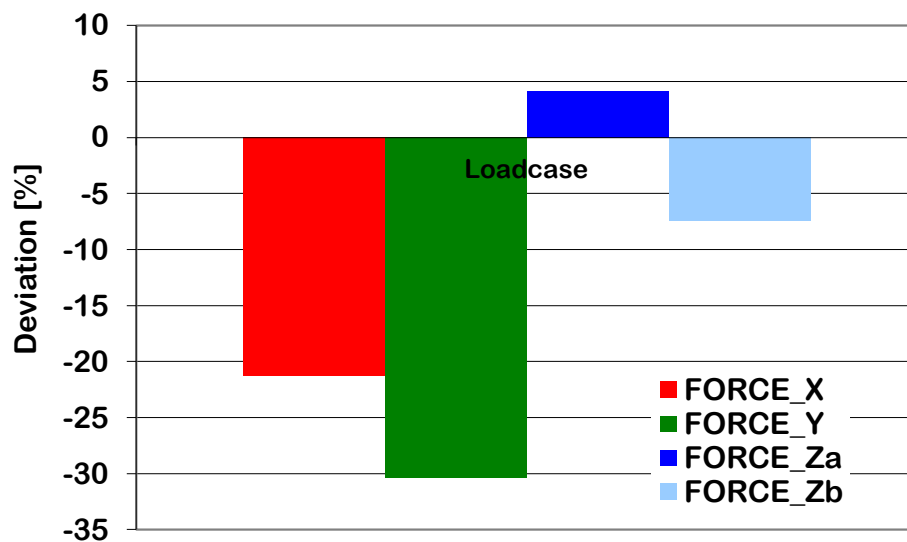Figure 5.6: The four different simulated static loadcases for machine B.

Figure 5.7: Comparison of simulated with measured static stiffness values for machine A (Force range for the four loadcases: $200N - 600N$).
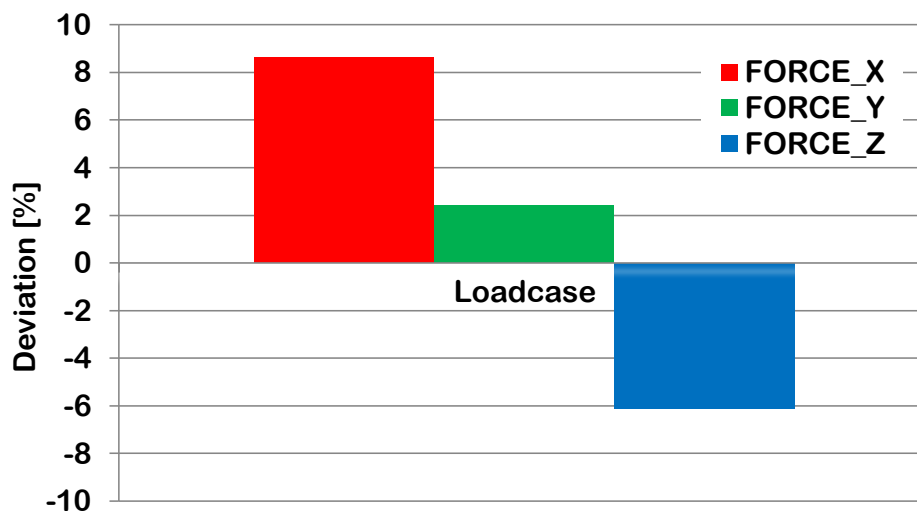
Figure 5.8: Comparison of simulated with measured static stiffness values for machine B (Force range for the three loadcases: $600N - 900N$).
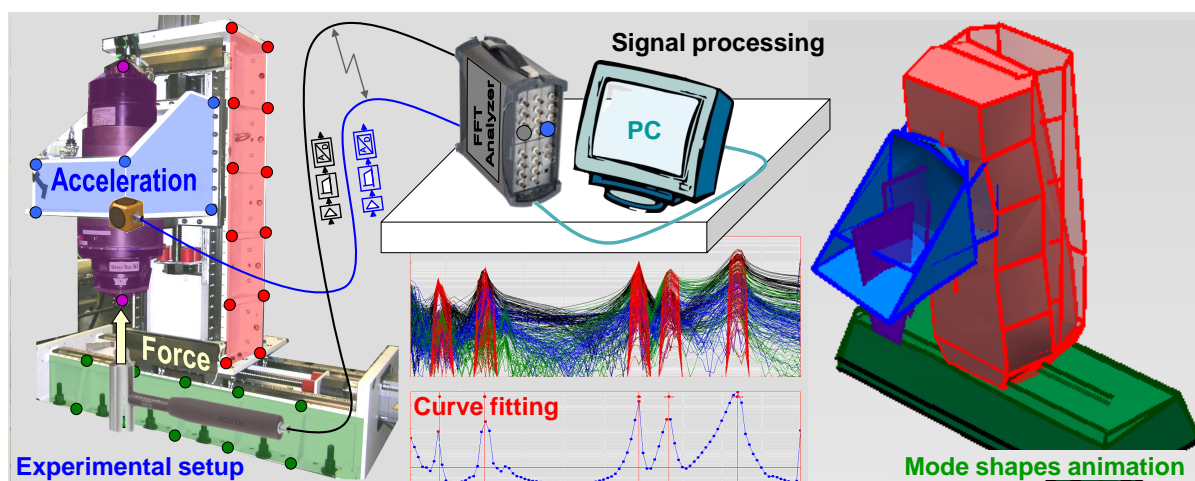

Figure 5.9: Complete process for an Experimental Modal Analysis (EMA).

The objective of the modal analyses carried out on the machine tools is to have a further validation tool, where the compliances of single parts and special boundary conditions are less relevant. On both machines A and B, an experimental modal analysis is conducted and the resonance modes and their respective frequencies are identified. The FE models used for the static analyses are then reconfigured for modal analyses and the eigenfrequencies and corresponding mode shapes are computed and compared with the experimental results.

The match between the simulated and experimental modes is systematically based on the deviations between corresponding eigenfrequencies and on the displacement characteristics of the corresponding mode shapes by visual inspection (same relative displacements between the machine bodies).

5.2.2 Validation of machine FE models with modal analyses

For machine A, the CAD geometry, one simulated mode shape and one experimental mode shape are exemplarily represented in figure 5.10. The matching of the FE model is based on the eigenmodes and the corresponding frequencies in a frequency range of $0 - 300 Hz$. The ratios of the FEM frequencies to the EMA frequencies for the identified modes 1 to 22 (except for modes 11 and 19, which could not be matched) are plotted in figure 5.11 and are within an error range of -10% to $+20\%$.
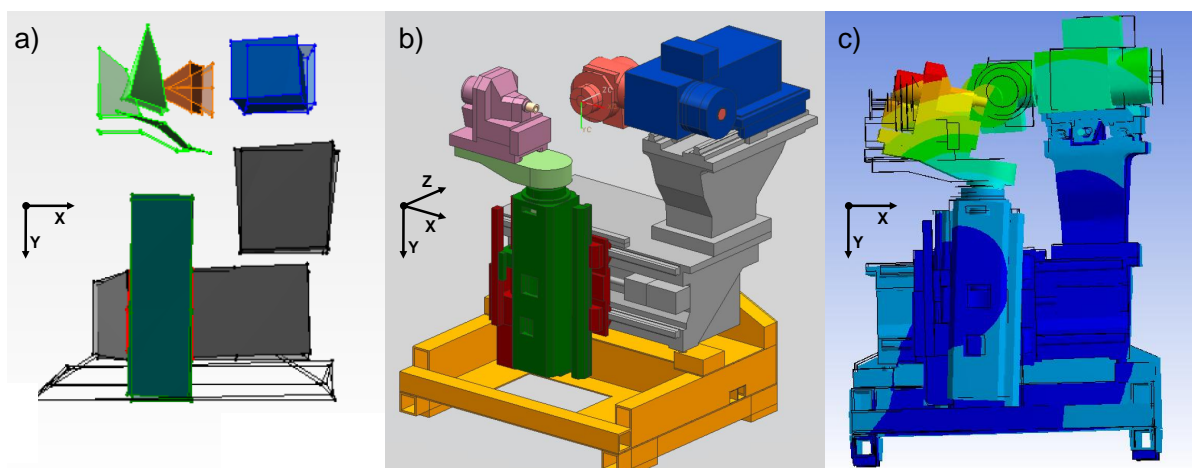

Figure 5.10: Model used for the matching of the experimental modal analysis of machine A.
a) Experimental modal analysis b) CAD model c) Finite element modal analysis

For machine B, the CAD geometry, one simulated mode shape and one experimental mode shape are represented in figure 5.12. The matching of the FE model is based on the eigenmodes and on the corresponding frequencies in a frequency range of $0 - 300 Hz$. The ratios of the FEM frequencies to the EMA frequencies for the identified modes 1 to 20 (except for mode 13, which could not be matched) are plotted in figure 5.13 and are within an error range of -15% to $+10\%$.

Considering the complete set of static and modal tests performed on two multi-axis machine tools, it can be stated that the matching between the measured and simulated deformations, resp. eigenfrequencies evidences a good concordance.
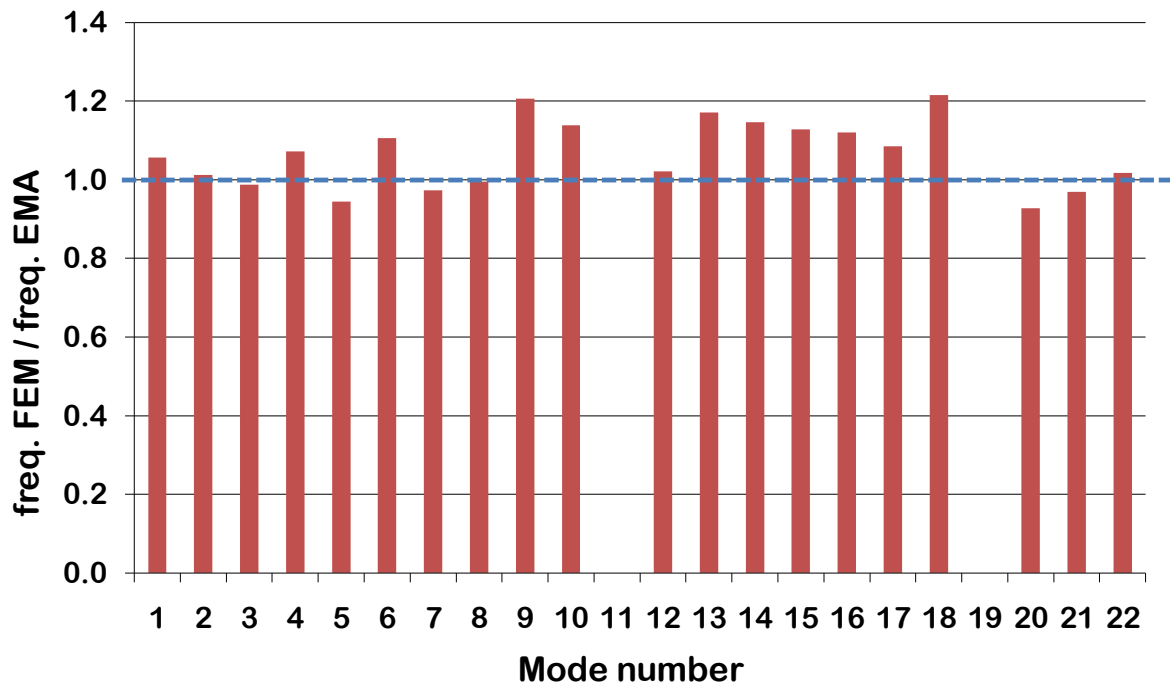
Figure 5.11: Comparison of simulated results with measured mode shapes for machine A.
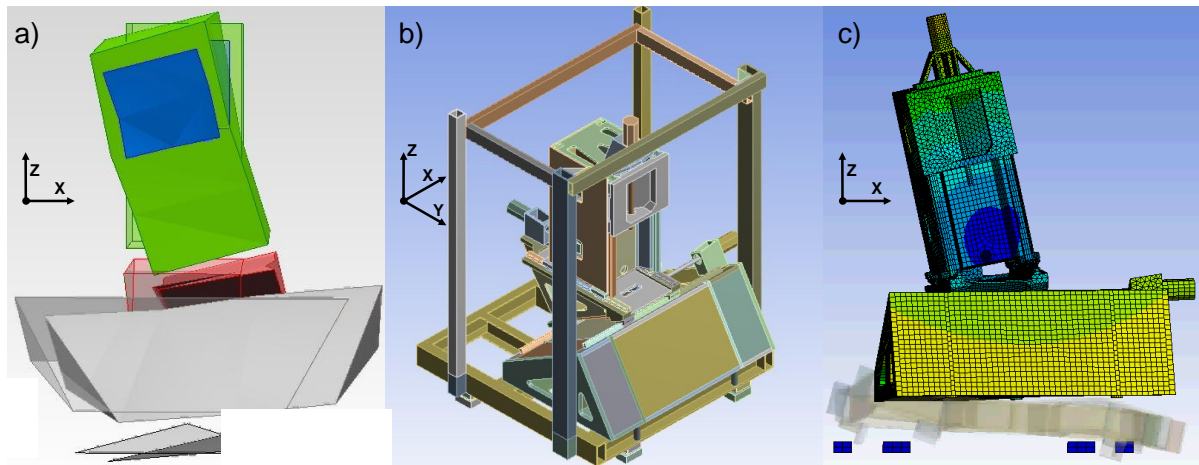

Figure 5.12: Model used for the matching of the experimental modal analysis of machine B.
a) Experimental modal analysis b) CAD model c) Finite element modal analysis

The FE models created with help of the established modeling guidelines provide thus a reliable basis for the subsequent analyses involving the rigid body approach and the order reduction technique.
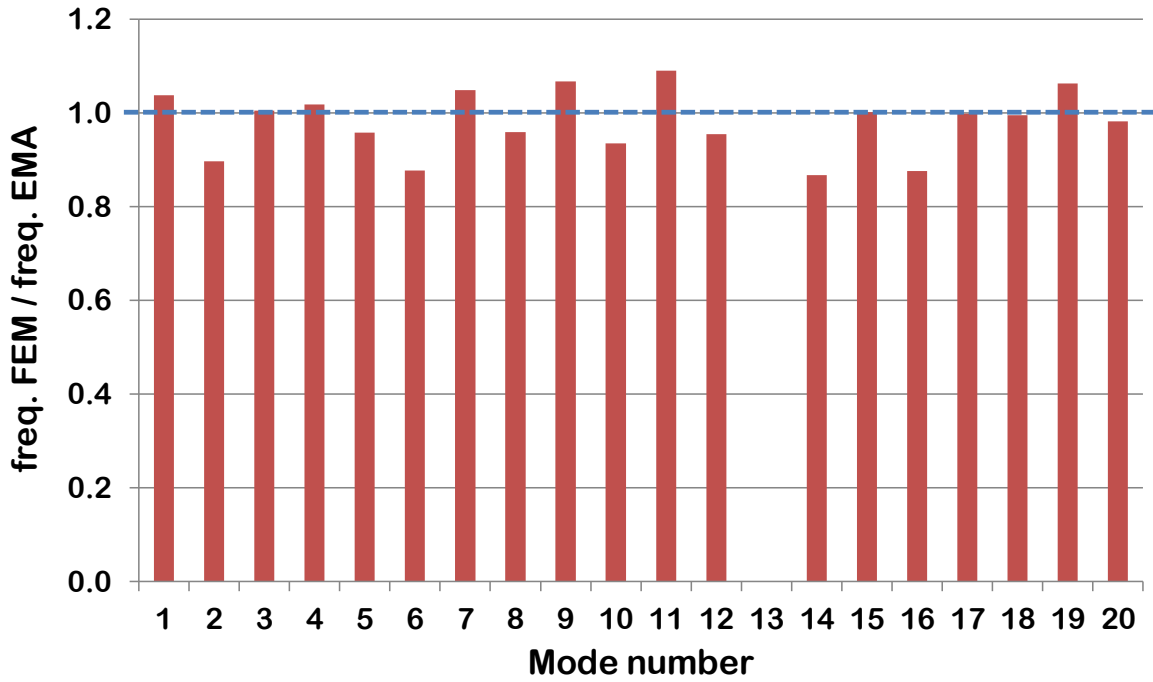
Figure 5.13: Comparison of simulated results with measured mode shapes for machine B.

5.3   Strain Energy Ratio R_ϵ

To bring the analysis of the results of the static and dynamic behavior of machine tools a step further, the *Strain Energy Ratio R_ϵ* (R epsilon) is defined (equation (5.1)), which represents the ratio of strain energy stored in all the axis coupling elements to the *Total Strain Energy*, for a defined loadcase. As a consequence, $(1 - R_\epsilon)$ is the ratio of *Structural Strain Energy* (deformation of the structure) to the *Total Strain Energy* (equation (5.2)).

$$R_\epsilon = \frac{\text{Couplings Strain Energy}}{\text{Total Strain Energy}} \tag{5.1}$$

$$\text{Total Strain Energy} = \text{Couplings Strain Energy} + \text{Structural Strain Energy} \tag{5.2}$$

The purpose of this strain energy ratio R_ϵ is first to identify how the deformation energy is distributed over the entire machine tool structure in order to, if necessary, enhance the stiffness of the coupling components evidencing the largest deformations. Secondly, the strain energy ratio provides a useful indicator which can be used for stiffness adjustments in simulations based on a rigid body approach, as later discussed in section 6.1.3.

When considering the modal analysis of a machine tool, in order to categorize the modal deformations of the machine, the eigenmodes are often distinguished between rigid body modes and structural modes. To quantify this attribute, the FE mode shapes of a simple three-axis machine tool (i.e. without rotary axes) as introduced in section 3.2 are computed. The strain energy ratio R_ϵ is computed for every eigenfrequency and the results plotted in figure 5.14 evidence that the ratio is frequency dependent. Hence the average R_ϵ in the frequency range $0 - 300Hz$ is ca. 0.55, whereas in the frequency range $300 - 600Hz$ it drops to ca. 0.35. Modes 3 and 13 e.g. feature a ratio close to 0.5, traducing mode shape deformations equally distributed over couplings and structure. Mode 4, with a ratio of 0.75, is an illustration of the extreme case characterized by deformations occurring mainly in the couplings (rigid body mode). The opposite case is illustrated by mode 17, with a ratio of 0.25, where the deformations are principally concentrated in the structure (structural mode).
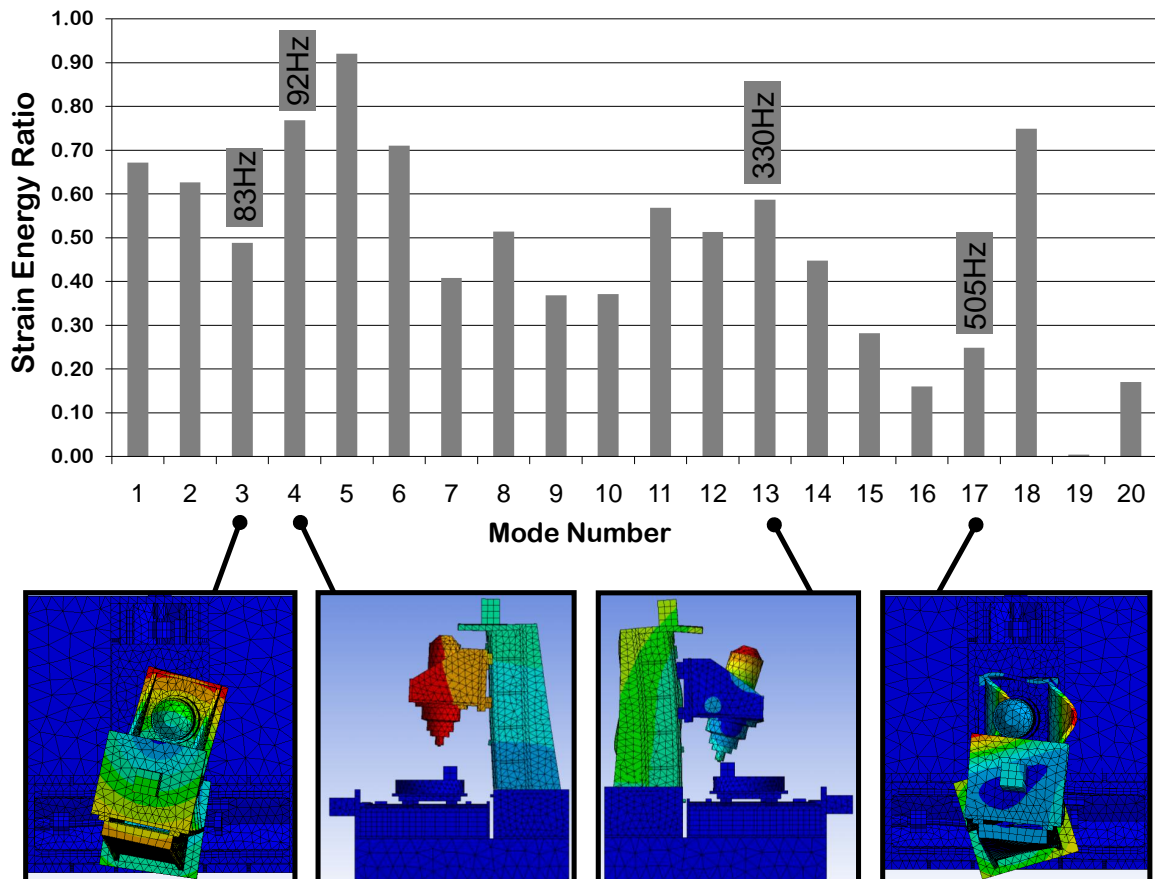

Figure 5.14: Variation of the strain ratio R_ϵ over the mode shapes of a 3-axis machine tool.

The investigation of the strain energy distribution can be done in more detail. For this purpose, the machine tool structure A introduced in section 5.1 serves as reference model. Three loadcases corresponding to forces at the TCP in directions X, Y ad Z are considered and the energy distribution in the linear axes, in the rotary axes and in the entire structure is examined.

The first analysis consists in focusing exclusively on the deformations in the couplings of the four linear axes (X1, X2, Y and Z) composing the machine. The plots in figure 5.15 show how important the variation of energy distribution in the linear couplings can be, depending on the loading conditions of the structure. For example, the ratio of strain energy in the Z axis goes from 10% for loadcase FZ up to 70% for loadcase FY.
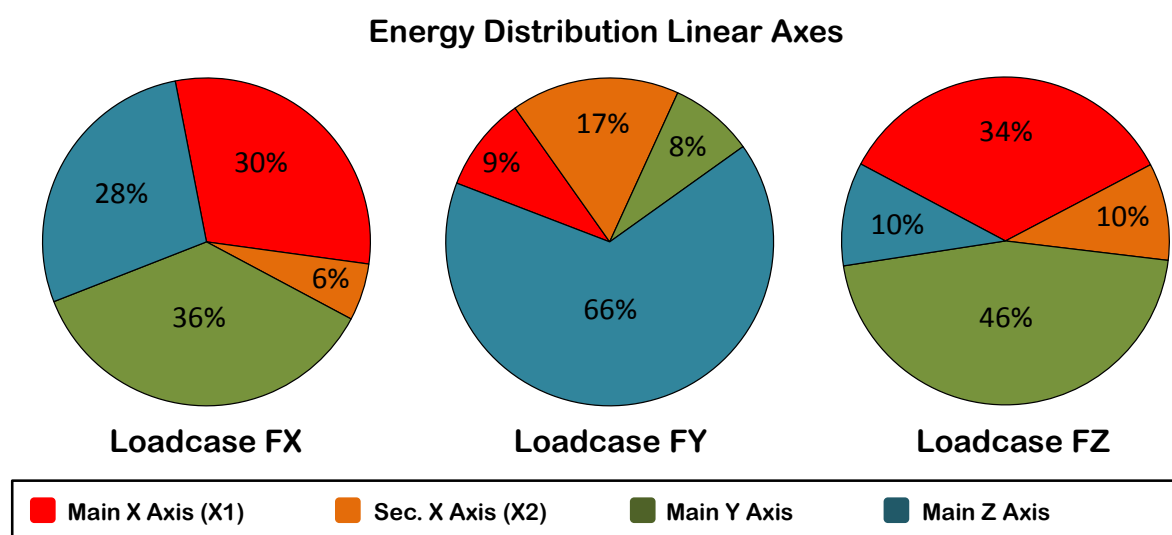

Figure 5.15: Distribution of strain energy in the linear axes for three static loadcases on machine A.

Within the linear axes it is also interesting to evaluate, for the case of linear guideways, the contribution of the rotational stiffness coefficients relatively to the translational stiffness parameters in terms of deformation (figure 5.16). From figure 5.17, it can be deduced that the amount of strain energy resulting from the roll (A), pitch (B) and yaw (C) rotations of the single carriages amounts to approximately 25% of the total strain energy within the linear guideways, for the three selected loadcases. Considering that on average 50% of the strain energy is stored in the couplings and that 25% of that energy is typically stored in the linear axes (figure 5.19), the total amount of energy in the rotative degrees of freedom of linear guideways ranges between 2% and 5%. This means that eventual uncertainties concerning the rotational stiffness coefficients of linear guideways are not significant for the evaluation of the dynamic behavior of machine tools.

The next analysis consists in focusing exclusively on the deformations in the couplings of the four rotary axes (A, B, Main and Workpiece spindles) composing the machine. The plots in figure 5.18 lead to same conclusions on the dependency of the energy distribution in the couplings relative to the loading conditions. For example the ratio of strain energy in the B axis goes from 10% for loadcase FY up to 80% for loadcase FZ.
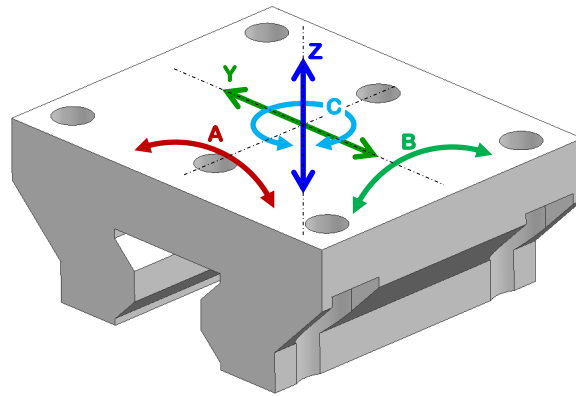
Figure 5.16: Sketch of translational (YZ) and rotational (ABC) displacements of linear guideways.
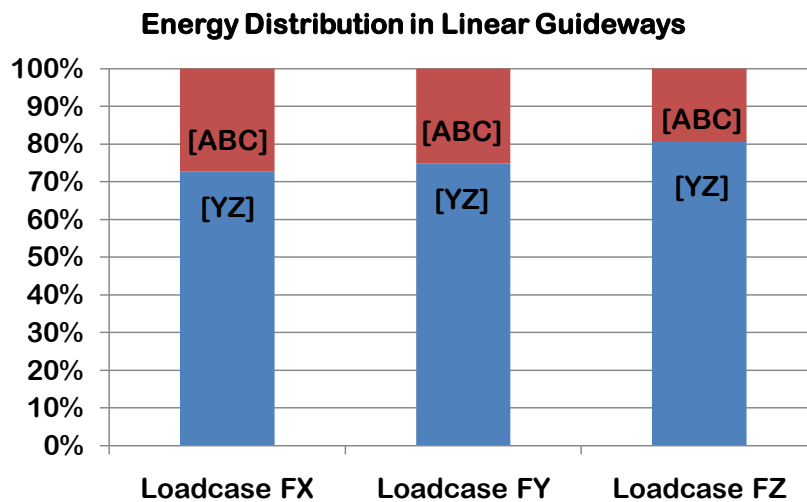
Figure 5.17: Translational (YZ) vs. rotational (ABC) strain energy ratio
in the linear guideways for three static loadcases on machine A.

Figures 5.15 and 5.18 evidence that, depending on the loading conditions, the couplings of certain linear or rotary axes are logically subject to more or less deformation, according to the kinematic arrangement. However, when proceeding to a unification of the data from the linear and rotary axes and additionally including the structural strain energy, the results take the form presented in figure 5.19. It can be observed that, whatever the direction of
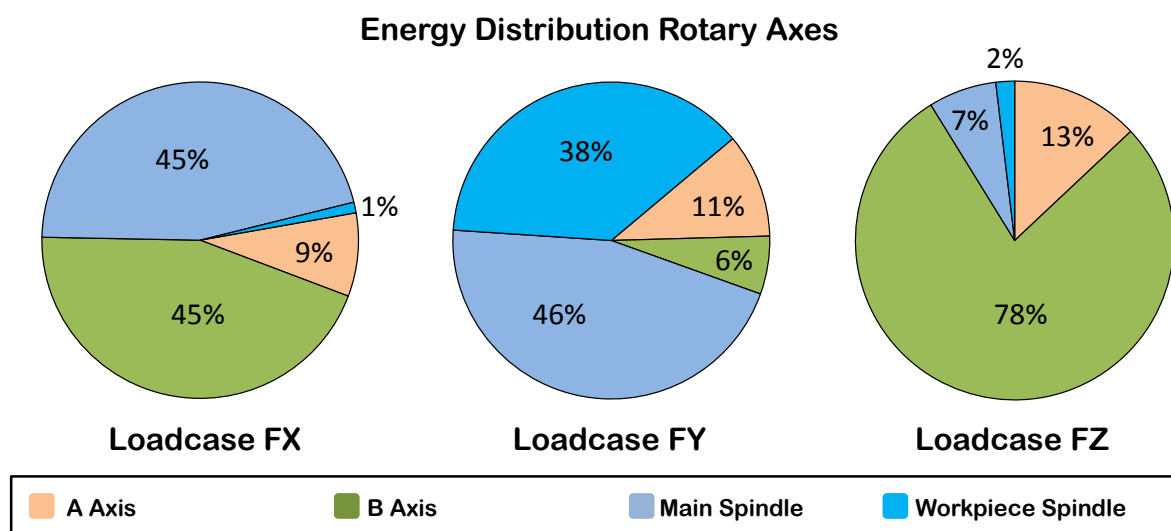
Figure 5.18: Distribution of strain energy in the rotary axes for three static loadcases on machine A.

the force, the Strain Energy Ratio R_ϵ remains stable, amounting to respectively 55%, 59% and 48% for the loadcases FX, FY and FZ. The results highlight a further aspect, namely that the deformation energy within the couplings is stored predominantly in the rotary axes. In the cases considered, the deformation energy ratio between linear and rotary axes varies indeed between 10% and 30%. This is mainly due to the fact that, for the applied static loadcases consisting of forces acting at the TCP, the rotary axes, located at the extremities of the kinematic chain of the machine structure, are directly affected by the transmitted forces.
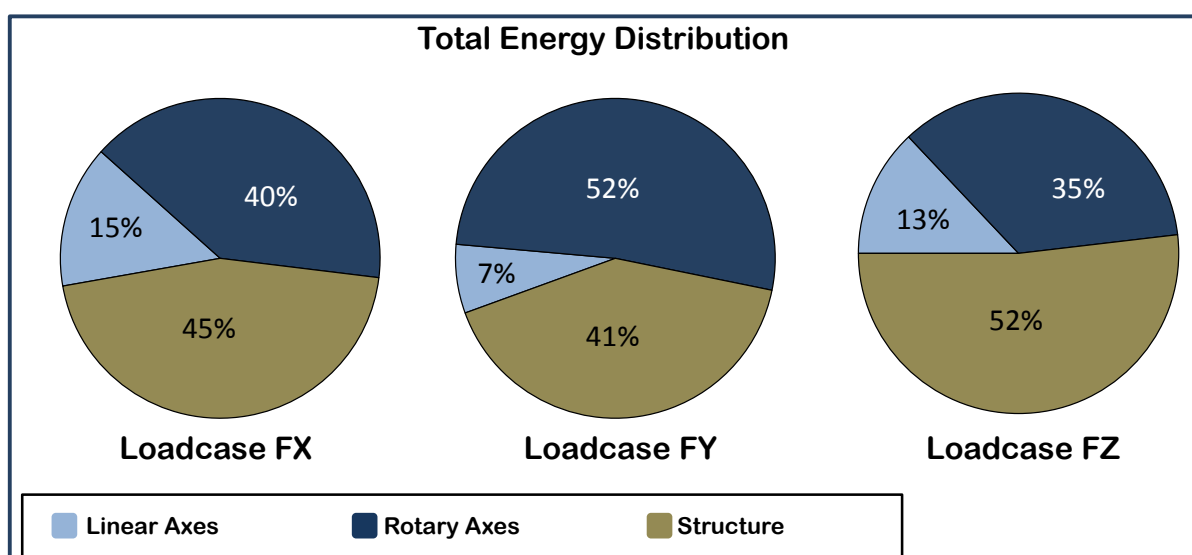

Figure 5.19: Distribution of strain energy in the entire structure for three static loadcases on machine A.

A last analysis proposes a check of the ratio R_ϵ for different configurations of the machine axes but with a load in constant direction. For the six positions considered, the linear and rotary axes of the machine are successively moved in order to have a single contact point between tool and workpiece (figure 5.20). A force in direction FX is applied at the TCP location and the strain energy ratio is evaluated in each case (figure 5.21). It can be noted that R_ϵ is fairly constant over the considered workspace.
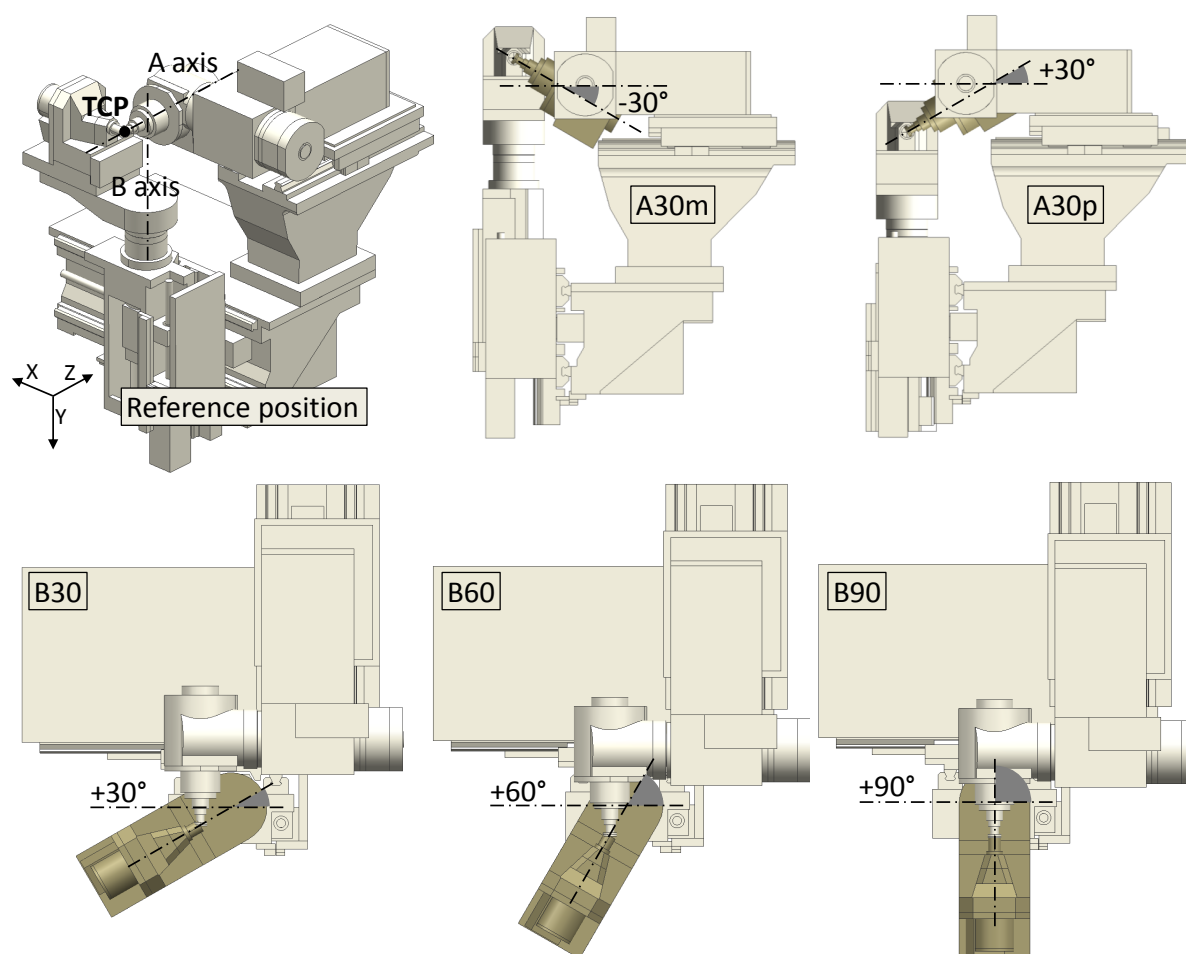
Figure 5.20: The 6 axis positions of machine A considered for the study of R_ϵ in the entire workspace.

These analyses demonstrate that, although the energy distribution in the structure varies in function of the force direction, the axis positions, the frequency, etc., the Strain Energy Ratio R_ϵ is a constant machine tool attribute, when considering the low-frequency range of modal analyses (figure 5.14) as well as any loading condition in static analyses (figures 5.19 and 5.21).

The tendency for the strain energy ratio to converge systematically towards 0.5 for the machine tools investigated in this thesis opens an interesting discussion. This symmetrical

Figure 5.21: Strain energy ratio R_ϵ in the six different axis positions of machine A.

compromise between structure and coupling compliance is probably not fully consciously purposeful but is rather a consequence of decades of experience in developing such structures, leading to a common sense of what proportions should be pursued. In figure 5.22, the sketch of an analytical justification is given, by schematizing the stiffness of the structure and of the joints by two respective springs: a varying spring k_1 and a constant spring k_2. From the represented plo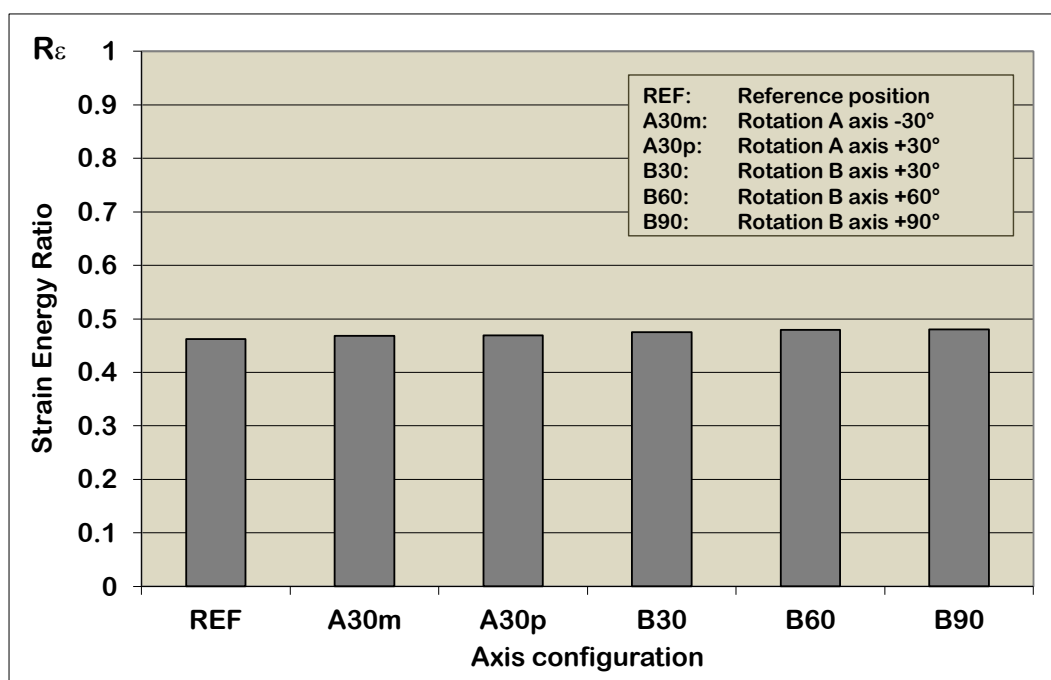t, some exemplifying data can be extracted, dictated by the serial connection of springs, whose weaker element dominates the overall behavior:

a. The start configuration has an overall joint stiffness of 0.5 and an overall structure stiffness of 0.8 (the units are here not relevant). An increase of the structure stiffness by 12.5% from 0.8 to 0.9 leads to a total stiffness increase of 4.5%. This low relative benefit may not be worth it, considering the mass gain which would probably result from such a structural reinforcement.

b. The next considered case consists of an overall joint stiffness of 0.2 and an overall structure stiffness of 0.5. By increasing the joint stiffness to 0.3, i.e. by 50%, the total stiffness increase is of 31.3%, which is a considerable gain. The underlying constructive measure could be in this case for example to upgrade the linear guiding systems from a size 25 to a size 35 and evaluate if the stiffness benefits are worth the consequently higher price and reduced workspace.

Such considerations are within the daily work of a design engineer. The awareness of an ideal proportion between $R_\epsilon = 0.4$ and $R_\epsilon = 0.6$ between structure and joints compliance has simply been revealed by the definition of the *Strain Energy Ratio*. The interpretation of the correlation between R_ϵ and machine tool design can hence be summarized as follows:

- The resulting stiffness of two springs in series is expressed as $k_{tot} = f(k_1, k_2)$

- From figure 5.22, it is deduced that a good compromise is $k_1 \approx k_2$

- On machine tool structures, this is traduced by a Strain Energy Ratio R_ϵ of ca. 0.5, which is often achieved by the reinforcement of the weakest part

- R_ϵ can be used as improvement/optimization criterion during the design of machine tool structures, trying as much as possible to move perpendicularly to the iso-lines on figure 5.22
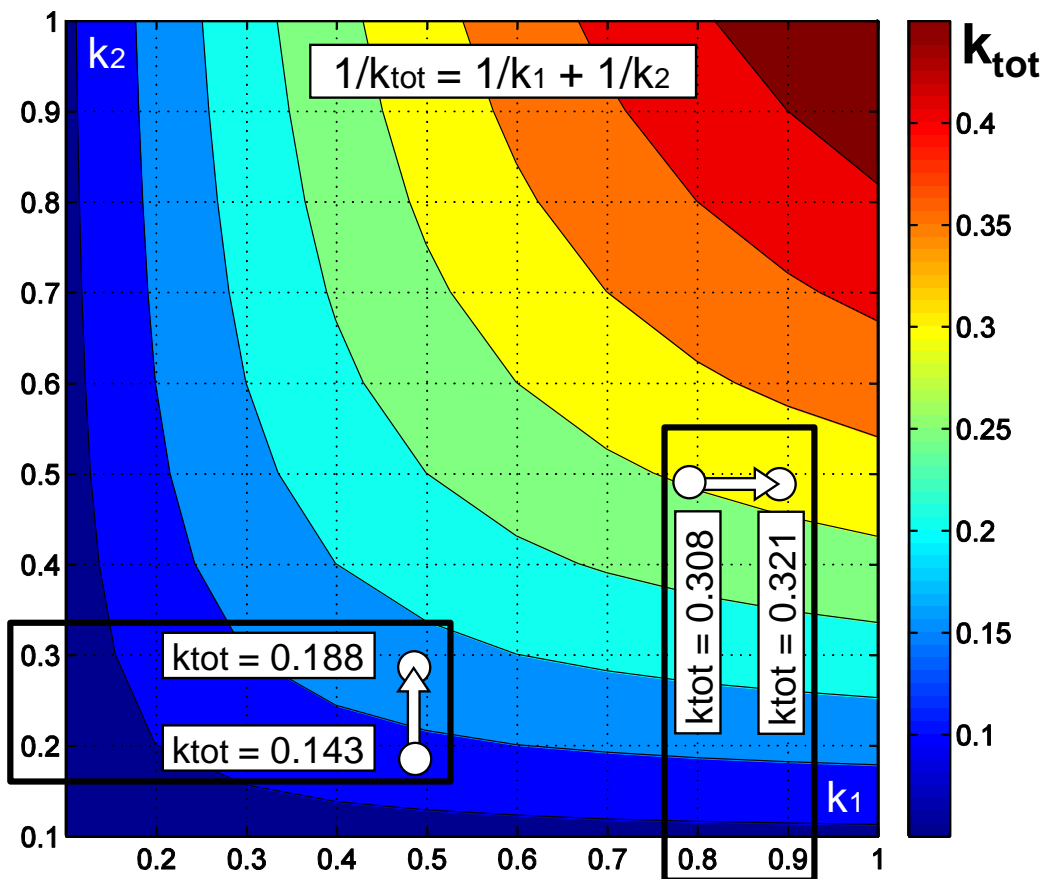

Figure 5.22: Schematization of structure and joint stiffness by serial connection of two springs.

Chapter 6

Stand-alone GUI for rigid body analysis

In the present chapter, the use of a novel stand-alone GUI based on Matlab is reviewed in detail. The program has been developed with the intent of filling the gap evoked in section 2.2, evidencing the needs of simulation tools offering simultaneously user-friendliness, application flexibility, computational efficiency and results accuracy, in order to align research-based knowledge with practical requirements of machine tool manufacturers.

6.1   SGI output for rigid body analysis

In section 3.3, the scripts developed in the *Structure Gateway Interface* have been discussed, leading to three analysis options depending on the user needs. The present section will be focusing on the option *RBS*, which exports the data of the FE model needed for rigid body analysis. The archived data set serves as input to the stand-alone GUI presented in the following sections 6.2, 6.3 and 6.4. The reason why the data for rigid body models are retrieved from a FE model lies in the discussed benefits of having a central platform for the creation of all the simulation models. On the one hand, the model can be very easily imported from a CAD program at every design stage, from simple cuboidal to detailed structures. On the other hand, the developed scripts for an automated implementation of the couplings and the developed routines for the export of all the mechanical properties of the bodies and of all the joint characteristics facilitate then the building of the complete RBS model.

6.1.1   Principle of export scripts for rigid body models

The *RBS* export procedure is based on figure 3.9, representing a two-axis machine tool model built using the aforementioned APDL pre-processing scripts. With help of the developed macros, the information required for rigid body analysis is retrieved in three distinct steps, executed individually in a loop over the machine bodies defined by the volume components (figure 3.5): writing of the mechanical properties of the axis bodies, writing of the geometrical properties of the axis bodies and writing of the joint properties of the axis couplings. The process and the successive functions executed by the RBS export scripts are illustrated in figure 6.1, with one loop over the volumes indicated by index i and one loop over the couplings indicated by index j.

6.1.2   Output data needed for rigid body models

The objective of the export operation using the *RBS* option is to extract the required data from the complex FE model, in order to obtain a simplified structure described by the basic mechanical properties of the bodies and of the joints connecting the bodies. In figure 6.2, the process leading from a detailed discretized model to a mathematical model built using a rigid body approach is illustrated.

To achieve the translation, the three steps referred to in section 6.1.1 are entirely implemented in ANSYS using APDL scripts and produce the following files, containing data specific to rigid body analyses:

- *body_parameters.txt* contains information related to the mechanical properties of the single bodies, retrieved using the elements grouped into the single volume components (figure 3.5)

- *body_geometry.dat* contains information related to the external hull of the bodies, selecting the external elements of the single volume components (figure 3.5). It is subsequently used for graphical purposes

- *coupling_parameters.txt* contains information related to the joint properties of all the machine axis couplings, referring to the area components, the coefficients contained in the two scripts STIFFNESS and DAMPING, the created interface nodes and the local coordinate systems (figures 3.6, 3.7 and 3.8)

The complete export data flow is recapitulated in figure 6.3, showing the succession of the writing operations, which are implemented to format the outputs according to the requirements of rigid body models of machine tools.
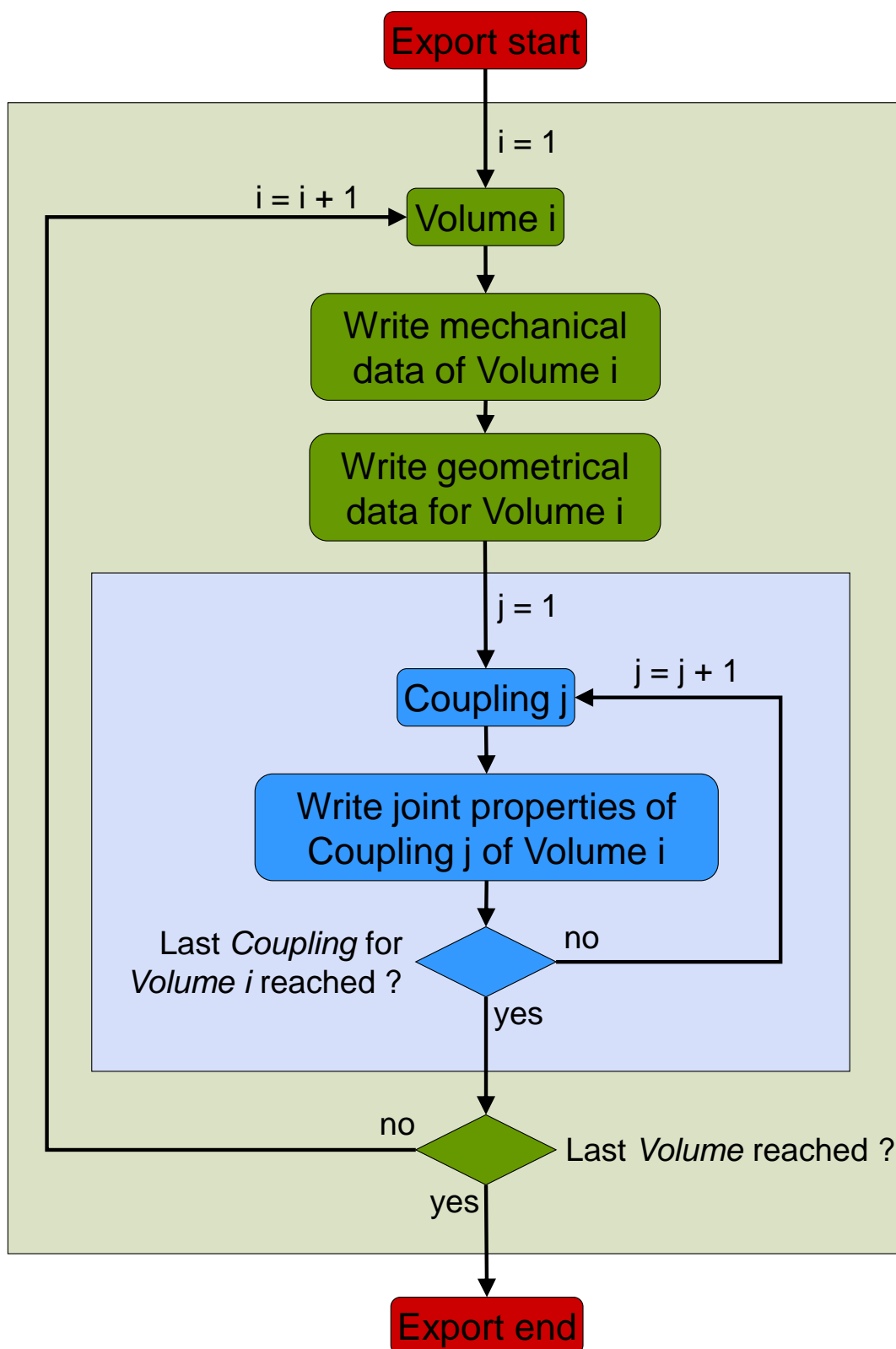
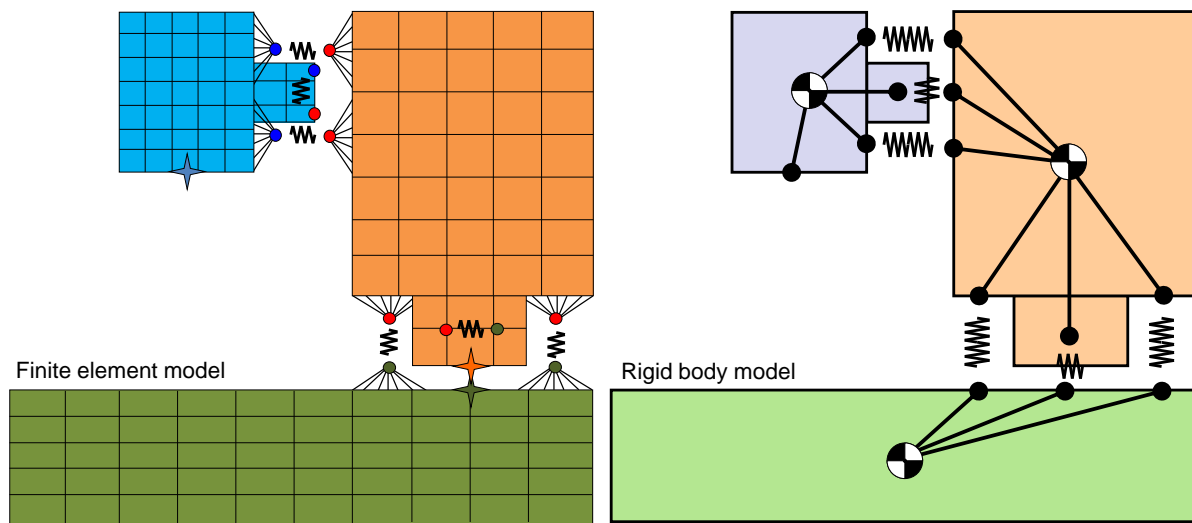Figure 6.1: Process flow diagram for export of RBS data.

Figure 6.2: Translation of a FE model into a rigid body model.

After the export is terminated, all volumes and couplings having been processed, the solve run in ANSYS is aborted. The output of the simulation consists of a set of text files, which are archived and made available for further use in the developed stand-alone environment presented in the next sections.

6.1.3   Coefficient adjustments for rigid body analysis

Before proceeding to the analysis capabilities available in the developed rigid body stand-alone GUI, it is important to spend some words on additional modeling rules, as enhancement to the conclusions drawn in section 4.2.1. The guidelines proposing preferential modeling techniques for linear guiding systems showed good results when comparing experimental data with FE simulations, as evidenced in sections 5.1 and 5.2.

However, the reflection needs to be taken a step further in order to reassess the validity of the established rules when integrating linear guideways into machine tool models based on different characteristics. Hence in rigid body analysis, the omitted local effects taking place in the structural parts must be taken into account somehow. The phenomenon is highlighted in figure 6.4: on the left-hand side is the case of a FE model, enabling deformations of the rail, the carriage and the adjacent structural parts, which all contribute to the overall joint compliance – confronted to the stiffer case on the right-hand side, where due to the non-deformable approach, the whole compliance is concentrated in the interface spring.
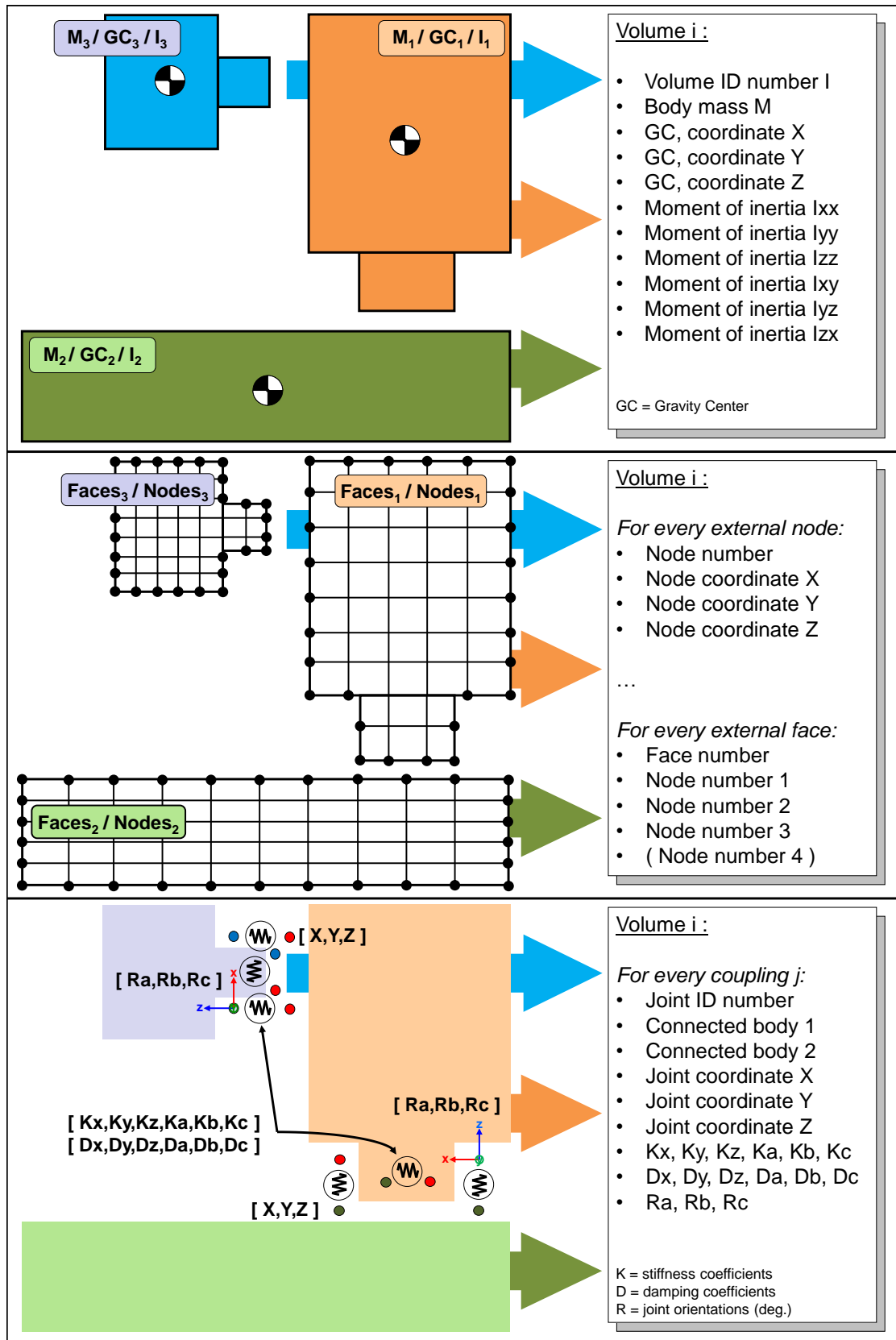
Figure 6.3: RBS data set: mechanical, geometrical and physical joint properties.
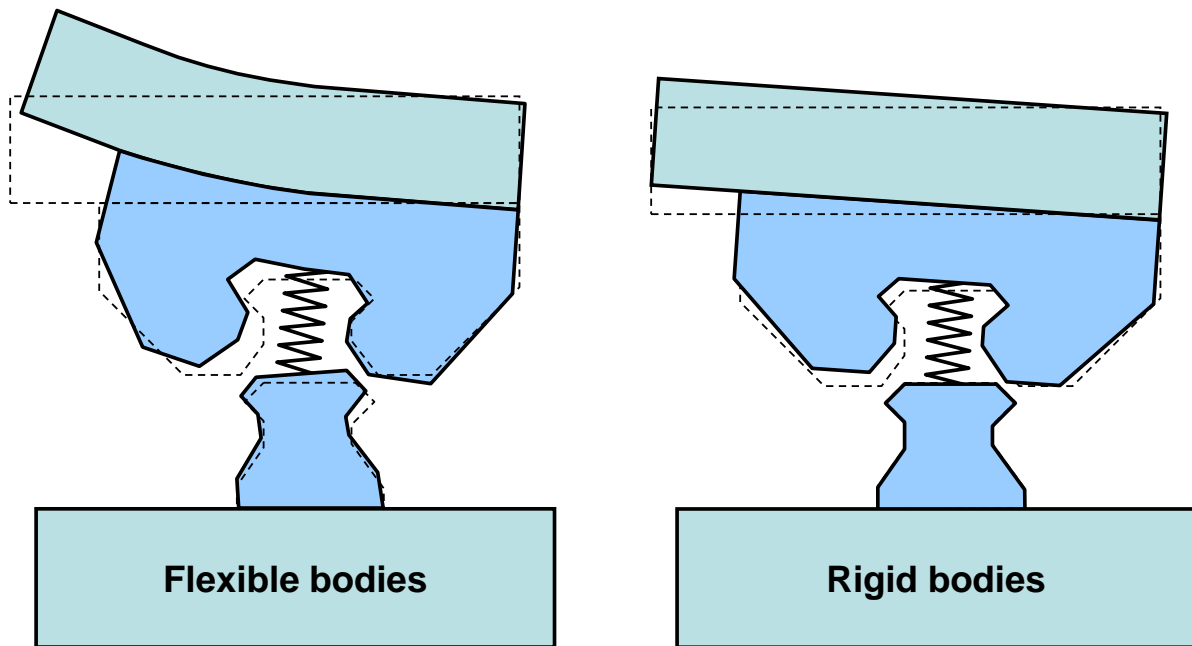
Figure 6.4: Local structural deformations taking place in and around the coupling zone of a FE model.

The question which arises is how the joint stiffness coefficients used in the FE models can be applied to rigid body simulations. As evident as this issue may seem, there are hardly any related indications found in the literature. The method proposed here consists in identifying a *stiffness scaling factor* R_s as general as possible to adjust the stiffness coefficients of any type of axis couplings. Its function is to compensate for the stiffening effect described in figure 6.4, with the purpose of achieving quantitatively reliable rigid body analyses of machine tools.

A valuable tool to help finding a convenient stiffness scaling factor is the *strain energy ratio* R_ϵ introduced in section 5.3. It gives the amount of potential energy stored in the axis couplings relative to the total deformation energy of the structure. As it has been demonstrated, is a constant attribute for a given machine tool.

To investigate the relation between the strain energy ratio and the stiffness scaling factor, a two-axis machine tool serves as example. The reference structure is taken from section 3.3 and the comparative study is based on the variation of the Young's modulus of the machine bodies. A static analysis (force at TCP in direction X) of five different models is computed and the corresponding strain energy ratios are calculated. The results are summarized in table 6.1, where the reference model is represented by a Young's modulus of 100% $(2.1 \cdot 10^5 MPa)$ and evidences a strain energy ratio R_ϵ of approximately 0.5, which as outlined in precedence in section 5.3, seems to be the average standard value for machine tools.

Table 6.1: Relation between Young's modulus and strain energy ratio R_ϵ resulting from the five static analyses on a two-axis machine tool.

E [GPa] (E / Eref)	105 (50%)	157.5 (75%)	210 (100%)	262.5 (125%)	315 (150%)
Rε	0.34	0.43	0.50	0.55	0.59

As default setting, it seems logical to choose a *stiffness scaling factor* R_s equal to the strain energy ratio R_ϵ. To further assess this intuition, the five static analyses carried out for different Young's moduli are reproduced in a rigid body environment. The observation is that, considering a static force applied to the tool tip, the relative error between the corresponding deviations of the FEM and the RBS models is minimum if $R_s = R_\epsilon$, as opposed to a constant R_s of 0.5 independent of R_ϵ. This statement is deducible from figure 6.5, where the model with the adaptive stiffness scaling factor evidences an error under 5% for any Young's modulus.
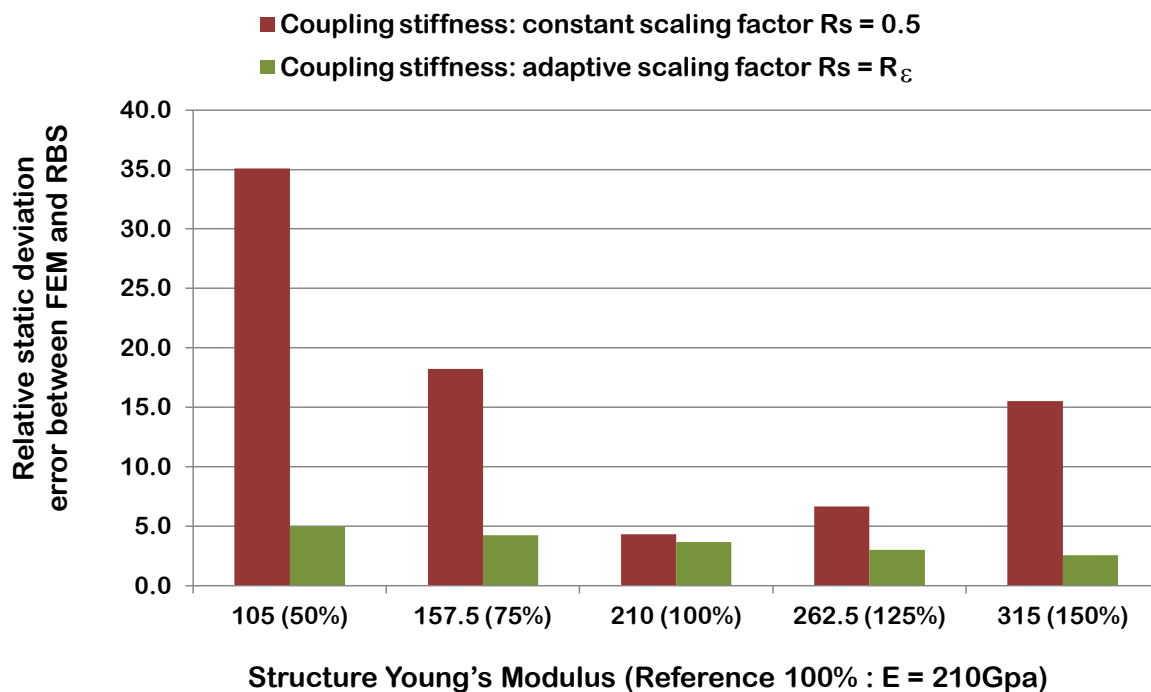

Figure 6.5: Relative static deviation error with constant and adaptive stiffness scaling factor R_s.

To conclude this section, an analog reflection on scaling of damping coefficients of coupling elements is needed. It has been suggested in several occasions that damping effects in machine tools are mostly concentrated in the axis connections, and this has been confirmed by the results on the test-bed in section 4.2.1. The damping parameters considered for linear guideways and bearings are nonetheless not exclusively a result of friction at the contact location between the rolling elements and the rail, resp. the carriage. The parameters also take into account the contributions coming from the adjacent structural parts, caused by friction effects in the mounting elements, like screws and bolts, used to assemble the carriages and the rails. For this reason, no damping scaling is actually needed between a FEM and a RBS simulation, since the joint parameter properties, responsible for practically the entire machine structure damping, are unaltered in the rigid body model. This aspect has not been thoroughly verified and would need further investigations.

The next three sections are dedicated to the application of the stand-alone GUI. In section 6.2, the inputs of the programm and the possible user-interventions for model modifications are discussed. In section 6.3, the various capabilities for model simulations are reviewed. In the last section 6.4, the results of the integrated analyses are validated by comparing them with the results obtained with equivalent FE models.

6.2   Introduction to the GUI functions

The start window of the newly developed stand-alone tool pictured in figure 6.6 is composed of seven distinct areas, each responsible for a specific task of checking, processing or analyzing the machine tool. For a better understanding, it is to note here that, since the GUI enables multiple axes for each motion direction, they are named $X1, X2, X3 \ldots$, $Y1, Y2, Y3 \ldots$, $Z1, Z2, Z3 \ldots$, etc. This means that if there is e.g. only one X axis, it is indifferently referred to as X or $X1$.

- The archived set of files resulting from the export option *RBS* in ANSYS Workbench serves as input to the program and is loaded using the *Import Model* button in the upper left corner.

- After completion of the import, a list containing *General Model Information* on the machine tool structure appears below the *Import* button, recapitulating the number of volumes, the coordinates of the tool (TCP) and the workpiece (WPP) reference positions, as well as the body identification numbers they belong to.

- The complete machine structure appears in the central *Graphical Area*. It represents here the three-axis machine tool (without spindle) introduced in section 3.2. It has
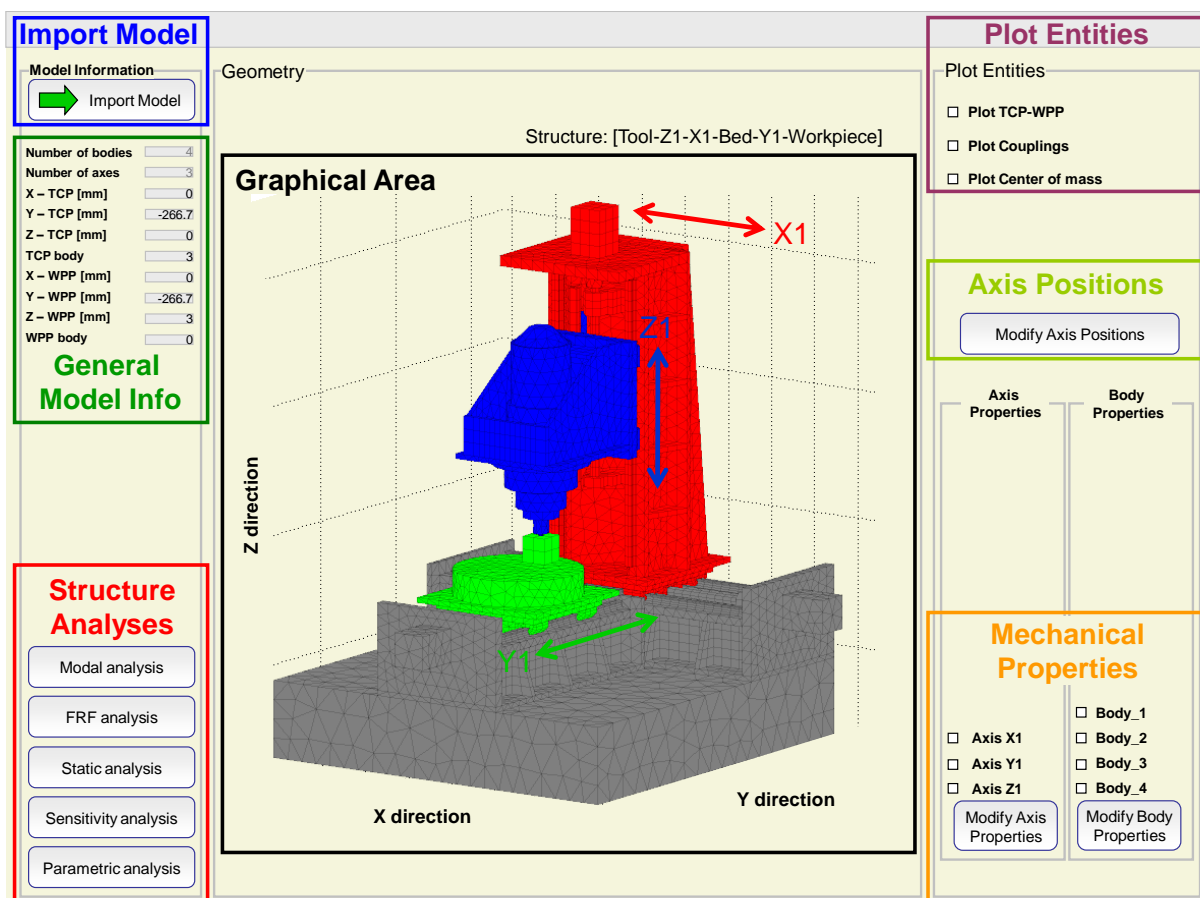
Figure 6.6: Start window of the stand-alone GUI with imported structure.

to be noted that, even though the volumes appear as being meshed, they have absolute rigid characteristics. The elements visible in the structure plot and which are exported from ANSYS have as only function to provide the geometrical boundaries of the bodies and enhance the graphical representation of the machine.

- The machine plot can be complemented by overlaying the TCP, the WPP, the axis couplings (geometrically described by the location and the orientation of the local coordinate system) and the center of mass of the axis bodies, all activated in the *Plot Entities* boxes in the upper right corner of the start window. This provides a direct visual check that the imported machine tool structure is correctly configured and that the axis bodies and their respective couplings are consistently defined.

- The positions of the machine axes can be changed at any time using the *Modify Axis Positions* button on the right hand side of the window. After selecting the axis to be moved, the position can be input using incremental values, in meters for linear axes and in degrees for rotary axes (figure 6.7).
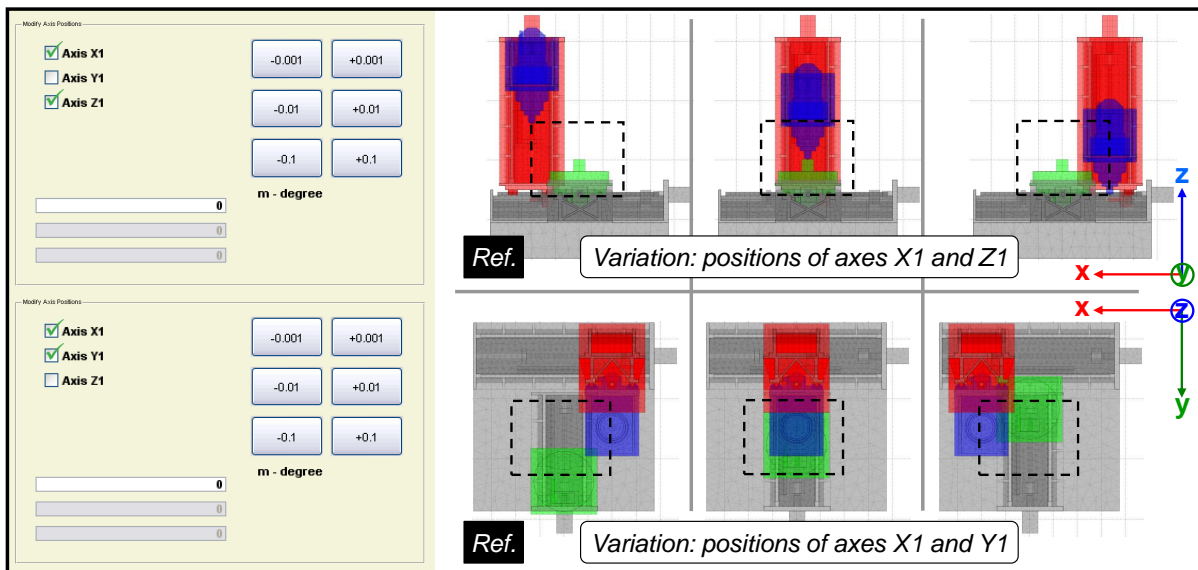
Figure 6.7: Additional pop-up window used to move the bodies along the machine axes.

- In the lower right corner, the main mechanical properties of the complete machine tool can be manually modified. By means of the option *Modify Body Properties*, it is possible to vary the mass and the corresponding inertial characteristics of the axis bodies (figure 6.8). With help of the option *Modify Axis Properties*, all the parameters and coefficients of the selected single axis couplings can be adjusted. Hence it is possible to update the physical stiffness and damping values of linear guideways, bearings, ballscrews, mounting elements, etc. Geometrical data of the coupling seen as a set of joints can also be redefined (figure 6.8).

- The *Structure Analyses* area in the lower left corner contains the command links to the five different analysis types provided for the user to investigate the complete behavior of the machine tool (reviewed in the next section 6.3).

6.3   Analysis capabilities

There are numerous ways of investigating the behavior of a machine tool, each covering specific issues related either to global vibrational problems or to concerns associated with static or dynamical relative deviations occurring at the TCP between the tool tip and the workpiece. In the presented stand-alone GUI, a menu of five analyses is proposed, which can be executed in an arbitrary sequence, depending on the interests of the user.

Figure 6.8: Additional pop-up windows used to modify the parameters of the axis couplings.

In order to illustrate the utilisation of each integrated simulation option, the basic machine structure introduced in figure 6.6 is used as accompanying example through the next sections to show, by means of some illustrative analyses, all potential applications offered by this new program. To give to the following results a higher pertinence, the structure is hereafter briefly described:

- Three axes according to the kinematic structure: [Tool-Z-X-Bed-Y-Workpiece]
- Mass X-axis: $\sim 760kg$ / Mass Y-axis: $\sim 290kg$ / Mass Z-axis: $\sim 470kg$
- Guideways: linear rolling elements, size $35mm$

6.3.1 Modal analysis

Sources of possibly perturbing structural resonances can be located and identified by means of a *Modal Analysis*. When such an analysis is performed, the program computes the complete set of eigenfrequencies and lists them in a new window. It is subsequently possible to display the corresponding mode shapes, either as picture or as animation. In figure 6.9, the first three eigenmodes are represented, superposed over the original structure.
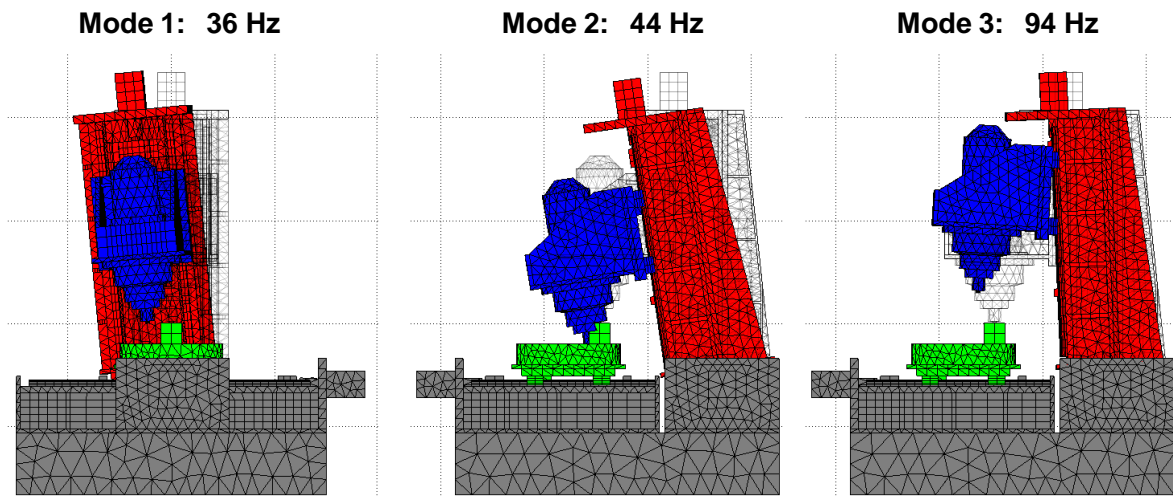
Figure 6.9: Plot of the first three mode shapes obtained by a rigid body modal analysis.

6.3.2 Harmonic analysis

By selecting the *FRF Analysis* option, the integrated harmonic analysis tool opens. The bodies and coordinates of the excitation and response points can be entered manually or alternatively taken directly from the original TCP and WPP definition. As a result, the relative displacements between the two points are evaluated and plotted, as shown in figure 6.10. The resonance peaks sorted by relative amplitude at the TCP can be additionally computed and listed.

A useful plot of the normalized frequency-dependent potential energy in the axis couplings (equation (6.1)) is a further qualitative indicator to determine possible weak spots in the

structure and can be called for every new excitation point or direction. As interpretation example, it can be observed in figure 6.11 that at $36Hz$ and $44Hz$, the most relevant energy amount is stored in the X1-axis, whereas at $290Hz$ the energy in the Z1-axis is prevalent and over $300Hz$ the predominant part of potential energy is stored in the Y1-axis.

$$E_i(\omega) = \frac{\sum_{j=1}^{N_i} \frac{1}{2} k_{ij} x_{ij}^2(\omega)}{\sum_{i=1}^{M} \sum_{j=1}^{N_i} \frac{1}{2} k_{ij} x_{ij}^2(\omega)} \ , \ \forall \ \omega \tag{6.1}$$

$$
\begin{aligned}
N_i &: \quad \text{number of couplings in axis } i \\
M &: \quad \text{total number of axes} \\
k_{ij} &: \quad \text{stiffness of coupling } j \text{ in axis } i \\
x_{ij} &: \quad \text{displacement of coupling } j \text{ in axis } i
\end{aligned}
$$
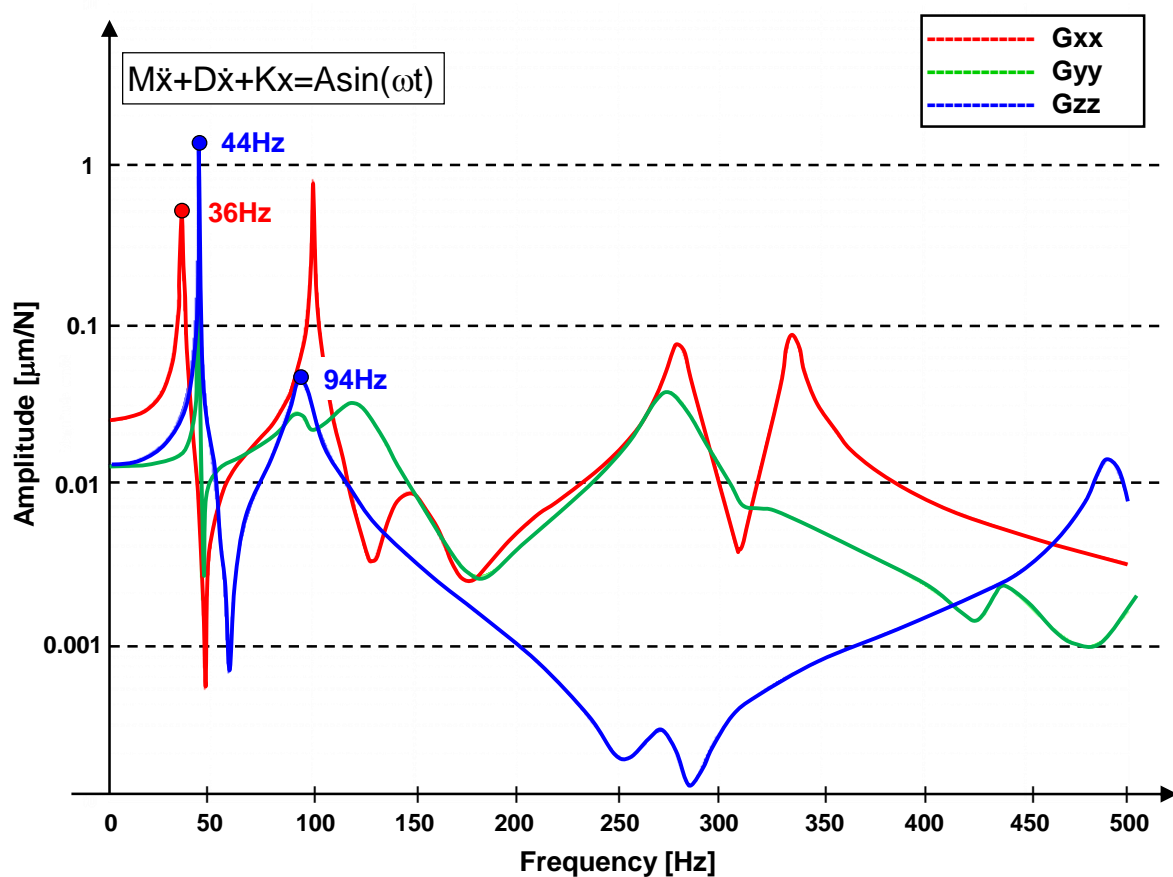
Figure 6.10: Plot of the three principal transfer functions G_{xx}, G_{yy} and G_{zz} at the TCP.
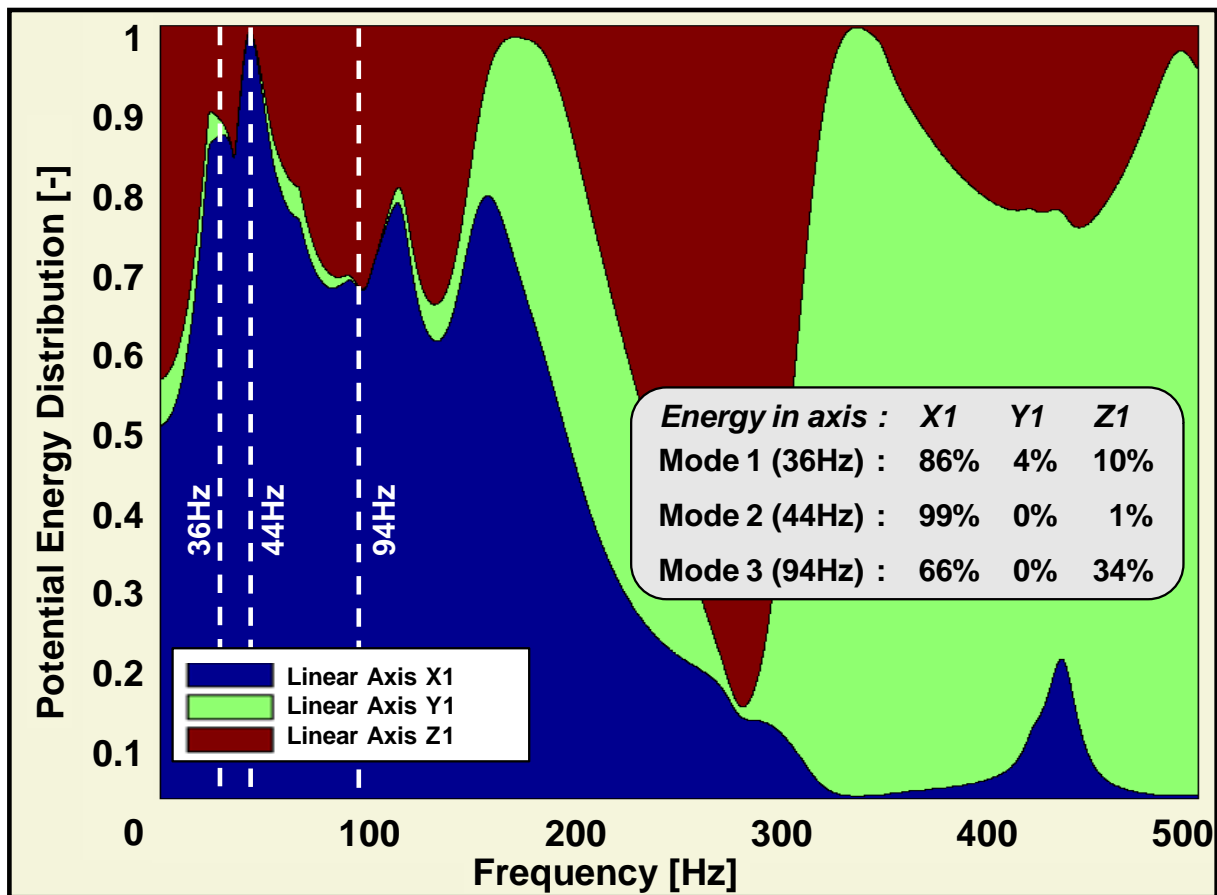
Figure 6.11: Graphical representation of the frequency-dependent distribution of
potential energy in the couplings for the harmonic loadcase considered in figure 6.10.

6.3.3 Static analysis

The *Static Analysis* option is a tool to evaluate the stiffness behavior of the entire structural
loop of the machine tool. By performing a static simulation, the displacements at the
TCP and WPP and the loads in the axis couplings are automatically computed for a set
of predefined loadcases:

- One loadcase where all bodies are subject to gravitational forces
- Three loadcases corresponding to forces in directions X, Y and Z
  between tool tip (TCP) and workpiece (WPP) $(1000N)$
- Three loadcases corresponding to torques about directions X, Y and Z
  between tool tip (TCP) and workpiece (WPP) $(1000Nm)$
- A set of quasi-static loadcases corresponding to individually applied
  reference accelerations of $10ms^{-2}$ of the single linear axes of the machine

In a new graphical window, the deformed structure for each loadcase can be displayed (figure 6.12 left). For every loadcase of the static analysis, the load amplitudes in every single joint are additionally computed. With the extra *Coupling Loads* function, a pop-up table is created giving the value and the position of the maximum load for every linear and rotary axis. The identified maxima are then plotted on the machine structure, as displayed in figure 6.12 right.
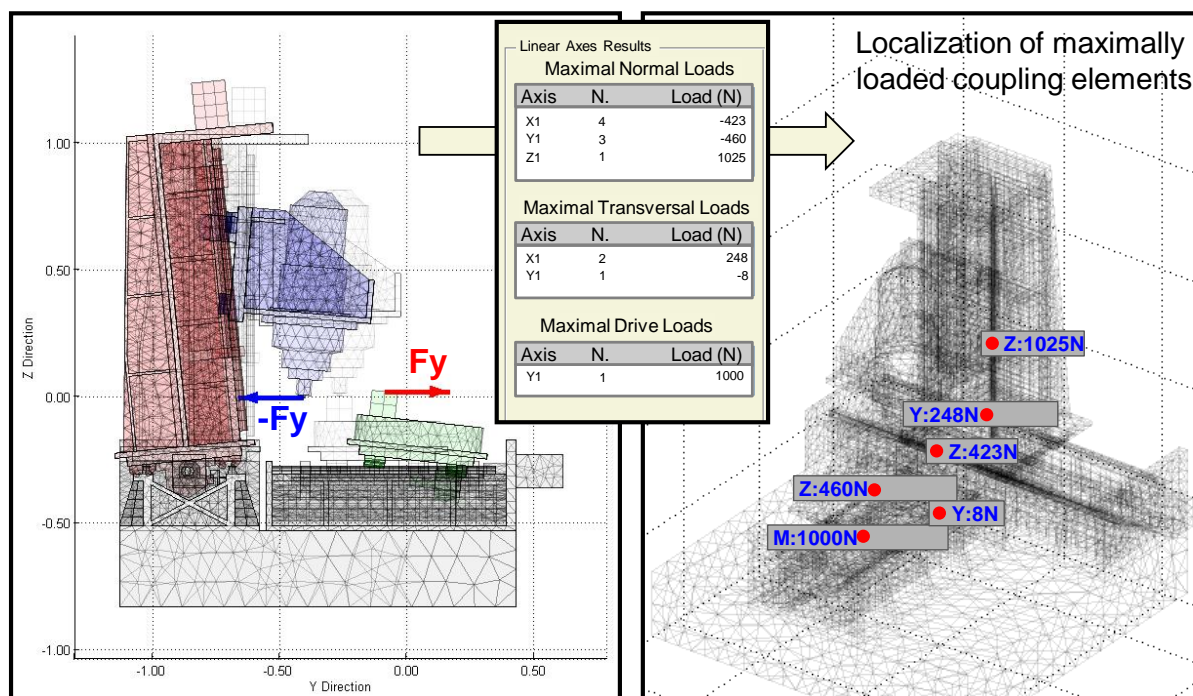
Figure 6.12: Deformed structure subject to a static loadcase F_y at the TCP (left) – with the corresponding maximum loads in the axis couplings (right).

6.3.4 Sensitivity analysis

The *Sensitivity Analysis* tool is a central feature of the stand-alone GUI. It gives at a glance all the locally linearized dependencies of machine tool specific output variables relatively to a set of predefined input parameters. In order to study the static and dynamic behavior of a machine tool in more detail, the following *quality parameters* are used:

– $KTCP\_X$:   Stiffness value at TCP in direction X
  $KTCP\_Y$:   Stiffness value at TCP in direction Y
  $KTCP\_Z$:   Stiffness value at TCP in direction Z

- 1st Peak: The frequencies of the highest three peaks
  2nd Peak: resulting from the harmonic responses at
  3rd Peak: TCP in directions X, Y and Z

- EX_Y, EX_Z: TCP displacement in direction X
  by an acceleration of axes Y resp. Z

- EY_X, EY_Z: TCP displacement in direction Y
  by an acceleration of axes X resp. Z

- EZ_X, EZ_Y: TCP displacement in direction Z
  by an acceleration of axes X resp. Y

The dependencies of these *quality parameters* are computed relatively to the following *design parameters*, whose variation during the sensitivity analysis is either relative or absolute, depending on the type of parameter:

- KN, KQ, KM: Local normal, transversal and drive stiffness parameters
  (available for linear axes)

- L, W: Length and width of a linear axis guideway system

- R_X: Orientation of a linear axis (rotation about motion direction)

- $PosYM$, $PosZM$:   Position of the driving point in the local directions Y and Z

- $PosX$, $PosY$, $PosZ$: Geometric centre of the coupling points of linear
  and rotary axes (see figure 6.8)

- KX, KY, KZ: Stiffness values in local directions X, Y and Z
  (available for bed mounting elements)

- $Krad$:   Local radial stiffness (available for rotary axes)

- Kax: Local axial stiffness (available for rotary axes)

The *quality parameters*, *design parameters* and the results of the sensitivity analysis appear in a table as the example shown in table 6.2 for the case of axis X1. In the leftmost column, the names of the *design parameters* are listed, with the respective nominal values in the second column. In the top row the *quality parameters* are found, with the respective reference values in the second row. A sensitivity analysis consists in varying every single design parameter by an absolute or relative amount (depending on the type of parameter)

and filling the table with the resulting absolute or relative (depending on the type of parameter) variations of the quality parameters. A short inspection of the output for each single axis provides immediate valuable indications on the most relevant factors influencing the behavior of the machine tool, as outlined in table 6.2 in the blue and red boxes. In each column, the largest values have to be taken into consideration. For the columns $KTCP\_X$, $KTCP\_Y$, $KTCP\_Z$, $Peak\_1$, $Peak\_2$ and $Peak\_3$, the values in the table correspond to a *percentage* variation of the quality parameter caused by a variation of the design parameters according to the settings indicated in the rightmost column. For the columns EX_Z1, EY_Z1, EY_X1, EZ_X1, EZ_Y1 and EX_Y1, the values in the table correspond to an *absolute* variation of the quality parameter caused by a variation of the design parameters according to the settings indicated in the rightmost column. For example:

- *Peak 1* (44Hz) increases by ca. 8.9% by a 10% increment of the distance *W_X1* between the carriages of axis X1.
- The cross-talk deviation *EY_Z1* decreases by 5.80μm if the median position *PosX_X1* of axis X1 is moved by 50mm

Table 6.2: Output of the sensitivity analysis of axis X1. Outlined are the most relevant design parameters.

		KTCP_X	KTCP_Y	KTCP_Z	Peak 1	Peak 2	Peak 3	EX_Z1	EY_Z1	EY_X1	EZ_X1	EZ_Y1	EX_Y1	
		40.9	80.4	78.0	44.0	100.4	35.9	0.4	0.6	0.1	-0.1	0.7	0.0	
	Ref.	N/μm	N/μm	N/μm	Hz	Hz	Hz	μm	μm	μm	μm	μm	μm	Incr.
PosX_X1	0.0 mm	0.97	-0.28	-0.21	-0.23	1.00	0.56	-2.94	-5.80	-0.92	0.00	0.00	0.00	+50 mm
PosY_X1	0.0 mm	0.00	0.02	6.01	1.81	0.00	0.00	0.26	-0.50	-0.07	-0.87	0.00	0.00	+50 mm
PosZ_X1	0.0 mm	0.00	2.73	0.13	4.09	0.00	0.00	-0.11	0.27	0.22	-1.52	0.00	0.00	+50 mm
RX_X1	0.0 °	-0.79	0.01	-0.01	0.00	1.19	-0.84	0.05	0.04	0.02	-0.08	0.00	0.00	+5 °
L_X1	321.0 mm	6.41	0.00	0.00	0.00	7.47	5.84	-0.06	-0.10	-0.02	0.00	0.00	0.00	10%
W_X1	338.0 mm	0.00	1.52	6.55	8.86	0.00	0.00	0.00	-0.01	-0.01	-1.55	0.00	0.00	10%
KN_X1	666.0 N/mm	0.45	0.79	3.59	4.31	0.60	2.50	0.00	-0.09	-0.02	-0.82	0.00	0.00	10%
KQ_X1	426.0 N/mm	2.77	0.39	0.00	0.23	3.08	0.56	-0.07	0.00	0.00	0.00	0.00	0.00	10%
KM_X1	168.0 N/mm	2.26	0.00	0.00	0.00	0.00	1.67	0.00	0.00	0.00	0.00	0.00	0.00	10%
PosYM_X1	0.0 mm	5.28	0.02	0.29	0.23	-0.70	1.67	-0.34	0.52	0.07	-0.05	0.00	0.00	+50 mm
PosZM_X1	-9.4 mm	1.59	0.16	0.06	0.23	0.20	3.34	0.13	-0.31	-0.24	-0.09	0.00	0.00	+50 mm
		%	%	%	%	%	%	μm	μm	μm	μm	μm	μm	

6.3.5 Parametric analysis

The last analysis option consists in varying design parameters between user-defined boundaries and graphically represent the results on selected quality parameters. The *Parametric*

Analysis opens a setup window where it is possible to select one or two design parameters, as well as a set of corresponding quality parameters, depending on the chosen analysis type:

- Static analysis – Force at TCP

    o $X - TCP$ stiffness
    o $Y - TCP$ stiffness
    o $Z - TCP$ stiffness

- Static analysis – Acceleration loads (cross-talk deviations)

    o Relative TCP–WPP displacement in X-direction
    o Relative TCP–WPP displacement in Y-direction
    o Relative TCP–WPP displacement in Z-direction

- FRF analysis – Force at TCP

    o 1st FRF peak
    o 2nd FRF peak
    o 3rd FRF peak
    o G_{xx} FRF response
    o G_{yy} FRF response
    o G_{zz} FRF response

The asset of a parametric analysis is, based on the results of the sensitivity analysis described in section 6.3.4, to extend the analytical investigation to a wider range of parameter variations. The sensitivity analysis specifies which design parameters should be preferentially targeted to improve a certain quality parameter; a subsequent parametric analysis allows to actually study the behavior of the machine tool with respect to the identified critical parameters in a more comprehensive manner. Referring to the results shown in table 6.2, two illustrative parametric analyses are performed: the first one consists in varying simultaneously the distance between the carriages of axes $X1$ and $Z1$ between $0.25m$ and $0.4m$ and representing in a 2D plot the resulting modification of the static stiffness in direction X at the TCP in $N/\mu m$ (figure 6.13). In the second analysis, the horizontal position (X and Y) of the couplings center of the axis X1 is varied between $-0.1m$ and $+0.1m$. The influence of these two parameters on the cross-talk deviation EY_Z1 at the TCP in μm, subject to an acceleration $a_x = 10ms^{-2}$ of the Z-axis is displayed in the corresponding 2D plot (figure 6.14).
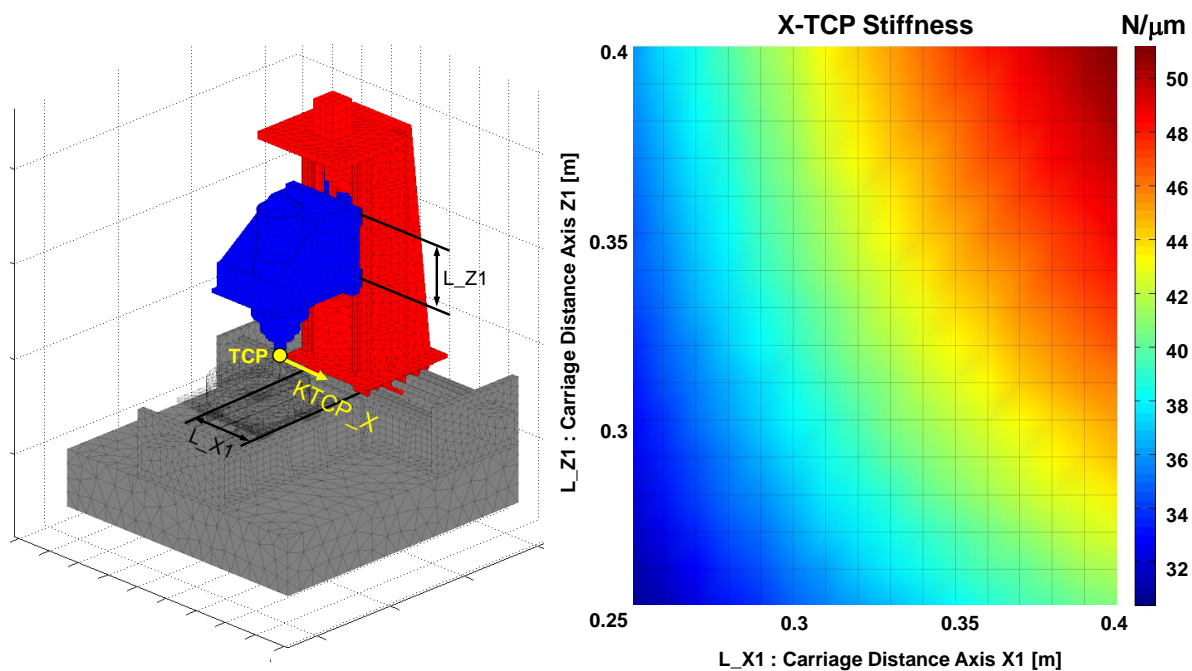
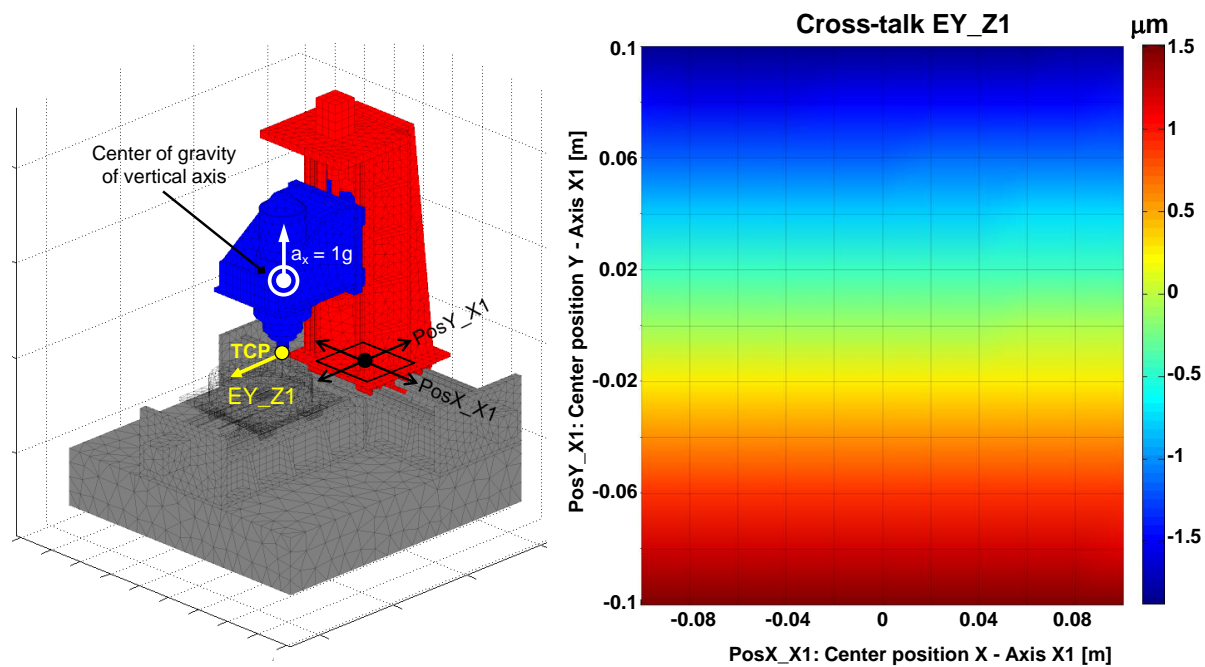Figure 6.13: X-TCP static stiffness vs. carriage distance of axes X1 and Z1.

Figure 6.14: Cross-talk deviation EY_Z1 at TCP vs. horizontal couplings position of axis X1.

6.4   Match between FEM and RBS models

Given the rigid body analysis capabilities presented in section 6.3 and the guidelines regarding a stiffness scaling factor for the adjustment of the joint behavior between FEM and RBS simulations, the next step is to verify the presented results on the two machine tools introduced in chapter 5.

The static and modal analyses carried out in ANSYS Workbench on the two machines serve as basis for comparison. As already mentioned, a rigid body model is supposed to correctly evaluate the behavior of a structure with the consciousness that the accuracy is limited compared to a detailed FE model. The objective is therefore not to find an optimal scaling factor adapted to a specific machine in a specific configuration and for a specific loadcase. The point is rather to have a generalized rule which provides satisfactory results for every machine, whatever the configuration or the loadcase, keeping in mind the limits of the modeling assumptions.

The scaling factors summarized in table 6.3 are applied to the rigid body models of machines A and B. The values of 50% are derived from the observed average *Strain Energy Ratio R_ϵ of 0.5*. For the stiffness coefficients K_Z and K_C of rotative bearings, a factor of 100% is assumed due to the supposed rigid nature of the axial and torsion connections. For the stiffness coefficients K_X, K_Y and K_Z of mounting elements, the scaling factor is strongly dependent on the way the feet are fixed to the machine bed (figure 6.15), that is why a range of $50 - 100\%$ is given. For a massive cast iron part, a stiffness scaling factor of 100% for K_X, K_Y and K_Z is appropriate, for a frame composed of O-profiles, a stiffness scaling factor of 50%, at least in the vertical direction K_Z, would be more adapted. For all the cases in between, a systematic study for the different mounting configurations and sizes would be needed to establish reliable scaling factors.

Table 6.3: Generalized scaling factors for rigid body models of machine tools.

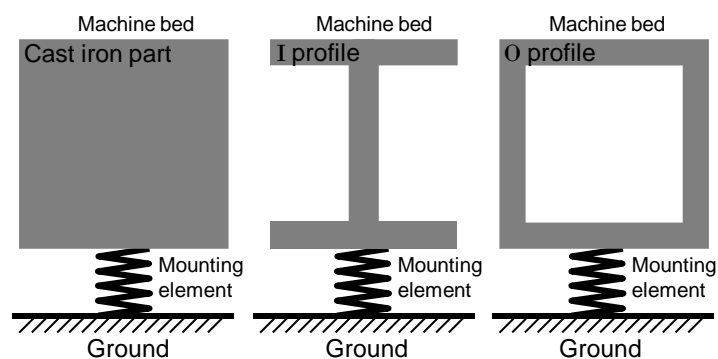| Axis type	Coupling type	Stiffness component	scaling factor for joint stiffness
Linear axis	Rail / Carriage	KY / KZ	50%
		KA / KB / KC	50%
	Ballscrew / Nut	KX	50%
Rotary axis	Rotative Bearing	KX / KY	50%
		KA / KB	50%
		KZ / KC	100%
Fixed axis	Mounting element	KX / KY / KZ	$50\% - 100\%$

Figure 6.15: Three illustrative examples of mounting elements between ground and machine bed.

6.4.1   Match between FEM and RBS with static analyses

For the matching of static analyses between FEM and RBS models, the simulation results already available in ANSYS are reproduced using the *Static Analysis* option of the stand-alone GUI (see section 6.3.3). The four loadcases applied to machine A and pictured in figure 5.3 are defined in the rigid body environment by adequately moving the axes and by resetting the corresponding position of the load application point using the coordinates of the TCP and WPP. The four resulting RBS models are found in figure 6.16.

The complete outcome of the static analyses is summarized in table 6.4, where it can be observed that the relative error of the RBS model reaches a maximal value of 17%. All the stiffness values are scaled relatively to the respective experimental results, listed in the right column. Considering the rigid body assumption and that the four loadcases are defined in such a way that excessive bending of structural parts of the machine are avoided, these results are the confirmation of the pertinence of the guidelines regarding the scaling factors of the axis couplings stiffness.

The results of machine B, on the basis of the static experiments of figure 5.5, are a good illustration of the limits of rigid body static analyses, in the particular case of forces or moments leading to important structural deformations like bending. The more pronounced the cantilever nature of a structural part, the more important becomes the error of the rigid body model. The stiffness scaling factors are able to compensate for the local deformations close to the joints, but cannot take into account global deformations of machine bodies. Loadcase FY, whose FE deformed state is shown in figure 6.17, is responsible for an important bending of both depicted rotary axes A and C. This is the reason why the relative error of the RBS model reaches a maximum value of 69%, as evidenced in table 6.5. Again, all the stiffness values have been scaled relatively to the respective experimental results, listed in the right column.
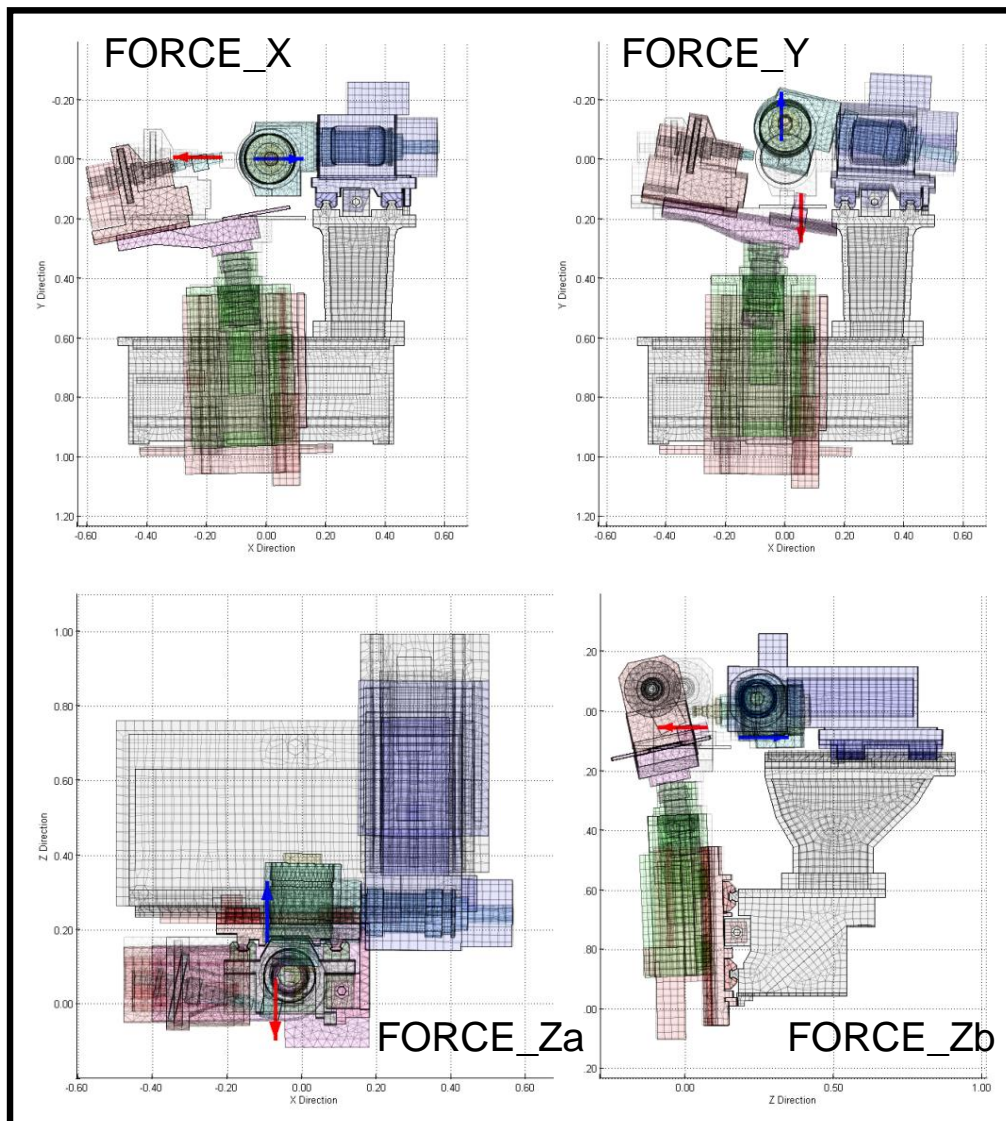
Figure 6.16: Rigid body simulations of the four loadcases of figure 5.3
(Axes in the same positions and forces depicted are applied between TCP and WPP).

6.4.2   Match between FEM and RBS with modal analyses

The second verification method to validate the rigid body models consists in computing the resonance frequencies and the mode shapes integrated in the stand-alone GUI (see section 6.3.1) and comparing them with the results of the modal analyses previously carried out in ANSYS Workbench. The matching principle is based on the visual inspection of the eigenmodes and the difference of the corresponding eigenfrequencies, as in the examples on figures 6.18 and 6.19.

Table 6.4: Results of static analyses with FEM and RBS models of machine A.

Static stiffness machine A	FEM	RBS	Deviation FEM-RBS		EXP
	K [N/μm]	K [N/μm]	abs.	%	K [N/μm]
FORCE_X	1.22	1.37	0.15	12	1
FORCE_Y	1.31	1.53	0.22	17	1
FORCE_Za	1.03	1.12	0.09	9	1
FORCE_Zb	1.13	1.24	0.11	10	1
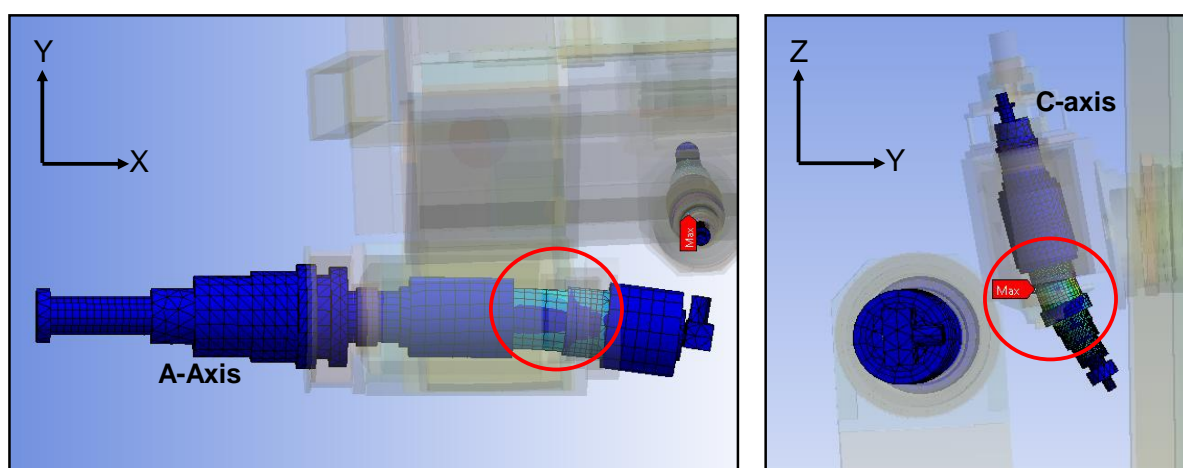
Figure 6.17: Deformed FE structure of machine B due to a force in direction FY at the TCP.

Following the same procedure as in section 5.2 for the matching between experimental and finite element modal analyses, the ratios of the RBS frequencies to the FEM frequencies for the identified modes are plotted.

In figure 6.20, it can be observed that the relative error over a frequency range of $0-300Hz$ varies between -25% and $+25\%$ for machine A. Mode number 15, characterized by a local structure deformation, could not be matched. The first two modes involve the compliance of the machine frame, on which the machine bed is mounted (figure 5.10). Modes 7 and 8 evidence a flexion mode of one of the rotary axes. These higher deviations are the consequences of the homogeneous scaling factors applied to the whole machine structure.
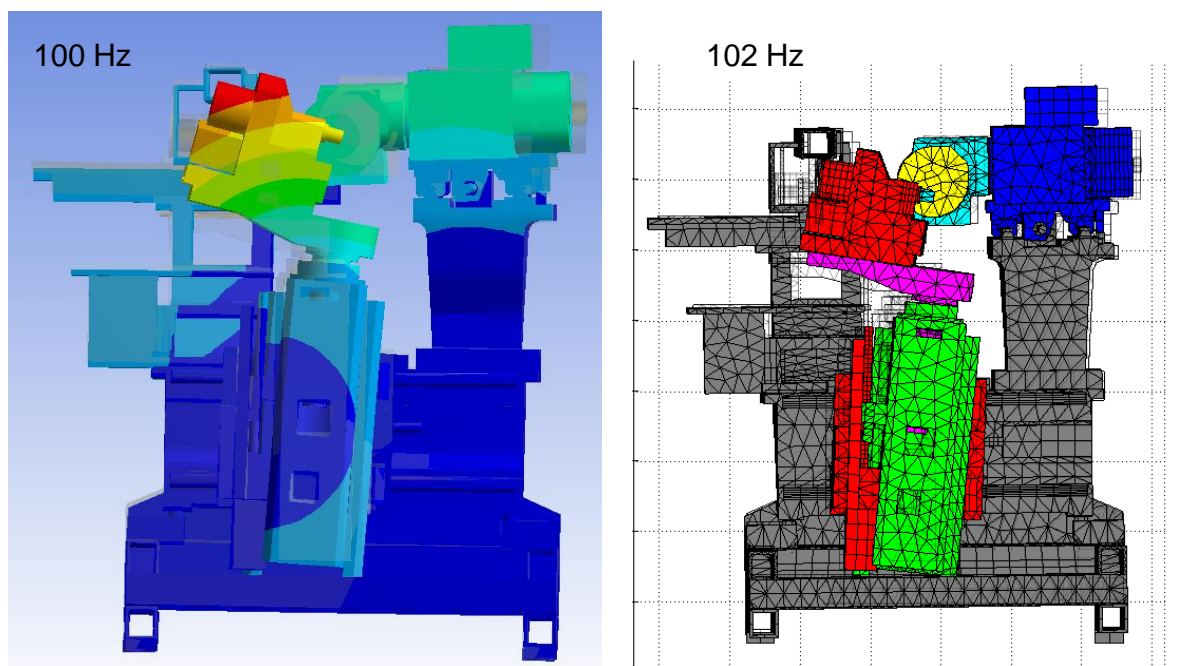
Figure 6.18: 8th mode (scaled frequency):
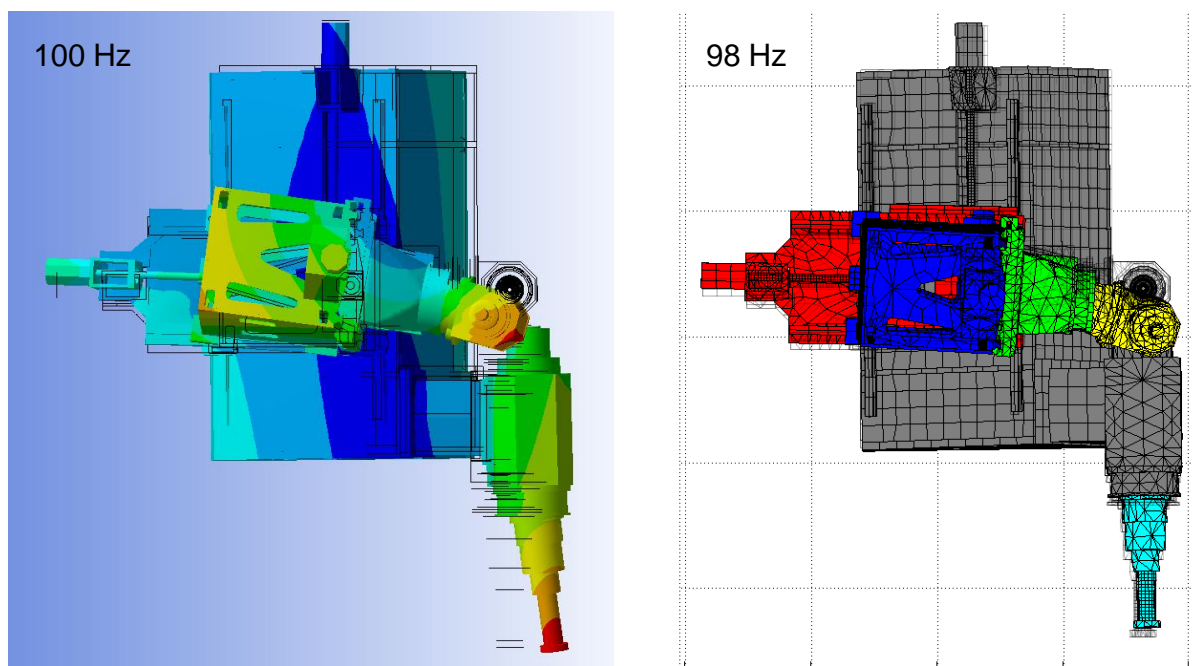illustrative matching between FEM and RBS modal analysis of machine A.

Figure 6.19: 8th mode (scaled frequency):
illustrative matching between FEM and RBS modal analysis of machine B.

Table 6.5: Results of static analyses with FEM and RBS models of machine B.

Static stiffness machine B	FEM	RBS	Deviation FEM-RBS		EXP
	K [N/μm]	K [N/μm]	abs.	%	K [N/μm]
FORCE_X	1.09	1.37	0.28	26	1
FORCE_Y	1.02	1.73	0.71	69	1
FORCE_Z	0.94	1.08	0.14	16	1

But even though some local effects might not be ideally modeled with the rigid body scaling guidelines, the maximal error deviations remain undeniably acceptable.

For machine B, the error lies between -10% and $+15\%$ for the same frequency range, as evidenced in figure 6.21. As it was the case for one mode in machine A, the missing modes in the plot all involve local deformations of the external frame visible in figure 5.12, which, for obvious reason, can't be reproduced with a rigid body model.
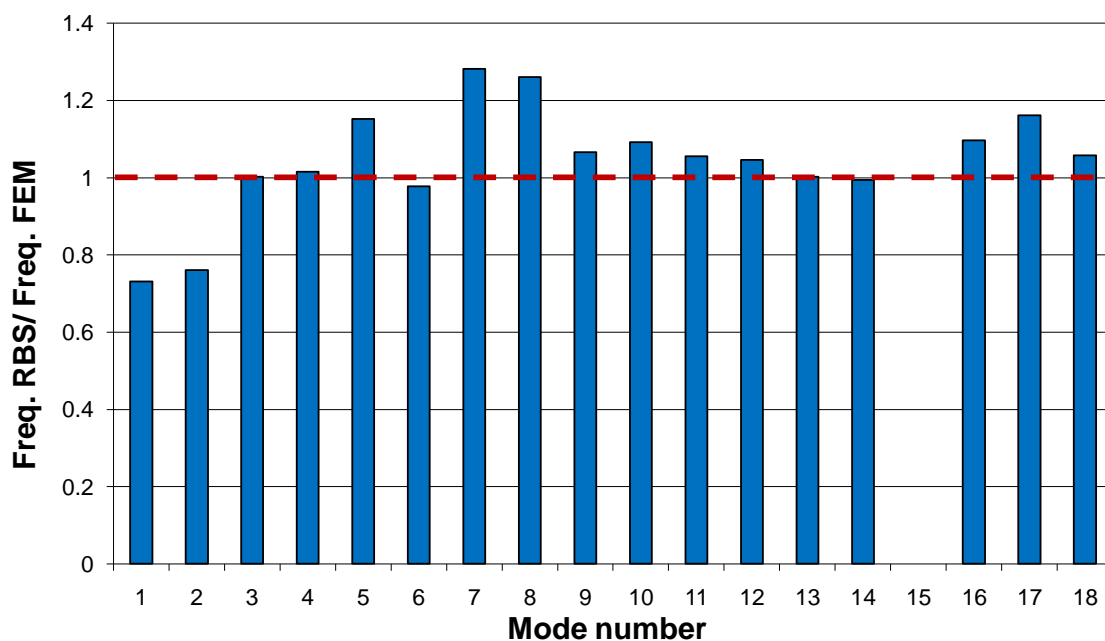
Figure 6.20: Results of modal analyses with the FEM and RBS models of machine A.
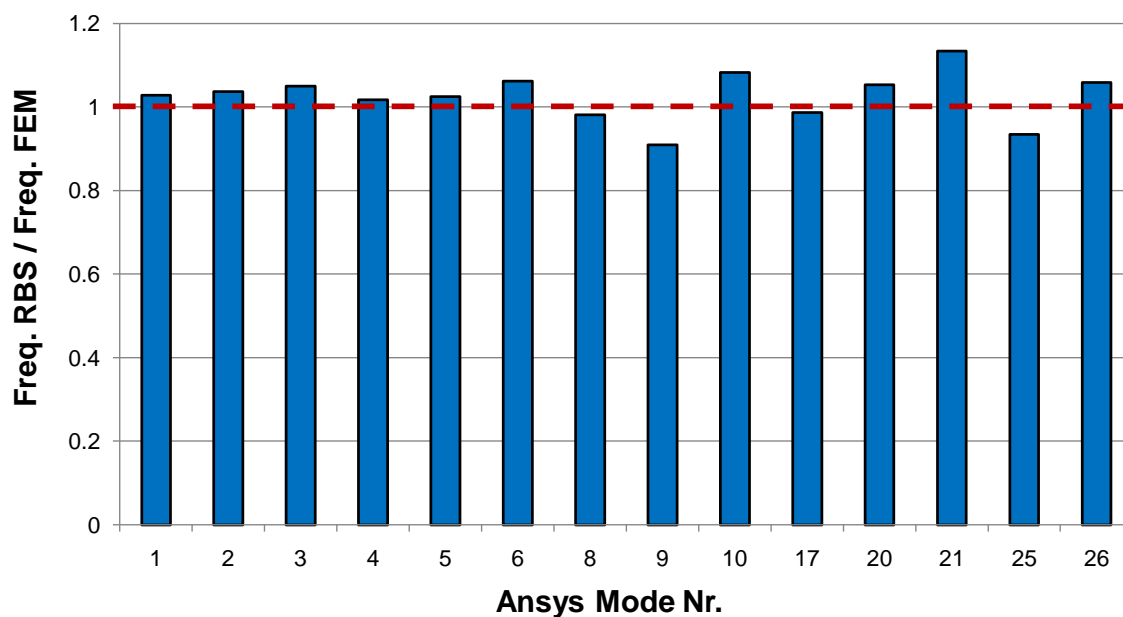
Figure 6.21: Results of modal analyses with the FEM and RBS models of machine *B*.

The two investigated machines have been compared using the complete versions of axis arrangements, i.e. including all linear axes, rotary axes, spindles and mounting elements. Sources of inaccuracies are therefore all the more possible, especially when comparing analyses ranging from static loadcases with forces in different directions to modal analyses considering all resonance modes up to $300Hz$. Given these conditions, it can be stated that the guidelines formulated at the beginning of section 6.4 have proved reliable and efficient for a multitude of structural analyses, making of the developed rigid body tool a very valuable support adapted to the requisites of modern machine design.

Chapter 7

Advanced mechatronic analysis of machine tools

Referring to section 3.3 pointing out the motivations behind a *Structure Gateway Interface* and the options available for the ANSYS user, the present chapter will be focusing on the option *CRS*. The developed mechatronic toolbox is based on *Coupled Reduced Simulations*, which extend the validity of the model by including the flexibility of the structural parts in form of reduced state-space matrices and by incorporating a control system at the interface between the machine tool axes.

7.1   SGI output for coupled reduced analysis

In this section, the scripts developed in order to export the data of the FE model needed for coupled reduced analysis in Matlab/Simulink are reviewed. The integration of the stored data into a complete mechatronic model of a machine tool is then described in the sections 7.2 to 7.6.

7.1.1   Principle of export scripts for order reduction

The *CRS* export procedure is illustrated based on the structure in figure 3.9, representing a two-axis machine tool model. The information required for coupled reduced analysis is retrieved in three distinct steps, executed individually in a loop over the machine bodies defined by the volume components (figure 3.5): writing of the full files containing the FE system matrices of the axis bodies, writing of the node properties of the axis couplings and writing of the joint properties of the axis couplings.

The process and the successive functions executed by the CRS export scripts are illustrated in figure 7.1, with one loop over the volumes indicated by index i and one loop over the couplings indicated by index j.

7.1.2   Output data needed for order reduction

The objective of the export operation using the *CRS* option is to extract the required data from the complex FE model, in order to obtain a simplified structure described by reduced system matrices of the machine bodies. In figure 7.2, the process leading from a detailed discretized model to a low-order model, without losing the information of the machine axis interfaces, is visualized.

To achieve the translation, the three steps referred to in section 7.1.1 produce the following files:

- the *body_matrices.full* file contains the complete set of system matrices of the single bodies (figure 3.5)

- the *body_nodes.txt* file contains information related to the coupling nodes defining the interfaces of the single bodies (figure 3.6)

- the *coupling_parameters.txt* file contains information related to the joint properties of the machine axes (figures 3.7, 3.8)

Instead of solving the system, APDL macros are developed to export the matrices. The exported ANSYS *full* file is characterized by the following properties: the finite element model (described by the system matrices), a loadcase (for structural analyses: a force or a moment, an application node and a direction), one or more evaluation nodes (in *output.txt*) and a frequency, defined within the options of the harmonic analysis.

The complete export data flow is recapitulated in figure 7.3, showing the succession of the writing operations, which are implemented to obtain the desired outputs in the desired format customized for machine tool models.

After the *CRS* export, the simulation run continues in Matlab/Simulink, where the following data and programs are required, in order to proceed to the building of a reduced mechatronic model of a machine tool:
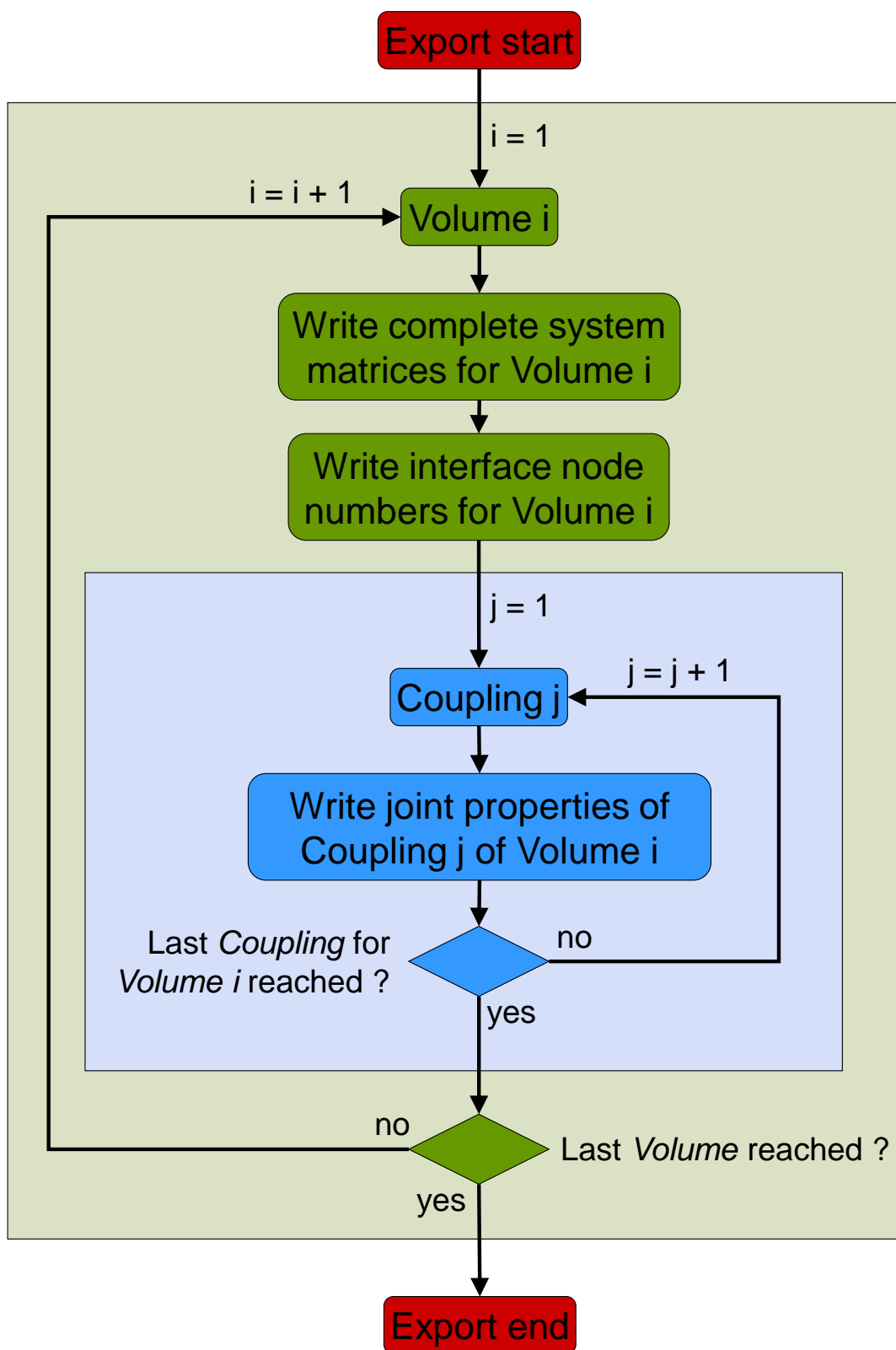
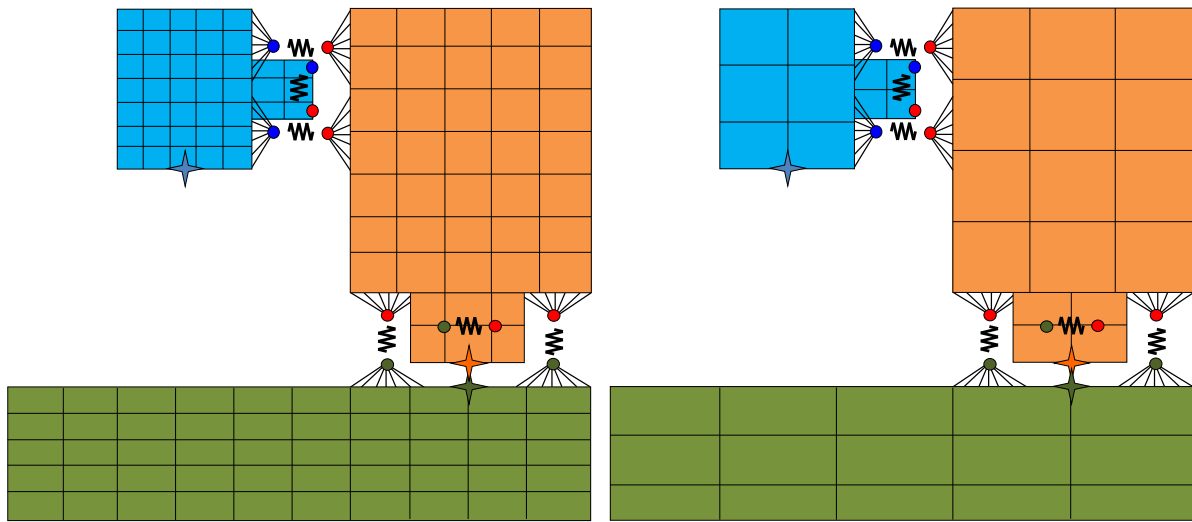Figure 7.1: Process flow diagram for export of CRS data.

Figure 7.2: Translation of a full FE model into a reduced FE model.

- Matlab software with Simulink toolbox

- MORforANSYS.exe, stand-alone reduction program based on the Krylov-Method and implementing the Arnoldi algorithm (section 2.1.3)

- The customized set of files exported using the ANSYS *CRS* option (section 7.1.2).

The operational flow in Matlab is outlined in figure 7.4. It is important to note that, except for the reduction parameters and the loadcase settings, the whole process is fully automated. The toolbox consists of a set of Matlab scripts developed specifically for mechatronic models of machine tools and has the function of implementing all the couplings, structural dynamics and control properties, independently of the number and nature of volumes, axes, couplings, loads, etc.

7.2 Model order reduction of machine bodies

After the export is terminated, all volumes and couplings having been processed, the solve run in ANSYS is aborted. The output of the simulation consists of a set of *full* and *text* files, which are archived and made available for further use in a dedicated mechatronic toolbox based on Matlab/Simulink.

The first operation in the creation of a mechatronic model consists in carrying out a model order reduction of the FE matrices exported from ANSYS. *MOR for ANSYS*, introduced in section 2.1.3 within the review of the various available reduction methods, is the reduction
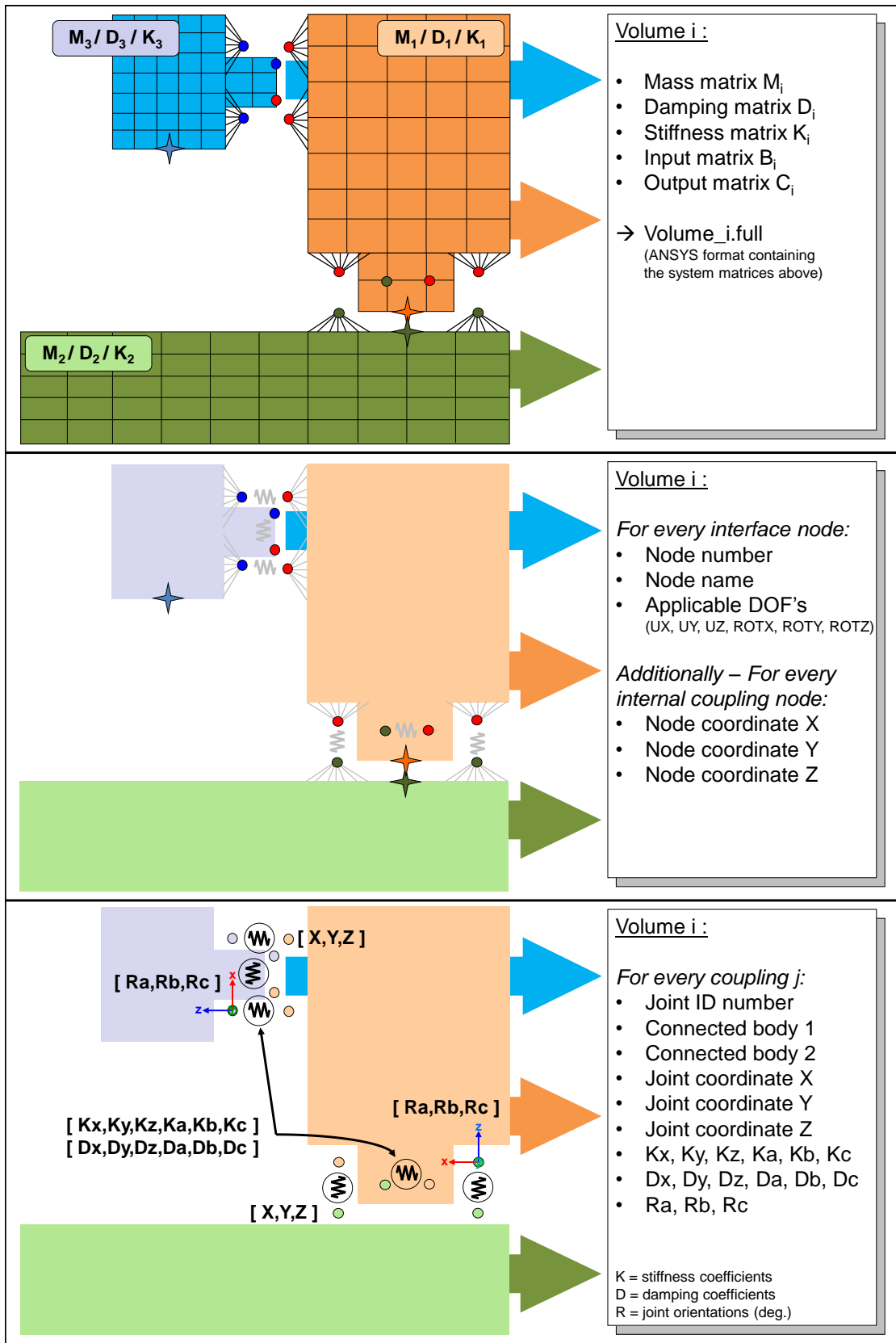
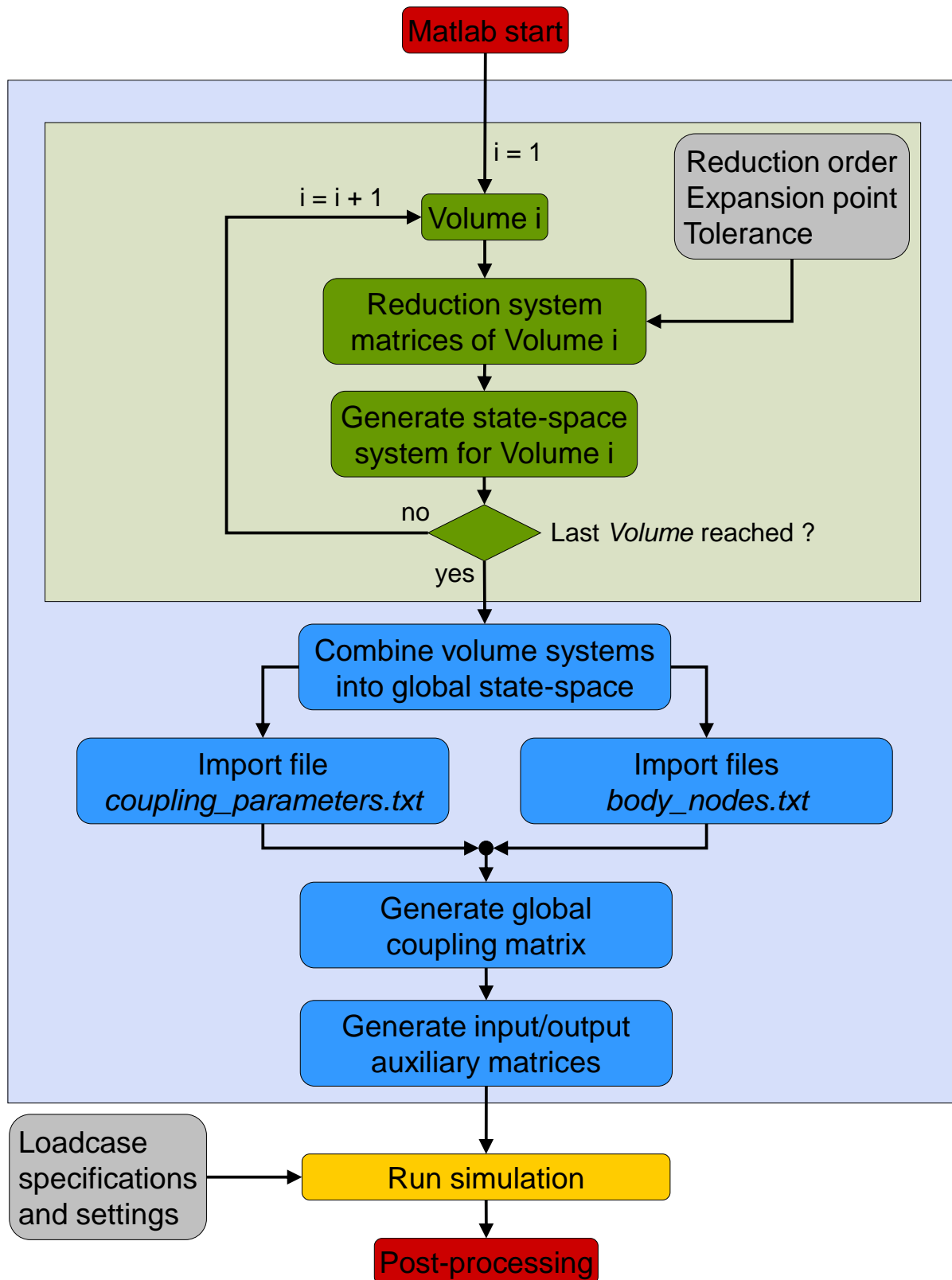Figure 7.3: CRS data set: system matrices, interface nodes and joint properties.

Figure 7.4: Operational flow leading to the mechatronic model in Matlab/Simulink.

algorithm selected to be integrated in the mechatronic simulation tool. This choice is motivated by different reasons:

- It is implemented to work with ANSYS files, which is the chosen FE program of the *Structure Gateway Interface*

- It is a stand-alone program, allowing a flexible and customizable application

- It has evidenced outstanding results in terms of computational time and accuracy compared to other reduction techniques

The commercial program MOR for ANSYS is integrated into the Matlab process and is executed for every volume which has been exported from ANSYS and corresponding to the sub-assemblies of the machine tool. For the case of the two-axis machine tool composed of three bodies, the following commands are required:

volume 1:

mor_for_ansys volume_1_f1.full volume_1_f1e10.full **-C** output_1.txt **-N** 50 **-o** body_1 **-t** 1e-15 **-x** 0

volume 2:

mor_for_ansys volume_2_f1.full volume_2_f1e10.full **-C** output_2.txt **-N** 50 **-o** body_2 **-t** 1e-15 **-x** 0

volume 3:

mor_for_ansys volume_3_f1.full volume_3_f1e10.full **-C** output_3.txt **-N** 50 **-o** body_3 **-t** 1e-15 **-x** 0

For each volume, two full files are actually needed for second order systems, obtained with two distinct frequencies, in order to obtain the matrices M, D and K from equation (7.1).

$$(-\omega^2 M + i\omega D + K)x(\omega) = F \tag{7.1}$$

The *output.txt* file contains the data related to the interface nodes, as described in figure 7.3. Additionally, the following options (which don't have to be the same for every volume) must be specified for the reduction algorithm:

- *-C* specifies, for each volume to be reduced, the text file containing the interfacing node numbers and the corresponding degrees of freedom

- *-N* specifies the desired dimension of the resulting reduced matrices

- *-o* specifies an arbitrary name for the resulting reduced matrix

- *-t* specifies the norm tolerance for deflation of the generated subspace vectors

- *-x* specifies the frequency point to be used during the Taylor series expansion

The standard commercial version of MOR for ANSYS provides the possibility, using the *-m* option, to include, into the same reduction process, one additional full file for every different loadcase defined in the ANSYS model. The reduction process combines the single B and C matrices (equation (7.2)), composed of *zeros* and *ones* filled in the right places, and computes one reduced matrix B and one reduced matrix C, which include the complete input/output information of the model.

For the specific characteristics of a machine tool model, where the axes are generally composed of at least four joints, each having to transmit loads in six directions (FX, FY, FZ, MX, MY and MZ) between the machine bodies, this solution is not optimal. Instead, a new custom-made option *-mp* has been integrated by the software provider, allowing the use of just the two original full files (with one arbitrary loadcase) The global B and C matrices, such as $B^T = C$, are subsequently assembled using the information in *output.txt*, considering every interface node as a potential loading point. This has the advantage of massively reducing both the export times and the memory storage requirements.

The resulting reduced matrices contain the structural properties of the single machine bodies, whose dynamical properties are described by the characteristic equation for second-order systems (7.2):

$$
\begin{aligned}
M\ddot{z} + D\dot{z} + Kz &= Bu \\
y &= Cz
\end{aligned}
\tag{7.2}
$$

Using the variable transformation in (7.3):

$$
\left.
\begin{aligned}
\dot{z} &= x_1 \\
z &= x_2
\end{aligned}
\right\} = x
\tag{7.3}
$$

the system is transformed into a first order system of double dimension (7.4):

$$
\begin{aligned}
M\dot{x}_1 + Dx_1 + Kx_2 &= Bu \\
y &= Cx_2
\end{aligned}
\tag{7.4}
$$

Or formulated in matrix form (7.5):

$$
\begin{bmatrix} M & O \\ O & I \end{bmatrix} \begin{bmatrix} \dot{x}_1 \\ \dot{x}_2 \end{bmatrix} + \begin{bmatrix} D & K \\ -I & O \end{bmatrix} \begin{bmatrix} x_1 \\ x_2 \end{bmatrix} = \begin{bmatrix} B & O \\ O & O \end{bmatrix} \begin{bmatrix} u \\ O \end{bmatrix}
$$

$$
y = \begin{bmatrix} O & C \end{bmatrix} \begin{bmatrix} x_1 \\ x_2 \end{bmatrix} \tag{7.5}
$$

By rearranging the equations (7.5), the resulting state-space model takes the form (7.6):

$$
\begin{bmatrix} \dot{x}_1 \\ \dot{x}_2 \end{bmatrix} = \begin{bmatrix} M & O \\ O & I \end{bmatrix}^{-1} \begin{bmatrix} -D & -K \\ I & O \end{bmatrix} \begin{bmatrix} x_1 \\ x_2 \end{bmatrix} + \begin{bmatrix} M & O \\ O & I \end{bmatrix}^{-1} \begin{bmatrix} B & O \\ O & O \end{bmatrix} \begin{bmatrix} u \\ O \end{bmatrix}
$$

$$
y = \begin{bmatrix} O & C \end{bmatrix} \begin{bmatrix} x_1 \\ x_2 \end{bmatrix} \tag{7.6}
$$

By defining matrix A and redefining matrices B and C as follows in equation (7.7),

$$
A = \begin{bmatrix} M & O \\ O & I \end{bmatrix}^{-1} \begin{bmatrix} -D & -K \\ I & O \end{bmatrix}
$$

$$
B = \begin{bmatrix} M & O \\ O & I \end{bmatrix}^{-1} \begin{bmatrix} B & O \\ O & O \end{bmatrix}
$$

$$
C = \begin{bmatrix} O & C \end{bmatrix} \tag{7.7}
$$

the reduced system is reformulated in the standard state-space form (7.8):

$$
\dot{x} = Ax + Bu
$$

$$
y = Cx \tag{7.8}
$$

As shown in figure 7.4, this transformation is done separately for each volume, i.e. there are a number of state-space systems corresponding to the number of volumes in the machine tool, which in the example considered here amounts to three.

7.3   Assembly of the machine tool model

In order to be able to analyse the system globally, the three systems need to be com-
bined back into one unique global state-space system. This is achieved by generating the
extended matrices A_{tot}, B_{tot} and C_{tot}, whose elements are composed block-wise by the
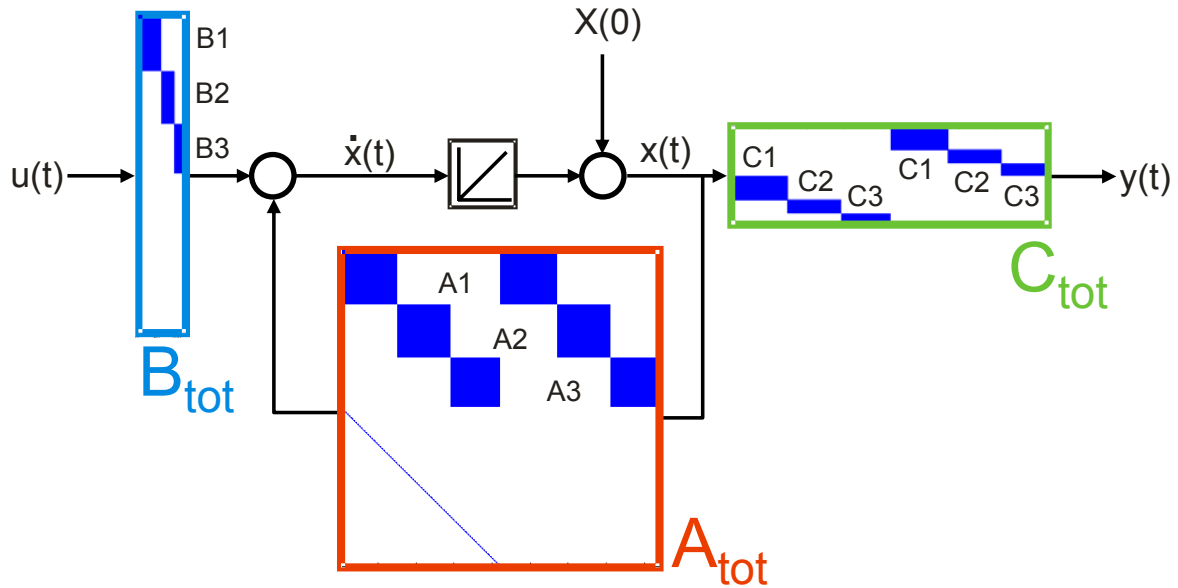matrices A, B and C of the single volumes, as pictured in figure 7.5:

Figure 7.5: Combination of the three state-space systems (A1,B1,C1,D1), (A2,B2,C2,D2) and
(A3,B3,C3,D3) into one global state-space space system by assembling the individual matrices.

The assembly of the new complete state-space systems $(A_{tot}, B_{tot}, C_{tot}, D_{tot})$, where due to
the system configuration D_{tot} is zero, is carried out automatically in Matlab, by a gene-
ralized adaptive script for an arbitrary number of volumes. The resulting system, whose
dimension equals the sum of the dimensions of the single systems, contains the reduced
dynamical characteristics, as well as the input/output information of the constitutive bo-
dies.

7.4   Integration of coupling elements

In order to correctly set the connections between the machine axes, the physical stiffness
and damping values, contained in the *coupling_parameters* text file, have to be incorporated
into the system. After processing the system outputs through an *Interface selector* in order
to select only the internal degrees of freedom (i.e. the degrees of freedom concerning the

axis couplings), the displacement and velocity outputs are automatically returned to the corresponding system inputs as *forces* by means of a *coupling matrix*, as evidenced in figure 7.6. The coupling matrix consists of a rearrangement of all physical stiffness and damping coefficients with the purpose of generating the internal loads, using the relative displacements and velocities of every pair of adjacent nodes in the axis couplings.
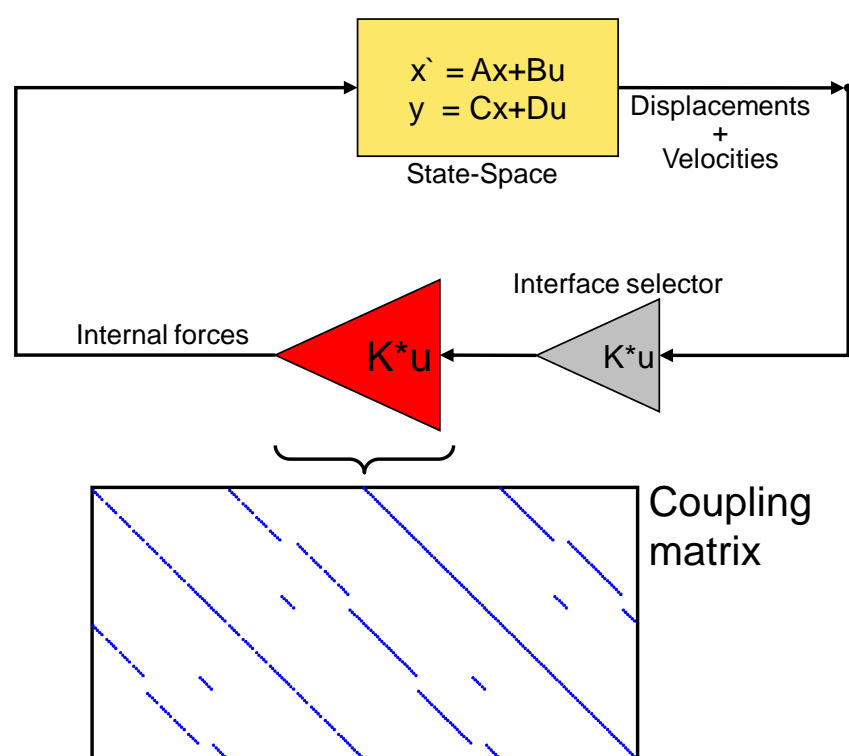

Figure 7.6: State-space system in Simulink extended with the coupling matrix, which automatically associates the internal inputs and outputs of the system.

The result is the fully defined model of a machine tool in figure 7.7, including the reduced structure flexibility of the machine bodies, the physical parameters of the connections between the bodies (stiffness and damping) and the required nodes for the evaluation of the machine tool (TCP, direct measuring system, etc.) The block *Input sorting* additionally allows a correct reordering of internal and external forces onto the single bodies.

This model represents an approximation of the complete dynamical characteristics of the original finite element structure, expressed by all the available transfer response functions between the selected excitation and response points.

To investigate the efficiency and the accuracy of the reduced model, a series of analyses of the three-axis machine tool introduced in section 3.2 are performed in ANSYS and reproduced using the model depicted in figure 7.7.
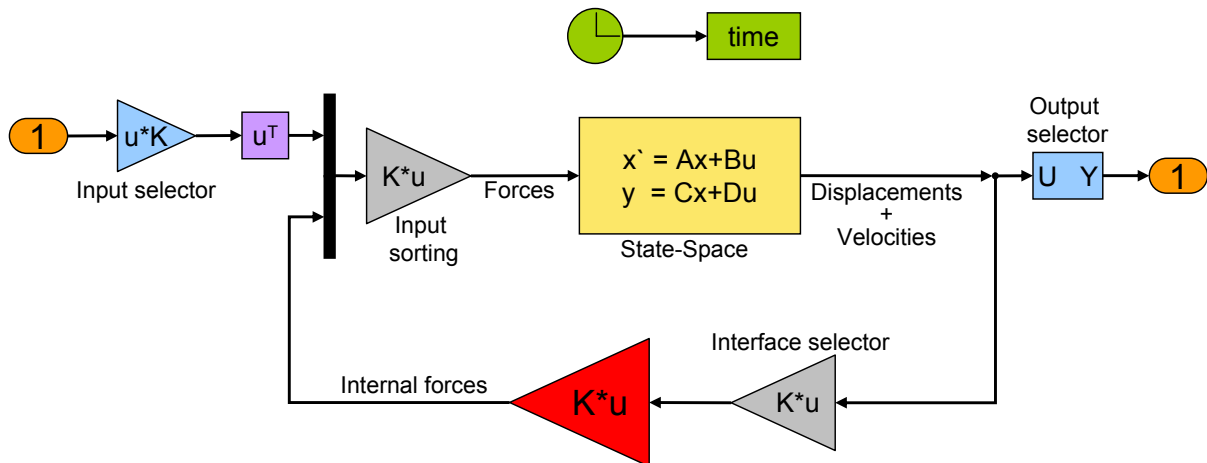
Figure 7.7: Simulink model of a reduced machine tool structure.

Two parameters of the reduction process have a significant influence on the final result: the dimension of the reduced model and the expansion point (see section 7.2). In a first step, the expansion point is set individually as the first natural frequencies of the four single bodies. The order reduction is then carried out for a varying dimension. The times required for the reduction process and the maximum relative error between the harmonic responses of the original ANSYS model and the reduced model (between 0 and 300Hz) are shown in figure 7.8. A satisfying error of 1.5% is reached at a dimension of 140, requiring a reduction time of ca. 900 seconds.

However, the assembled model, composed of the four bodies and the couplings, has much lower natural frequencies as those of the single bodies. In a next study, the reduction dimension is set to 100 and the expansion point is varied within the frequency range of interest, i.e. between 0 and 300Hz. The plot in figure 7.9 shows that for an expansion point between 50 and 200Hz, the relative error lies below 1%. There is therefore, depending on the application, a compromise to find between the order of the reduced model and the expansion point, in order to have the smallest possible model with the lowest error in the frequency range of interest.

A reduction order of 100 and an expansion point of 100Hz are selected to illustrate the method. In table 7.1, the first fifteen resonance frequencies of the modal analysis are shown for a full FEM computation in ANSYS and for a reduced *CRS* computation in the Matlab mechatronic toolbox. The depicted table outlines the quality of the reduced model, able to exactly describe the modal behavior of the structure in a frequency range of $0Hz - 500Hz$.
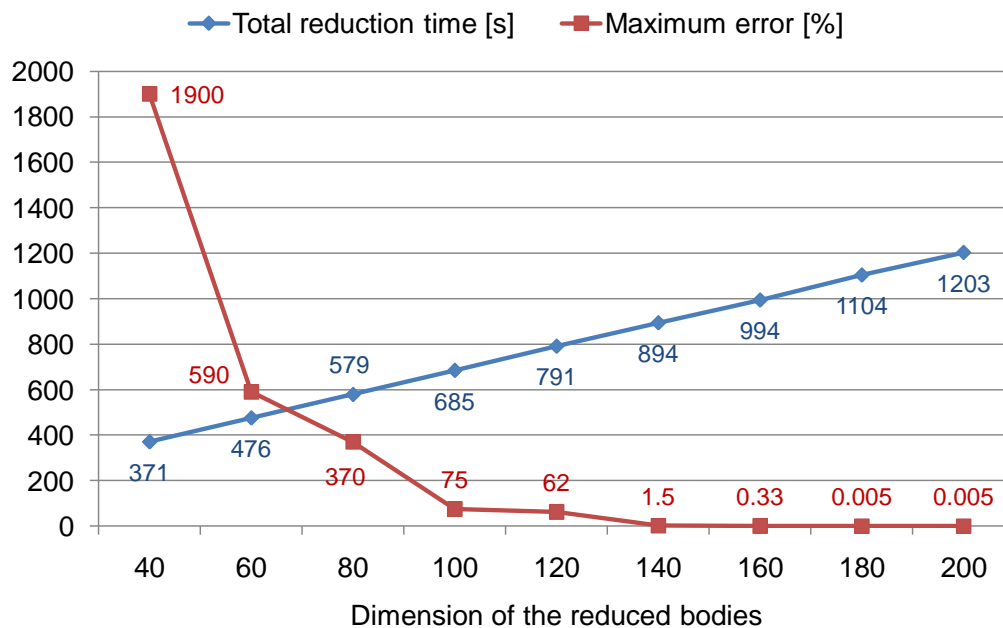
Figure 7.8: Maximum error vs. reduction time between a FEM and a CRS harmonic analysis in a frequency range 0-300Hz (expansion point corresponding to the first natural frequencies of the single bodies) .
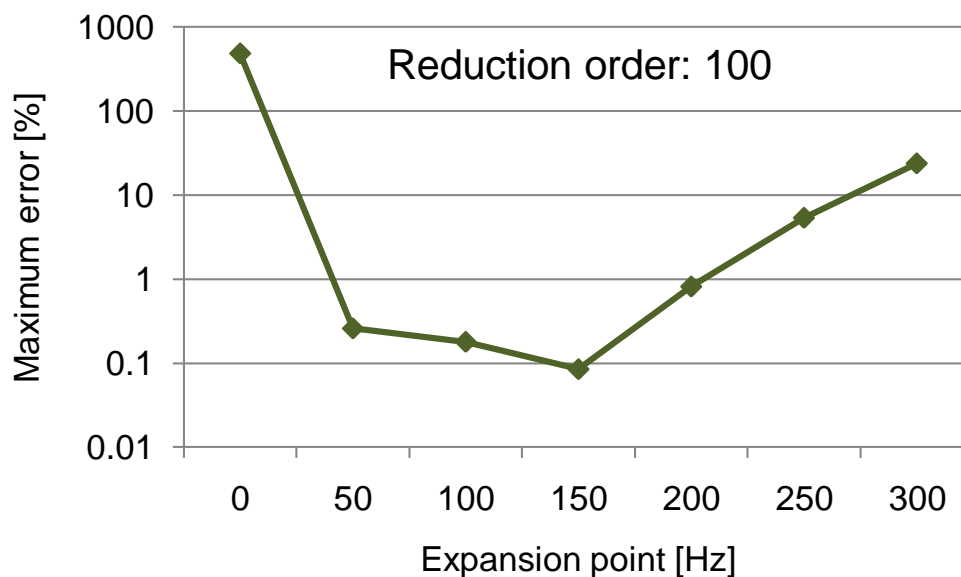

Figure 7.9: Maximum error vs. expansion point between a FEM and a CRS harmonic analysis in a frequency range 0-300Hz (reduction order set to 100) .

Table 7.1: Comparison between the first fifteen corresponding modes of a FEM modal analysis and a *CRS* modal analysis.

Mode Nr.	FEM	CRS
1	35.97	35.98
2	44.67	44.67
3	84.36	84.39
4	96.39	96.55
5	131.09	130.82
6	145.27	145.41
7	218.67	218.53
8	249.78	250.65
9	281.32	281.15
10	303.38	303.68
11	327.85	327.86
12	335.06	334.40
13	335.91	335.92
14	446.28	447.45
15	492.40	493.31

In figure 7.4, the building process in Matlab is schematically represented and it can be observed that, besides the reduction specifications listed in section 7.2, some settings relative to the loading conditions are required in order to perform harmonic analyses. These settings act on the blocks *Input selector* and *Output selector* found in figure 7.7.

- Excitation body ID numbers, where forces are applied
  - direction of forces
  - output number for each excitation body
- Response body ID numbers, where results are evaluated
  - direction of displacements and velocities
  - output number for each response body

The quality of the reduced model is confirmed by the match of the two harmonic responses, representing the response function at the TCP in direction X. The plots of the full ANSYS

simulation (blue spots) and of the reduced simulation (in red) are superposed in figures 7.10 and 7.11, evidencing a very good match between $0Hz$ and $300Hz$. The comparison of the harmonic analysis is limited to a few points, because of the restrictions resulting from the ANSYS model, in terms of computation time and memory capacity.
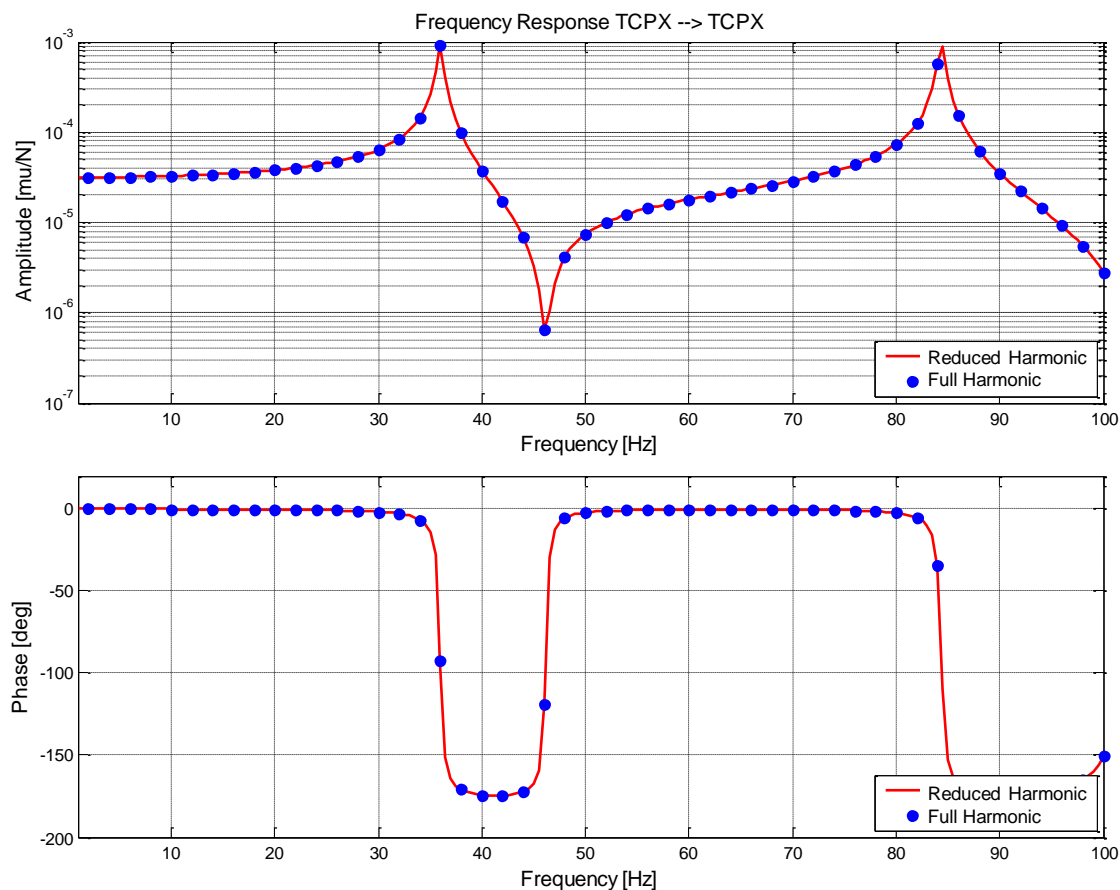
Figure 7.10: Comparison between full FEM harmonic analysis and *CRS* harmonic analysis (0-100Hz).

The above considerations point out the efficiency and accuracy of the method. The quality of the results of the reduced model shows that it is possible to achieve a considerable diminution of the computation time without deteriorating the dynamical behavior of the machine tool. In order to quantify the benefits obtained by a reduced simulation, table 7.2 summarizes the sizes of the models, the memory requirements and the times needed for a full harmonic analysis in ANSYS and for the different steps of the *CRS* process. The advantages of the method are tangible, and become even more significant if one considers the fact that, for each further loadcase (e.g. for various stiffness and damping coefficients in the couplings) in ANSYS, the time required is 150 minutes, whereas it remains limited to less than a couple of minutes for each further analysis in Matlab.
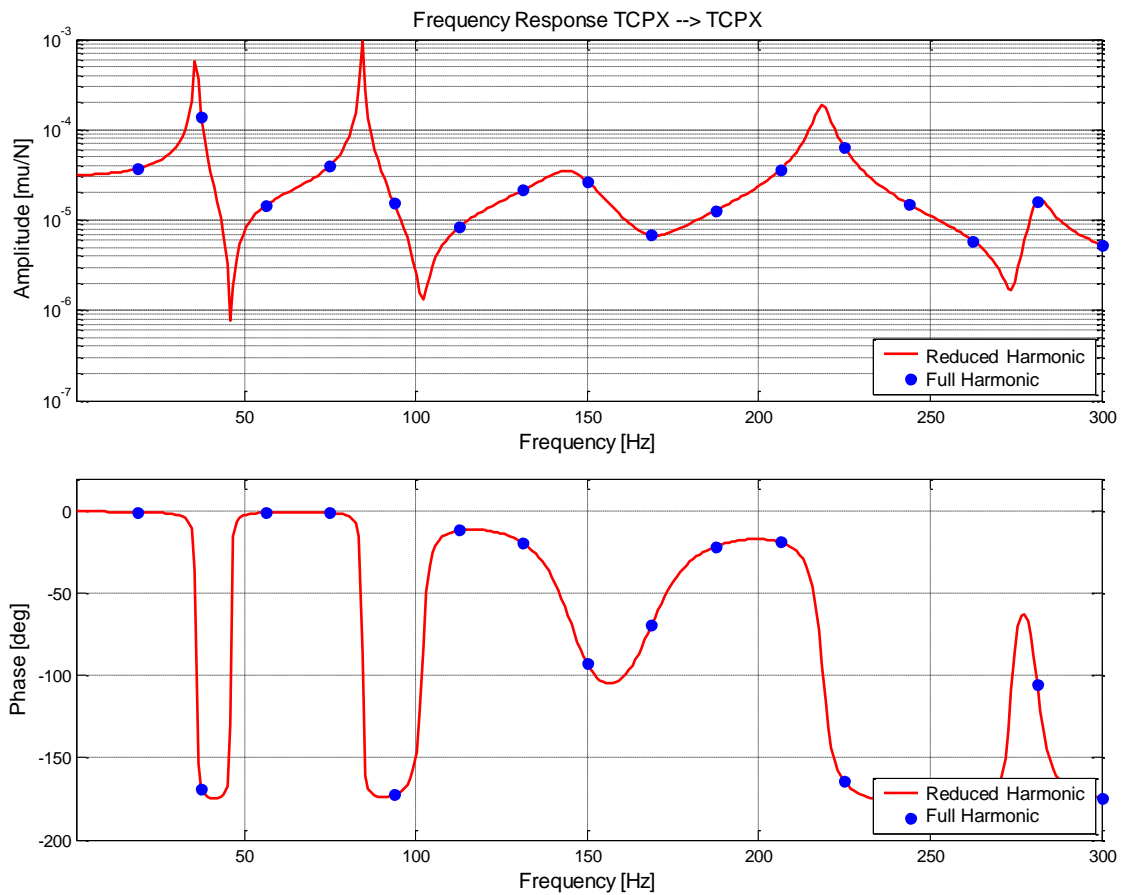
Figure 7.11: Comparison between full FEM harmonic analysis and *CRS* harmonic analysis (0-300Hz).

7.5   Motivation for a modular model reduction

At first glance, this whole method of reducing the single bodies separately can appear to be laborious. If one is interested in the frequency response between two points of the global system, previous studies have shown that it is actually more adequate to operate a single model order reduction of the whole system, as schematized in figure 7.12. The disadvantage of performing modular model reduction is especially evident with increasing number of volumes and couplings composing a machine tool. In the examined example, the four bodies are connected by three axis couplings leading to a total number of 90 internal inputs and outputs to manage. In a more complex structure, as for example machine *A* in chapter 5, with three linear axes, three rotary axes, one spindle and two serial sets of mounting elements, it can reach 250 internal inputs and outputs. It was therefore a prerogative during the development of this mechatronic toolbox to implement a fully automated model assembly process in Matlab/Simulink, in order to make the tool applicable to any type and size of machine structure.

Table 7.2: Comparison of simulation times for the full ANSYS model and the reduced model
(performed on a 64bit computer with a 3GHz processor and 16Gb RAM).

Model size	FEM	CRS
Number of DOF's	380'000	400
Computing Times		
Matrices writing from ANSYS		2 min
Order reduction with MOR for ANSYS		11 min
State-space model building in Matlab		< 1 min
Harmonic response analysis	150 min	< 1 min
Total	**150 min**	**< 15 min**
Memory usage		
Size of resulting files	14 Gb	0.7 Gb

This drawback being solved, the following aspects unequivocally speak in favor of modular
model order reduction:

- For complex machines having up to several millions degrees of freedom, the reduction
  of the full system matrices can be extremely time consuming and requires notable
  computing resources. Splitting the structure into axis components minimizes RAM
  requirements.

- With global model order reduction, it is impossible to integrate additional effects
  or functions within the reduced system. The connections between the moving axes
  are especially sensitive in this regard. Most FE-analyses (modal and harmonic an-
  alyses e.g.) are performed under the assumption that the system is linear. This is
  acceptable for the structural investigation of the single bodies, but if couplings are
  involved (guideways, drives, bearings, transmissions or any other system implying a
  relative motion between two parts), it only constitutes a linearized approximation
  affecting the dynamical behavior of the whole machine tool. By reducing single
  bodies separately, more detailed modeling steps can be added subsequently in the
  environment of the reduced system: carriages for example can be complemented by
  non linear phenomena like hysteresis, or transmission gears can incorporate backlash

effects. Hence subsequent transient analyses can be performed. This modular form also turns out to be of great help for investigating and identifying the properties of axis couplings. After a global reduction, the user does not have access to any internal degree of freedom, the resulting compact model has a fully defined dynamic behavior, which does not enable any change. As shown in section 4.2, where the present toolbox has been used for the illustrated simulations, a modular model allows an extremely facilitated variation of the Young's modulus, the β proportional damping and the density (mass) of the single bodies, as well as of every single stiffness and damping coefficient in the couplings, without having to repeat the process starting from the ANSYS FE-model.

- In the present case, the interest of the described method consists in having the possibility of integrating a control algorithm to the single machine tool axes (section 7.6) and thus being able to study the structural behavior under motion and the corresponding effects at the TCP. This allows the investigation of dynamical effects in function of velocity, acceleration and jerk settings, as well as the optimization of the control system layout in an early stage of the development of a machine with drastically reduced computing time.

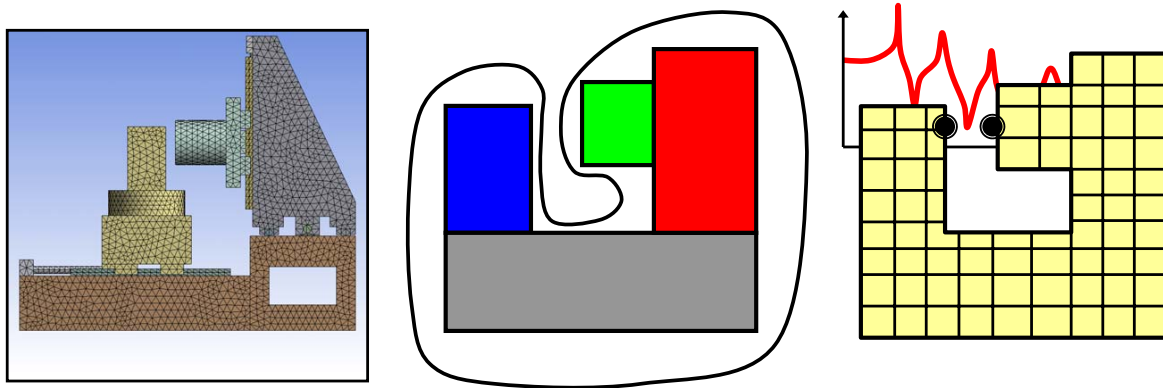Figure 7.12: Standard approach: global model order reduction of a machine tool.

7.6   Incorporation of axis control systems

As already suggested in the previous section, the next complexity step, leading to the completion of a mechatronic system, consists in extending the Matlab/Simulink model with a set of actuators, sensors and the corresponding feed controls closing the feedback loops of

the machine axes. This is achieved by deactivating (i.e. setting to zero) the drive stiffness in the direction of motion and by replacing it with a drive force or torque, depending of the axis type. The axis displacements are detected by the relative deviations of the degrees of freedom corresponding to the linear scale and the reader head. In figure 7.14, two control systems are integrated into the model of the two-axis machine tool represented in figure 7.13
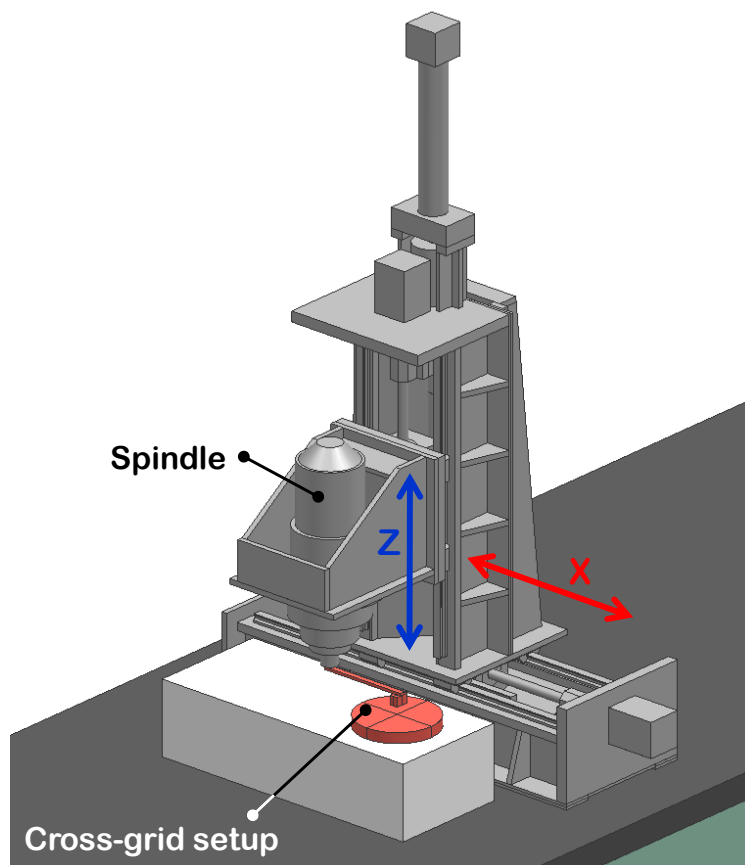
Figure 7.13: Two-axis machine tool used for the integration of the controlled axes X and Z and to reproduce the measured cross-talk deviations according to figure 7.16.

In the control system box in figure 7.14, reference paths are fed to the machine axes. The trajectory deviations, given by the errors of the actual positions and velocities relative to the nominal values, are measured at the locations of the direct measuring systems. The resulting forces to correct the errors are reinjected into the model by acting at the locations of the drives.

Special measuring equipment, specifically developed for the geometric evaluation of machine tools, is often adopted in order to evaluate the relative displacement between the tool tip and the workpiece reference point at the TCP in various configurations of the

Figure 7.14: The complete Simulink model containing the model of the machine tool structure, as well as two basic cascaded control systems for the two motion directions X and Z.

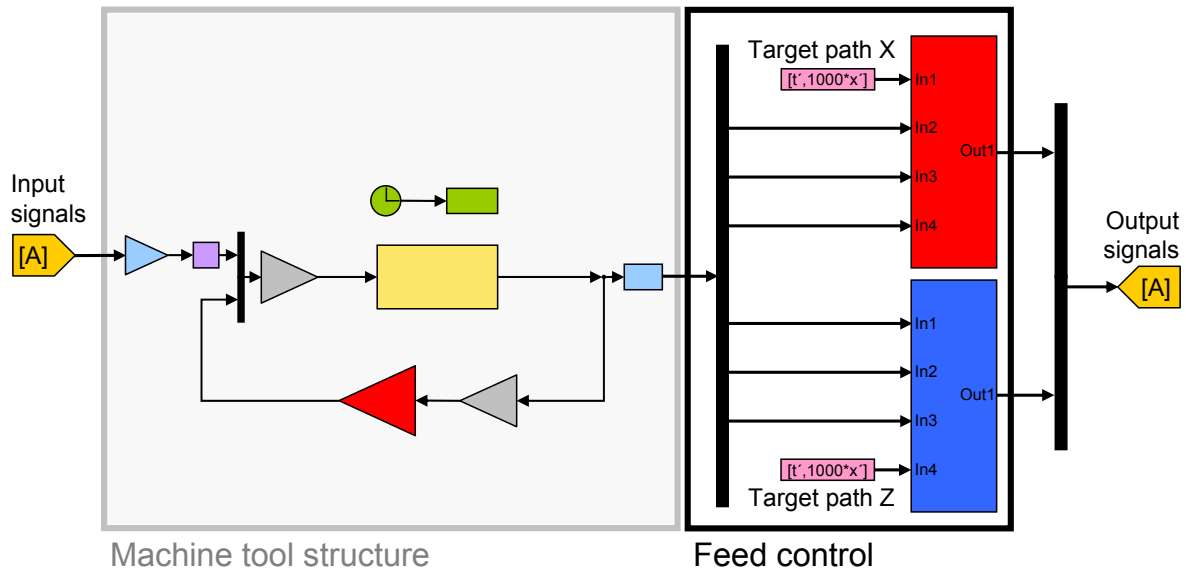machine axes or along predefined paths. This also facilitates the interpretation of geometric errors in linear and rotary axes and provides useful data for the calibration of the machine [127, 128, 129, 130]. Some of these techniques have recently also been used to evaluate the dynamic behavior of machine tools in order to identify weak spots in the structural arrangement of axes and guiding systems [131, 132], in presence of loads due to acceleration and/or constant path velocity.

In order to verify experimentally the mechatronic model, a series of measurements according to the above references are conducted on the existing machine. The test consists in feeding a path of $s = 100mm$ to the X-drive and measuring the cross-talk deviations EY_X at the TCP by means of a cross-grid. Inertial cross-talk is a displacement orthogonal to the direction of nominal motion during acceleration phases caused by the offset between the drive force and the center of mass and by the offset between the TCP and the center of mass, as illustrated in figure 7.15.

For the purpose of evidencing this effect on the two-axis machine, an offset of $X = 300mm$ is added to the TCP in the direction of motion in order to magnify the cross-talk deviations and improve the comparability between measurement and simulation. The required measuring devices are mounted on the machine as shown in figure 7.16.

For the experiments, the velocity and jerk values are kept at a constant value of $v = 15mmin^{-1}$, respectively $j = 300ms^{-3}$. The acceleration is successively set to $a = 1ms^{-2}$, $a = 2ms^{-2}$ and $a = 3ms^{-2}$, in order to evaluate the effects of the inertial loads on
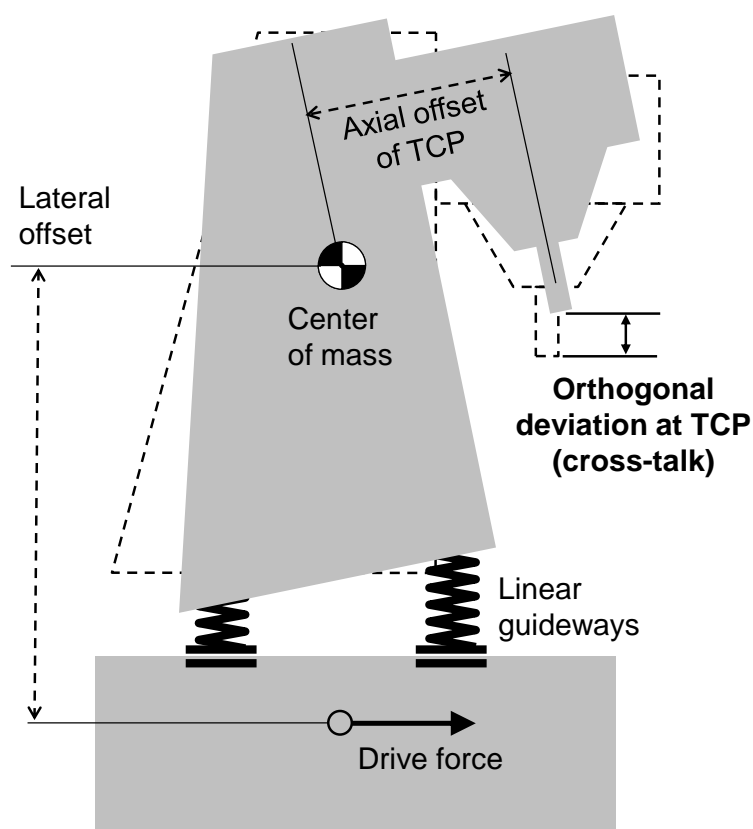
Figure 7.15: Schematic of inertial cross-talk effects at the TCP on a machine tool.

the cross-talk deviations. These measurements are then reproduced using the reduced simulation model depicted in figure 7.14. The settings of the model controller are set to the values of the real controller and the three corresponding acceleration values are assigned to the path generator in Simulink. The experimental results and the simulation results are shown in figure 7.17. From the inspection of the plots, two things can be outlined: first, the quasi-linear correlation between acceleration and cross-talk values, which has already been emphasized in several occasions on analogue structures, and secondly, asserting the conclusion drawn in section 7.4, the validity of the reduction method. The reduced model is capable of matching the measured cross-talk effects in the acceleration phase, despite not rigorously accurate controller parameters and the assumption that the global dynamic behavior of the structure is constant over the small considered X-position motion range.

The reduction toolbox, starting from a complex FE model, generates, in a highly auto-mated way, a reduced system capable of reproducing all the relevant mechanical properties of the axis structural parts and of the axis couplings. Dynamic path deviations induced by axes motions can be modeled integrating the control systems of the machine tool, as evidences the recapitulation in table 7.3.
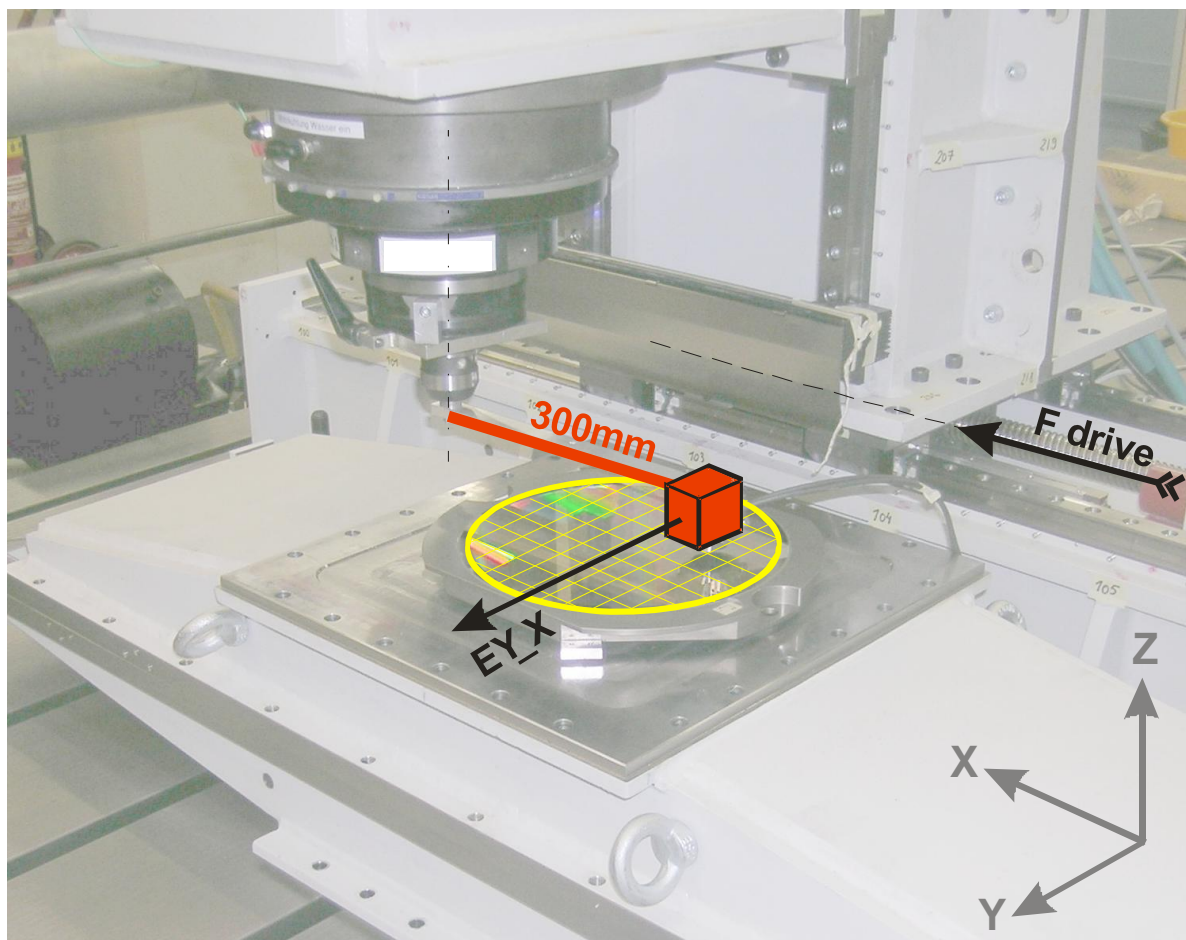
Figure 7.16: Cross-grid experimental set-up - Motion in X through $Fdrive$ and measurement of EY_X.

Table 7.3: Recapitulation of measured and simulated cross-talk deviations.

	1 m/s^2	2 m/s^2	3 m/s^2
Measured Cross-Talk deviation EYX	3.4 ± 0.5 μm	6.0 ± 0.5 μm	8.0 ± 0.5 μm
Simulated Cross-Talk deviation EYX	3.5 ± 0.5 μm	5.8 ± 0.5 μm	7.6 ± 0.5 μm
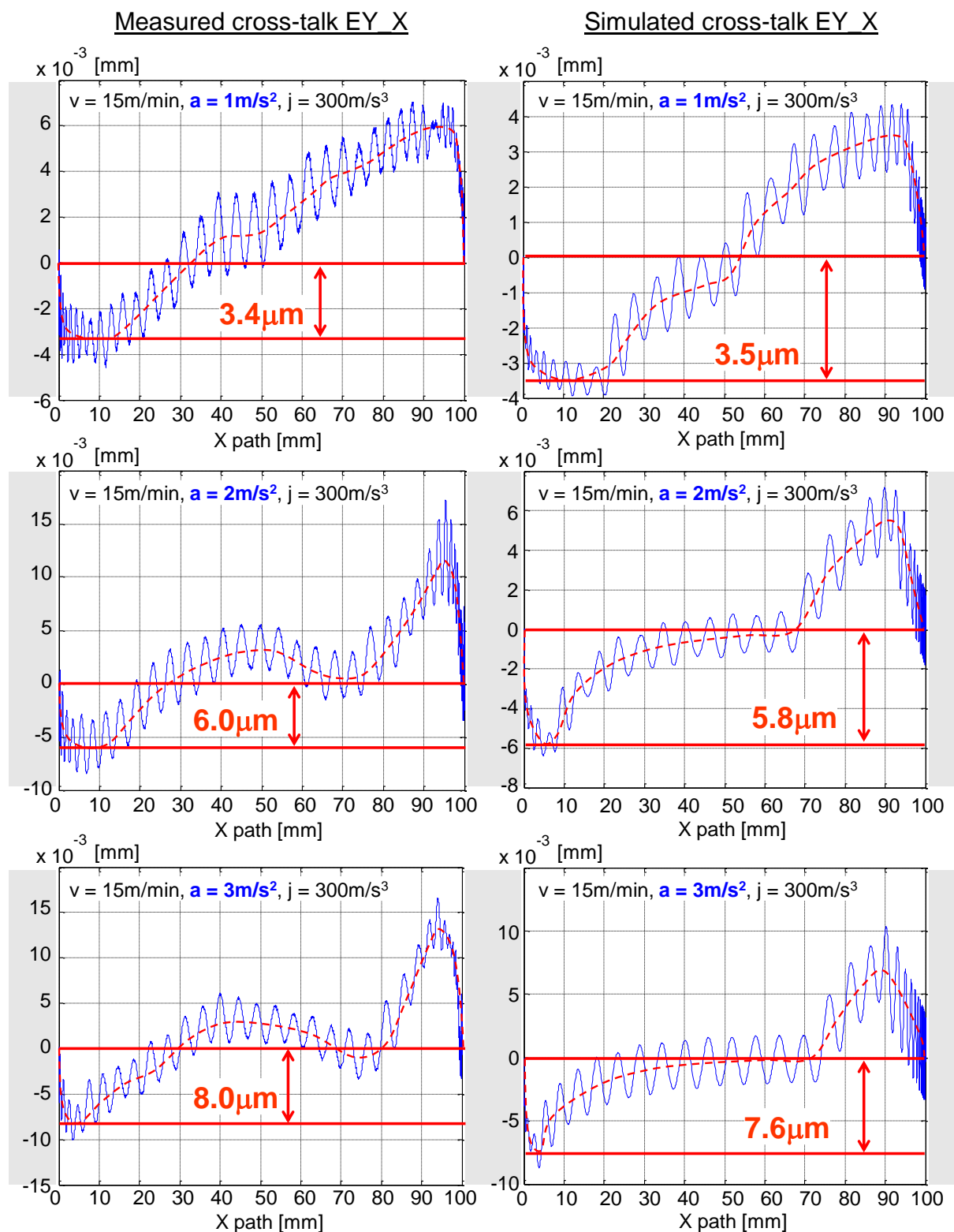
Figure 7.17: Measured (left) and simulated (right) cross-talk values by variable acceleration values.

Chapter 8

Summary and Outlook

There is a large potential to be exploited regarding the utilization of simulation during the development of machine tools. The methods currently in use for the study of the dynamical behavior of multi-axis machine structures can be divided into two categories: Rigid Body Simulation and Finite Element Method. The usual simulation deployment often looks like in figure 8.1, showing the deficient integration between different environments dedicated to the study of various aspects of the machine tool structure, leading to considerable effort for the creation and transfer of the models.

The concept of *Structure Gateway Interface* (SGI) has been developed within the framework of the presented thesis to concretize the application of simulation tools on a large scale. The *SGI* has proven to be an ideal central exchange platform to support the designer in the steps involved in obtaining a functional simulation model, as illustrated in figure 8.2. Representing a unique link between the CAD geometry and the final simulation models, it is supported by the three fundamental constitutive modules handled throughout the described developments: the properties of the *couplings*, the behavior of the body *structures* and the characteristics of the *controls*.

The techniques for the modeling of the couplings, like linear guideways, rotative bearings and ballscrew systems, have been the object of experimental studies. First the correct integration of stiffness coefficients provided by the manufacturers of linear guideways has been extensively investigated by means of a test-bed. The matching of the results of a series of measurements with the corresponding FE models helped to establish modeling rules to be applied on entire machine structures. The validation has been achieved by carrying out static and dynamic experimental tests on two multi-axis machine tools, which evidenced a good concordance with the simulations. Resonance peaks of single frequency responses have then been used to identify physical damping parameters in the carriage-rail interfaces, illustrating the efficiency of the matching method based on a simplified flexible model.
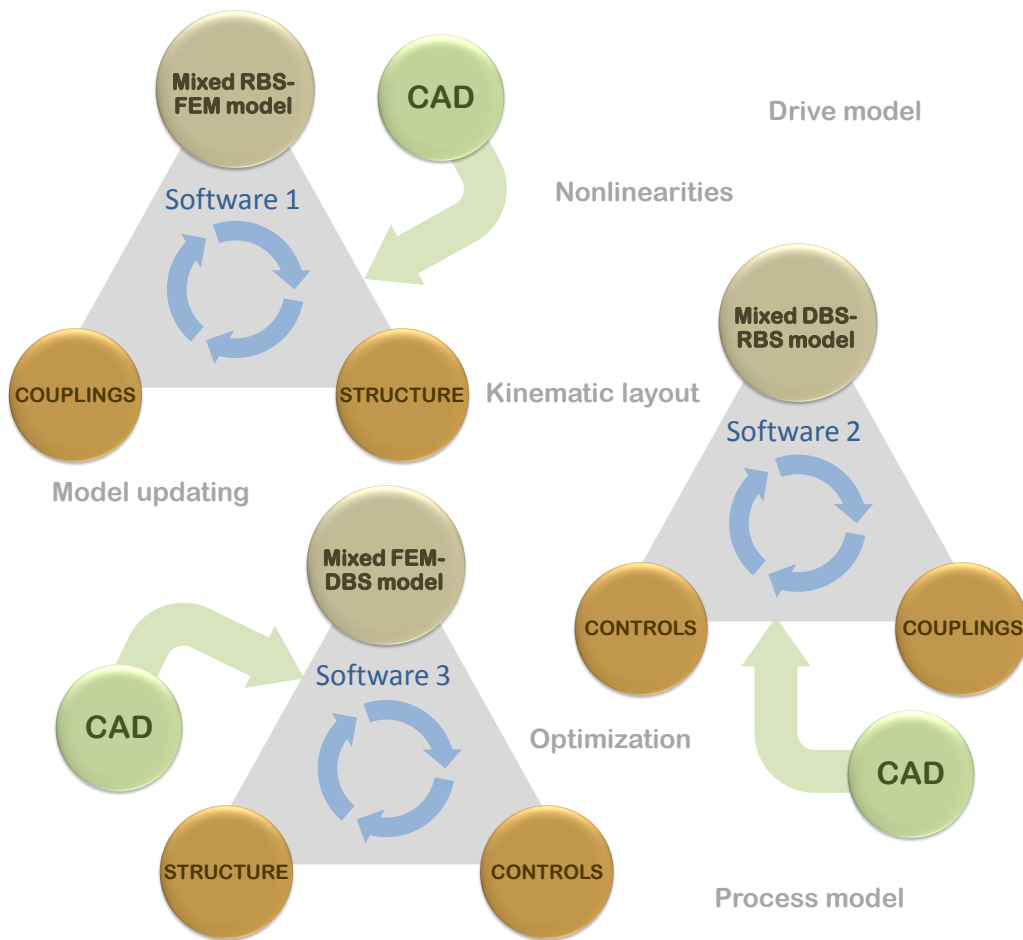
Figure 8.1: Distributed simulation tools, reflecting the actual use of simulation.

Relying on the specified rules for the FE modeling of machine tool structures, a set of macros has been developed to facilitate the creation and export of models from ANSYS Workbench. The scripts, taking into account the specific features of machine tools, are used to automatically describe the kinematics of the structure and to automatically define the properties of all linear and rotary axes, spindles and mounting elements. After completion of the model, three options are provided by the SGI, enabling to solve directly the model in ANSYS, to export the data necessary for rigid body simulation or to export the data necessary for coupled reduced simulation.

A stand-alone GUI has been developed with the intent of making rigid body analysis of machine tools industrially accessible. The entire mechanical and geometrical description of the machine, exported from ANSYS, is imported into the stand-alone program. A primordial condition to the applicability of the resulting rigid body simulations was the validation of the models by means of the original FE models. The high simplification degree
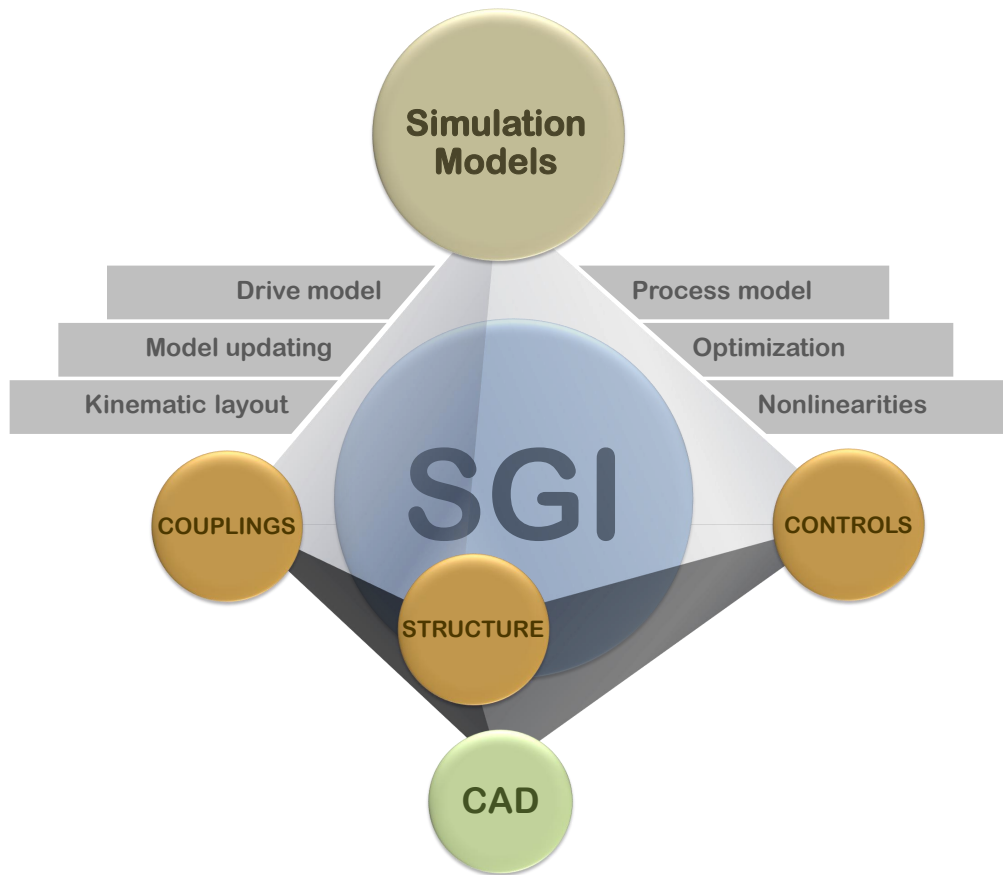
Figure 8.2: Integrated simulation tools, illustrating the role of the *Structure Gateway Interface* (SGI).

leads to obvious limits regarding the accuracy of the rigid body analyses, but it was shown that with an appropriate adjustment factor of the stiffness coefficients of the axis couplings, a good correlation between FEM and RBS results has been obtained. This adjustment factor proved to be strongly dependent of the *Strain Energy Ratio* R_ϵ, defining the relative amount of potential energy in the couplings with respect to the elastic deformation energy in the structure. In the GUI, a broad range of analysis capabilities have been implemented, useful to investigate all aspects concerning the static and dynamic behavior of a machine tool. Static, quasi-static, modal and harmonic analyses, focusing primarily on the relative deviations between the TCP and the WPP, are the fundamental integrated functions. Advanced functions like sensitivity and parametric analyses are successively used to explore in detail the properties of the structure by varying the parameters defining the basic configuration. Thanks to the implementation of very valuable graphical representations of the results, they allow an extremely fast and efficient improvement of selected static and dynamic characteristics in the whole admissible workspace.

For the purpose of detailed analyses of machine tools including the complex interactions of the structural behavior with the control of the feed axes, a Matlab toolbox for advanced mechatronic analyses has been developed. Based on the finite element system matrices, the process leading to the structural model includes the modular order reduction of the single machine volumes using the commercial program MOR for ANSYS, the assembly of the reduced state-space systems and the addition of the coupling properties. The scripts of the toolbox have been developed in such a way that various axis positions within the envisaged workspace are possible, by switching between the corresponding sets of reduced bodies. Given the large number of volumes and connections arising from machine tool structures with numerous linear and rotary axes and in varying positions, a priority of the toolbox implementation was the automated handling of the interfacing degrees of freedom. The integration of the control algorithms constitutes the next step, leading to a full mechatronic model of a machine tool. By means of cross-talk measurements on a real two-axis machine, the validity of the method has been verified by reproducing the experiments on the corresponding reduced model. The results showed that it is possible to obtain an excellent match between the measurements and the simulations, within extremely reduced computation times.

In chapter 1, the main optimization objectives and the corresponding variable parameters applicable to mechatronic models of machine tools have been listed. This work didn't aim at developing the actual optimization tools, but rather at providing the basis for the various optimization tools. The reliability of the different simplified simulation methods having been systematically experimentally assessed, they constitute a solid integrated tool to be applied during the design phase.

- Hence the rigid-body GUI is potentially an ideal tool for model updating, which consists in adjusting a selected set of uncertain parameters by matching simulative and experimental results. The implementation of mathematical comparison criteria like the MAC (Modal Assurance Criterion) can be useful to more rigorously identify specified parameters using the mode shapes resulting from experimental modal analyses. Automated matching criteria between measured and simulated FRFs, for the identification of specific stiffness or damping parameters, is a further model updating method which can have many profitable applications for machine tools.

- The computational efficiency of rigid body models is an advantage for the investigation of more complex problems, involving the inverse dynamics: given the tolerances of a workpiece and the resulting required stiffness at the TCP, critical components like linear guideways and rotative bearings can be dimensioned with respect to their stiffness, or drive systems can be dimensioned with respect to their forces and torques.

- A logical extension of the GUI is also, based on the various static and dynamic analyses already implemented, to integrate evolutionary optimization algorithms, which are well adapted to act on the fundamental configuration of the machine axes. Static and dynamic TCP stiffness values, eigenfrequencies, cross-talk deviations and workspace can be optimized by varying e.g. the positions of the linear guideways and bearings, the stiffness coefficients in the couplings, the distribution of the masses and moments of inertia, etc.

- The optimization on the structural level is also conceivable using a reduced flexible model created with the developed mechatronic toolbox. By implementing a loop between a parameterized ANSYS model and a simplified Matlab model, the reduced computation times can be capitalized to optimize the stiffness and mass properties of single structural parts, by varying for example wall thicknesses or hole diameters. An interesting research field would further consist in developing a method to operate local stiffness changes directly on the reduced model and to then define how these mathematical improvements are practically realized in the physical FE model.

- The automated routine to export, reduce and assemble an arbitrary number of versions of the original model in different axis positions has been implemented in prevision of the simulation of entire paths. The combined motions of tool and workpiece, involving complex configurations, could hence be simulated under the condition of an appropriate interpolation between the discrete axis positions.

- The integration of the control system should be extended to take into account the entire drive chain dynamics (motors, gears, transmission belts, etc.), to consider advanced control algorithms or to implement non-linearities in the couplings, like e.g. friction laws or stick-slip and hysteresis effects.

- The final link completing the dynamical loop of the machine tool structure is the process model. It closes the gap between the TCP and the WPP and turns the system into a closed kinematic chain, which is obviously necessary, since the accuracy issues are particularly important during the contact between the tool and the workpiece. The demonstrated accuracy and the observed computational efficiency of a reduced flexible model enable the integration of the process loads in order to investigate instability problems and optimize the parameters of the machining process.

The developed SGI is only the premise to what the future design process of machine tools could look like. Supported by innovative, robust and powerful geometric defeaturing methods, the pre-processing phase becomes fully automated. The optimally meshed model

serves as basis for further simulations. The long-term objective is to perform the subsequent reduced simulations in a fully stand-alone program, combining rigid body models, flexible models, the control algorithms and the process model into one single environment. Along with the design maturation of the machine structure, the complexity level of the simulation model is upgraded to achieve an effective merging of virtual machine tools and real product development. At the most advanced design stage, the inputs are the geometry, the material and the precision requirements of the workpiece. The visionary integrated program runs the complete dynamic simulation along the target path to optimize process, control and structural parameters.

Bibliography

[1] Y. Altintas, C. Brecher, M. Weck, and S. Witt. Virtual Machine Tool. *CIRP Annals - Manufacturing Technology*, 54(2):115–138, 2005.

[2] R. Neugebauer, B. Denkena, and K. Wegener. Mechatronic Systems for Machine Tools. *CIRP Annals - Manufacturing Technology*, 56(2):657–686, 2007.

[3] Wolfgang Knapp. Kurs Prüfen von Werkzeugmaschinen, Institut für Werkzeugmaschinen und Fertigung, ETH Zürich, 2010.

[4] Bernhard Bringmann. *Improving geometric calibration methods for multi-axis machining centers by examining error interdependencies effects*. PhD thesis, ETHZ, 2007.

[5] Josef Mayr. Thermische Messungen auf Werkzeugmaschinen. In *2. Symposium Simulation von Werkzeugmaschinen*. IWF/inspire, ETHZ, 2009.

[6] Markus Ess. Thermische Simulation von Werkzeugmaschinen. In *2. Symposium Simulation von Werkzeugmaschinen*. IWF/inspire, ETHZ, 2009.

[7] Oliver Zirn. Machine Tool Analysis – Modelling, Simulation and Control of Machine Tool Manipulators, Institut für Werkzeugmaschinen und Fertigung (IWF), ETH Zürich, 2008.

[8] J. Vesely and M. Sulitka. Machine Tool Virtual Model, 2008.

[9] M.F. Zaeh, Th. Oertli, and J. Milberg. Finite Element Modelling of Ball Screw Feed Drive Systems. *CIRP Annals - Manufacturing Technology*, 53(1):289–292, 2004.

[10] Thomas Oertli. *Strukturmechanische Berechnung und Regelungssimulation von Werkzeugmaschinen mit elektromechanischen Vorschubantrieben*. PhD thesis, TU Muenchen, 2008.

[11] J. Hamann, U. Ladra, and E. Schaefers. System Design for Machine Tools. In *The 12th Mechatronics Forum – Biennial International Conference*, 2010.

[12] Sascha Weikert. *Beitrag zur Analyse des dynamischen Verhaltens von Werkzeugmaschinen*. PhD thesis, ETHZ, 2000.

[13] Daniel Siedl. *Simulation des dynamischen Verhaltens von Werkzeugmaschinen während Verfahrbewegungen*. PhD thesis, TU Muenchen, 2008.

[14] Daniel Zaugg. Virtueller Prototyp mit Matlab/Simulink. In *3. Symposium Simulation von Werkzeugmaschinen*. IWF/inspire, ETHZ, 2010.

[15] R. Coleman. Simulation and Design of active Isolation Systems taking into Acount the Stage Dynamics. In *3. Symposium Simulation von Werkzeugmaschinen*. IWF/inspire, ETHZ, 2010.

[16] Bernhard Bringmann. Simulationsbaukasten mit SimMechanics. In *3. Symposium Simulation von Werkzeugmaschinen*. IWF/inspire, ETHZ, 2010.

[17] Sergio Bossoni. *Geometric and Dynamic Evaluation and Optimization of Machining Centers*. PhD thesis, ETHZ, 2009.

[18] Thomas Lorenzer, Sascha Weikert, and Konrad Wegener. Decision-making Aid for the Design of Reconfigurable Machine Tools. In *The 2nd International Conference on Changeable, Agile, Reconfigurable and Virtual Production*, pages 720 – 729, 2007.

[19] Gerald Kress. Kurs Strukturanalyse mit FEM, Institut für Mechanische Systeme, ETH Zürich, 2010.

[20] Michel Del Pedro and Pierre Pahud. *Mécanique vibratoire*. Presses polytechniques et universitaires romandes, CH–1015 Lausanne, 3rd edition, 1997.

[21] P. Koutsovasilis and M. Beitelschmidt. Comparison of model reduction techniques for large mechanical systems. *Multibody System Dynamics*, 20:111–128, 2008. 10.1007/s11044-008-9116-4.

[22] P. Benner. Novel Model Reduction Techniques for Control of Machine Tools. In *ANSYS Conference & 27th CADFEM Users' Meeting, Leipzig*, 2009.

[23] T. Bonin, A. Soppa, J. Saak, M.F. Zaeh, H. Faßbender, and P. Benner. Modale versus moderne Ordnungsreduktionsverfahren: Effiziente Simulation von Werkzeugmaschinen. *Mechatronik*, 117:11–12, 2009.

[24] T. Bechtold. *Model order reduction of electro-thermal MEMS*. PhD thesis, Albert-Ludwigs Universität Freiburg im Breisgau, 2005.

[25] A.C. Antoulas and D.C. Sorensen. Approximation of large-scale dynamical systems: An overview, Rice University, Houston, 2001.

[26] Roy R. Craig and Mervyn C.C. Bampton. Coupling of Substructures for Dynamic Analyses. *AIAA*, 6:1313–1319, 1968.

[27] Ulf Sellgren. Component Mode Synthesis - A method for efficient dynamic simulation of complex technical systems, 2003.

[28] P. Maglie. Einsatz von Reduktionsmethoden für die Simulation von Werkzeugmaschinen. In *ANSYS Conference & 26th CADFEM Users' Meeting, Darmstadt*, 2008.

[29] G. Bianchi, F. Paolucci, P. Van den Braembussche, H. Van Brussel, and F. Jovane. Towards Virtual Engineering in Machine Tool Design. *CIRP Annals - Manufacturing Technology*, 45(1):381–384, 1996.

[30] P. DeFonseca, D. Vandepitte, H. Van Brussel, and P. Sas. Dynamic model reduction of a flexible three-axis milling machine. In *International Conference on Noise and Vibration Engineering*, pages 185–194, 1998.

[31] Maira M. DaSilva, Oliver Brüls, Bart Paijmans, Wim Desmet, and Hendrik Van Brussel. Concurrent simulation of mechatronic systems with variable mechanical configuration. *Proceedings of ISMA 2006*, pages 1–12, 2006.

[32] R. Maj, F. Modica, and G. Bianchi. Machine Tools Mechatronic Analysis. In *Proceedings of the Institution of Mechanical Engineers, Part B: Journal of Engineering Manufacture*, volume 220, pages 345–353. Professional Engineering Publishing, 2006.

[33] Michael R. Hatch. *Vibration Simulation Using Matlab and Ansys*. Chapman & Hall/CRC, 2001.

[34] J. Berkemer. *Gekoppelte Simulation von Maschinendynamik und Antriebsregelung unter Venvendung linearer Finite Elemente Modelle*. PhD thesis, Universität Stuttgart, 2003.

[35] J. Fleischer, C. Munzinger, and M. Kipfmüller. Aufwandsreduktion bei der Werkzeugmaschinensimulation – Anforderungen. *wt Werkstattstechnik online*, 98:321–326, 2008.

[36] P. Maglie. Anwendung von FE-basierten Reduktionsmethoden. In *VDI-Mechatronik*, 2009.

[37] Peter Benner and Jens Saak. Efficient balancing based MOR for second order systems arising in control of machine tools, TU Chemnitz, 2009.

[38] Florian Fässler and Fritz Bircher. Flexible Mehrkörpersimulation zur Optimierung moderner Fertigungssysteme. In *15. Schweizer CADFEM Users' Meeting, Zürich*, 2010.

[39] Christopher Beattie and Serkan Gugercin. Interpolatory projection methods for structure-preserving model reduction. *Systems & Control Letters*, 58(3):225–232, 2009.

[40] Marcus Meyer. Computational Model Order Reduction of Linear and Nonlinear Dynamical Systems, 2006.

[41] Zhaojun Bai, Karl Meerbergen, and Yangfeng Su. Arnoldi Methods for Structure-Preserving Dimension Reduction of Second-Order Dynamical Systems. In *Dimension Reduction of Large-Scale Systems*, volume 45 of *Lecture Notes in Computational Science and Engineering*, pages 173–189. Springer Berlin Heidelberg, 2005.

[42] R. Eid, B. Salimbahrami, and B. Lohmann. Parametric Order Reduction of Proportionally Damped Second-Order Systems. *Journal of Sensors and Materials*, 19:149–164, 2007.

[43] Serkan Gugercin. An iterative SVD-Krylov based method for model reduction of large-scale dynamical systems. *Linear Algebra and its Applications*, 428(8-9):1964–1986, 2008.

[44] Heike Fassbender and Andreas Soppa. Machine tool simulation based on reduced order FE models. *Mathematics and Computers in Simulation*, In Press, Corrected Proof, 2010.

[45] T. Bechtold, E.B. Rudnyi, and J.G. Korvink. Error Estimation for Arnoldi-based Model Order Reduction of MEMS. *Technical Proceedings of the 2004 NSTI Nanotechnology Conference and Trade Show*, 2:430 – 433, 2004.

[46] Tamara Bechtold, Evgenii B. Rudnyi, and Jan G. Korvink. Error indicators for fully automatic extraction of heat-transfer macromodels for MEMS. *Journal of Micromechanics and Microengineering*, 15(3):430–440, 2005.

[47] Christian Moosmann. *ParaMOR – Model Order Reduction for parameterized MEMS applications*. PhD thesis, Albert–Ludwigs Universität, Freiburg im Breisgau, 2007.

[48] Evgenii B. Rudnyi, Jan Lienemann, Andreas Greiner, and Jan G. Korvink. mor4ansys: Generating Compact Models Directly from ANSYS Models. In *Technical Proceedings of the 2004 Nanotechnology Conference and Trade Show, Nanotech 2004, March 7-11, 2004*, pages 279–282, 2004.

[49] E.B. Rudnyi and J.G. Korvink. Model Order Reduction for Large Scale Engineering Models Developed in ANSYS. In *Applied Parallel Computing*, pages 349–356. Springer, 2005.

[50] Andreas Greiner, Jan Lienemann, Evgenii Rudnyi, Jan G. Korvink, Lorenza Ferrario, and Mario Zen. Automatic Order Reduction for Finite Element Models. In *9th National conference on Sensor and Microsystems, AISEM 2004*, pages 8–11, 2004.

[51] Jeong Sam Han, Evgenii B. Rudnyi, and Jan G. Korvink. Efficient optimization of transient dynamic problems in MEMS devices using model order reduction. *Journal of Micromechanics and Microengineering*, 15(4):822–832, 2005.

[52] Jan Lienemann, Dag Billger, Evgenii B. Rudnyi, Andreas Greiner, and Jan G. Korvink. MEMS Compact Modeling Meets Model Order Reduction: Examples of the Application of Arnoldi Methods to Microsystems Devices. In *Technical Proceedings of the 2004 Nanotechnology Conference and Trade Show, Nanotech 2004, March 7-11, 2004*, pages 303–306, 2004.

[53] M. Zaeh and D. Siedl. A New Method for Simulation of Machining Performance by Integrating Finite Element and Multi-body Simulation for Machine Tools. *CIRP Annals - Manufacturing Technology*, 56(1):383 – 386, 2007.

[54] H. Weule, J. Fleischer, W. Neithardt, D. Emmrich, and D. Just. Structural Optimization of Machine Tools including the static and dynamic Workspace Behavior. In *Proceedings of the 36th CIRP International Seminar on Manufacturing Systems (ISMS)*, pages 269–272, Saarbrücken, 2003.

[55] Martin Kipfmüller. *Aufwandsoptimierte Simulation von Werkzeugmaschinen*. PhD thesis, Karlsruher Instituts für Technologie, 2009.

[56] O. Zirn and R. Montavon. Gekoppelte Simulation von FE- und Mehrkörpermodellen für Werkzeugmaschinen. In *ASIM*, 2008.

[57] Raphaël Montavon and Oliver Zirn. Couplage des modèles d'analyses par éléments finis et corps–rigides en machines–outils, 2008.

[58] Marc Brandenberger. Coupled Simulation using FEM, MBS and Control Simulation Tools using the example of a machine tool. In *NAFEMS Seminar: Mechatronics in Structural Analysis*, 2004.

[59] Jixiang Li. Flexible Multibody Simulation Using Substructuring in ANSYS Workbench. In *ANSYS Conference & 26th CADFEM Users' Meeting, Darmstadt*, 2008.

[60] J. D. Beley. Multibody Dynamics and Joints Simulation in ANSYS. In *ANSYS Conference & 28th CADFEM Users' Meeting, Aachen*, 2010.

[61] F. Maggio. Multi-Body Simulation and Multi-Objective Optimization Applied to Vehicle Dynamics. In *ANSYS Conference & 26th CADFEM Users' Meeting, Darmstadt*, 2008.

[62] Sascha Weikert, Christian Jaeger, Sergio Bossoni, and Konrad Wegener. Efficient Evaluation of early machine concepts in the frequency domain including control issues, 2008.

[63] Thomas Lorenzer, Sascha Weikert, and Konrad Wegener. Efficient Modelling and Simulation of Reconfigurable Machine Tools Using Predefined Structural Modules. In Herbert Utz, editor, *3rd International Conference on Changeable, Agile, Reconfigurable and Virtual Production*, pages 214–223, Muenchen, Germany, 2009.

[64] R. Altenburger. Simulative Kopplung der Maschinenstruktur mit der Antriebsregelung. In *1. Symposium Simulation von Werkzeugmaschinen*. IWF/inspire, ETHZ, 2008.

[65] Albert Albers, Dieter Emmrich, and Pascal Haeussler. Automated structural optimization of flexible components using MSC.ADAMS/Flex and MSC.Nastran Sol200. In *1st European MSC.ADAMS User Conference*, 2002.

[66] Jürgen Fleischer and Alexander Broos. Parameteroptimierung bei Werkzeugmaschinen – Anwendungsmöglichkeiten und Potentiale. In *Weimarer Optimierungs- und Stochastiktage*, 2004.

[67] P. Haeussler, D. Emmrich, O. Mueller, B. Ilzhoefer, L. Nowicki, and A. Albers. Automated Topology Optimization of Flexible Components in Hybrid Finite Element Multibody Systems, 2001.

[68] G. Ding, Z. Qian, and S. Pan. Active Vibration Control of Excavator Working Equipment with ADAMS. In *International ADAMS User Conference*, 2000.

[69] A. Drivet. Virtual Prototyping of an active Suspension using ADAMS/View and Matlab. In *MSC.Software VPD Conference*, 2006.

[70] P. Haese and C. Decking. Investigation of Drive Systems using ADAMS and Matlab/Simulink. In *ADAMS/Rail User Conference*, 2000.

[71] F. Ying, G. Yiming, and Z. Hongni. Control for Vehicle Handing Stability Based on ADAMS and Matlab. In *International Conference on Computer Application and System Modeling (ICCASM)*, 2010.

[72] R. Alber. An approach for the Coupled Simulation of Structure and Control Engineering in ANSYS – ingplusplus, 2007.

[73] G. Kehl. Integrierte Simulation von Strukturdynamik und Regelungstechnik an Bearbeitungszentren. In *1. Symposium Simulation von Werkzeugmaschinen. IWF/inspire, ETHZ*, 2008.

[74] Edward Chlebus and Bogdan Dybala. Modelling and calculation of properties of sliding guideways. *International Journal of Machine Tools and Manufacture*, 39(12):1823–1839, 1999.

[75] Y. Cao and Y. Altintas. Modeling of spindle-bearing and machine tool systems for virtual simulation of milling operations. *International Journal of Machine Tools and Manufacture*, 47(9):1342–1350, 2007. Selected papers from the 2nd International Conference on High Performance Cutting, 2nd CIRP International Conference on High Performance Cutting.

[76] M. Ebrahimi and R. Whalley. Analysis, modeling and simulation of stiffness in machine tool drives. *Computers & Industrial Engineering*, 38(1):93–105, 2000.

[77] Yasar Deger. Optimisation of the Dynamic Behaviour of a Machine Tool Mounting Device. In *FENET / NAFEMS Seminar*, 2001.

[78] Y. Lin and W. Chen. A Method of identifying Interface Characteristic for Machine Tools Design. *Journal of Sound and Vibration*, 255(3):481–487, 2002.

[79] Keivan Ahmadi and Hamid Ahmadian. Modelling machine tool dynamics using a distributed parameter tool-holder joint interface. *International Journal of Machine Tools and Manufacture*, 47(12-13):1916 – 1928, 2007.

[80] M. Thurneysen and G. Demaurex. Modalanalyse von komplexen Maschinen, praktische Überprüfung. In *1. Symposium Simulation von Werkzeugmaschinen.* IWF/inspire, ETHZ, 2008.

[81] Won-Jae Lee and Seok-Il Kim. Joint stiffness identification of an ultra-precision machine for machining large-surface micro-features. *International Journal of Precision Engineering and Manufacturing*, 10:115–121, 2009. 10.1007/s12541-009-0102-4.

[82] Jaspreet S. Dhupia, A. Galip Ulsoy, Reuven Katz, and Bartosz Powalka. Experimental Identification of the Nonlinear Parameters of an Industrial Translational Guide for Machine Performance Evaluation. *Journal of Vibration and Control*, 14(5):645–668, 2008.

[83] Yao Man Zhang, Zhi Kun Xie, and Yong Xian Liu. Modeling and Calculation of Dynamic Performances of NC Machine Tool Considering Linear Rolling Guideway. *Applied Mechanics and Materials*, 16–19:510–514, 2009.

[84] D.M. Shamine, S.W. Hong, and Y.C. Shin. Experimental Identification of Dynamic Parameters of Rolling Element Bearings in Machine Tools. *Journal of Dynamic Systems, Measurement, and Control*, 122(1):95–101, 2000.

[85] I. Zaghbani and V. Songmene. Estimation of machine-tool dynamic parameters during machining operation through operational modal analysis. *International Journal of Machine Tools and Manufacture*, 49(12-13):947–957, 2009.

[86] T. Hoshi and N. Takenaka. Parameters of Mounting and Foundation affecting the Structural Dynamics of Machine Tools. *Annals of the CIRP*, 1973.

[87] H. Schulz and R.G. Nicklau. Designing machine tool structures in polymer concrete. *International Journal of Cement Composites and Lightweight Concrete*, 5(3):203 – 207, 1983.

[88] E. Saljé, H. Gerloff, and J. Meyer. Comparison of Machine Tool Elements Made of Polymer Concrete and Cast Iron. *CIRP Annals - Manufacturing Technology*, 37(1):381 – 384, 1988.

[89] J. Meschke. *Verbesserung des dynamischen Verhaltens von Werkzeugmaschinen durch Erhöhung der Systemdämpfung.* PhD thesis, TU Braunschweig, 1994.

[90] Ping Xu and Ying-Hua Yu. Research on steel-fibber polymer concrete machine tool structure. *Journal of Coal Science and Engineering (China)*, 14:689–692, 2008. 10.1007/s12404-008-0444-z.

[91] D.I. Kim, S.C. Jung, J.E. Lee, and S.H. Chang. Parametric study on design of composite-foam-resin concrete sandwich structures for precision machine tool structures. *Composite Structures*, 75(1-4):408–414, 2006. Thirteenth International Conference on Composite Structures - ICCS/13.

[92] M. Schnabel. Improvement of Machine Characteristics of a Machining Center with Parallel Kinematics by Using an Alternative Material for the Machine Frame. In *5th Parallel Kinematics Seminar, Chemnitz*, 2006.

[93] I. Chowdhury and S. Dasgupta. Computation of Rayleigh Damping Coefficients for Large Systems. *The Electronic Journal of Geotechnical Engineering*, 8, 2003.

[94] S. Adhikari. Damping modelling using generalized proportional damping. *Journal of Sound and Vibration*, 293(1-2):156–170, 2006.

[95] C. Cai, H. Zheng, M.S. Khan, and K.C. Hung. Modeling of Material Damping Properties in ANSYS. In *ANSYS Conference & 20th CADFEM Users' Meeting, Friedrichshafen*, 2002.

[96] B. Denkena. Grundlagen der Werkzeugmaschinen - 3. Dynamisches Verhalten von Werkzeugmaschinen, 2003.

[97] F. Albertz. *Dynamikgerechter Entwurf von Werkzeugmaschinen-Gestellstrukturen*. PhD thesis, TU Muenchen, 1995.

[98] J. Becker and L. Gaul. CMS Methods for Efficient Damping Prediction for Structures with Friction. In *IMAC XXVI: Conference & Exposition on Structural Dynamics*, 2008.

[99] F. Hoffmann. *Optimierung der dynamischen Bahngenauigkeit von Werkzeugmaschinen mit der Mehrkörpersimulation*. PhD thesis, RWTH Aachen, 2008.

[100] V.L. Popov, S.G. Psakhie, E.V. Shilko, A.I. Dmitriev, K. Knothe, F. Bucher, and I. Ertz. Friction coefficient in rail-wheel contacts as a function of material and loading parameters. *Physical Mesomechanics*, 5:17–24, 2002.

[101] J. DeVicente, J.R Stokes, and H.A Spikes. Rolling and sliding friction in compliant, lubricated contact. *Proceedings of the Institution of Mechanical Engineers, Part J: Journal of Engineering Tribology*, 220:55–63, 2006.

[102] F. Al-Bender and W. Symens. Characterization of frictional hysteresis in ball-bearing guideways. *Wear*, 258(11-12):1630–1642, 2005.

[103] P. Dietl. *Damping and Stiffness Characteristics of Rolling Elements Bearings.* PhD thesis, TU Wien, 1997.

[104] P. Dietl, J. Wensing, and G.C. van Nijen. Rolling bearing damping for dynamic analysis of multi-body systems - experimental and theoretical results. *Proceedings of the Institution of Mechanical Engineers, Part K: Journal of Multi-body Dynamics*, 214:33–43, 2000.

[105] E. Albert and H. Rossteuscher. Dynamische Kennwerte für Profilschienenführungen. *Antriebstechnik*, 1:22–23, 2008.

[106] C. Brecher, M. Kunc, M. Key, and W. Klein. Reibungs- und Dämpfungseigenschaften von Profilschienenführungen. In *15. Dresdner Werkzeugmaschinen-Fachseminar*, 2010.

[107] R. Neugebauer, C. Scheffler, M. Wabner, and M. Schulten. Advanced state space modeling of non-proportional damped machine tool mechanics. *CIRP Journal of Manufacturing Science and Technology*, 3(1):8 – 13, 2010.

[108] H. Rossteuscher. Bestimmung der dynamischen Kennwerte von Profilschienenführungen. In *2. Symposium Simulation von Werkzeugmaschinen*. IWF/inspire, ETHZ, 2009.

[109] James Shih-Shyn Wu, Jyh-Cheng Chang, and Jui-Pin Hung. The effect of contact interface on dynamic characteristics of composite structures. *Mathematics and Computers in Simulation*, 74(6):454–467, 2007.

[110] P. Groche and T. Hofmann. EFB-Forschungsbericht Nr. 238 - Einfluss des dynamischen Übertragungsverhaltens von Stösselführungen auf die Arbeitsgenauigkeit von Umformpressen, 2005.

[111] B. Schlecht. *Maschinenelemente 2: Getriebe, Verzahnungen und Lagerungen.* Pearson, 2010.

[112] W. Steinhilper and B. Sauer. *Konstruktionselemente des Maschinenbaus 2 - Grundlagen von Maschinenelementen für Antriebsaufgaben.* Springer, 6th edition, 2008.

[113] Shigeru Aoki. Dynamic characteristics of welded structures. *Nuclear Engineering and Design*, 160(3):379 – 385, 1996.

[114] Eberhard Abele, Madhu Munirathnam, and Michael Roth. Dynamic behaviour of protective covers in machine tools. *Production Engineering*, 1:199–204, 2007. 10.1007/s11740-007-0013-0.

[115] S. Bograd, A. Schmidt, and L. Gaul. Modeling of damping in bolted structures, 2007.

[116] Hongliang Tian, Bin Li, Hongqi Liu, Kuanmin Mao, Fangyu Peng, and Xiaolei Huang. A new method of virtual material hypothesis-based dynamic modeling on fixed joint interface in machine tools. *International Journal of Machine Tools and Manufacture*, 51(3):239 – 249, 2011.

[117] S. Pietrzko. *Verfahren zur Identifikation der Dämpfungsmatrix mechanischer Systeme*. PhD thesis, EMPA, 1992.

[118] G. Petuelli. *Theoretische und experimentelle Bestimmung der Steifigkeitseigenschaften normbelasteter Fügestellen*. PhD thesis, TU Aachen, 1983.

[119] Ulrich Fuellekrug. Computation of real normal modes from complex eigenvectors. *Mechanical Systems and Signal Processing*, 22(1):57–65, 2008.

[120] R.J. Allemang and D.L. Brown. *Harris' Shock and Vibration Handbook*, chapter 21: Experimental Modal Analysis. McGraw-Hill, 5th edition, 2002.

[121] P. Avitabile. Experimental Modal Analysis – A Simple Non-Mathematical Presentation. *Sound and vibration*, 2001.

[122] C. Schedlinski and I. Seeber. Computerunterstützte Modelanpassung von Finite Elemente Modellen industrieller Grössenordnung. In *MSC Anwenderkonferenz*, 1999.

[123] R.J. Allemang. The Modal Assurance Criterion – Twenty Years of Use and Abuse, 2003.

[124] R.B. Randall and Y. Gao. Updating modal models from response measurements. In *Proceedings of ISMA*, 2003.

[125] Johannes Guggenberger and Eddy Dascotte. Anwendung von Model Updating mit FEMtools. In *ANSYS Conference & 23rd CADFEM Users' Meeting, Bonn*, 2005.

[126] J. Sauer. Closing the Data Gap Between Simulation and Modal Test with Virtualized Testing for an Improved FE Model Update. In *ANSYS Conference & 28th CADFEM Users' Meeting, Aachen*, 2010.

[127] S. Weikert and W. Knapp. KGM-plus - Device for Simultaneous Measurement in Six Degrees of Freedom on Machine Tool Trajectories. In *Proceedings of the ASPE*, 1999.

[128] S. Weikert and W. Knapp. R-Test, a New Device for Accuracy Measurements on Five Axis Machine Tools. *Annals of CIRP Annals - Manufacturing Technology*, 53:429–432, 2004.

[129] B. Bringmann, J.P. Besuchet, and L. Rohr. Systematic evaluation of calibration methods. *CIRP Annals - Manufacturing Technology*, 57(1):529 – 532, 2008.

[130] B. Bringmann and W. Knapp. Machine tool calibration: Geometric test uncertainty depends on machine tool performance. *Precision Engineering*, 33(4):524 – 529, 2009.

[131] B. Bringmann and P. Maglie. A method for direct evaluation of the dynamic 3D path accuracy of NC machine tools. *CIRP Annals - Manufacturing Technology*, 58(1):343 – 346, 2009.

[132] Markus Steinlin, Sascha Weikert, and Konrad Wegener. Open Loop Inertial Cross-talk Compensation Based on Measurement Data. In *25th Annual Meeting of The American Society for Precision Engineering*, Raleigh, USA, 2010. The American Society for Precision Engineering.